U. S. WEATHER BUREAU

THE INTERNATIONAL METEOROLOGICAL SATELLITE WORKSHOP

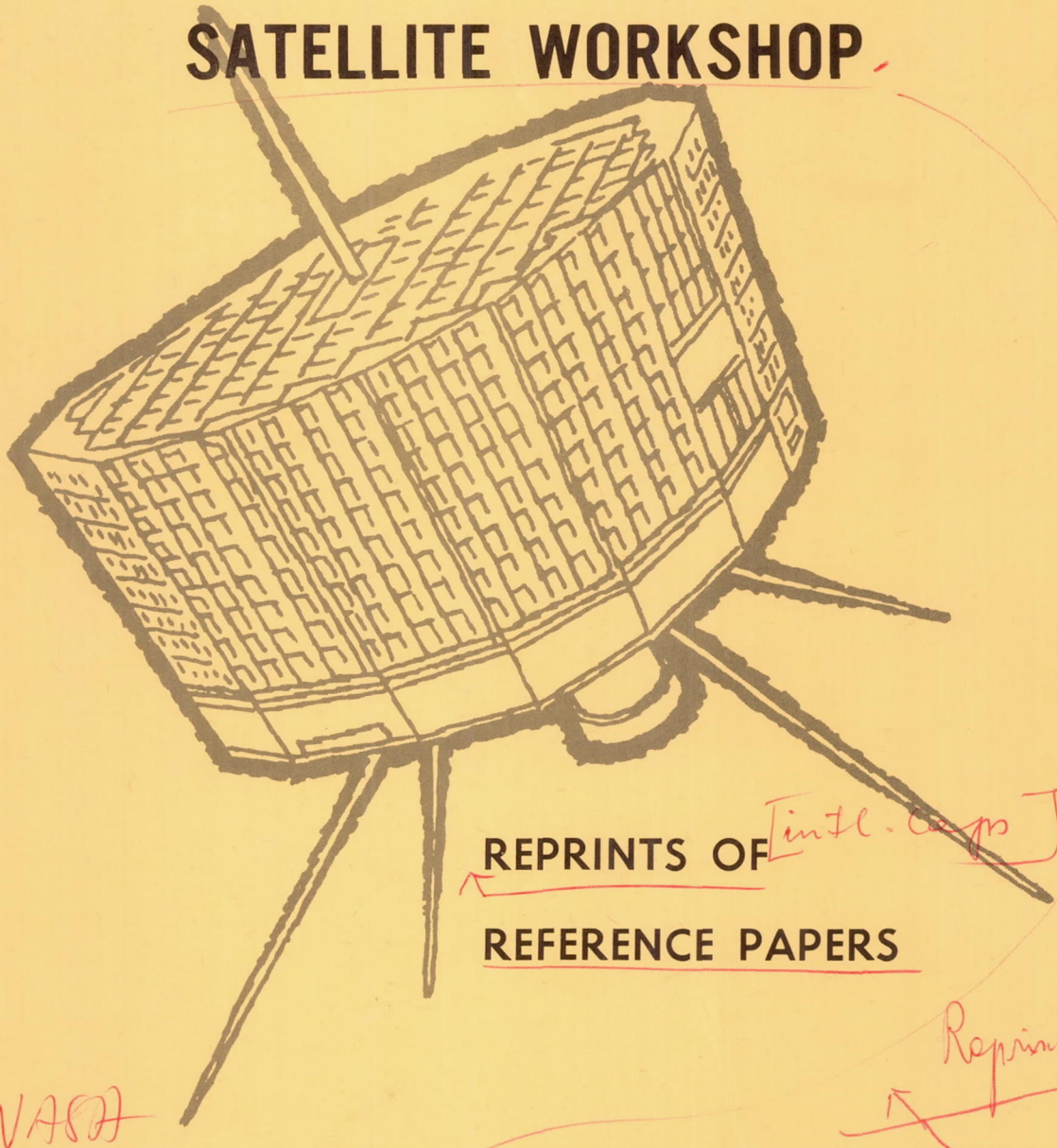

REPRINTS OF REFERENCE PAPERS

WASHINGTON, D. C. NOVEMBER 13–22, 1961

LIST OF REPRINTS

Bristor, Charles L. – *TIROS I Photographs of the Midwest Storm of April 1, 1960.*

Fritz, Sigmund – *Cloud Pictures from Satellite TIROS I; Satellite Cloud Pictures of a Cyclone over the Atlantic Ocean.*

Hubert, Lester F. – *A Southern Hemisphere Case Study with TIROS I Data; A Subtropical Convergence Line of the South Pacific: A Case Study Using Meteorological Satellite Data.*

Jones, J. B. – *A Western Atlantic Vortex Seen by TIROS I.*

Krueger, Arthur F. – *Cellular Cloud Patterns Revealed by TIROS I.*

Schuetz, John – *Cloud Streets over the Caribbean Sea.*

Stroud, W. G. – *Meteorological Measurements from the TIROS Satellites.*

Tepper, Morris – *TIROS Program Results.*

Wark, D. Q. – *On Indirect Temperature Soundings of the Stratosphere from Satellites; TIROS I Observations of Ice in the Gulf of St. Lawrence.*

Wexler, H. – *Meteorological Satellites.*

Whitney, Linwood F. – *A Tornado-Producing Cloud Pattern Seen from TIROS I.*

Winston, Jay S. – *Cloud Structure of an Occluded Cyclone over the Gulf of Alaska as Viewed by TIROS I; Satellite Pictures of a Cut-Off Cyclone over the Eastern Pacific; Some Aspects of a Cycle of Available Potential Energy.*

(*From the* QUARTERLY JOURNAL OF THE ROYAL METEOROLOGICAL SOCIETY, Vol. 87, No. 373, July 1961)

Satellite cloud pictures of a cyclone over the Atlantic Ocean

By S FRITZ

Meteorological Satellite Laboratory, U.S. Weather Bureau, Washington

551.507.362.2 : 551.515.12 : 551.576 : 77

Satellite cloud pictures of a cyclone over the Atlantic Ocean

By S. FRITZ

Meteorological Satellite Laboratory, U.S. Weather Bureau, Washington

(Manuscript received 26 January 1961; communicated by J. S. Sawyer)

SUMMARY

A composite of Tiros 1 pictures describing the cloud system in a mature cyclone, centred in the Atlantic Ocean to the west of Ireland, is described. Comparison of the pictures with conventional meteorological data shows that a stratiform cloud surrounding the storm was identical in position with a warm moist tongue of air flowing around the storm. In the centre of the storm where the clouds were more broken, giving the appearance of cumuliform clouds, a large mass of cold, dry air extended from the surface up to the tropopause above 400 mb. A few areas of steady precipitation were present in the stratiform cloud regions while more scattered showers existed in the central cumuliform region. An area of relatively high winds circled the storm, in conformity with the expectations from the thermal wind relation when cold air and warm air layers reside side by side. A brief comparison is made between the vertical motion computations based on conventional data and the cloud areas.

1. INTRODUCTION

The meteorological satellite, Tiros 1 (Sternberg *et al.*) launched on 1 April 1960 has photographed many interesting patterns of clouds (Staff, Met. Sat. Lab. 1961; Fritz and Wexler 1960; Wexler and Fritz 1960; Fritz 1960; Bristor and Ruzecki 1960; Winston 1960). The satellite did this with the aid of two television cameras; one, a wide-angle camera, photographed an area of approximately 800 × 800 mi when the camera axis was pointed straight down, and the second, narrow-angle, camera then covered an area of about 80 × 80 mi. Under these circumstances the wide-angle camera resolution was about 2 mi, whilst in the narrow-angle pictures the resolution was about $\frac{1}{2}$ mi.

During the second day of its existence, on 2 April 1960, Tiros 1 sped over the North Atlantic Ocean; and at about 1110 GMT, it began taking a series of snapshots spaced at 30 sec intervals. These photographs included the cloud system associated with an old, well-developed cyclonic vortex centred about 400 mi west of Ireland. About 100 min later, during the next orbital pass, Tiros again photographed the same storm. From these photographs, two composites have been prepared which clearly show the pattern of the clouds associated with the cyclone. Fig. 1 (a), (Plate VIII) contains the composite made from several frames taken during the first orbit, and Fig. 1 (b) is a composite made from frames in the next orbit.

2. DESCRIPTION OF TIROS CLOUD PICTURES

(*a*) *Wide-angle pictures*

To facilitate discussion and to orient the pictures geographically, the major features of the clouds in Fig. 1, (Plate VIII) have been sketched on a polar-stereographic map* in Fig. 2, (Plate VIII). Fig. 1 (a) best describes the clouds which occupied the western, northern and eastern parts of the cloud system, while Fig. 1 (b) shows the western, southern, and eastern portions best. We see that the clouds in the pictures of Fig. 1 extended from a point in the Atlantic Ocean, over 1,000 mi west of the European Coast, eastward into the European continent, covering much of the intervening Atlantic Ocean and the countries bordering the Atlantic.

* A separate study showed that the major cloud features were located within about 60 mi of their exact locations.

TIROS I PHOTOGRAPHS OF THE MIDWEST STORM OF APRIL 1, 1960*

CHARLES L. BRISTOR AND MARY ANN RUZECKI

Meteorological Satellite Laboratory, U.S. Weather Bureau, Washington, D.C

[Manuscript received October 10, 1960; revised October 26, 1960]

ABSTRACT

The midwest cyclone of April 1, 1960 is described from the standpoint of a series of TIROS cloud photographs. Cloud features having different appearances are related to the air masses and mechanisms involved. The cloud pictures are also used in outlining a possible application for objective weather map analysis in sparse data regions.

1. INTRODUCTION

TIROS I, the first photographic meteorological satellite, was launched on April 1, 1960. More than 20,000 photographs of the earth's cloud cover were received during its useful life span of 76 days. The satellite was equipped with both wide- and narrow-angle television cameras. A more detailed description of the engineering aspects of TIROS I may be found elsewhere [1].

One of the first storms photographed by TIROS I as it circled the earth was the Midwest storm of April 1, 1960 (fig. 1). Among the most striking cloud patterns photographed by TIROS I are large-scale vorticies, such as can be seen in frames B and C of figure 2. Frame B has been used as an example previously [2] owing to its classical structure of cyclonic center and frontal position. In this report it will be studied in greater detail as an integral part of the storm situation.

The Midwest storm developed as a lee disturbance to the east of the Rockies in conjunction with an intrusion of polar maritime air from the west. Individual TIROS cloud photographs presented in figures 2, 3, and 4 indicate the details of the cloud structure in various portions of the storm. The letter label attached to each photo appears on the map in figure 1—capitalized to indicate the satellite's position and in small type to locate the optical center of the picture. Photos A, B, and C in figure 2 were taken near 2028 GMT, April 1 looking back along the orbit as the satellite moved southeastward off the Louisiana coast. The remaining photos, D, E, F, G, and H in figures 3 and 4 were taken near 1843 GMT on the preceding orbital pass looking northwestward over the upper Plains and Great Lakes region. The areas viewed in narrow-angle photos G and H are indicated on the wide-angle photos D and F. The wide-angle photos were fitted with computer-produced perspective geographic grids. Sample grids are presented for frames B (fig. 2) and E (fig. 3). Precision of the gridding procedure requires knowledge of the satellite spin axis with respect to some frame of reference when the picture was taken. This involves knowing the spatial location of the optical axis of the camera systems and an accurate estimate of the time when the picture was taken. A more complete discussion of the gridding process may be found elsewhere [3].

One hundred photographs were taken by the TIROS wide- and narrow-angle cameras during the two passes of interest here. Fortunately, some of these pictures provide an excellent view of the entire storm area. After careful examination of the photographs, two composite sketches were created from eight gridded photos to provide a schematic representation of cloud brightness and coverage. Although individual cellular patterns and filament structures are indicated, there has been no attempt to obtain cell-for-cell accuracy. The mosaic sketch on a standard map base is broken into two segments because of the mis-match arising from movement of cloud features during the 100 minutes between pictures which overlap geographically from one pass to the next. Figure 5 presents the mosaic of the southern portion of the storm and figure 6 indicates the northern portion. The entire cloud pattern in outline form is also indicated with light stippling in figure 1. The mosaic sketches of figures 5 and 6 have been divided into Roman-numbered regions to facilitate the discussion. It will be convenient to indicate the sub-regions of the sketches by number and also refer to the individual photos by letter without regard to figure number in order to reduce wordage. Since the paper largely involves the description of pictorial details, the reader is cautioned to relate the discussion continuously to the corresponding pictures in order to maintain meaningful continuity.

The discussion in this paper represents an attempt to relate some of the outstanding features of the cloud

*This research has been supported by the National Aeronautics and Space Administration.

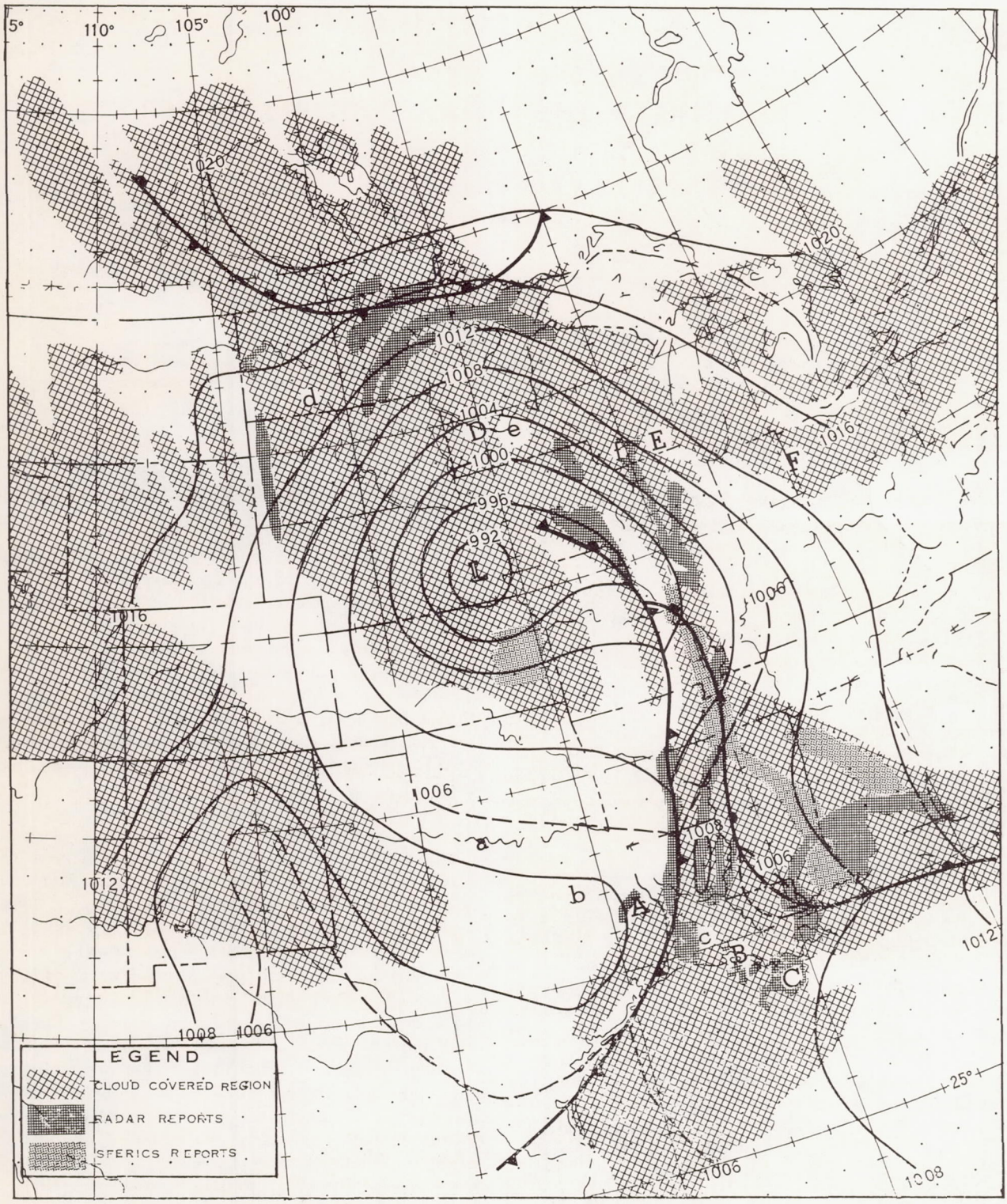

FIGURE 1.—Sea level chart, 2100 GMT, April 1, 1960, with cloud cover area and radar and sferics reports. Letters refer to satellite photographs.

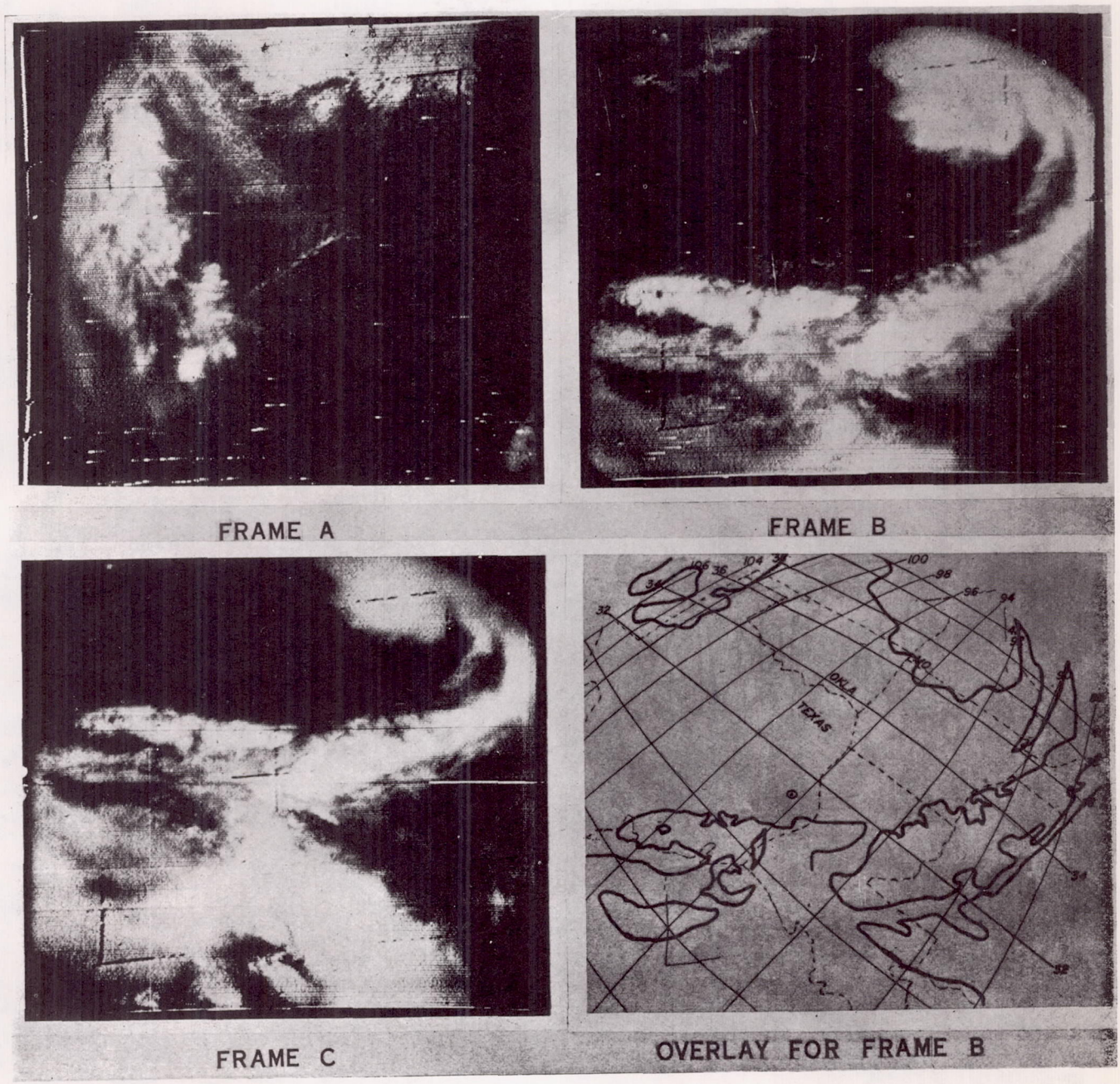

FIGURE 2.—TIROS wide-angle cloud photographs taken over points A, B, and C of figure 1, and a grid overlay for frame B. (The dotted circle gives the optical center of the picture.)

photos to other meteorological observations and analyses. In particular, comparisons are made between the cloud cover pattern and objective weather analyses pointing up the potential usefulness of the cloud information for improvement of such analyses in sparse data regions.

2. CLOUD PHOTOS

The following comments concerning the individual photos are designed to point out the main features in each picture and to relate them to the composites in figures 5 and 6. Also, somewhat in the manner of a cloud atlas, an effort is made to identify the types of clouds being viewed, but without discussing the weather situation in its entirety. This identification is however dependent upon corroborating evidence obtained from the standard meteorological observations of clouds and weather, both from the ground and from airplane reports. Relationships of the cloud pictures to circulation patterns and other

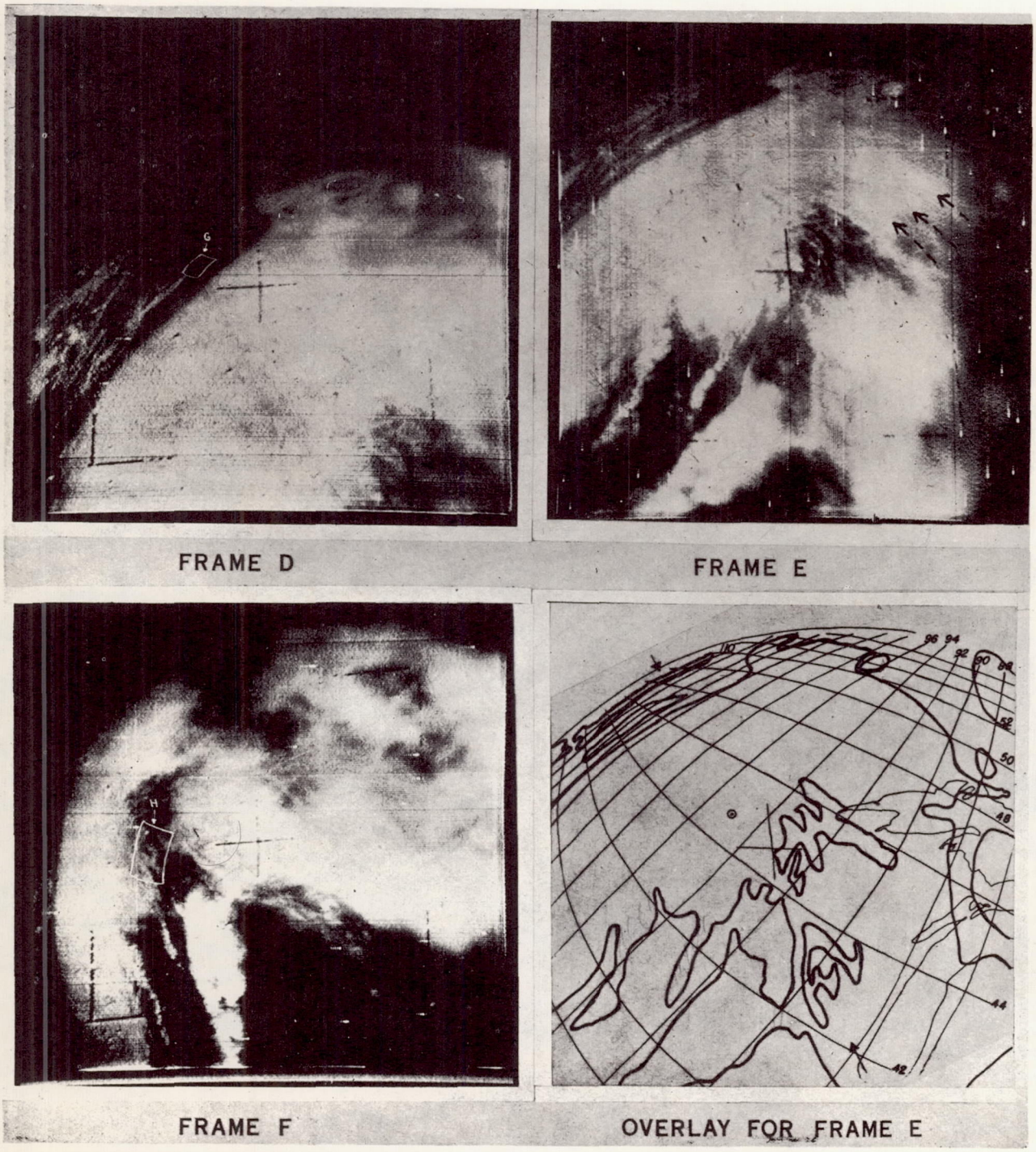

FIGURE 3.—TIROS wide-angle cloud photographs taken over points D, E, and F of figure 1, and a grid overlay for frame E. (The dotted circle gives the optical center of the picture.)

meteorological mechanisms will be treated in the ensuing section of the paper.

In the right foreground of frame A (See also fig. 5) is a predominantly clear region extending from eastern Texas into Missouri. The textured edge of a dense overcast region is visible at the top of the frame over Kansas. The cloud mass to the left has a marked cellular structure throughout, with a suggestion of thin upper clouds. The leading clump of cells is near Lubbock, Tex. The main portion of this cloud mass extends over most of New

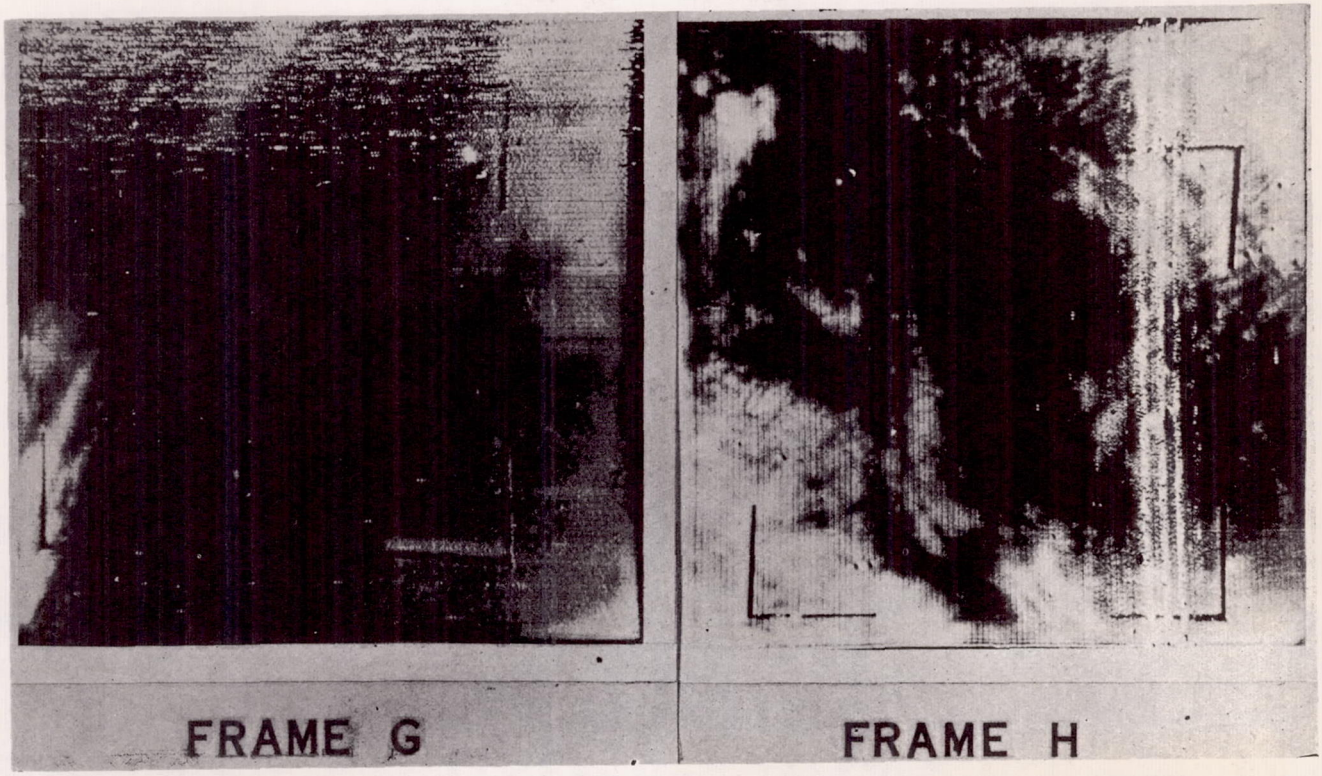

FIGURE 4.—TIROS narrow-angle cloud photographs taken over areas G and H shown in frames D and F of figure 3.

Mexico and northwestward. A filmy veil of clouds appears to emanate from the upper left of the photo (near Denver) and terminates in a brighter streak near the center (intersecting the southern Oklahoma border).

Frame B was taken one minute after frame A. The Texas-New Mexico cloud now appears much foreshortened near the top of the picture. More of the solid overcast region is now visible in the upper right. The overcast extends over much of Nebraska as indicated by the accompanying geographic overlay.

A wealth of new detail appears in the foreground. Faint patches of stratocumulus are lined up horizontally across the photograph along the lower boundary of the clear area. These wisps continue to the right into a brighter wedge of cloud containing cumulonimbus and upper cloud at its junction with the overcast region in the upper right portion of the photo. The features described above are located in the mosaics of figure 5 along a line through central Arkansas and northward into Iowa. Much brighter clouds of great variety extend across the photo in a broad belt immediately below and paralleling the features just described. Widespread shower activity with cumulus and cumulonimbus clusters, together with middle and high clouds, occupies the band from the upper right down to the bright "finger" in the lower central foreground of the picture. A cloud system, with parts almost as bright, extends on to the left. The brighter portion of this left branch near the center of the photo, is a region of cold frontal shower activity. Two sizable clear patches appear as black spots farther to the left in a post-cold-frontal region of waning shower activity. The larger, relatively clear, horizontal areas below this cloud region are located over the Gulf of Mexico near the northern portion of the Texas coast.

Frame C was taken 30 seconds later and largely overlaps frame B. The important extension of the viewed area is in the foreground. The bright region at the lower edge of frame B is now located near the center of the picture with a broad, very bright band extending to the lower right. This band, extending from New Orleans eastward along the Gulf coast consists of an almost solid mass of cumulonimbus activity with extensive middle and upper cirriform overcast. The gray area to the lower left extending off the Louisiana coast contains patchy lower clouds with little or no upper cloud cover. The darker region in the lower right, covering parts of central and northern Mississippi and Alabama represents mostly high, broken cloudiness with a few patches of lower, cumulus shower activity.

Frame D of figure 3 is predominantly a view of the extension of the dense overcast area over Kansas and Nebraska as seen in frames A, B, and C. Most of the part shown here, covering the Dakotas, appears equally dense and uniform. These are multi-layered, precipita-

569382—60——4

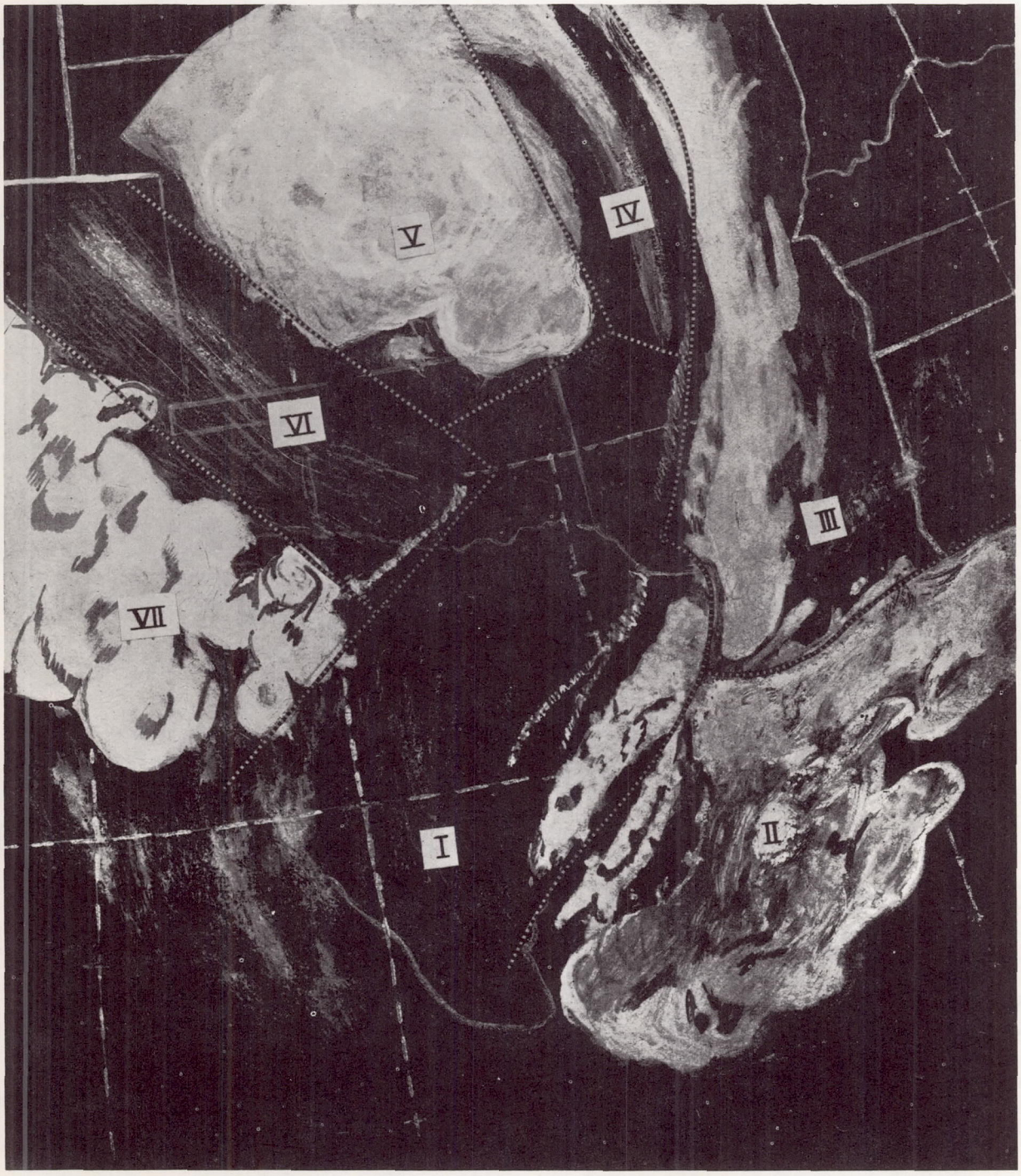

FIGURE 5.—Mosaic representation of TIROS wide-angle cloud photographs taken near 2028 GMT, April 1, 1960.

tion-bearing clouds. The possibility of an effect of snow cover is discussed later. A narrow-angle picture,* viewing the center of the lower half of this frame gives only a faint suggestion of a cellular pattern. Frame G of figure 4 presents a detailed narrow-angle camera view of the west flank of this large overcast in the area marked on frame D. The bright cloud in the lower left evidently contains rows of cumuliform clouds. There also appear to be streaks of thin clouds parallel to the edge of the large overcast. The cloud pattern to the left in frame D is located over Wyo-

*Unfortunately, strong electronic interference contaminated this photo making the printing reproduction marginal in quality.

FIGURE 6.—Mosaic representation of TIROS wide-angle cloud photographs taken near 1843 GMT, April 1, 1960.

ming with the streaks oriented roughly north-south. Some thin cirrus clouds exist here but the brighter portions are rows of towering cumulus clouds in a relatively dry environment. The hook-shaped cloud near the horizon (top, center) extends into Canada beyond Edmonton, Alberta. The clouds near the western edge are cirrus with small cumulus beneath. At the southern edge of the hook-shaped cloud and to the right of the dark spot, low stratus and stratocumulus and drizzle prevail, perhaps with some upper cloud cover. Farther to the right, cirrus and altocumulus clouds are thinner and there are no low clouds. The somewhat square, bright patch farther to the right is apparently a view of the northern portion of Lake Winnipeg with a covering of snow and ice, since only broken upper clouds are reported in that area.

Frame E, taken one minute after frame D, reveals much detail to the east and northeast of the large overcast region. The slightly brighter parallel cloud bands which appear as arcs to the upper right of the picture center (indicated by thin arrows) are of particular interest. In this area over northern Minnesota, radar echoes (fig. 1) form a remarkably similar pattern of concentric arcs. (An independent diagnosis of this banded structure from the photos alone would likely be rather difficult because of the lack of contrast in the images.) The bright cloud mass to the lower left extends over eastern Iowa. This is the northern portion of the thundershower structure discussed under frame B. The partly cloudy darker region from the lower left corner of the frame is the extension of the cloudless wedge also shown in that frame. Here, however, much greater detail is available in what appeared in frame B to be a single cloud band pointing southward into the clear area. One hundred minutes later, in frame E, at least two streets of bright shower cloud masses are apparent in this region, along with other isolated groups of cells.

Frame F, taken one minute after frame E, contains a gray region to the left of center which is also visible slightly to the right of the center of frame E. Frame H presents a narrow-angle camera view of a portion of the region indicated on frame F and located near La Crosse, Wis. In this narrow-angle photo a few large cumulus clouds appear in the upper left, with multi-layer frontal precipitation cloudiness commencing in the lower left. Stratocumulus in various banded arrays appears toward the top and right of the central partly cloudy area. Frame F also presents a clear area in the lower right corner which is located along the Ohio Valley. The bright band extending to the right is a mass of low stratus extending eastward along the lower Great Lakes. A cirrus veil covers the stratus and extends northward. No middle cloud exists in this area as indicated by the radiosonde reports.

3. CLOUD FEATURES AND THE SYNOPTIC WEATHER SITUATION

The above discussion permits one to locate geographically the various cloud features seen in the photos. The two composite cloud representations in figures 5 and 6 will next be related to the storm structure. Reference will be made to the 2100 GMT sea level chart in figure 1 as well as to the isentropic chart in figure 7 and the north-south and east-west cross sections in figures 8 and 9, all based upon information at 0000 GMT, April 2.

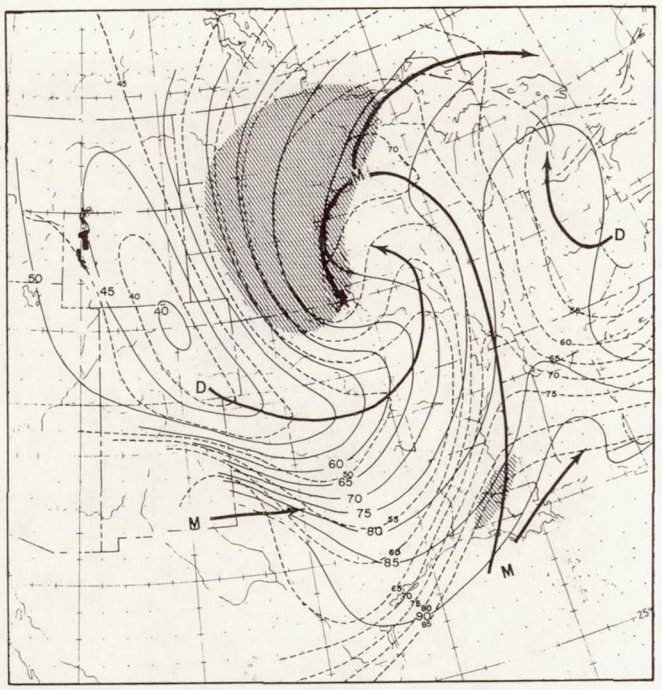

FIGURE 7. Isentropic chart for 300° K.; pressure in solid lines and condensation pressure in dashed lines, 0000 GMT, April 2, 1960. Shading indicates approximate area of saturation.

Region I of figure 5 is the post-cold-frontal section of the storm. Considering the fact that the pictures were taken near mid-afternoon local time, it may seem remarkable that this region is so free of even convective-type clouds. The air was extremely dry, however, as indicated by surface reports such as that for Fort Worth which had a temperature of 72° F. and dew point of 28° F. Immediately to the rear of the front along the Texas coast there is a broad band of clouds, which appears brightest to the northeast and also has some small, distinct clear spots embedded in it. Reports from stations along the Texas coast show that this post-frontal cloud band consisted of towering cumulus and stratocumulus types. Reports of any major shower activity in this area, either from surface reports, radar, or sferics, were lacking, however. These clouds were very likely entirely within the warm air above the cold front. Figures 8 and 9 show that the cold air was rather shallow for some distance behind the front so that warm-air cloudiness could have had bases as low as about 5,000 ft. The deeper cold, dry air was not reached until farther west of the front. The faint patches of stratocumulus in frame B may mark the leading edge of the deep cold air.

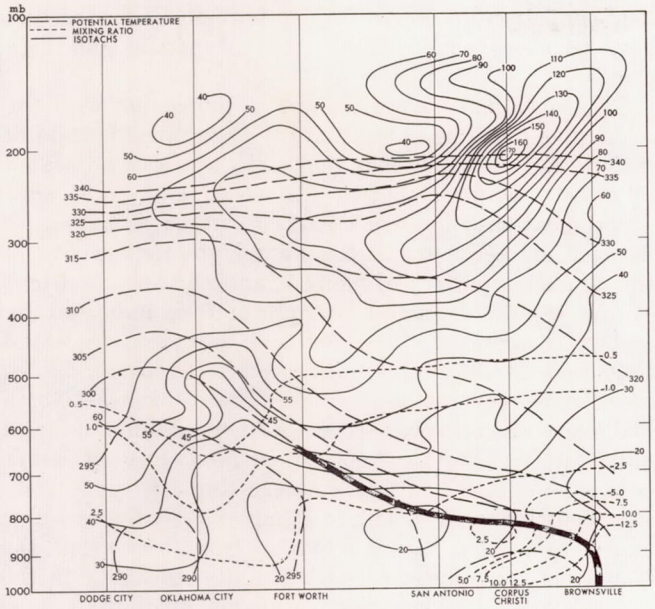

FIGURE 8.—North-south vertical cross-section (isotachs in 10-knot intervals) 0000 GMT, April 2, 1960.

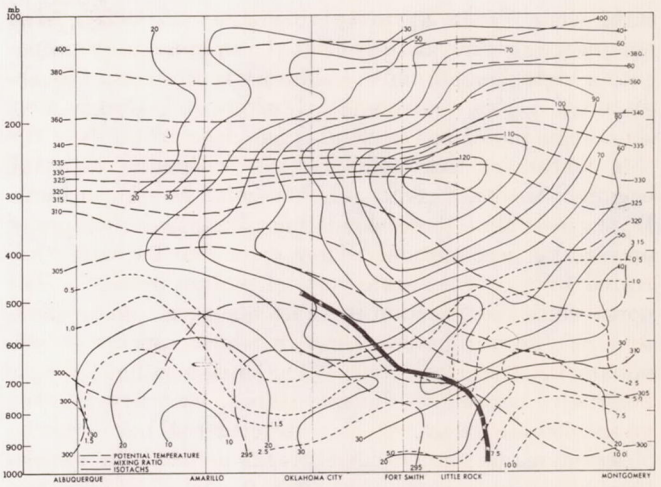

FIGURE 9.—East-west vertical cross-section (isotachs in 10-knot intervals) 0000 GMT, April 2, 1960.

Region II is very moist as indicated by the high condensation pressures on the isentropic surface displayed in figure 7. Clusters of radar echoes shown in figure 1 marked the frontal thunderstorms from Lake Charles, La. northward toward Little Rock, Ark. Heavy clusters of radar echoes and sferics reports blanketed another large thunderstorm area which extended from New Orleans eastward in the warm-frontal zone along the Gulf coast. Upper-level charts indicated a branch of the jet stream extending from near the Mississippi Delta toward central Florida. One might thus speculate that the marked contrast in cloudiness and precipitation, indicated in frame C by the bright coastal cloud band and the reduced activity offshore (see also bottom and lower left in frame B), may reflect differences in the large-scale vertical motion pattern on either side of the jet axis. Aircraft reports indicated a cirrus overcast between 300 and 400 mb. which extended over the thundershower area, but also ended at the Gulf coast.

Region III includes the warm tongue shower activity which extended in a band northward along the Mississippi River to southeastern Iowa. Although surface reports did not generally indicate high humidity in this band, there was evidence of a well developed moist tongue on the isentropic chart (fig. 7). A line of sferics fixes extended through this band from Jackson, Miss. to St. Louis, Mo. Clusters of radar echoes marked the bright "finger" of cloud in frame B near the southern end of this band and similar echoes marked the equally bright cloud clusters in frames E and F to the north.

Region IV is an extension of the post-frontal and frontal region. Close inspection of frame B suggests a veil of thin upper clouds covering the easternmost dark wedge. Radar and surface reports located thundershowers in the northern portion of the brighter central cloud area and southwesterly upper winds could have carried convectively produced upper clouds into the dark wedge. Surface reports required that the occluded front be placed near Des Moines, Iowa at 2100 GMT in the central cloud area. Thus the eastern dark wedge of reduced cloudiness is in the warmer air to the east of the cold front. This is in agreement with reports from stations such as St. Louis which reported partly cloudy skies in the southerly warm flow. If we may digress slightly into region IX (fig. 6), we see similar indications of the frontal position there. Surface data at 1800 GMT suggest that the left-most bright appendage in the dark area in the lower left of frame E is associated with the cold front over southwestern Iowa. Stations with partly cloudy skies were located well to the east of the front, but west of the bright shower band in the moist tongue.

Region V is the southern portion of the area of upslope precipitation. The pattern of ascending, saturated air is indicated on the isentropic surface (fig. 7) by the southwestward curving branch of the moist tongue. Rain and snow had ended in the southeastern portion of this cloud mass and pressures were rising. However, by the time of these photos, new snowfall from the storm had enlarged the area of snow cover to include northeastern Nebraska and the eastern Dakotas. The apparent brightness and lack of texture may thus result, in part, from the presence of the snow field. The question of image contamination by snow fields does not arise insofar as the southern and western cloud boundary is concerned, since snow cover limits are well within the cloudy area. The rather well defined edge of these clouds suggests the desiccating power of the descending motion pattern around its perimeter.

The thin cloud veil in region VI appears to have been generated by shower activity farther to the northwest. The sounding at Lander, Wyo. indicated extremely un-

stable showery air up to approximately 16,000 ft. The northwesterly flow at such heights was apparently propagating high clouds from this showery source region southeastward across Oklahoma. Denver and Dodge City soundings indicated a cloud base near 620 mb. The thin texture of this cloud veil, as contrasted with the brighter streaks of cloud over Wyoming as seen in frame D, suggests that these clouds may be poor indicators of upward vertical motion. They appear to be barely tolerated by the broad-scale vertical motion pattern. The north-south cross section in figure 8 suggests an explanation for the abrupt cloud streak which appears to terminate the thin cloud veil. (The cross section, fig. 8, is essentially normal to the mid-tropospheric flow as seen on the 500-mb. chart, fig. 11.) Kuettner [4] has discussed observations of similar cloud streaks or bands in association with jet streams. Although the jet stream in this case was far removed from the cloud streak, there is evidence of considerable variation in horizontal wind shear oriented in the same direction as the cloud streak. Close examination of frame B on the original film strip reveals not only the bright cloud line but a faint resumption of cloud farther to the southeast. There is thus an impression that vertical motions in response to the streaks in the horizontal shear created an undular pattern in the cirrus veil—augmenting the cloud in regions of ascending motion and subduing it where sinking motion occurred. The bright streak is located about midway between Oklahoma City and Fort Worth, near the zone of maximum cyclonic shear on the cross section.

In region VII the isentropic chart (fig. 7) suggests that a broad-scale ascending motion area existed in the middle troposphere with air being lifted along the flank of the cold dome. In figure 9 between Albuquerque and Amarillo, air with slightly higher moisture content is noticeable. Soundings in this sector had extreme instability in the lower layers. Dry adiabatic lapse rates extended upward beyond 700 mb. at Albuquerque, N. Mex., and Amarillo and Midland, Tex. The unstable air terminated at the tropopause near 400 mb. The cellular structure in frame A thus appears to be made up of a cirrus veil above large cumulus groups.

Region VIII contains a variety of cloud types. Unfortunately, the foreshortened view precludes any serious attempt to distinguish one type from another. The "hook-shaped" western boundary of the cloud is located in an air mass of Pacific origin where the previously mentioned cirrus and small cumulus clouds were reported. The sharpness of this western edge may reflect an orographic downslope motion to the east of the Canadian Rockies since westerly winds aloft were reported in the Edmonton–Calgary area. Farther east the quasi-stationary front shown in figure 1 bounded a colder and much drier polar continental air mass. The stratiform clouds along the west limb of the front were probably covered by middle and upper clouds which extended eastward into the partly cloudy area over the colder air mass. No low clouds were reported in the dry polar air—the dull gray patches being thinner areas of middle and high clouds.

Region IX has been discussed in connection with the overlapping regions to the south. The central portion of the widespread continuous rain and snow area is located in eastern South Dakota. The cloud and radar echo areas, mentioned in connection with frame E, appear to be near the perimeter of the frontal upslope activity in the isentropic pattern of figure 7, and on the very fringe of the region of frontal precipitation as indicated by surface reports. In this area and to the north, cloud brightness in the photos may be affected partly by an older snow cover extending into north central North Dakota and eastward across northern Minnesota and northern Wisconsin. Another isolated line of radar echoes is indicated in figure 1 near Rapid City, S. Dak.

In contrast to the northern Minnesota cloud arcs which existed in a region having a marked frontal inversion, the Rapid City sounding revealed extreme instability in the lower layers. The north-south alignment of the echoes with the flow at lower levels over the western Dakotas suggests a band of convective activity induced from the ground rather than from frontal lifting. It is quite remarkable that all cloud activity ceases rather abruptly at the western edge of the large frontal cloud mass. A combination of factors seems to be involved since the edge appears to coincide at all cloud levels. Reversal of the mid-tropospheric vertical motion from ascending to descending at the cloud edge may have been the predominant factor. The filmy appearance of the edges of cloud bands in frame G, coupled with the suggestion of downslope motion over the Canadian and Montana Rockies, suggests that lateral mixing of dry air may also have assisted the process of middle and upper cloud decay along this western edge. At lower levels, moist northeasterly trajectories within the upslope cloud mass, in contrast with drier northwesterly trajectories farther west, may have favored such an abrupt edge within the convective layers.

Region X presents the situation in the eastern portion of the storm's perimeter. The isentropic chart in figure 7 indicates an eastward-branching moist tongue with a lateral admixture of drier air from Kentucky and Tennessee. No middle clouds were indicated by the soundings, nor by the isentropic chart which intersected above a strong low-level inversion in this area. Presumably a pattern of overrunning motion farther aloft produced clouds, since aircraft reported cirrus in conformity with the filmy white clouds seen throughout the central and eastern Lakes region in frame F. Soundings at Dayton, Ohio, Flint, Mich., and Pittsburgh, Pa. indicated a strong temperature inversion and moisture lapse at 3000–5000 ft. Reports of fog accompanying the low clouds in this strong inversion area suggest a rather solid layer of fog, stratus, and stratocumulus from the ground up.

One of the main features of the cloud pictures is the broad band of stratiform cloud which, in Figs. 1 (a), 1 (b) and 2, terminates in the arrowhead-like cloud near the centre of the vortex. The figures show that the stratiform cloud is a quasi-circular band of cloud. Starting with the protuberance in the wall of the cloud, near 50°N 30°W, the cloud sweeps southward in a band about 300 mi wide, joining with a widespread cloud mass over western Spain (eastern Spain is nearly cloud-free). The cloud over Spain may, in part, be enhanced by orographic effects, but it extends also to the south-southwest into the Atlantic Ocean just west of Gibraltar, suggesting the existence of a weak frontal system there.

The main stratiform cloud continues over Spain into France, but contains some fairly large holes over the Bay of Biscay region (Figs. 1 (a) and 2). The stratiform cloud continues to circle the storm area passing over England and Ireland, and then, moving out over the Atlantic Ocean near latitude 55°, it divides into two parts. One part goes into the arrowhead cloud near the centre of the vortex, and the other part completes the circuit by joining the protuberance just to the west of the ' arrowhead '; the continuity of the cloud around the northern side of the vortex can be better seen in an individual frame (shown in Fig. 1 (c)). In addition, Fig. 1 (c) suggests that the cloud may have had a fairly sharp boundary in its northern section.

In the pictures, this quasi-circular stratiform cloud encircles a swirling galaxy-like mass of more broken, cumuliform clouds which lies near the centre of the cloud system. In addition, we note that very narrow cloud streets seem to originate in the wall of the stratiform cloud, most prominently near the west-wall protuberance. These cloud streets, several hundred miles in length, circle south of the ' arrowhead ' cloud and sweep into the cumuliform, central cloud mass.

It is interesting to note the similarity of several cloud features in Figs. 1 (a) and 1 (b) in view of the fact that 100 min had elapsed between the two sets of pictures. The arrowhead and the protruding cloud in the inner west wall of the stratiform cloud persist essentially unchanged. The very narrow cloud streets which seem to issue from the inner west-wall protuberance and to sweep south of the arrowhead into the cumuliform mass in the centre are clearly evident in both Figs. 1 (a) and 1 (b). Certainly the form of the cloud system had hardly changed at all in this 100 min interval.

(*b*) *Narrow-angle pictures*

During the second pass when the pictures in Fig. 1 (b) were observed, the narrow-angle camera also photographed a swath across the centre of the cloud system, and a composite of these narrow-angle pictures is shown in Fig. 3, Plate IX, together with associated wide-angle pictures. Actually the composite in Fig. 3 stretches farther to the west than the pictures in Fig. 1 (b) because there is evidence that the narrow-angle camera started photographing the Earth somewhat earlier than did the wide-angle camera.

Fig. 3 (a) shows the narrow-angle pictures taken in the western half of the cyclonic pattern of Fig. 1 (b). The approximate boundaries of the narrow-angle pictures swath is shown in the wide-angle picture, Fig. 3 (b), by the broken lines. In Fig. 3 (c) the narrow-angle pictures for the eastern half of the cyclone cloud pattern is shown. Fig. 3 (d) shows the swath which contains the composite of Fig. 3 (c). The letters A, B and C are given to indicate the corresponding positions in the wide-angle and narrow-angle pictures. Position A is the place where the cloud ' streets ' emerge from the stratiform cloud; position B is the end of the arrow-head cloud; and position C is near the inner edge of the stratiform cloud on the eastern side of the cyclonic cloud pattern. In Fig. 3, the rather uniform stratiform clouds on both the western and eastern sides of the cloud pattern can be seen to have almost no small-scale detail, but they do contain relatively large patches of dark area denoting thinner clouds or actual holes*. The cumuliform cloud

* The narrow-angle pictures contain a defect which makes the stratiform clouds appear less uniform than they really are. In Fig. 3 the apparent thinning of the cloud occurs in a narrow band across the whole composite, and is especially noticeable in the stratiform cloud. Note, for example, the darker areas along the satellite path in the upper left-hand frames of Fig. 3 (a). These darker areas which are oriented along the length of the pictures in Fig. 3 are spurious.

seems to be made up of small elements, especially in the cloud streets; but, near the tip of the arrow head cloud (position B) and in the 'galaxy-like' cloud (between B and C), the elements are fairly large and bright, sometimes over 40 mi in length. They were, doubtless, the cloud elements associated with the scattered shower activity reported in the surface observations.

3. The meteorological situation

The cloud system of Figs. 1, 2 and 3 is, of course, the result of physical processes in the atmosphere. To relate these processes to the cloud pictures we need to examine the meteorological state of the atmosphere at the time of the pictures. To facilitate the discussion, the meteorological charts which are presented here contain an outline of the stratiform cloud area taken from Fig. 2. The surface and 500 mb analyses were prepared by the National Weather Analysis Center, independent of the cloud pictures.

(*a*) *Surface data*

At the time Tiros took the pictures of Fig. 1, a large, mature cyclone was centred about 400 mi west of Ireland. The sea-level pressure chart for 1200 GMT, 2 April, 1960 (Fig. 4) shows the cyclone with its central pressure of about 974 mb. The cyclone was characterized by practically circular isobars and strong pressure gradients, which were associated with reported surface winds of up to 50 kt. A weak front, which has been entered on the map along the west coast of Europe, sweeps southward and westward across the Azores.

The cloud amount and cloud forms, observed from the earth's surface, are also shown in Fig. 4, and we note that near the frontal zone a band of overcast sky was present, in which low and middle cloud (as seen from the surface) predominated. Cirrus cloud forms were also reported over parts of Spain and France. Surrounded by the overcast band, an area of broken clouds predominated in the surface reports over the ocean although scattered clouds were also reported there. The low clouds in this non-overcast area were mainly cumulus clouds in various states of development, and stratocumulus types. Altocumulus and cirrus clouds were also reported. Along the inland edge of the overcast band, cirriform clouds predominated.

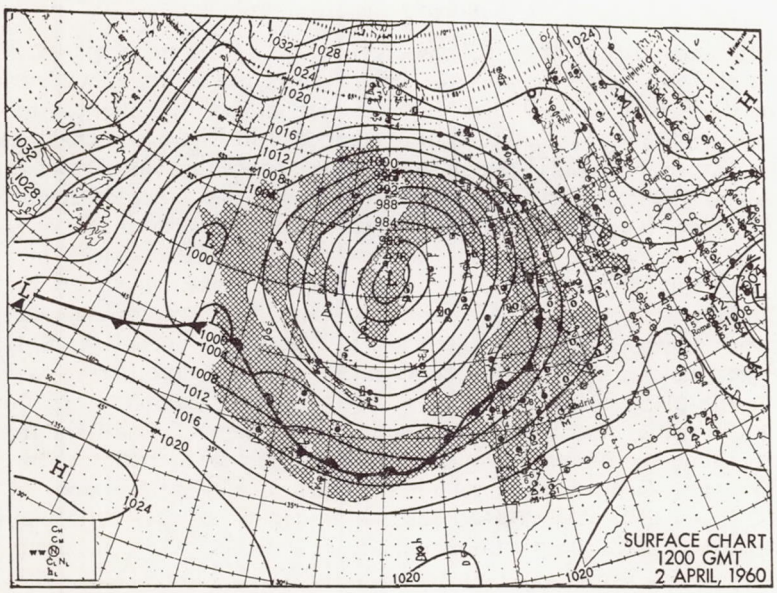

Figure 4. Sea-level chart for 1200 GMT, 2 April 1960, showing mature cyclone with outline of stratiform cloud area from Fig. 2 superimposed. Surface cloud observations are also shown.

Precipitation occurred in a few reports. More steady rain was reported in the overcast band near the frontal zone, over and near Spain and the British Isles, and over some adjacent ocean areas; a few showers were also noted in the central overcast region over the ocean.

Although the surface cloud reports were not sufficient, even in this rather dense shipping zone, to outline the cloud areas completely, similarity between the surface reports (Fig. 4) and the Tiros picture (Figs. 1 and 2) is apparent.

(*b*) *Upper-air data*

The cyclone in Fig. 4 was quite symmetrical with height. The ' low ' centre on the 500 mb chart (Fig. 5), at a height of about 16,800 ft, was located nearly above the surface low-pressure centre.

Fig. 5 contains an analysis of the temperature field; and the dew-point temperatures are also plotted near each reporting radiosonde station. If we denote the centre of the cyclone by the position of the lowest height on the 500 mb chart, then we note that a cold, dry mass of air resided close to, but somewhat to the southeast of, the centre; the exact positions cannot, of course, be given with the data available. Moreover a warm, moist mass of air circles the centre from the Azores, across Spain and England and into the Atlantic.

A region of relatively strong winds, with up to 60 kt reported, encircles the southern and eastern sides of the 500 mb vortex. This weak jet stream lies in or near the inside edge of the semi-circular zone of warm moist air, and therefore near the inner edge of the cloud system in Fig. 1.

The flow of the moist air around the cyclone is seen even more clearly on the 300°K isentropic chart (Fig. 6). On this chart, both the relative humidity and water-vapour mixing ratio are given; and isolines of pressure and of mixing ratio have been analysed. This isentropic chart reaches a pressure of less than 400 mb in its centre, indicating the deep cold air which had already been noted on the 500 mb chart (Fig. 5). Moreover, the moist air (high-mixing ratio) flows with the winds around the vortex, and especially

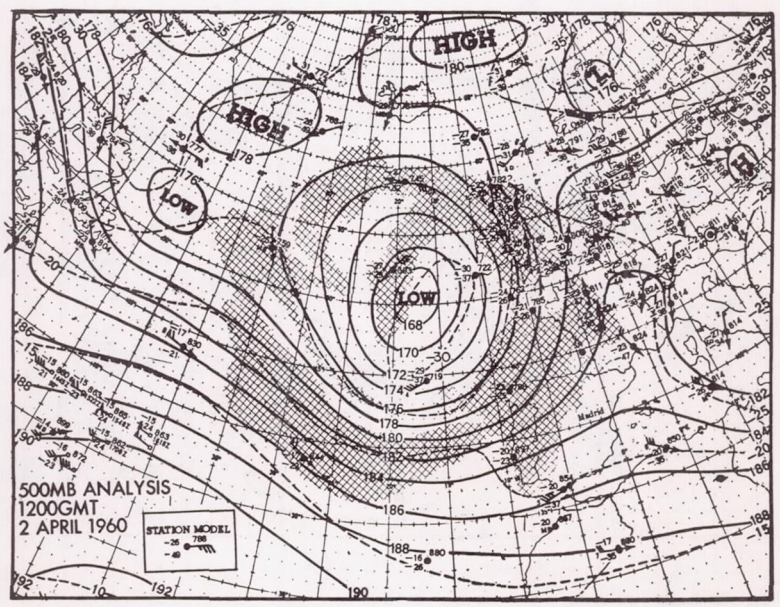

Figure 5. 500 mb chart for 1200 GMT, 2 April 1960. Solid lines are 200 ft contours, dashed lines are isotherms. Dew-point temperatures are shown at lower left of each station circle.

on the eastern side of the centre the air flows up the isentropic surface. The presence of condensation obscures the real significance of this chart, but the existence of overcast clouds and precipitation in this region (Figs. 2 and 4) attests to the reality of the ascent in this case.

In order to note the vertical extent of the cold, dry air in the vortex centre, and of the warm, moist air around the periphery of the vortex, several cross-sections have been prepared. One of these cross-sections, along the line marked A-A in Fig. 6, is shown in Fig. 7. Here the cold air is shown to reach from the earth's surface to the tropopause near 300 mb. Relative humidity is also shown in Fig. 7, since this moisture quantity is readily discussed in relation to clouds. It is clear that except for the levels near the ocean surface, the air above ship station *K* is much drier than the air over ship station *J* up to the 400 mb level. To the south of ship *K*, over the Azores, the air has about the same relative humidity as that at station *K*; small differences do appear but may not be reliable in view of the inaccuracies in humidity measurement.

Commercial air-plane cloud reports (K.L.M. and Alitalia) indicated that near latitude 56°N in this cross-section (Fig. 7), a stratiform cloud top was located at a height of 10,000 to 12,000 ft. This information is shown in the cross-section. The latitude where the cross-section crosses the inner edges of the stratiform cloud as seen by Tiros (Fig. 2) have also been included in Fig. 7.

Finally, since the cloud formation is generally associated with vertical motion in the atmosphere, the vertical motion chart for the 600 mb pressure level deduced by the Joint Numerical Weather Prediction Unit (U.S.W.B.) is shown in Fig. 8. The vertical motion is shown to be slightly downward in the north centre of the cloud pattern. In the overcast cloud region the vertical motion often changes sign, denoting alternations between upward and downward motion.

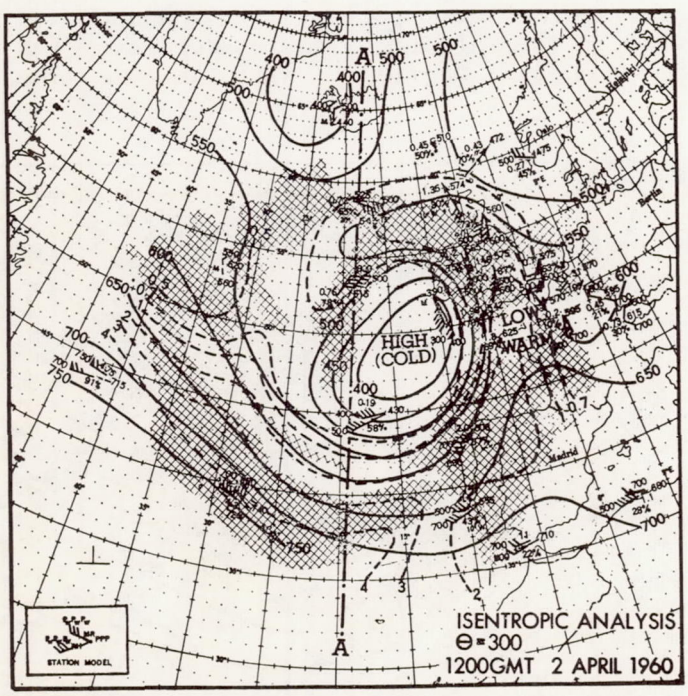

Figure 6. Isentropic chart ($\theta = 300$°K), 1200 GMT, 2 April 1960, showing deep core of cold air with warm moist air flowing around it. Solid lines are isobars on the isentropic surface; dashed lines are lines of constant water vapour (mixing ratio). Line AA shows the region of the cross-section in Fig. 7. The winds are shown at two pressure levels near the level of the isentropic chart. High and low refers to the elevation of the isentropic surface.

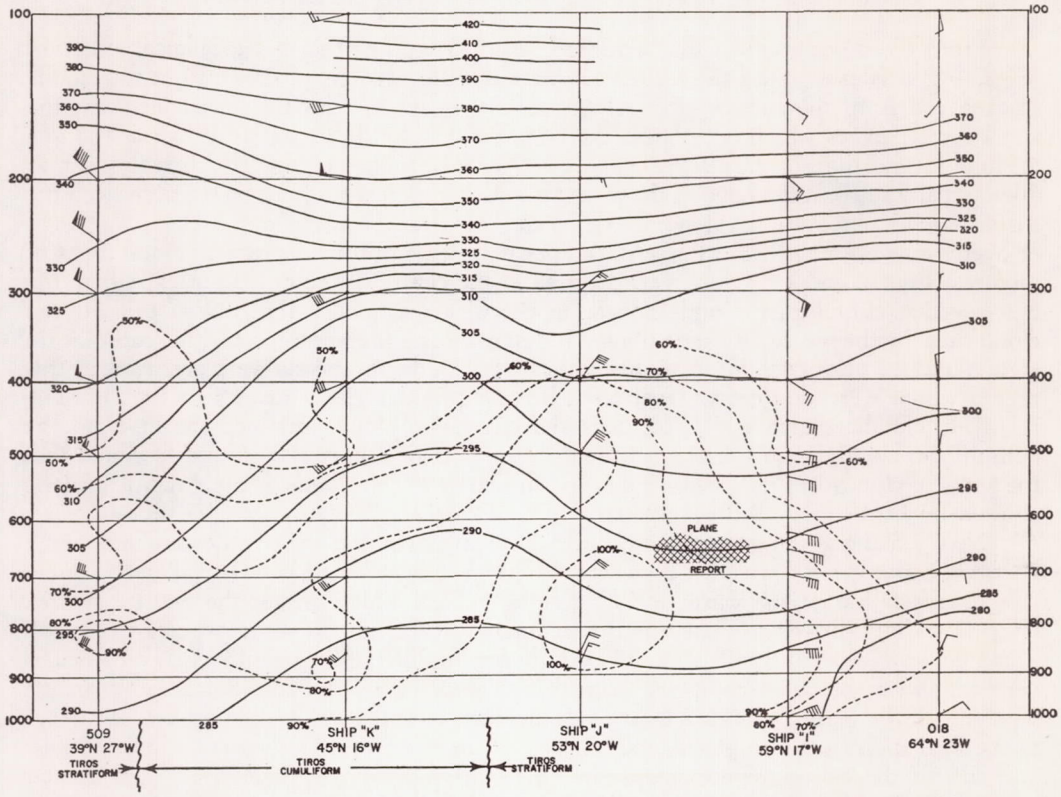

Figure 7. North-south cross-section through the atmosphere along the line AA of Fig. 6, 1200 GMT, 2 April 1960. Solid lines are lines of constant potential temperature; dashed lines are lines of constant relative humidity. The inner boundaries of the stratiform cloud (from Fig. 2) are shown below the diagram.

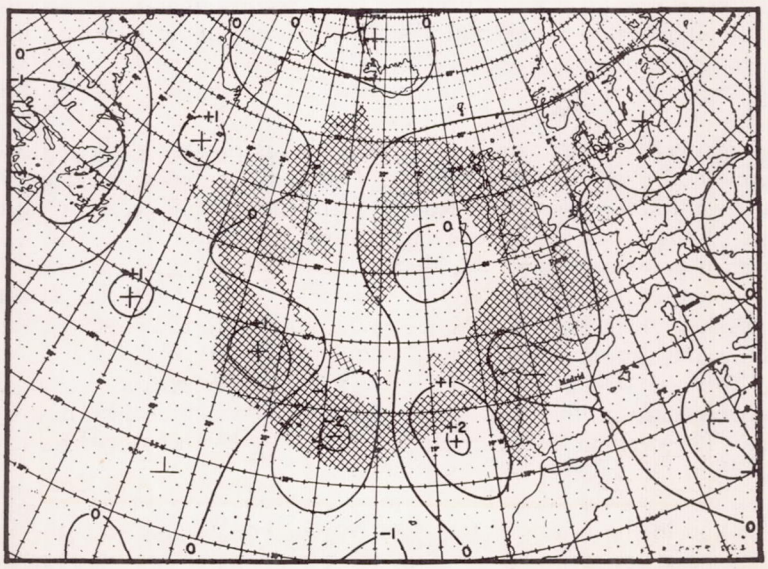

Figure 8. Vertical motion chart for 600 mb at 1200 GMT, 2 April 1960, computed by JNWP Unit. Units are cm sec^{-1}. + denotes upward motion; − denotes downward motion.

4. Comparison of Tiros cloud pictures with meteorological data

From the description of the pictures (Figs. 1-3) and of the meteorological situation (Figs. 4-8) it is easy to see the association between the two sets of data. First the clouds as observed from the surface (Fig. 4) agree, as they must, with the Tiros pictures; the small discrepancies which occur near the edges of the cloud picture patterns may be due to slight mislocations of the cloud elements in Fig. 2, or to the fact that the surface observer does actually see past the edge of the overcast. Although it would not be possible from the surface-cloud observations alone to delineate the details of the cloud field, the areas of overcast as observed from the surface appear in the uniform, stratiform cloud areas of pictures (Figs. 2 and 4). Moreover, the area in the centre of the cloud vortex, where the non-overcast cumuliform clouds appear in the pictures, is also the broken to scattered cloud area in the surface observations. Judging by the surface reports, the cumuliform area contained also some altocumulus and cirrus clouds. Some showers occurred in this region which were doubtless associated with the brighter cloud masses in Fig. 1. The relatively cloudless area which parallels the stratiform cloud and separates it from the cumuliform cloud, is more difficult to find in the surface reports. It should be noted that the array of clouds in Fig. 1 bears a marked similarity to the clouds in the Atlantic cyclone studied by Ludlam and Miller (1959).

Now looking at the gross features, it is quite apparent that the stratiform cloud which covers the European coast and then spirals into the arrowhead cloud of Figs. 1 and 2 is a manifestation of the warm moist ' tongue ' of air which circles the 500 mb vortex (Fig. 5) and appears as an ascending moist tongue in the 300°K isentropic chart (Fig. 6).

Furthermore, the broken cloud area in the middle of the cloud vortex coincides very well with the deep, cold, dry mass of air. Judging by the continuous cloud in the west side of the vortex, this cold mass of air has been cut off from its cold air source further to the west and is now completely encircled by warm moist air. The variation in brightness and size of the cumuliform elements in Fig. 1 (b) suggests that the clouds had greater vertical extent to the east of the arrowhead cloud than to the west of it. Thus the pictures suggest that the air was more stable in the northerly flow to the west of the arrowhead cloud, and more unstable in the southerly flow near the cyclone centre. Ludlam and Miller (1959) found similar distribution of the height of the cloud tops.

The stratiform cloud doubtless slopes downward from the arrowhead towards the north. This can be ascertained from the cross-section in Fig. 7. At ship station *J*, judging by the high relative humidities, the cloud top was about 23,000 ft high (near the 400 mb level). At ship station *I*, the relative humidities are much lower at that level suggesting a lower cloud level and the airplane reports support the cloud existence at 12,000 ft.

An area of relatively strong winds (about 60 kt) is present along the inner edge of the stratiform cloud near the 500 mb level. This is to be expected since the wind will increase with height in the region between the warm and cold air according to the thermal wind relation. Thus strong winds are bound to appear in this region.

Moreover, it is interesting to note that the cloud streets of Figs. 1 and 2 lie closely parallel to the contour lines of the 500 mb chart (Fig. 5); but since the ' streets ' join the central cloud mass which is near the lowest 500 mb height, the streets apparently cross the contours as they approach the centre. Since the wind direction was constant with height (Fig. 7) these streets serve as good wind-direction indicators and also suggest (Fig. 1) a convergence into the ' galaxy-like ' cloud mass, which is itself near the centre of low pressure. These cloud streets could not of course be discovered from the surface observations alone.

Finally, a word should be said about the vertical motion chart (Fig. 8). The slight downward motion in the centre of the cloud vortex would agree with the fact that the stratiform cloud did not appear there, although the bright broken cloud may have been associated with clouds existing or built up to high levels. It would also suggest that most of the central cumuliform cloud was below 600 mb (about 13,000 ft). This was perhaps

truer near the cloud streets near station *K* and in the dim clouds west of the arrowhead than in the central cloud mass itself.

In the stratiform cloud-area, the computed upward motion also agrees with the cloud's existence. However, the strong downward motions near 37°N, 25°W seem questionable; although one cannot prove that upward motion was occurring *at that instant*, the presence of the cloud casts doubt on the existence of strong downward motion in the area in the recent past. Had the motion actually been upward, where downward motion had been computed in the stratiform cloud region of Fig. 8, the initial conditions which were used in the numerical computation model would have been different; and the forecast resulting from the real conditions might have been different. Thus the cloud pictures may eventually serve as a valuable additional observation to aid in the determination of the actual state of the three-dimensional motion in the atmosphere, as well as of the moisture and temperature structure.

5. Conclusions

The stratiform clouds observed by Tiros in Fig. 1 were clearly associated with a warm, moist tongue of air which encircled the vortex in the Atlantic Ocean at 1200 GMT, 2 April 1960. In the centre of the vortex a cold, relatively dry mass resided, apparently cut off from its main cold-air source. This cold air was associated with the non-overcast, galaxy-like cloud area which was surrounded by the stratiform cloud. This region between the cold and warm air is also the region of maximum jet-like winds, and is therefore to be expected near the inner edge of the stratiform cloud. Finally, cloud streets, which cannot be seen from surface observations, serve to outline the wind flow, in the mature storm in which the wind direction does not change much with height.

Finally, a great deal of additional detail is evident in the photographs. The pattern in the form of a nearly closed circle over the European coast near North Germany (Figs. 1 (a) and 2) is an interesting example. Is this the counterpart of a meso-scale eddy in the atmosphere ? Was the shape of the arrowhead cloud in Fig. 1 (a) produced by meso-scale eddies ? Looking southward along the ' arrow,' in Figs. 1 (a) and 2, the appearance of the cloud suggests the possibility that a small cyclonic eddy existed on the eastern side near latitude 50°N, and an anticyclonic eddy on the western side of the arrowhead.

It will of course be interesting to examine other cloud patterns which appear like that of Fig. 1 to see if similar meteorological conditions are associated with them and to see if generalizations can be formulated.

Acknowledgment

This work has been supported by the National Aeronautics and Space Administration.

References

Bristor, C. L. and Ruzecki, M. A.	1960	' Tiros I photographs of the Midwest storm of April 1, 1960,' *Mon. Wea. Rev.*, **88**, p. 315.
Fritz, S.	1960	' Cyclone prints from satellite, Tiros I,' *Interavia*, **15**, p. 1,384.
Fritz, S. and Wexler, H.	1960	' Cloud pictures from satellite, Tiros I,' *Mon. Wea. Rev.*, **88**, p. 79.
Ludlam, F. H. and Miller, L. I.	1959	' Research on the properties of cloud systems.' Imperial College Sci. and Tech., London, *Tech. (Final) Rep.* No. AF-61 (514)-1,292.
Staff, Meteorological Satellite Laboratory, (U.S. Weather Bureau)	1961	' Some meteorological results from Tiros I,' in ' Report on Tiros I,' *Nat. Aeronaut. and Space Admin.* (to be published).
Sternberg, S. *et. al.*	1960	' Roundup of Tiros I,' *Astronautics*, **5**, p. 32.
Wexler, H. and Fritz, S.	1960	' Tiros reveals cloud formations,' *Science*, **131**, p. 1,708.
Winston, J. S.	1960	' Satellite pictures of a cut-off cyclone in the Eastern Pacific,' *Mon. Wea. Rev.*, **88**, p. 295.

axis, they are invisible against the lower stratus and fog. The lower troposphere streamlines are shown here because the clouds near the Andes at 48° to 50° S. were embedded in this layer. The "bridge" of tenuous clouds at 48.5° S., 69° W. appears to be cirrus streaming across the lower cloudless area. Conditions over the pictured area of South America were unfavorable for mountain waves to occur. The sounding at Puerto Montt shows no stability in the middle and upper troposphere [2]. Probably therefore, the small cloud rows at 50° S., 70° W., lying east of the Andes, *are not* wave-produced lenticular clouds.

Figure 2 shows both jet axes transferred from figure 10 and the 200-mb. wind report from Stanley. In the upper right, the cloud area (probably middle and high clouds) 48° to 46° S. appears to have a western edge near 72° W., that is, to the cyclonic shear side of the northern jet. The cloud bands in the pattern (e.g., at 64° W.) are transverse to the wind directions at jet levels. The transverse pattern seems continuous with the bright band across the picture center which in turn lies on the equatorward side of the high-latitude (southern) jet axis. A cloud band extending from 50° S., 56° W. to 46° S., 54° W. was along the jet axis. Because of the possible error in fitting these grids to the pictures, the position of the jet axis shown here relative to this cloud band may be somewhat in error. However, this feature has the same location on an adjacent picture (not shown) and is estimated to be correctly placed within 60 to 100 miles. In any event, the main band and the finer-scale streamers are very near the jet axis, parallel to it, and probably on the equatorial side, as shown. The dark area just to the east is almost cloudless. This is associated, in the low troposphere, with a high pressure ridge containing few clouds, while at high levels there may be descent associated with the jet.

The clear area centered at 53° S., 66° W. is in the lee of the South American continent and may reflect downward motion on the lee side of the continent.

Figures 3, showing the jet axis nearer the horizon, displays more of the cloud pattern on the cyclonic shear side of the high-latitude jet. The difficulties in obtaining exact consistency between locations of the same cloud features on two different pictures are evident here when small features are compared with figure 2. Nevertheless the band of clouds and the clear areas associated with the jet axis are probably located with an accuracy of 60–100 miles and more of the general pattern near the jet can be seen. The cumuliform clouds near 47° S., 43° W. mark the transition from the high pressure ridge to the cyclone, in the low troposphere—features that are discussed below in connection with the surface analysis.

Figures 4, 5, and 6 show clouds, associated with the cyclone, which no doubt are both low and middle clouds as well as cirrus. These pictures will be used to modify the surface analysis of figure 12.

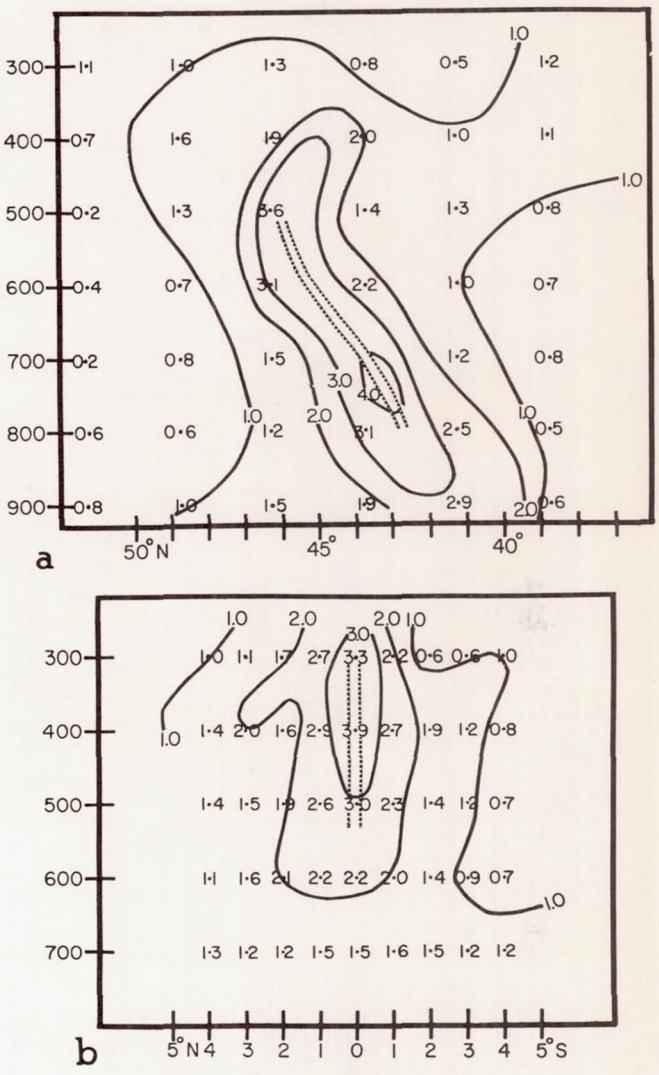

FIGURE 8.—Potential temperature gradients (°C. per 60 n. mi.) for Northern Hemisphere. Doubled broken line shows position of maximum gradient. (a) For 12 winter cases, (b) for 4 autumn cases; abscissa labeled in degrees of latitude north and south of jet axis.

5. MODIFICATION OF SURFACE ANALYSIS WITH PICTURE DATA

Comparison of the nephanalysis, figure 7, with the surface analysis, figure 12, shows that the low pressure area at 41° W. corresponds to the area covered with scattered to a few cumuliform clouds. While the Argentine analysis does not extend to 17° W., it does not seem reasonable that cyclones existed at both 41° W. and 17° W., with one showing the classical cyclonic spiral pattern and the other largely cloud-free. The surface cyclone was undoubtedly placed as shown in figure 12 on the basis of

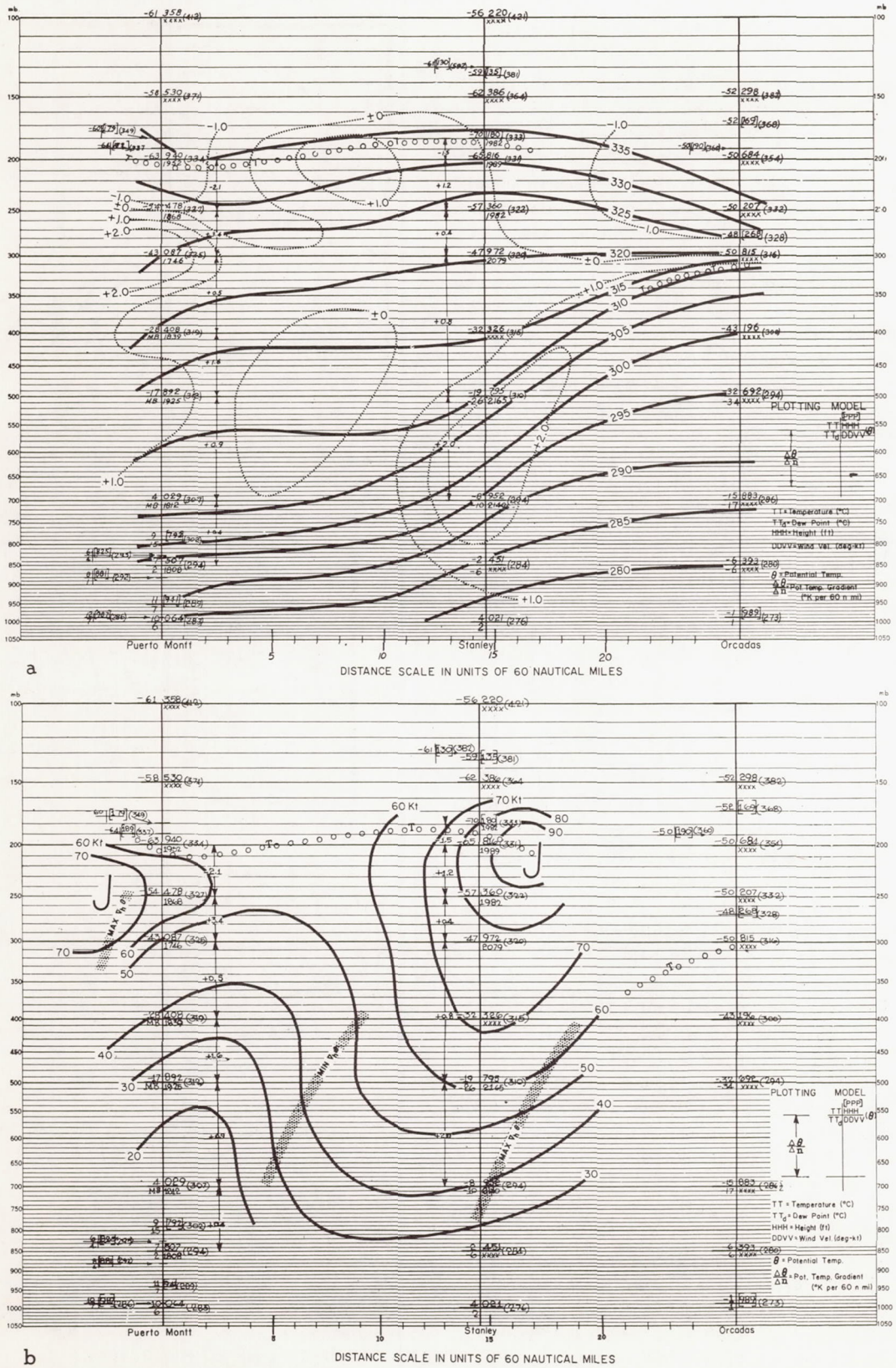

FIGURE 9.—Space cross sections for 1200 GMT, April 28, 1960; (a) showing isentropes (solid lines) and isopleths of $\Delta\theta/\Delta n$ (°C. per 60 n. mi., broken lines), and (b) showing axes of minimum and maximum temperature gradient (stippled lines) and isotachs (solid lines). Large "J" indicates best estimate of jet core location.

FIGURE 10.—300-mb. chart for 1200 GMT, April 28, 1960.

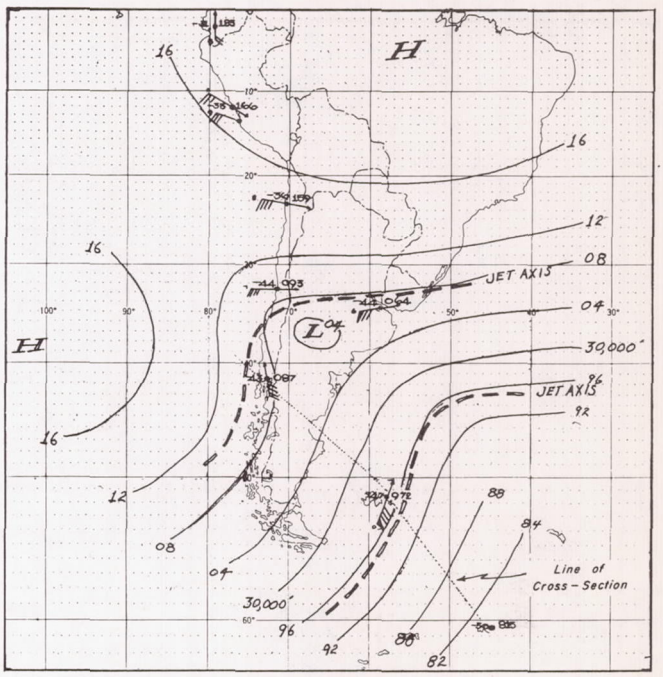

FIGURE 11.—Soundings for the three stations used in cross section (fig. 9). 1200 GMT, April 28, 1960.

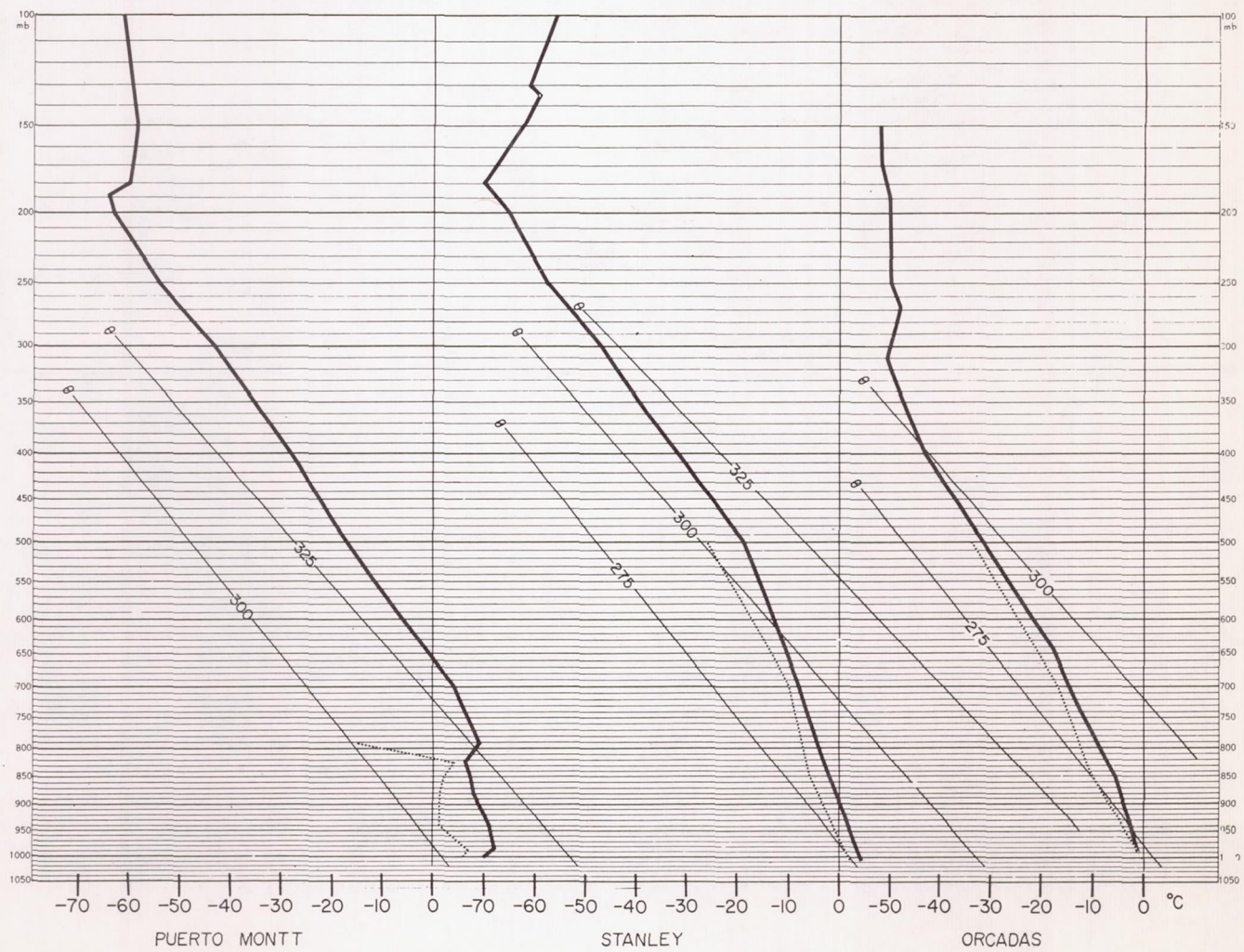

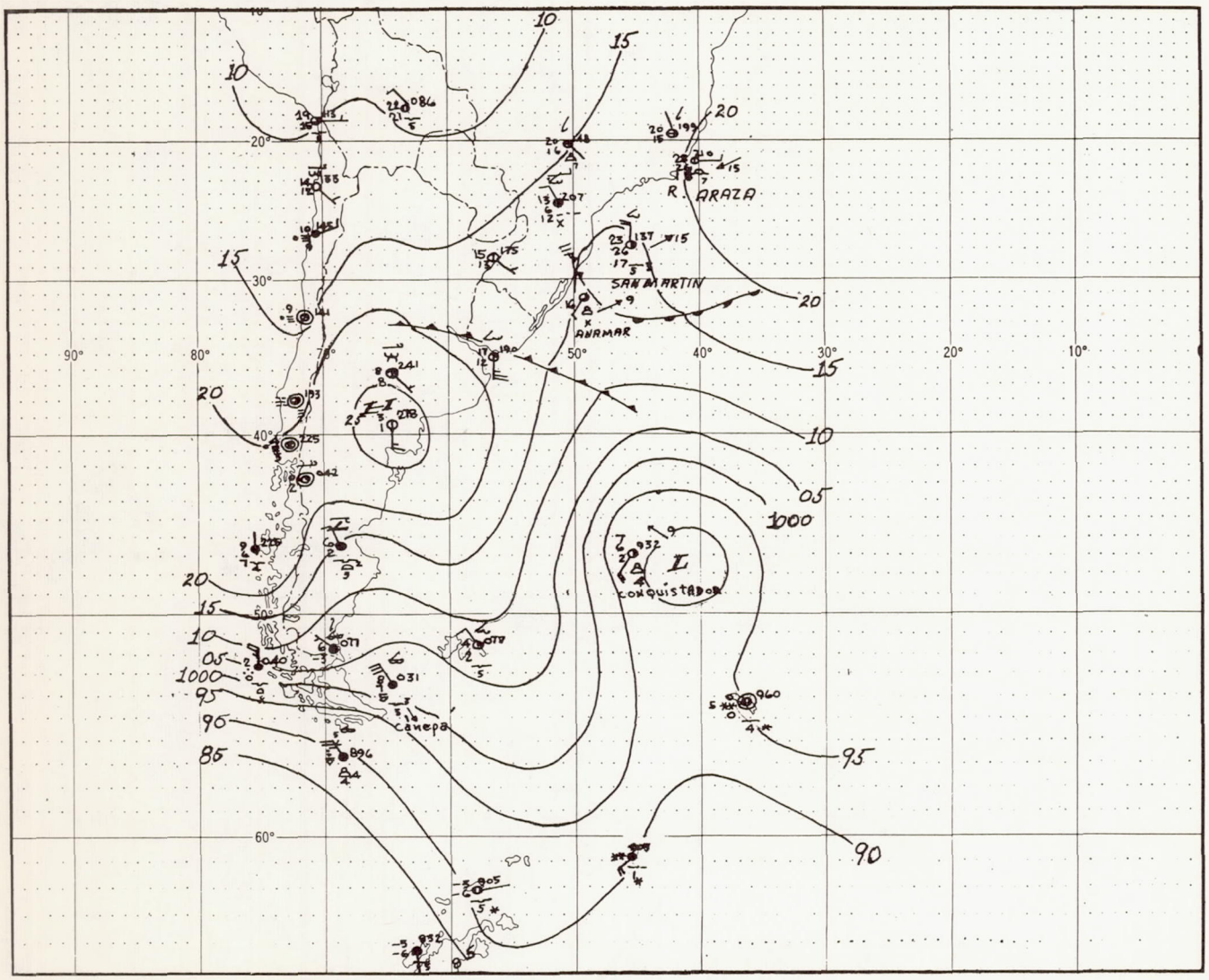

FIGURE 12.—Copy of surface data and analysis made by Argentina Meteorological Service. 1200 GMT, April 28, 1960.

the single ship report at 47° S., 45° W. In the absence of any other data the position of the Low seems entirely reasonable, but with the addition of picture data, the ship pressure appears questionable. Once doubt is thrown on the report, the analyst must decide whether the cloud type and wind speed are consistent with a deep Low so nearby. It appeared to this writer, in light of the picture data, that the ship pressure, and perhaps even the wind observation, or else the ship position, were in error. The picture data were therefore used as a basis to reanalyze the oceanic portion of the surface chart. The modified analysis is shown in figure 13.

First, the ridge line that lies on the east coast at 60° W. was extended into the zone of scattered cumuliform clouds at 50° S., 45° W. Second, an occluded cyclone (fig. 6) was located at 45° S., 17° W. That this cyclone was in the mature stage is inferred from the fact that the dry (cold) air had apparently circulated completely around the north (equatorial) side of the center and was producing a

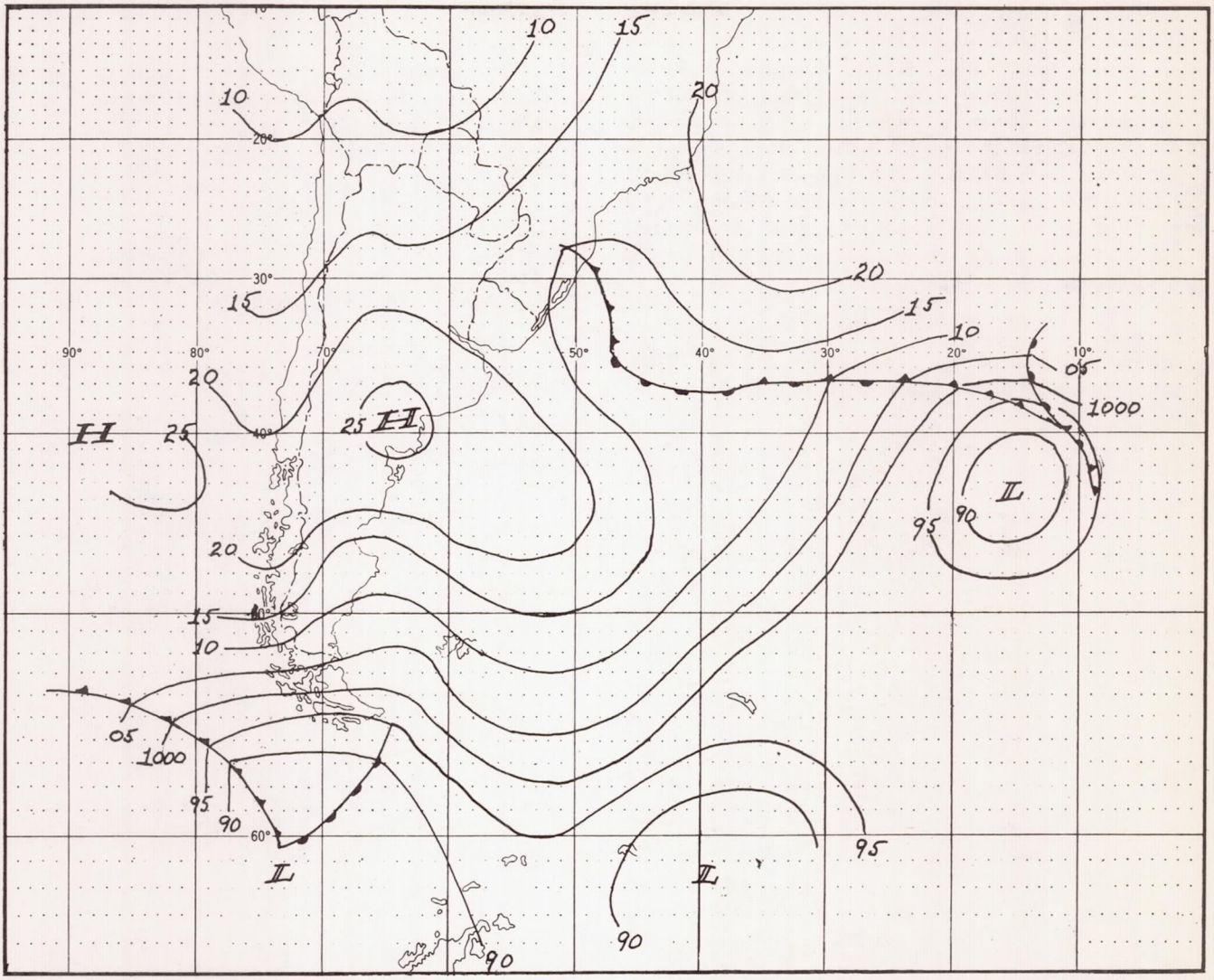

FIGURE 13.—Modification of figure 12 by use of TIROS pictures.

scattered to cloudless projection toward the center from the northeast.

Third, fog and stratus down to 52° S. along the west coast of South America indicate no front or cyclone in that immediate vicinity, but the sharp line marking the edge of the stable air implies it is a line between air masses of significantly different trajectory, and for that reason the pressure pattern southwest of South America is suggested. This portion of the analysis is of course completely outside any meteorological or picture data available at this writing and is thus little more than speculation. The cyclone in the Atlantic is, however, located with a high degree of confidence as is the ridge line extending southeastward from the continent.

6. CONCLUSIONS

This case study illustrates:

(1) The cloud patterns associated with cyclones and fronts are of a sufficient scale and simplicity to enable meteorologists to extract much valuable diagnostic data from satellite pictures.

(2) Cloud patterns associated with jet streams (and perhaps many other synoptic models of the upper atmosphere) are so varied and complex, that much more research must be completed before the meteorologist can exploit satellite pictures by themselves for location of the jet stream. This is true partly because the fine detail of patterns near the jet that have been documented by surface and airplane photographs are largely invisible on the currently available satellite pictures. The investigation of jet cloud patterns for satellite use must concentrate on the larger-scale distribution.

ACKNOWLEDGMENT

The computation of the locator grids for the TIROS pictures illustrates one of the essential support functions of the Computation Section of the Meteorological Satellite Laboratory.

The work on this study has been supported by the National Aeronautics and Space Administration.

REFERENCES

1. E. Palmén, and C. W. Newton, "A Study of the Mean Wind and Temperature Distribution in the Vicinity of the Polar Front in Winter," *Journal of Meteorology*, vol. 5, No. 5, Oct. 1948, pp. 220–226.
2. M. A. Alaka, "Aviation Aspects of Mountain Waves," World Meteorological Organization, *Technical Note No. 18*, WMO-No. 68, TP. 26, 1958, 48 pp.

USCOMM-WB-DC

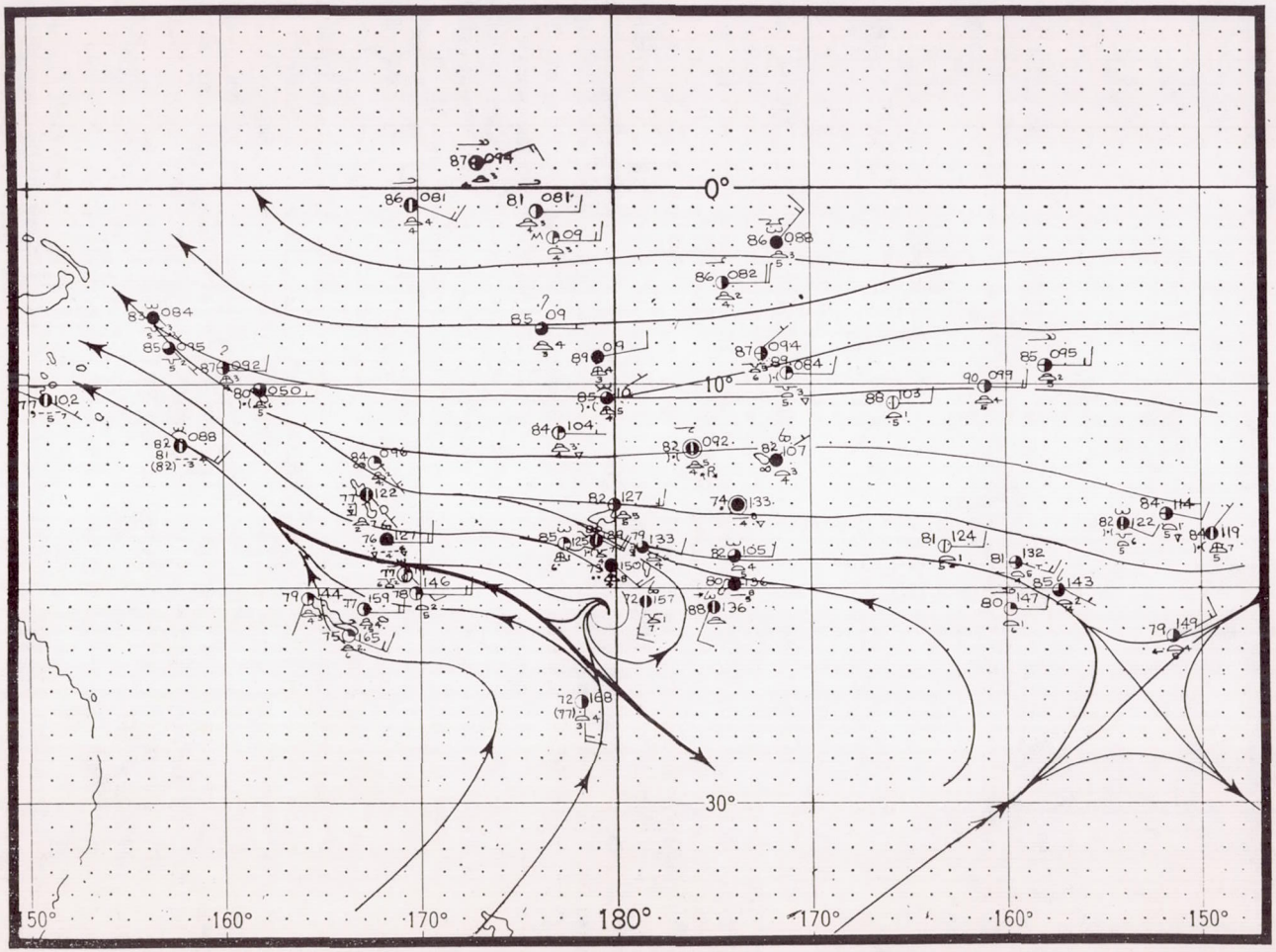

Fig. 11*b*. Surface streamline analysis for 0000 GMT, May 12, 1960.

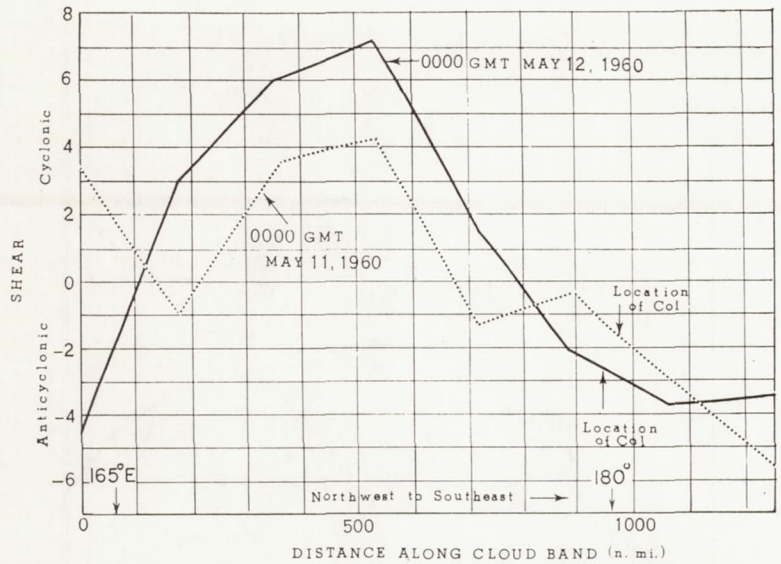

Fig. 12. Computed shear across major cloud band in units of knots per 180 nautical miles; positions of col shown for beginning and end of May 11, 1960.

(16°S, 152°W) all show typical trade wind flow with easterlies throughout the low and middle troposphere. Of this group only Guadalcanal has a radiosonde and this shows a typical trade wind layer overlain with deep easterlies, and a moist layer from the surface to about 12,000 ft. The great distance between stations leaves ample room for undetected perturbations and the winds are cited only to point out that the nonperturbed surface flow in the vicinity of those stations is confirmed by the upper air observations.

Two wind reports that were taken on opposite sides of the major cloud band are interesting because they detect flow directed toward the cloud band from opposite sides, in the layer between the surface and about 7000 ft. The pibal taken at 15°S, 167°E indicates light winds, northeast, just north of the band, and at 22°S, 166°E the winds are all south of east. Again the latitudinal span of 7 degrees between these observations may contain a complicated circulation pattern; one can only point out that the data do not conflict with the convergence asymptote shown on the surface analysis.

The only other upper-air data available in the area of interest are radiosonde and wind observations at Nandi (17.6°S and 177.6°E). It has already been mentioned that the layer from 2000 to 7000 ft contained east winds, but the winds changed to westerlies at greater height; at about 10,000 ft at the beginning of this 24-hr period, at 8,000 ft at 1200 GMT, and at 3,000 ft during the last 6 hours of the 11th. Because a trough line extending from higher latitudes moved over Nandi during this interval, and because the westerlies increased with height, it is quite certain that these were midlatitude westerlies overlying the very shallow easterlies at the surface. No doubt clouds were associated with this polar trough but no good pictures were obtained of the high latitude portion of the trough.

Tiros Pictures as Complementary Meteorological Data

The pictures presented here show features not discussed up to this point that illustrate the potential of satellite data in synoptic analysis. An intermittent zone of increased cloudiness is visible on Figures 2, 4, 6 and 8 from 10°S to 12°S indicating a line of weak convergence roughly parallel to the major subtropical band to the south, a feature only vaguely indicated by the surface data. The tropical analyst would note this weak convergence at this map time and forecast no extreme weather for the pictured area in the near future.

When any one wind report shows a significant deflection from east in the trade wind region, the tropical analyst must scrutinize all evidence in an attempt to explain it. This evidence consists of the past record, indicating whether the cause might be a sea breeze or other local effect, the reputation of that particular station for reliability, and the previous weather analysis of the upstream area to see if a wave may have been developing unnoticed. In cases like this even the negative information of pictures showing no well-developed waves is useful because the 'detective work' is enormously eased. An example of this occurred during the analysis of the map series necessary to produce Figures 11*a* and 11*b*. On 0000 GMT, May 10, the surface wind at Christmas Island (2°N, 158°W) was south; 20 kt and 24 hours later it had returned to southeast. Because the map series was being analyzed independently of the pictures, considerable time was spent in attempting to account for this wind shift by a strong disturbance extending both north and south of the equator, extrapolating its motion downstream to see if appropriate wind changes at other stations verified a traveling disturbance. Finally, with no other changes occurring downstream, it was concluded that no significant disturbance had moved into the pictured area, and Figures 11*a* and 11*b* show uniform easterlies in the tropical area east of 170°W. Turning then to the pictures, a brief inspection verified the absence of an intense wave (see Figs. 2 and 8). Use of the pictures during the analysis would have eased the analyst's chore and lent confidence to the final result.

Because the camera was viewing well above the horizon while the satellite was south of 30°S, pictures of the higher latitudes are less satisfactory than pictures of the tropics. Nevertheless some excellent pictures of the patterns within the subtropical anticyclone were obtained. The area near the horizon in the westernmost strip composite of Figure 1*a* and the individual frame in Figure 5 show a curved pattern of clouds curving from left to right toward Australia on the horizon. This pattern delineates the northern limb of an anticyclone that was shown on the Australian encoded analysis. According to that source, a high was centered at 30°S, 158°E, at 0500 GMT, May 11, 1960.

These pictures of clouds in the anticyclone are of interest because a large number of vortex patterns so prominent in the Tiros data are associated with cyclones where the low-level convergence produces copious cloudiness that arranges itself in the characteristic spiral patterns. Here, however, is anticyclonic circulation that is undoubtedly producing surface divergence and subsidence, yet there are sufficient clouds (probably no more than a few tenths) to show this curved pattern. Purely from meteorological reasoning one can be moderately confident that the cloudiness is suppressed cumulus limited by an inversion or by a dry stable layer.

Summary

This study has shown that a dense network of surface observations (by tropical standards) provided only a tentative indication of lines of convergence in the low troposphere. Based only on surface cloud data the presence of disturbed weather near the major convergence line was suggested, but it was not possible to delineate a continuous band of clouds and thereby a continuous convergence line. Furthermore, efforts to detect a line of vorticity failed to show a significant magnitude of cyclonic shear along the convergence line. One might therefore conclude that the evolution of the system producing the major cloud band had passed through the frontal stage and even the shear line characteristic was dissipating. In any event, an excellent surface data network in the tropics is not adequate to describe the quasi-stationary type of system studied here because the effect on the field of horizontal motion is so small that it is virtually undetectable when the systems are quasi-stationary. The standard data must be complemented by more complete cloud observations such as those provided by satellite observations. The pictures provided by the four passes showed nearly 2000 miles of a vigorous band of middle and low clouds that apparently maintained its position over the main convergence asymptote at the surface, a very good pictorial evidence of a persistent line of convergence.

Acknowledgements. This work has been carried out in the Meteorological Satellite Laboratory of the U. S. Weather Bureau and was made possible only by the use of the Computation Section and other supporting facilities in that laboratory. The

work is supported by the National Aeronautics and Space Administration.

References

Bandeen, W. R., and W. P. Manger, Angular motion of the spin axis of the Tiros I meteorological satellite due to magnetic and gravitational torques, *J. Geophys. Research, 65*, 2992–2995, 1960.

Jordan, C. L., Comparison between observed and geostrophic winds. *Quart. J., Roy. Meteorol. Soc., 79*, 153–156, 1953.

Palmer, C. E., Tropical meteorology, *Quart. J., Roy. Meteorol. Soc., 78*, 126–163, 1952.

Palmer, C. E., C. W. Wise, L. J. Stempson, and G. H. Duncan, The practical aspects of tropical meteorology, *Air Force Surveys in Geophysics*, no. 76, 195 pp., 1955.

Ramage, C. S., Notes on the meteorology of the tropical Pacific and Southeast Asia, *report to Geophysics Research Directorate*, Contract No. AF 19(604)-1942, University of Hawaii, 174 pp., 1959.

Riehl, H., *Tropical Meteorology*, McGraw-Hill Book Co., New York, 392 pp., 1954.

(Manuscript received December 12, 1960.)

A WESTERN ATLANTIC VORTEX SEEN BY TIROS I

J. B. JONES, MAJOR, USAF

Air Weather Service Member, Meteorological Satellite Laboratory, U.S. Weather Bureau, Washington, D.C.

[Manuscript received April 14, 1961; revised June 29, 1961]

ABSTRACT

TIROS I observed an extratropical cyclone near Bermuda on three occasions in early May 1960 during the last 86 hours of the life cycle of the storm. A study of this case was undertaken with three objectives in mind: (a) to describe interesting features of the organization manifested in the cloud patterns and compare these with conventional analyses; (b) to present a subjective interpretation of some of the cloud images and discuss the criteria which form the basis for interpretation; and (c) to show examples of practical application of these pictures of the storm to routine frontal analysis and nephanalysis.

1. INTRODUCTION

During early May 1960, TIROS I took pictures of a small extratropical vortex located in the western Atlantic between Bermuda and the southeastern United States. Pictures were obtained during the mid-afternoon on May 5, 7, and 8. On May 6 the orbital passes over the region were too far east or west of the vortex for the satellite to view the associated cloud patterns. Included in this paper are a brief synoptic history of the storm, a description and subjective interpretation of the cloud images, a brief discussion of the apparent relation between the cloud patterns and conventional analyses, and finally a demonstration of the practical utility of the cloud pictures obtained by a satellite.

In recent months, storms observed by TIROS I over the eastern Pacific Ocean, the central United States, and the northeastern Atlantic Ocean have been studied [1, 7, 12, 15]. Some of these studies deal essentially with a single observation of the storm [1, 12]. In other cases successive views of the same system have permitted a study of persistent and transient features of the associated cloud patterns over time intervals varying from 100 minutes to approximately 24 hours [7, 15]. For the case presented in this paper, a fortuitous set of circumstances provided pictures of the same storm at 48- and 24-hour intervals over a 4-day period, recording on film the degeneration of a vigorous cyclone.

2. SYNOPTIC HISTORY

Indications of a wave formation on the polar front in the Atlantic immediately east of Florida appeared on the NAWAC surface analysis for 0000 GMT, May 3, 1960 (fig. 1a). During the next 72 hours, the wave continued to develop and apparently reached maximum intensity at about 0000 GMT, May 6 (figs. 1b-d). Subsequently the low center retrograded (figs. 1e-f), the associated frontal system became diffuse and ill defined, and finally during the period 0000 GMT to 1200 GMT May 9, the vortex filled and disappeared (figs. 1g-h).

3. THE PICTURES

ORGANIZATION

The storm was first viewed by TIROS on May 5 near 2200 GMT as it was reaching maximum intensity (fig. 2a). Photographs obtained near 2200 GMT, May 7 and 2100 GMT, May 8 show the cloud distribution in and near the vortex as the storm center weakened (figs. 3a, 4a). Satellite subpoints and principal points in the area viewed in these pictures are shown in figure 1, maps d, f and g, respectively.

Perhaps the most striking feature of the photographs is the degree of organization manifested by the spiral bands of clouds. These bands, which converge toward the "cloud crest" at A, give the viewer an immediate impression of a cyclonic circulation. Comparing figures 2a and 4a, it is apparent that in that length of time the number of bands associated with the storm decreased and the "crest" at A became more broken—a likely sequence of events considering the synoptic history of the vortex (fig. 1). However, it is interesting to note that even as the Low filled, the general pattern, or "cyclone print" [6], of the storm persisted throughout the period of decay. The persistence of the pattern between figures 3a and 4a, a time span of 23 hours, is quite remarkable.

The spiral bands associated with the vortex display a considerable dimensional variation—apparently unrelated to the vigor of the storm center. For example, the band DD′, figure 2a, measures about 600 n.mi. in length and varies in width from 15 to 30 n.mi. Close inspection of this band on the original positive transparency shows the main band to be composed of a number of smaller bands or streets. These component streets appear to vary in

605661—61——2

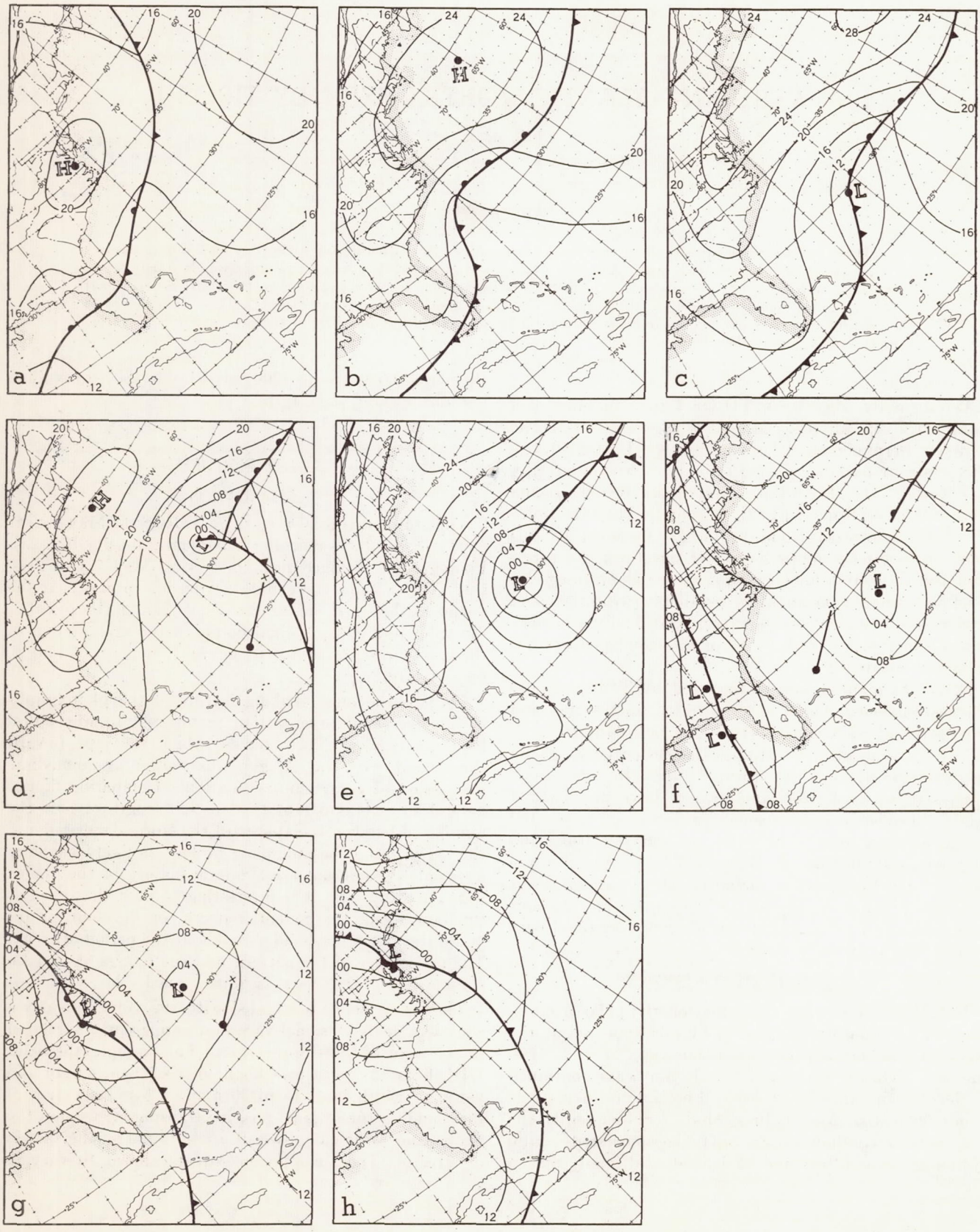
a
b
c
d
e
f
g
h

Särtryck ur Tellus nr 1, 1961

Cellular Cloud Patterns revealed by Tiros I[1]

By ARTHUR F. KRUEGER and SIGMUND FRITZ, U.S. Weather Bureau

(Manuscript received November 11, 1960)

Abstract

In this report some satellite (TIROS I) photographs of cellular cloud patterns are related to conventional meteorological observations. These cellular patterns occurred at the top of convective layers which were heated from below; and through which there was little vertical variation in wind velocity.

1. Introduction

On April 1, 1960 the National Aeronautics and Space Administration placed a meteorological satellite, called TIROS I, into orbit around the Earth. The primary function of this satellite was to photograph the Earth's cloud cover between about 55° N latitude and 55° S latitude; and for this purpose it utilized two cameras, one a wide angle camera capable of viewing a swath 800 miles wide, and another, a narrow angle camera, capable of examining in considerable detail a smaller area located within the larger area. The experiment proved to be remarkably successful, and during its two and one-half-month lifetime TIROS I photographed many interesting cloud features, some of which have already been described (FRITZ and WEXLER, 1960; WEXLER and FRITZ, 1960; STAFF MEMBERS, 1961). For a description of the satellite and its components the reader is referred to a series of articles published in the June 1960 issue of Astronautics (STERNBERG ET AL, 1960).

One of the cloud features revealed by TIROS I was a cellular pattern having horizontal diameters as large as 30 to 50 mi and consisting of clear centers bounded by ring- or U-shaped cloud elements about 10 to 15 mi wide. Such features are too broad to be recognized by a single observer at the Earth's surface, and yet small enough to remain undetected by even the best distribution of standard synoptic reports.

Three examples of such a cellular pattern are shown in fig. 1. The first picture (fig. 1a) was taken while the satellite was over the Atlantic Ocean, 650 naut mi northeast of Bermuda at 1612 GMT, April 4, 1960; the second (fig. 1b) was taken over the central Pacific, looking north westward towards the Aleutians at 2341 GMT, April 1, 1960; and the third (fig. 1c) was taken from a point 750 naut mi northeast of Hawaii at 2250 GMT, April 4, 1960.

The primary aim of this report is to relate this cloud pattern to the available meteorological observations. Emphasis is mainly on the Atlantic case (fig. 1a) since more extensive observations were available for this case than for the other two. These observations consist of the standard surface reports, radiosondes, pilot balloon observations, and aircraft reports including several dropsondes. Later, the problem of cellular convection, as treated by laboratory and theoretical studies, will be discussed briefly in relation to these TIROS observations.

[1] This work has been supported by the National Aeronautics and Space Administration.

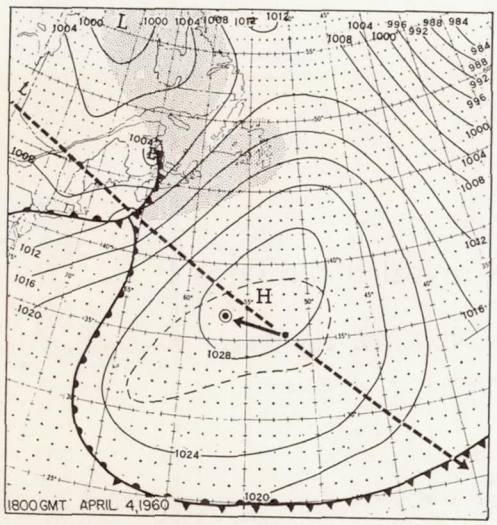

Fig. 3. Surface weather map for 1800 GMT, April 4, 1960. Track of TIROS I, subsatellite point (dot), and picture center (circled dot) are indicated. The area occupied by cellular cloud pattern in fig. 1a is outlined by dashed line.

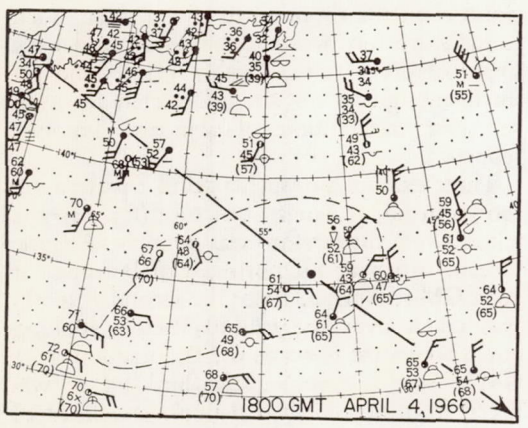

Fig. 4. Surface synoptic reports for 1800 GMT, April 4, 1960. Plotting model is abbreviated. Figures in parentheses are ocean surface temperatures. Track of satellite again indicated; and area occupied by cellular cloud patterns of fig. 1a is outlined.

2. Synoptic Analyses

The Atlantic Case.

To establish location and scale, a latitude-longitude grid[2] has been superimposed on

[2] The method for calculating these grids is described in another report (STAFF MEMBERS, 1961) and will not be discussed here.

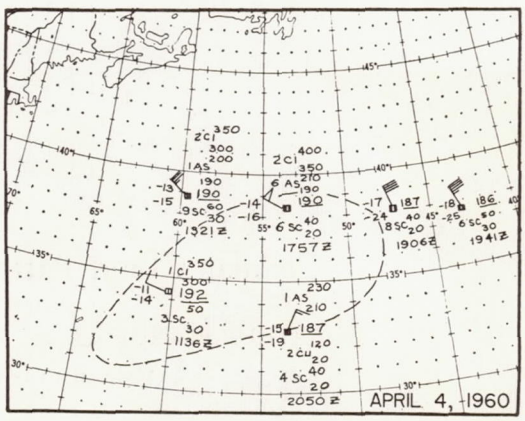

Fig. 5. Aircraft reports for period 1200 GMT-2300 GMT, April 4, 1960.

fig. 1a. This is shown in fig. 2, where it is readily apparent that the cellular cloud pattern in the foreground occupies a large area, extending in the picture about 650 naut mi in a west-east direction and 300 naut mi in a north-south direction. These cells have diameters ranging from 20 naut mi near the picture center to about 40 or 50 naut mi in the lower right portion of the figure.

The surface weather map corresponding most closely in time with this photograph is for 1800 GMT, April 4, 1960 (fig. 3). It shows an intense anticyclone with a maximum pressure of 1029 mb dominating the picture area. Northwest of this high pressure center, extensive middle and low cloudiness were reported with rain occurring near Nova Scotia and Newfoundland (fig. 4). This cloudiness, having the appearance of a stratiform type, is apparent toward the northwestern (upper left) portion of fig. 2. However, in the cellular cloud region of fig. 2 only low clouds, chiefly stratocumulus and cumulus, were reported (fig. 4). These observations were verified by a few aircraft in the vicinity which estimated these clouds to have bases around 2000—3000 ft. and tops ranging from 4000 ft. in the northern to 12,000 ft. in the southern part of the picture area (fig. 5).

The buoyancy of these cumuliform clouds arises in part from heating of the air mass at the ocean surface. Ships in this region, for example, reported ocean temperatures averaging about 3° C warmer than the air just above, with the smallest differences on the western

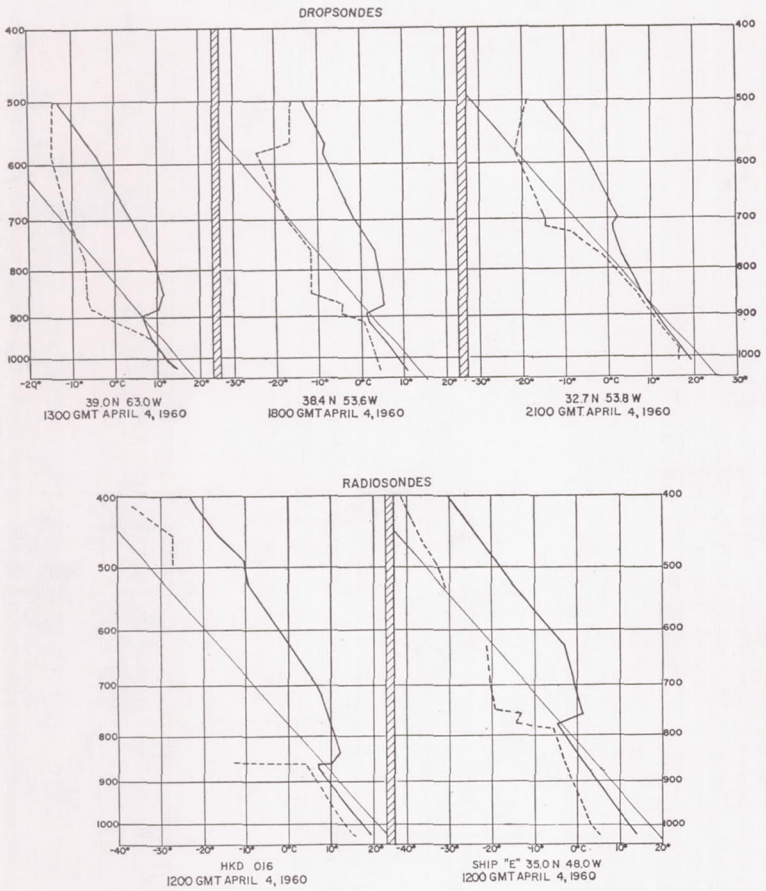

Fig. 6. Aircraft dropsonde observations at locations indicated and radiosonde observations at Bermuda and ship E between 1200 GMT and 2100 GMT, April 4, 1960. Solid lines show temperature distributions; dashed lines, dew point distributions.

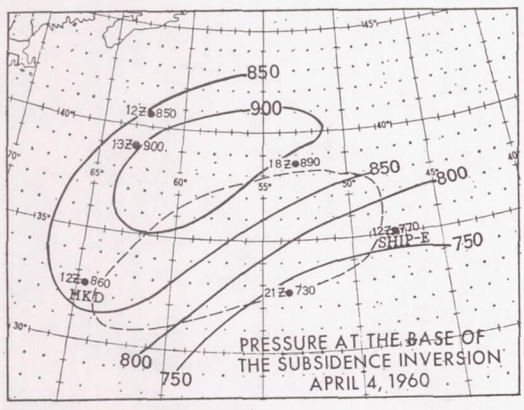

Fig. 7. Topography of the base of the subsidence inversion from data primarily in fig. 6. Analysis is for intervall of 50 mb.

side of the high pressure center and the greatest on the east where the surface wind had a northerly component (fig. 4). Radiational cooling at the cloud tops should also contribute to the destabilization of this air mass.

Radiosonde observations for Bermuda and ship "E" (35° N, 48° W) for 1200 GMT, as well as dropsondes from reconnaissance aircraft are illustrated in fig. 6, while the position of the soundings are shown in fig. 7. The sounding closest in time (1800 GMT) was a dropsonde at 38.4° N, 53.6° W taken near the edge of an altostratus deck (see figs. 2 and 4). This sounding showed a marked subsidence inversion at 900 mb (about 3000 ft.) capping a moist lower layer in which the temperature lapse-rate was close to dry adiabatic. Any con-

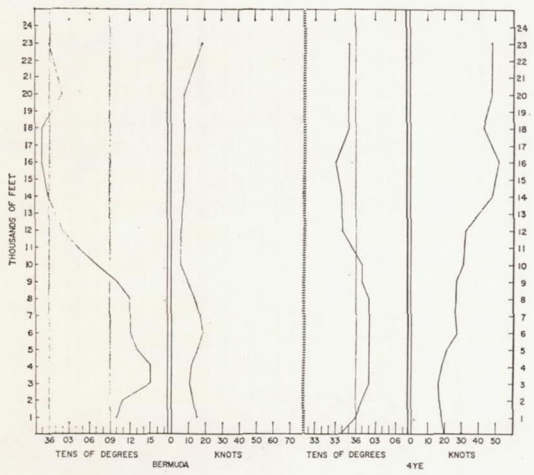

Fig. 8. Upper-wind soundings for Bermuda (1200 GMT) and ship E (1800 GMT), April 4, 1960.

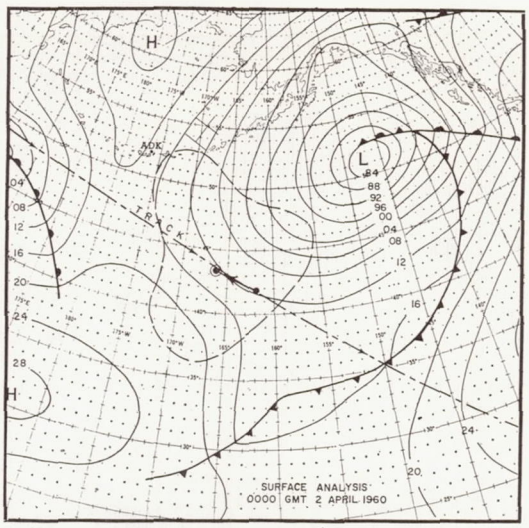

Fig. 9. Sea-level isobars and fronts, 0000 GMT, April 2, 1960. Track of TIROS I, sub-satellite point (dot), and picture center (circled dot) are indicated. The area occupied by cellular cloud pattern is outlined by dashed line.

vective clouds below this inversion presumably would be shallow since the condensation level was only 20 mb below the inversion. The presence of a higher cloud deck was indicated by increasing moisture with height above 600 mb.

A similar low-level structure, but with considerable variation in the height of the inversion and also convective cloud thickness, was indicated by the other soundings. The highest inversion (730 mb or about 9000 ft.) occurred in the southern part of the picture region (32.7° N, 53.8° W) with the thickest clouds also indicated (bases about 2000 ft, tops about 12,000 ft.). This seems to be connected with larger cloud elements and also larger clear spaces in the lower right portion of fig. 2.

The systematic spatial variation in depth of the moist lower layer is seen in fig. 7 which is an analysis of the topography of the subsidence inversion based on the few soundings available taken during the period 1200—2100 GMT. The average depth of this layer was about 850 mb, or approximately 5000 ft. Thus, if the cellular pattern is considered to include the entire convective layer rather than just the visible cloud, the horizontal scale is about thirty times the vertical scale.

Upper-wind soundings (fig. 8) were available only for Bermuda (1200 GMT) at the western extremity and ship "E" (1800 GMT) at the eastern end of the region. These showed a

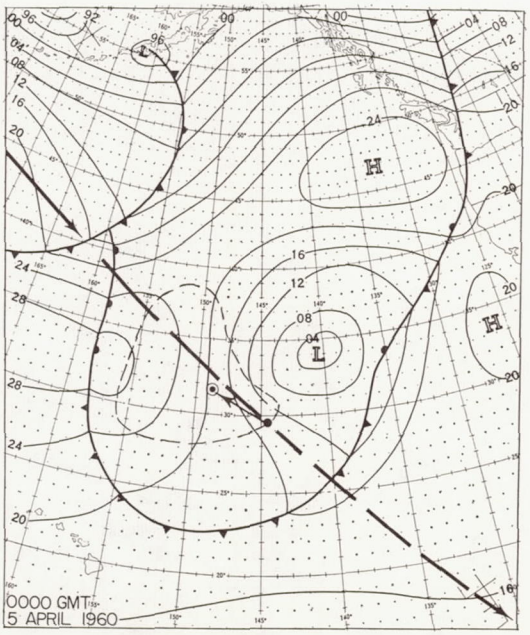

Fig. 10. Sea-level isobars and fronts, 0000 GMT, April 5, 1960. Track of TIROS I, sub-satellite point (dot), and picture center (circled dot) are indicated. The area occupied by cellular cloud pattern is outlined by dashed line.

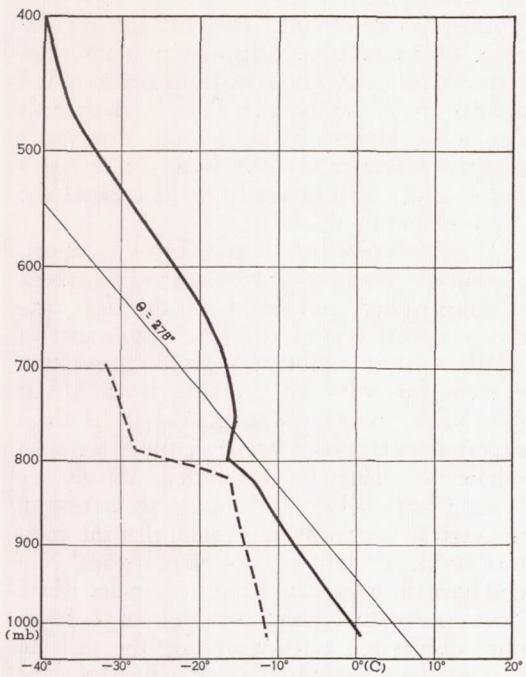

Fig. 11. Radiosonde observation for Adak, Alaska, 0000 GMT, April 2, 1960.

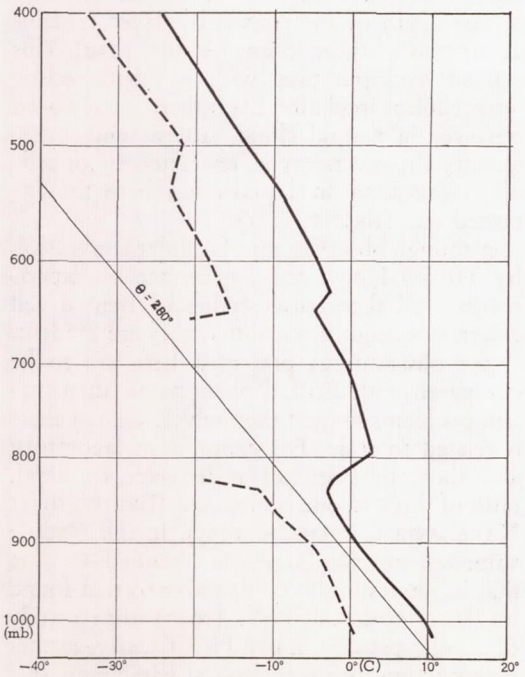

Fig. 12. Radiosonde observation for ship NHXN (34.9° N, 150.4° W), 0000 GMT, April 5, 1960.

veering of the wind up to 3000 ft. with a small decrease in wind speed. Above 3000 ft. the wind speeds increased about 10 kt to 6000 ft, while the wind direction remained uniform up to the base of the inversion (4000 ft. at Bermuda, 7000—8000 ft. at "E"). Above the inversion the winds backed to a northerly direction indicating cold air advection.

The Pacific Cases.

The surface map corresponding with fig. 1b is shown in fig. 9, and that for fig. 1c in fig. 10, again with the track of the satellite indicated and the area occupied by a cellular cloud pattern outlined. The synoptic conditions accompanying fig. 1b will be discussed first.

As may be seen in fig. 9, the surface flow in the region outlined varied from anticyclonic to cyclonic, in contrast to the anticyclonic flow accompanying fig. 1a. But surface reports in the area, except for the Aleutians, were almost non-existent. The available reports did, however, indicate considerable amounts of stratocumulus clouds. Such a northerly current from the Bering Sea, as was observed over the area, would also be expected to undergo considerable heating at the ocean surface. The only radiosonde observation available was from Adak, 730 mi to the northwest of the picture center, and was quite similar to those for the Atlantic case. Here the subsidence inversion was at 800 mb (fig. 11). Whether this sounding was representative of conditions in the central part of fig. 1b may be questioned, for it is generally expected that cyclonic flow is more unstable throughout a deeper layer than anticyclonic flow (PETTERSSEN, ET AL, 1946). That this may not be the case here is suggested by the JNWP vertical motion computations (not shown). That chart, applicable at 600 mb, showed subsiding motion over the picture area; thus an inversion should have formed at the base of this subsiding layer with the cellular pattern confined to the convective layer at some level below 600 mb. Some indication of greater vertical development, however, is suggested in the immediate foreground of fig. 1b, where a blurred appearance may have represented either anvil cirrus or patches of altostratus clouds.

The second Pacific case (fig. 1c) shows the smallest cellular pattern of the three cases. These are located in northerly flow with the

isobar curvature again varying from anticyclonic to cyclonic across the area and occur to the rear of the cutoff low discussed by WINSTON (1960, see also STAFF MSL). In this area stratocumulus clouds were reported, and surface heating was indicated from the sea-air temperature difference. One radiosonde observation available in the area was quite typical of the others cited earlier (fig. 12). Another significant difference of this case from the Atlantic case was in the surface wind velocities. Here they ranged up to 30—35 kt compared with 12—20 kt for the Atlantic case. Pilot balloon observations were not available except from a ship about 300 naut mi to the south and this indicated little variation in direction or speed up to 5000 ft.

Summary

A study of the synoptic observations accompanying the three satellite pictures of cellular cloud formations described in this report indicated that: (1) a layer of moist air about 5000 ft. deep was heated at the ocean surface resulting in an adiabatic lapse-rate, (2) superimposed over this layer was another of greater stability which served to inhibit the convection and (3) throughout the convective layer there appeared to be little variation in wind speed and direction above that portion influenced by surface friction.

These distinctive cloud patterns, especially those in fig. 1a, have the appearance of Benard cells. There are, however, many important physical differences between the patterns observed by TIROS I and those observed in the laboratory.

3. Physical Nature of Cellular Convection

Cellular convection was studied in detail by Benard early in the century (cf BRUNT, 1951). The patterns he observed in unstable liquids consisted of cells with upward motions in the center and descent at the periphery. His findings led him to suggest that certain cloud patterns, such as cirrocumulus, might represent cellular convection. Stimulated by his pioneering, other investigators undertook the study of these Benard cells and attempted to relate their findings to atmospheric cloud patterns. Theoretical work was originated by RAYLEIGH (1916) who determined the criterion for the onset of convection. This criterion indicates that Benard convection will not occur unless the density at the top of a fluid layer exceeds that at the bottom by an amount that varies directly as the molecular heat conductivity and viscosity, and inversely as the cube of the depth of the fluid.

The cloud patterns illustrated in this report, presumably with upward motion and cloudiness at the periphery and descent in the clear centers, are more typical in general appearance to cellular patterns obtained from convection experiments with an unstable layer of air (CHANDRA, 1938; GRAHAM, 1933). In these experiments smoke-laden air confined within a suitable container is destablized, usually by heating from below. If no shearing motion in the vertical is present, it is found that the mixture breaks up into a series of polygonal cells that have the intracellular motion just described. The observed polygonal pattern is an unsteady one, displaying a tendency for the cells to join into long rolls and the rolls in turn breaking up into polygonal cells. Increasing the depth of the chamber results in an increase in the cellular diameter, but the ratio of this diameter to the depth of the convective layer remains about two or three to one (AVSEC, 1939). This cellular configuration with its characteristic intracellular circulation has hitherto rarely been observed in natural cloud patterns, and consequently the reverse type, characteristic of cellular convection in liquids, has been the expected one (BRUNT, 1951).

Although observations of cellular convection by TIROS I have the appearance of experimental and theoretical studies of Benard cell convection, significant differences are evident. If the observations presented here are to be compared with Benard phenomena, then certain problems suggest themselves. One of these is related to scale. For example in laboratory and theoretical studies a diameter to depth ratio of three to one is obtained (BRUNT, 1951; NAKAGAWA & FRENZEN, 1955). In this study a value ten times as large was obtained—a ratio that is, interestingly, comparable to that found by WOODCOCK and RILEY (1947) from a study of cellular patterns in pond ice. Clearly, further investigation into the physical parameters that determine scale is required.

METEOROLOGICAL MEASUREMENTS

from

THE TIROS SATELLITES

by

W. G. STROUD

GODDARD SPACE FLIGHT CENTER

National Aeronautics and Space Administration

Washington, D. C.

August 1961

ABSTRACT

The three TIROS Meteorological Satellites containing television and solar and thermal radiation-detecting instruments have yielded a vast quantity of meteorological and geophysical information on the earth and its atmosphere over the past year and one half. Large numbers of photographs have revealed the unexpected extent of the organization of cloud systems over the earth. Clouds associated with tornados, with mountains and with hurricanes have been brought under observation by the satellites. The radiation detectors have provided maps of the distribution of radiation, both reflected and thermal, over large areas and, in addition to providing knowledge of the distribution of the energy balance have permitted the estimation of cloud heights and temperatures.

The analysis and interpretation of the staggering amount of information that has been acquired is a continuing task.

ACKNOWLEDGEMENT

The preparation of this paper and the scope of the TIROS Project activities have required that the author draw extensively on the work of many of his colleagues and fellow participants in the Meteorological Satellite Program. He is especially indebted to Dr. R. Hanel and his co-workers for the solar and thermal radiation maps and many discussions on the data. The Meteorological Satellite Laboratory staff of the United States Weather Bureau kindly furnished the Hurricane Anna nephanalyses of figures 5 and 6.

The many scientists, engineers, and technicians who prepared the satellites and launched the rockets are an unidentified but very real part of this paper.

INTRODUCTION:

There have been three Television and Infra Red Observations Satellites (TIROS) launched during the past two years for the purpose of making meteorological observations of the earth. Four more are planned. This is a logical point in the program to assess it as an experiment in our studies of the atmosphere and its motions. In addition, the individual satellites have varied in details and in degrees of success; the usual difficulties the experimental physicist encounters, exaggerated by the unusual laboratory in which he is conducting the experiments.

The value of satellites as an observational tool has been long recognized by the geophysicist, and discussed in the literature (1, 2, 3). But the technology of launch vehicles, telemetry and other practical considerations have only recently permitted the realizations of these ideas. The satellite brings to the geophysicist simultaneous observations of large areas of the earth, of regions that he cannot practically put under observation by any other technique, and provides him an entirely new view of the earth -- as a planet.

The method of these experiments is exploratory; as early examples of the exploitation of a new technology they are obviously limited by the lack of knowledge of what parameters are best measured from the satellite and by the experimenter's ability to make the measurement -- his lack of adequate sensors.

Since the clouds are visible manifestations of the thermodynamic processes of the atmosphere and could be photographed by techniques adaptable to

the satellite, they have been the first atmospheric phenomenon brought under observation (4) from rockets and satellites. A more refined measurement has been that of the radiation reflected and emitted by the earth and its atmosphere (5). The early rockets, Viking and Aerobee, and satellites, Vanguard II and Explorer VII, measurements, complemented by the continuing development of the launch vehicle technology laid the groundwork for the TIROS system and convinced the experimenters that valid and significant geophysical experimentation could be conducted from a satellite platform.

The TIROS system may be considered as composed of four elements (a) the spacecraft (or satellite) itself, (b) the launch vehicle, (c) the data acquisition sites, and (d) the results and their utilization. This paper addresses itself primarily to the results of the three satellites and the description and analysis of data obtained. Brief descriptions of the spacecraft and the sensory instruments; the launch vehicles, the Thor-Delta rocket; and the data acquisition sites at Wallops Island, Virginia and San Nicholas Island, California are included for logical reasons.

The Spacecraft

The TIROS satellite is a 285 pound pillbox, 42 inches in diameter, 19 inches high, containing a complex of optical, sensory, electronic, and magnetic and mechanical devices for the detection, storage and transmission of the data and for the control of these functions (6). Figure 1 shows the satellite and its major TV components. Figure 2 shows the radiation experiments subsystem. There are four sensory subsystems in the TIROS III satellite, a number which has varied somewhat from TIROS I, which had only the two vidicon camera subsystems. These are the two, wide-angle vidicon cameras, each capable of photographing a 750 by 750 mile area when the satellite is viewing a sun-illuminated area of the earth. The camera characteristics are listed in Table I.

TABLE I

Characteristics of TIROS Cameras

	TIROS I		TIROS II		TIROS III	
	CAMERA 1	2	CAMERA 1	2	CAMERA 1	2
Field of View	104°	12.7°	104°	12.7°	104°	
Lens Speed	8/1.5	8/1.8	8/1.5	8/1.8	8/1.5	
Shutter Speed	1.5 millisec		1.5 millisec		1.5 millisec	
Lines per Frame	500		500		500	
Video Band Width	62.5 kc		62.5 kc		62.5 kc	
Resolution per Raster line, zero nadir angle	1.5-2 mi.	1.2-0.5 mi.	same		1.5-2 mi.	

The five-channel scanning radiometer has been described elsewhere (7); the spectral sensitivities of the five sensors and of the other radiation detectors are listed in Table II.

TABLE II

The Radiation Experiments on the TIROS Satellites

Channel	Purpose	Spectral Sensitivity	Field of View
1	Water Vapor	6.0 - 6.5 microns	5x5 degree
2	Window	8 - 12 "	"
3	Albedo	0.2 - 6.0 "	"
4	Thermal	7.5 - 30 "	"
5	"Vidicon"	0.55 - 0.75 "	"
Wide Field Cone			
a.		Total (black)	35°
b.		Thermal (white)	35°
Hemispheres			
a.		Total (black)	Disc of Earth
b.		Thermal (white)	"

In addition to these sensors there are the solar-cell Ni-CD battery power subsystem and the horizon sensor for attitude determination, the north indicator for picture azimuth indication, and the magnetic orientation control for varying the coupling between the magnetic moment of the satellite and the earth's magnetic field (8).

In all the spacecraft have performed quite well. A summary of the present status of the satellites is given in Table III.

TABLE III

The Launch Vehicle:

The Thor-Delta, a three-stage, liquid-liquid-solid vehicle has been used to successfully launch TIROS II and III. An early version of this rocket, the Thor-Able II, utilizing basically the same propulsive units but different guidance and sequencing, was used for the TIROS I launch. This vehicle has placed the TIROS' into nominal 400 n.m. nearly-circular orbits of 100-minute periods and 48 degrees inclination. Table IV summarizes the orbit characteristics of the three launches.

The statistics for the Thor-Delta launch vehicle are tabulated in Table V. At launch the rocket stands 92 ft. high, is of about 8 ft. diameter and has a lift-off weight of about 112,000 pounds. The performance of the Thor-Delta has been excellent -- five of the six vehicles were successfully fired.

TABLE IV

Orbital Characteristics of the TIROS Satellites

(September 1, 1961)

	TIROS I	TIROS II	TIROS III
Altitude (Apogee	464.4 s.mi.	454.7	507.1
Altitude (Perigee	432.5 s.mi.	384.6	459.7
Inclination	48.39°	48.53°	47.89°
Period	99.24 min.	98.25 min.	100.4 min.
Launch Vehicle	Thor-Able II	Thor-Delta	Thor-Delta

TABLE V

The Thor-Delta Launch Vehicle

	Stage I	Stage II	Stage III
Fuel	Lox and Kerosene	MDMH and RFNA	Solid
Nominal Thrust (lbs)	150,000	7,500	3,000
Burning Time (sec)	160	109	40
Source	Douglas (Thor)	Aerojet General (AJ10-104)	Allegany Ballistics Lab. (X-248)

The Data Acquisition Stations

For all three TIROS there have been two data acquisition stations, one essentially on each coast of the United States. The TIROS-peculiar ground equipment has been the same throughout the operation, but the type of antenna used to acquire the data has varied.

The basic characteristics of the antenna are that it be of about 30 db gain at 240 mc and be trainable. Despite the fact that 65-foot parabolic "dishes", as well as the General Bronze multiple-helices array, have been used, each of the antennas is capable of automatically tracking the satellites at the data transmission frequency. At present the two stations in use are at Wallops Island, Virginia, the site of the NASA small-rocket range; and, at San Nicholas Island, California, a part of the Pacific Missile Range.

The satellite tracking is done by the Minitrack network of stations; the computed orbital elements are published by the Space Computing Center of NASA.

The operation of the stations is directed by the TIROS Technical Control, a Project function, located at Goddard Space Flight Center. Since TIROS, because it is a spin-stabilized body with fixed camera orientation, can take pictures only when the cameras are directed toward a sun-illuminated area of the earth, this Control Center gathers and analyzes the data on attitude of the satellite, the power balance, the orbital elements and the interesting weather situations in various areas of the earth and computes the programs that the data acquisition sites will use to command the satellite to take pictures over the acceptable areas of the earth. In addition, the Center evaluates the performance of the satellite, institutes emergency procedures for handling unexpected difficulties, either in the satellite or on the ground. In contrast to the picture data, the radiation experiments collect full 100-minute orbits of data and transmit it on command to the ground station without special programming.

On the average, seven orbits of data (about 450 pictures and seven radiation tapes) are obtained each 24 hours. The locations of the two stations is not optimal, -- one acquires five of the seven orbits and there is some overlap -- but have been dictated by practical considerations such as land areas on which to build.

The Utilization of the Data

The data received from the satellite are recorded in several formats at the ground stations. The telemetry data which handles all the "housekeeping" parameters, such as voltages, currents, positions, etc. which measure the performance of the instrumentation, are recorded on strip charts in analog form

for immediate analysis. The geophysical data are recorded in two formats, one magnetic tape and two as pictures. Both the picture and radiation data are recorded on high fidelity magnetic tape. These tapes are shipped to GSFC for processing and archival purposes.

For immediate operational use at the station, the picture data are recorded on 35 mm film by means of a photo-kinescope. This film strip is rapidly processed at the station and teams of meteorologists, by projecting the pictures on rough latitude-longitude grids, which are machine-computed right at the stations, are able to prepare nephanalyses of the areas photographed by the satellite. These nephanalyses are prepared in a format for facsimile transmission so that within three to six hours after a satellite pass the "fax" nephanalyses are transmitted to the National Weather Center at Suitland, Maryland, and thence, over the national weather communication circuits to the field users of meteorological data. Within these time intervals these nephanalyses of limited areas of the earth appear at all major Weather Bureau stations throughout the country, on ships at sea, and at many of the U.S. Military installations around the world.

The original film containing the pictures is returned by mail to the Naval Photographic Center in Washington, where it is processed and positive and negative copies are made and distributed to all research users of the data. After gridding, the master film is sent to National Weather records Center in Asheville, North Carolina, from which Center 100-foot strip copies may now be purchased.

The radiation tapes are mailed to GSFC where they are processed in a

two-step procedure; first, to a digital magnetic tape format which contains the raw radiation information as a function of time; then, by mating this tape with a similar tape containing the orbital elements and with calibration and attitude data, to a final meteorological radiation tape (again in a binary format) which is the basic method of publication of the data. From this tape, by means of appropriate computer programs and printout equipment, tabulations, grid prints and contour maps on various scales may be obtained. Fifty selected orbits of TIROS II radiation data in the form of 1 in 6 million and 1 in 30 million grid-prints are now in publication as a NASA Technical Report.

The entire processing is an outstanding example of the complexities and the amount of work involved in handling the huge volume of data obtained by the meteorological satellite. References (7b) and (9) give detailed accounts of the radiation data reduction.

RESULTS OF THE TIROS EXPERIMENTS

There have been a number of interesting technological results from the TIROS satellites -- the coupling between the earth's magnetic moment and that of the satellite (8), the long term operation of bearings in the hard vacuum of space, etc. (10); but, this paper will be concerned with the geophysical results. The results may be grouped into three classes: (a) the operational use of the picture data in meteorology; (b) the research use of the picture data in meteorology and geophysics; and, (c) the research use of the radiation data. Only limited examples of each group will be possible in this paper. Much has been published or is in publication (7, 10, 11, 12) and if the quantity of data being collected is any measure, much more will be published.

An example of one of the operational nephanalyses produced by the TIROS satellite is shown in Figure 3.

The pictures taken by the satellite were projected one by one on latitude-longitude grids of the areas photographed after identification of the cloud types and characteristics, standard symbols were marked on the map and the boundaries of the cloud systems and the satellite coverage noted. The area from West Africa to Western United States, north to Canada and south to Colombia has been brought under observation. The following figure (4) is an example of one of the roughly 200 photographs used to produce the nephanalyses of Figure 3.

A good example of the value of the nephanalyses is shown in Figure 5

wherein the TIROS III was tracking Hurricane Anna. And, in Figure 6, one of the photographs used in the July 21st nephanalysis is shown.

Whereas the nephanalyses are largely produced at the data acquisition sites, the research use of the pictures for meteorology and geophsics is done in the more leisurely atmosphere of the laboratory. Here the study of special events and phenomena such as the Benard-cell-like cloud forms over the Pacific, the cloud structure of an occluded cyclone, mountain clouds, the intensity, size and distribution of northern and southern hemisphere cyclones, the distribution of mountain snow, ice formations and flow in the St. Lawrence estuary, and the variations in coloration of the land surface, the glint from the sea -- may all be conducted (13). Figures 7, 8, 9 and 10 are examples of these observations.

The reflected and emitted electromagnetic radiation measurements which are briefly designated as radiation measurements in the following text seem to be the most significant data being acquired by the satellites. The reduction of the data to a format from which they can be readily assimilated and studied has been quite difficult (7b), but is now becoming somewhat routine. At present, only a fifty-orbit sample of the TIROS II data have been processed to grid-prints and printouts that permit analysis and interpretation.

Despite the difficulty of precise, absolute radiometric measurements, even in the laboratory, the TIROS II and III experiments have shown that significant measurements can be made from the satellite. The data from Orbit 88, taken on November 29, 1960 over the Atlantic Ocean and North

Africa are shown in Figures 12, 13, 14, 15 and 16 with the surface weather chart nephanalysis shown in Figure 11. Only the data from the five-channel scanning radiometer are given in these figures which are described briefly in the legend to each.

Some general comments about the group are pertinent. The values of radiation received at the satellite from the area on the map are given in watts per square meter. The weather system at the time of the satellite pass over the area was obtained by conventional techniques since TIROS II cloud photographs of the area were not available (Figure 11). A frontal system extended from Ireland over the ocean toward the southwest. Over large areas of the ocean, French West Africa and Algeria, no cloud data (NCD) were available.

CONCLUSIONS

There are available from the TIROS meteorological satellites a tremendous range of new geophysical data. The major problem confronting the experimenters involved is the task of adequately sifting through the vast quantities of photographs and maps to make sense of them; to find the patterns and the continuity which permit one to deduce and to relate the new information to the present theories and concepts.

It is a sizeable task, but probably the only practical means by which the atmosphere as a global phenomena will be brought within man's understanding.

TABLE III

Performance of the TIROS Satellites

September 1, 1961

	TIROS I	TIROS II	TIROS III
Launched	April 1, 1960	November 23, 1960	July 12, 1961
Days of Data Transmission	78*	Still Transmitting	Still Transmitting
Approx. No. of Pictures Transmitted	23,000	35,650	12,000
Orbits of Radiation Data Obtained	**	1,601***	367
Major Failures:	1. Narrow angle camera out between orbits Nos. 22 & 572.	1. Wide angle lens coated by rocket exhaust, pictures poor.	1. One camera shutter hung up.
	2. Relay failure destroyed battery power system.	2. Decay of interference filters on two scan radiometers after several months.	2. Decay of interference filters on two scan channels of radiometer.

*Beacons still transmit when in sunlight.

**The radiation experiments were not included in TIROS I.

***Five channel radiometer motor stopped 4/27/61. Balance of subsystem still operating.

FIGURES AND LEGENDS

FIGURE 1: The TIROS Satellite and Its Major Components.

The base plate with the TV camera lenses, projecting downward among the antennas and topped by the "hat", covered with solar cells, is readily identified. In the lower left is a vidicon camera with lens - in the front center is the video tape record for storage of the camera pictures. In the left rear the five bright discs identify the five-channel scan radiometer. The other components are beacons, control circuits, diplexer and switches all mounted on the base plate.

FIGURE 2: The Radiation Subsystem of the TIROS Satellite.

The 100 minute tape recorder is shown in the left rear with the DC/DC converter deck in front. Front center is the electronics deck containing the seven-channel telemetry and the tuning-fork clock for keeping time in the satellite. The 235 mc transmitter is right front. All components and decks are mounted in the pressurized can.

FIGURE 3: The TIROS III Nephanalyses for July 18, 1961 Over the Atlantic-from Seven Orbits.

The standard meteorological cloud symbols have been used and are in the legend in the lower left. The boundaries of satellite coverage are shown by heavy lines, the cloud boundaries are lighter. A vortex was visible and is indicated off the West coast of Africa. The eastern United States iscovered with a heavy overcast. In many areas, such as over the Yucatan peninsula, tongues of clouds and clear areas indicate a circulation pattern. Broken cloud patterns cover the major Caribbean islands, while the water areas are clear. Much of the area is not under the observation afforded by the satellite.

FIGURE 4: An Example of Cloud Photographs Used to Produce Nephanalyses Like Figure 3.

Shown is the West Coast of Africa between Cape Blanco at the top right and Dakar at the bottom center. The area out over the water is covered with broken, cumuliform clouds.

Figures and Legends (Continued)

FIGURE 5: Successive Nephanalyses from TIROS III of the Caribbean Area and Hurricane Anna, July 20 through 23, 1961.

The upper left frame shows the vortex off Venezuela and the photograph that was used to identify it and the cloud cover of the surrounding area. In the upper right frame the hurricane is more centered in the satellite pass and the vortex has moved about seven degrees due west in one day. The lower frames, taken July 22nd and July 23rd indicate the hurricane moving toward Honduras and dissipating over the land. The hurricane was not noticed on the nephanalyses of Figure 3 taken on July 18, two days before it appeared on Orbit 117 photographs.

FIGURE 6: Hurricane Anna on July 21, 1961:

The hurricane is shown off the coasts of Venezuela and Colombia, which run across the picture from lower right to upper left. The Lake Maracaibo in Venezuela may be discerned in the lower center of the photograph. The eye of the hurricane is not visible at this time, but the circulation pattern is.

FIGURE 7: TIROS III Photograph of Florida.

Well-developed convective cumulus clouds covering the land areas may be identified by their brightness. A squall line running east-west lies out over the Gulf of Mexico to the west of Tampa, Florida.

FIGURE 8: The Iberian Peninsula and the Straits of Gibralter, July 15, 1961.

A bright cloud bank lies over the Pyrenees Mountains. At the top of the picture may be seen the circular pattern of a cyclonic storm in the North Atlantic.

FIGURE 9: The Sahara Desert of North Africa and the Gulf of Sidra, Off Libya.

This is a dramatic view of the desert coloration so often observed. The Oasis of Kufra, a plateau area of Libya, is the dark patch on the right center of the picture.

FIGURE 10: A TIROS III-Located Tropical Storm Named Liza.

This example of a storm from an area of no weather reports lies west of Lower California. TIROS III located the center on July 19, 1961 at 25°N and 123°W.

Figures and Legends (Continued):

FIGURE 11: A Nephanalysis from Surface Weather Data on TIROS II Orbit 88, Over the Atlantic Ocean and North Africa.

The sub-satellite path is the heavy dashed line through the center of the figure. The boundaries of coverage by the five-channel radiometer are defined by the heavy shaded areas. The satellite made measurements within this entire area. No cloud data (NCD) were available over large areas (see text).

FIGURE 12: TIROS II Scanning Radiometer Water Vapor Channel at 6.0 - 6.5 Microns, Orbit 88.

The narrow spectral band and the low energies available make the precision of the absolute values of radiation poorer than on other channels. The corresponding blackbody temperatures of the "hot" region over Spanish West Africa are 253°K. The physical meaning of this region, which is not apparent on other channels, is not clear.

FIGURE 13: TIROS II Scanning Radiometer Atmospheric Window Channel at 8 to 12 Microns, Orbit 88.

This channel has yielded the most accurate and readily-interpreted results. The low values of radiation, $\bar{W}$ = 13 watts per square meter, equivalent to a blackbody temperature of 223°K, are identified with the high cloudy area associated with the front and storm center out over the Atlantic - to the left. Temperatures of 240°K ($\bar{W}$ = 20) were observed quite often - the maximum temperature was 293°K over the desert. Notice the cold region (clouds ??) over the Atlas Mountains. It is possible to estimate the heights of the clouds from these data!

FIGURE 14: TIROS II Scanning Radiometer, Albedo Channel at 0.2 to 6.0 Microns, Orbit 88.

This reflected solar energy map appears very often like the reverse of the window or the thermal channel. High cloudiness is bright, so clouds will reflect less solar energy, unless the surface albedo is high, as it is over the desert. Thus, the maps by themselves may lead to erroneous conclusions. This channel is sensitive to solar elevation angle, so computation of the values of albedo for the various surfaces is difficult. The clear bright area over the Sahara (on right) has an albedo of 28 percent, whereas, the Moroccan area has a low albedo of 6 percent, suggesting some vegetation.

References (Continued):

11. Staff, Aeronomy & Meteorology Division, Goddard Space Flight Center, and Meteorological Satellite Laboratory of U.S. Weather Bureau: Final Report of TIROS I Meteorological Satellite System, NASA Technical Report, In publication, September 1961.

12. Hanel, R.A., and Stroud, W. G., "The TIROS II Radiation Experiment"- In publication, Tellus, November 1961.

13. a)Wark, D,.Q., and Popham, R.W., "TIROS I Observations of the Ice in the Gulf of St. Lawrence", Monthly Weather Review 88, 182 (1960).

    b)Winston, J.S. and Tourville, L., "Cloud Structure of an Occluded Cyclone Over the Gulf of Alaska, as viewed by TIROS I", Bulletin American Meteorological Society 42, 151 (1961).

    c)Hubert, L.F., "A Subtropical, Convergence Line of the South Pacific", Journal of Geophysical Research 66, 797 (1961).

Tiros Program Results

(CONTINUED FROM PAGE 29)

addition, there were three achievements in different technological areas which are worthy of specific mention:

a. *Spin-up rockets.* In Tiros I, approximately seven weeks after launch, a pair of spin-up rockets were successfully fired on command from the ground to improve the spin-axis stability. The spin rate was increased from 9.5 to 12.85 rpm (the design increase value was 3 rpm). This was the first known demonstration of a rocket motor on any satellite or space vehicle being fired successfully after such a long period in the space environment. In Tiros II the spin-up rockets were again successfully used, although this time only two days after launch.

b. *Magnetic attitude control of the spin axis.* The torque produced by the interaction of an induced magnetic dipole in the satellite with the earth's magnetic field was determined to be the main cause of the Tiros I spin axis wandering from its predicted (space-stationary) position. For Tiros II, 250 turns of fine wire capable of carrying a variable current were incorporated in the satellite to provide a controllable magnetic dipole. By means of the predicted torques, it was hoped to provide some control of the satellite orientation and thus improve the observational conditions. This magnetic orientation coil has been activated several times with very satisfactory results.

c. *Lubricated ball bearings.* In precision instruments such as the IR radiometer, where the alignment of optical elements must be preserved and wear on the bearings must be minimized, ball bearings with conventional lubrication techniques are essential to gain the necessary low power drain, long life, and reliability. By proper design and careful fabrication, it has been possible to reduce the rate of oil flow out of the bearing assembly and to reduce the rate at which the lubricant volatilized under space condition of low pressure. As of the time of this writing, after 4 mo of operation in space, the bearing is still functioning properly, as attested by the transmission of meaningful data by the radiometer systems.

Serious Failures

The Tiros engineering subsystems did not all work flawlessly. There have been failures, the following being

Tiros II Radiation Chart

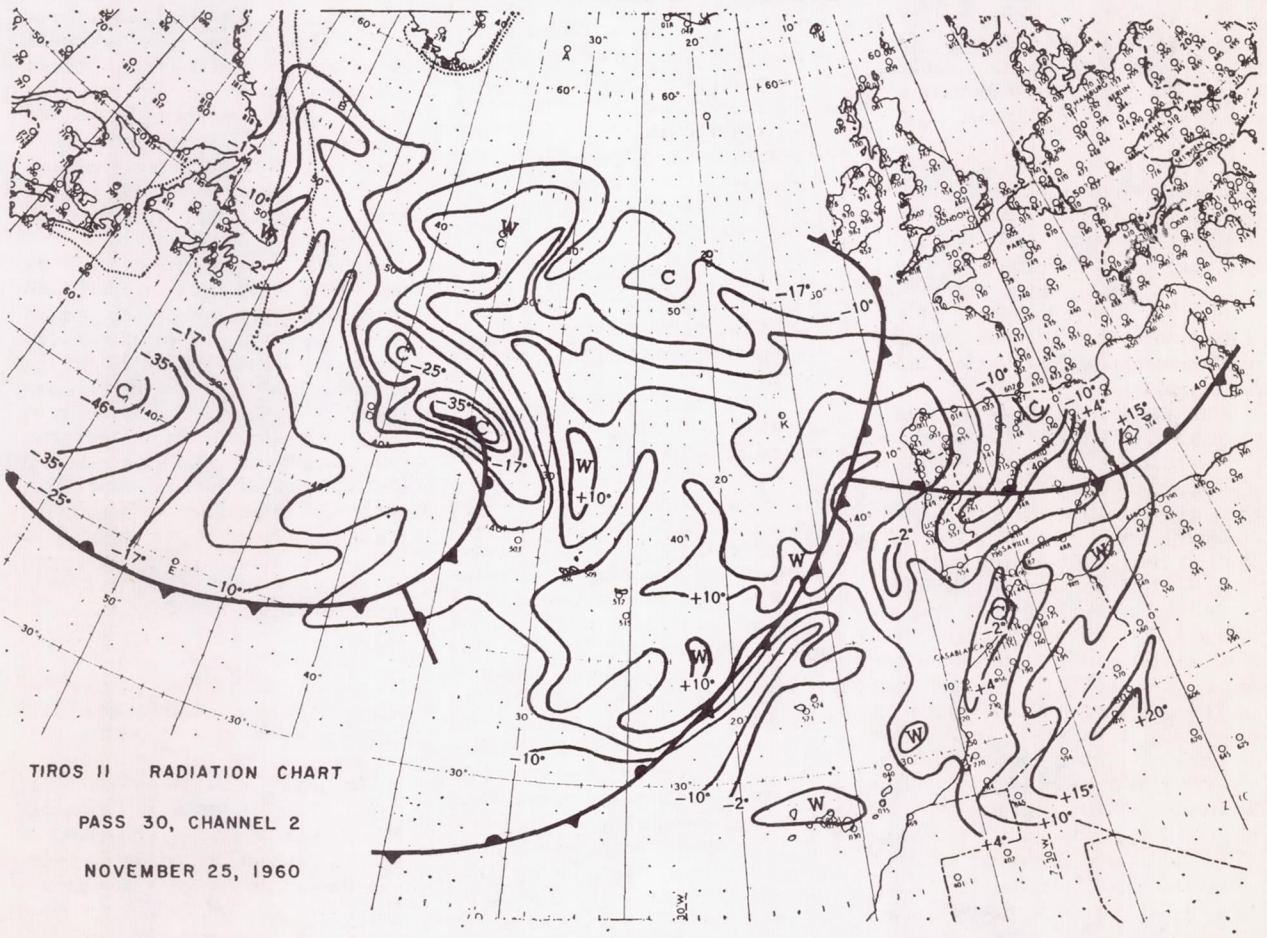

Shown in this figure by Hanel and Wark are two weather frontal systems which lay in the Atlantic as Tiros II passed over and the temperatures derived from the satellite's radiation measurements. Associated with the one on the left is a region of marked low temperatures (indicated by "C" for cold) coming from the tops of the cold clouds usually found in the low-pressure center of the system. The frontal system to the right lies through a region of high temperatures (marked "W" for warm) off the coast of Spain. This would seem to indicate that this front is weak here and no longer has much cloudiness associated with it, so that the radiation is coming from the ocean or from the tops of low, and therefore warm, clouds. The higher-pressure region between the two frontal systems, in the mid-Atlantic, is a region of high temperature also, indicating that there is a lesser amount of cloudiness here.

among the more serious:

a. The horizon-sensing attitude indicator subsystem of Tiros I did not produce the desired information. Satellite attitude had to be computed primarily by the application of photogrammetric techniques to the photographs themselves. In Tiros II the highly successful IR radiation subsystem provides the required attitude information.

b. In Tiros I a relay became stuck in the command circuit, preventing the turning off of the TV transmitter. Continued transmitter operation drained the batteries and caused general failures. As a consequence, after orbit number 1302, about midnight June 29, 1960, it was decided to discontinue operations.

c. In Tiros II, a malfunction in the clock system for the remote-operation mode of the wide-angle camera caused the discontinuance of operations in that operational mode in order not to jeopardize the successfully operating subsystems. Direct wide-angle pictures, direct narrow-angle pictures, and remote narrow-angle pictures are still being taken at the time of this writing.

d. The Tiros II satellite occasionally responds to spurious and unexplained command signals.

All in all, however, the satellite engineering systems worked very well and established without doubt the feasibility of meteorological satellites.

2. *Would the satellite measurements contain useful meteorological information?*

With the receipt of the very first pictures from Tiros I, it became apparent that the satellite system was photographing clouds, cloud formations, and cloud patterns. The meteorological research teams at the U.S. Weather Bureau, Air Force Cambridge Research Center, Naval Weather Research Facility and other institutions attacked the problem of interpreting the Tiros pictures in terms of weather information content. The first step was to compare the photographs with meteorological analyses from other available and more conventional observations, as reported by Winston and Tourville in the American Meteorological Society bulletin for March. The studies soon indicated excellent correspondence between the cloud formations and meteorological patterns, such as the following:

Low-pressure cyclonic storm systems (these appeared as spiral cloud formations in the satellite photographs), cold fronts, large areas of stratus cloudiness, unstable areas having cellular shaped clouds, local severe storms, jet stream, and mountain clouds. As a matter of fact, these findings confirmed previous suggestions based on limited photographs from high-altitude rockets that nature was drawing a weather map by means of clouds.

By matching together overlapping photographs, it was possible to construct mosaics covering very large areas, such as the one of a family of several storms shown on page 28, drawn from V. J. Oliver, "Tiros Pictures of a Pacific Frontal Storm," *Weatherwise*, Oct. 1960. This mosaic covers almost 5000 mi, from the mid-Pacific to the central U.S. With it is shown the meteorological frontal analysis on which has been based the nephanalysis—the analysis of clouds as indicated in the photographs. The correspondence is excellent, but the detail afforded by the picture's cloud analysis is totally lacking in the broad brushstroke meteorological one.

Cloud Details Studied

Such detail is being studied to determine whether differences in the cloud patterns can yield information on the stage of development of a storm system or on its severity. In one such project, reported by R. Boucher at the AMS meeting in January, the cloud patterns have been studied in relation to the evolution of a "cyclone system" from its emergence as an "open wave" to the time of its "occlusion." If this study is successful, it may be possible to tell from the photographs alone the stage of development of a cyclone system.

The extraction of meteorological information from Tiros II IR data is proceeding at a much slower rate. This data is received in analog form, and for more rapid processing must be converted to digital representation and then married to the orbital data for position and look-angle reference. The data must then be plotted so as to be represented as a field. This process has been quite laborious, and only a limited amount of data has been analyzed. In general, however, results have been very satisfying. As expected, areas of low temperature have been associated with cloud zones (where the radiating surface is at higher and cooler altitudes) and areas of higher temperatures have been associated with cloud-free, high-pressure regions, as reported by Hanel and Wark at the AOS meeting in March, and indicated in one of their charts on page 63.

The answer to the question posed is again YES.

3. *Could the meteorological information contained in the satellite data be extracted and transmitted to the weather services in time to be of value in analysis and forecasting?*

It would have been significant enough had Tiros been successful only in providing new and detailed data about atmospheric processes. This would undoubtedly lead to a more thorough understanding of the weather and the factors that produce it. But a bonus was yet to come. In anticipation of the possible utilization of Tiros data for operational meteorological purposes, teams of civilian, military, and contracted meteorologists were at the data-acquisition stations to study the incoming data in "real time." Within 60 hr after Tiros I was launched, picture data less than 6 hr old was being interpreted and the analyses forwarded via facsimile transmission to the National Meteorological Center of the U.S. Weather Bureau at Suitland.

The chart on page 29, a copy of one of those transmissions, is of the system of the family of storms pictured on page 28. The cloudy areas are clearly depicted, as are the cloud bands themselves. The storm center south of the Aleutian Islands is clearly outlined by these cloud bands. Transmissions such as these were incorporated into the regular analyses and forecasts of the Weather Bureau; copies were also relayed to our air and naval services both in this country and overseas. The many reports which we have received, both from civilian and military field users, have been extremely enthusiastic about the usefulness of such data. Reports of the operational utilization of the Tiros II data, despite the degraded quality of the pictures from the wide-angle camera, have been even more enthusiastic. The operational weather services have indicated that these cloud analyses established, confirmed, or modified surface frontal positions, assisted in the briefing of pilots on accurate weather, were used in direct support of overwater deployment and aerial refueling of aircraft, gave direct support to an Antarctic re-supply mission, confirmed the position of a Pacific typhoon, and verified or amplified local analyses particularly over areas with few conventional reports, etc.

The quality of the IR radiation data from Tiros II has been excellent. However, as indicated, they have to be reduced and plotted on maps before they can be properly interpreted. From this point of view, until rapid processing techniques can be developed, the IR data are not as useful as the TV data for operational use.

Thus, the answer to the last question is again YES.

The operational utilization of Tiros data has captured the imagination of the weather services and has made them all the more impatient for the

establishment of an operational meteorological satellite system to provide such data continuously and over the entire earth. Plans for the implementation of such a system are currently being developed by an interagency committee of experts.

What needs to be done now? The successful operation of the Tiros satellite system has brought into sharper focus the required direction toward which the meteorological satellite program should be heading. The areas which require development at this time are as follows:

a. *Satellite system improvement.* In particular, a larger spacecraft is required, to carry additional new and improved sensors. For global coverage, a polar orbit will be necessary and the spacecraft should be earth-oriented to increase earth-viewing time. These features are being planned for the next family of meteorological satellites—Nimbus.

b. *Data analysis.* The volume of data already acquired by the Tiros satellites and the volume of data to be expected from future meteorological satellites is enormous. The Weather Bureau is developing procedures for processing, storage, and retrieval of these data. Attempts are being made to encourage increasing numbers of investigators to study these data through aggressive contacts with the meteorological community in general and with university research groups in particular.

c. *Data transmission.* A critical part of the data-volume problem is transmitting the meteorological content of data to operational meteorologists in as near real-time as possible. This involves determination of the significant meteorological content of satellite output (of interest to the weather forecaster) and development of rapid transmission techniques to make this content available to the user in time for use. Satellite on-board analysis, ingenious techniques for data presentation, automatic-analysis instrumentation, improved transmission facilities, advanced communications relays—all are developments which are of current concern. ♦♦

JOURNAL OF GEOPHYSICAL RESEARCH VOLUME 66, NO. 1 JANUARY 1961

On Indirect Temperature Soundings of the Stratosphere from Satellites

D. Q. WARK

U. S. Weather Bureau
Washington, D. C.

Abstract. Outgoing radiation from the atmosphere is calculated at several frequencies in the 15-μ carbon dioxide band according to the random Elsasser band model and the Curtis-Godson approximation to the mean line width. From the resulting values, an inversion of the problem is performed, with simplifying assumptions, to recover the temperature structure of the upper part of the atmosphere. This abbreviation of the experiment proposed by Kaplan would yield the temperatures and the lapse rates in two layers of the atmosphere from three measurements of the outgoing radiation. Results from three model atmospheres indicate that calculated mean lapse rates and mean temperatures in the two layers, as they might be deduced from measurements made from a satellite, are in good agreement with actual temperature structures.

Recently, *Kaplan* [1959*a*] proposed a method for determining the temperature structure of the atmosphere by making measurements from a satellite of the upward radiation in the 15-μ band of carbon dioxide. It was suggested that a set of ten measurements, each confined to a narrow spectral interval of about 5 cm^{-1} and properly selected within the 15-μ band, would allow one to infer the temperatures within ten layers of the atmosphere. It was assumed that carbon dioxide is uniformly mixed in the atmosphere, an assumption which seems to be well supported [*Hagemann, Gray, Machta, and Turkevich,* 1959].

A complete experiment of this sort, however, is difficult because of clouds which obscure the lower layers of the atmosphere. A proposal was therefore put forth [*U. S. Weather Bureau,* 1959] that a simpler investigation might be conducted in which only three or four spectral intervals would be examined. These would be confined to the central part of the 15-μ band, so that even in the most transparent interval the outgoing radiation would arise almost entirely from the stratosphere. Clouds are mostly limited to the troposphere and would not interfere.

To test this method of determining the temperature structure of the stratosphere, it was first necessary to calculate the specific intensity of the radiation leaving the top of the atmosphere. In a narrow spectral interval $\Delta\nu$, in which the Planck function can be regarded as constant over the interval, the radiative transfer integral equation can be written

$$I(\theta) = B(T_2) + \int_{T_2}^{T_0} \tau \frac{\partial[B(T)]}{\partial T}\, dT \qquad (1)$$

where $I(\theta)$ is the mean specific intensity in the interval; $T = T(p) = T(z)$ is the temperature, which is a function of the pressure p or of the height z; the subscripts 2 and 0 refer to the top of the atmosphere and to any point below which τ is effectively zero, respectively; and τ is the mean transmission (over the spectral interval) of the radiation passing from a point in the atmosphere to the top of the atmosphere, and is defined by

$$\tau = \int_{\nu_0-\Delta\nu/2}^{\nu_0+\Delta\nu/2} \exp\left[-\int_z^{z_2} k(\nu)\rho \sec\theta\, dz\right] d\nu \qquad (2)$$

in which $k(\nu)$ is the mass absorption coefficient at the frequency ν, ρ is the density of the gas, and ν_0 is the central frequency of the interval. Equation 1 is the integration by parts of the more common form of the transfer integral equation,

$$I(\theta) = B(T_s)\tau_s + \int_{\tau_s}^{1} B(T)\, d\tau \qquad (3)$$

where s refers to the surface conditions. Equation 3 may easily be interpreted in physical terms [see *Greenfield and Kellogg,* 1960], but equation 1

reveals its nature less readily. It is often advantageous, however, to calculate the transmission and the differential of the Planck function, rather than the reverse forms of these functions which appear in equation 3.

The last term in (1) can be written as a summation if the layers of the atmosphere are sufficiently thin so that $\overline{B(T)} = B(\bar{T})$ and $\Delta\tau \ll 1$ in each layer. Then

$$I(\theta) = B(T_2) + \sum_{i=1}^{i=n} \tau_i \left(\frac{\partial[B(\bar{T})]}{\partial \bar{T}}\right)_i (\Delta T)_i \qquad (4)$$

where the nth layer is at T_0; $\bar{T}$ is the mean temperature in the layer; and τ_i is evaluated at the central pressure in the layer.

The principal hurdle in most radiative transfer problems is the determination of τ. For carbon dioxide it is possible to approximate certain portions of the band by an Elsasser band [*Elsasser*, 1942]. Carbon dioxide is a linear molecule, so that its P and R branches have lines almost equally spaced and, in general, the lines vary little in strength over a spectral interval containing two or three lines. With very little error, the transmission over a spectral interval equal to the line spacing can be expressed by

$$\tau = 1 - \sinh\beta \int_0^y \exp(-y\cosh\beta) J_0(iy)\, dy \qquad (5)$$

where

$$y = \frac{Sm}{D\sinh\beta} \qquad (6)$$

and

$$\beta = \frac{2\pi\alpha}{D} \qquad (7)$$

in which S is the line strength, defined as the integrated absorption coefficient over the line, α is the line half-width, D is the line spacing, and m is the mass per unit area of the absorbing gas. This relation will not hold near the band center, where there is a contribution by the Q branch.

In the 15-μ band there are several individual bands. The strongest band contributing to the absorption is the ν_2 fundamental, centered at 667.40 cm^{-1}. In addition, however, there is significant absorption by overtone and combination bands, even at the peaks of the P and R branches of the ν_2 fundamental. *Kaplan* [1953] introduced the random Elsasser band: if the lines due to the several sub-bands contributing to the absorption are randomly spaced, the most probable value of the transmission is given by

$$\tau = \prod_{i=1}^{i=m} \tau_i \qquad (8)$$

where τ_i is the transmission due to an individual band.

In equation 5 it is assumed that the absorbing gas is homogeneous. In the atmosphere, of course, this condition is not met. *Curtis* [1952]

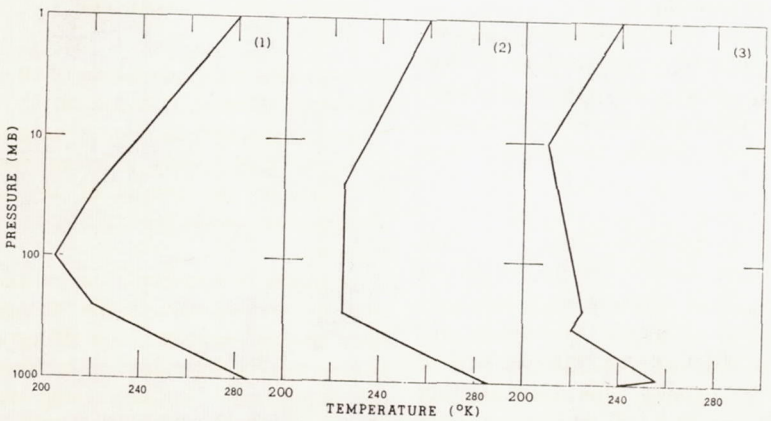

Fig. 1. Three sample atmospheric models, showing temperature versus the logarithm of pressure. The carbon dioxide content is 0.0310 per cent by volume in each atmosphere.

DEPARTMENT OF COMMERCE
FREDERICK H. MUELLER, Secretary

WEATHER BUREAU
F. W. REICHELDERFER, Chief

Reprinted from

MONTHLY WEATHER REVIEW

Volume 88
Number 3

MARCH 1960

Closed May 15, 1960
Issued June 15, 1960

CLOUD PICTURES FROM SATELLITE TIROS I*

S. FRITZ AND H. WEXLER

U.S. Weather Bureau, Washington, D.C.

[Manuscript received April 29, 1960; revised May 5, 1960]

ABSTRACT

Some of the more striking examples of cloud phenomena revealed by the first pictures that have come from the experimental weather satellite, TIROS I, are presented, and broad-scale patterns in the pictures are interpreted in terms of general features of the associated weather maps. These preliminary results show that a vast variety of scales appear in the cloud patterns associated with cyclonic vortices. Marked differences, as well as similarities, in cloud patterns associated with several types of cyclones are pointed out; the cyclones discussed include mature vortices in the Atlantic and Pacific Oceans, younger cyclones over and near the United States, and a typhoon in the South Pacific Ocean. The cloud cover over an extensive area is portrayed by means of preliminary mosaics of TIROS pictures and by a schematic cloud map made from the pictures.

1. INTRODUCTION

TIROS I, an experimental weather satellite (c.f. [1]) containing two television cameras was launched on April 1, 1960, by the National Aeronautics and Space Administration. The characteristics of the satellite, its cameras, and its orbit have been reported elsewhere [2]. By April 22, it had made about 300 orbits (apogee 461.3 stat. mi.; perigee 436.0 stat. mi.; inclination 48.4°; period 99.24 min.) and its cameras had taken about 6,000 pictures of various cloud formations. The purpose of this preliminary note is to present a few examples of these cloud pictures and to show their relation to observed weather patterns.

From among these first pictures that have come from TIROS some of the more striking examples have been selected. These have been put together in two ways. The first category portrays the large-scale vortex or cyclonic storm, several hundred miles in diameter. Pictures of seven individual vortices have been selected and their relationships to features of sea level weather maps are discussed. The location of the satellite in its orbit and the direction of view of its cameras at the time of each picture have not yet been determined precisely. However, approximate locations and directions that will serve the purpose of this preliminary report are indicated on the maps.

The second category is a composite array. One array consists of two mosaics of about 30 different prints and extends from a region about 800 miles west of Ireland to the Near East. Another array, in the form of a schematic representation of clouds, extends from the Pacific coast of the United States eastward over the Mediterranean to the Near East.

2. CLOUD PATTERNS OF CYCLONIC STORMS

The first category, figures 1–8, contains seven different examples of vortices observed by TIROS in both the Northern and Southern Hemispheres. With each picture, except figures 7 and 8, is shown the weather map associated with the vortex. The weather analyses were copied from the sea level maps of the National Weather Analysis Center, U.S. Weather Bureau, Suitland, Md.

Figure 1 shows the storm that was picked up in the

*This work has been supported by the National Aeronautics and Space Administration.

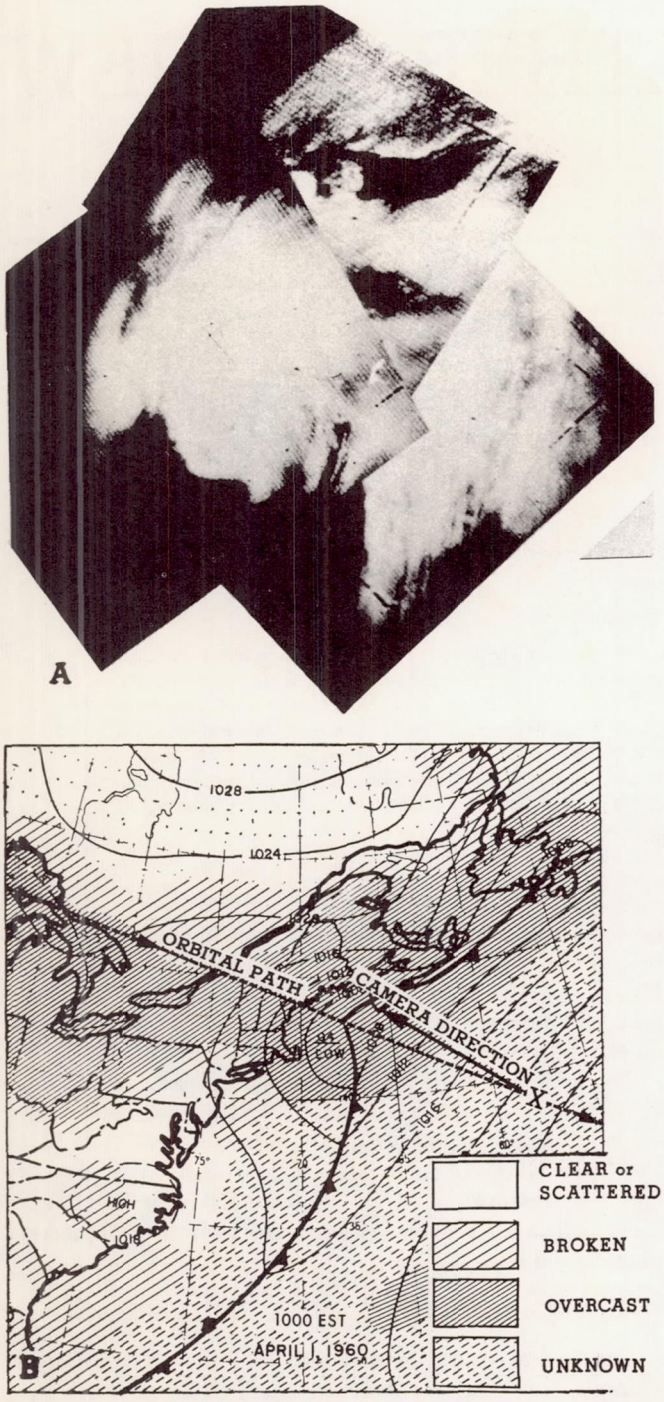

FIGURE 1.—(A) Three overlapping TIROS pictures showing extratropical cyclone centered about 120 miles east of Cape Cod, April 1, 1960. (B) Sea level weather map, 1000 EST, April 1, 1960. Point X denotes approximate location of satellite and the arrow indicates camera direction when pictures were taken.

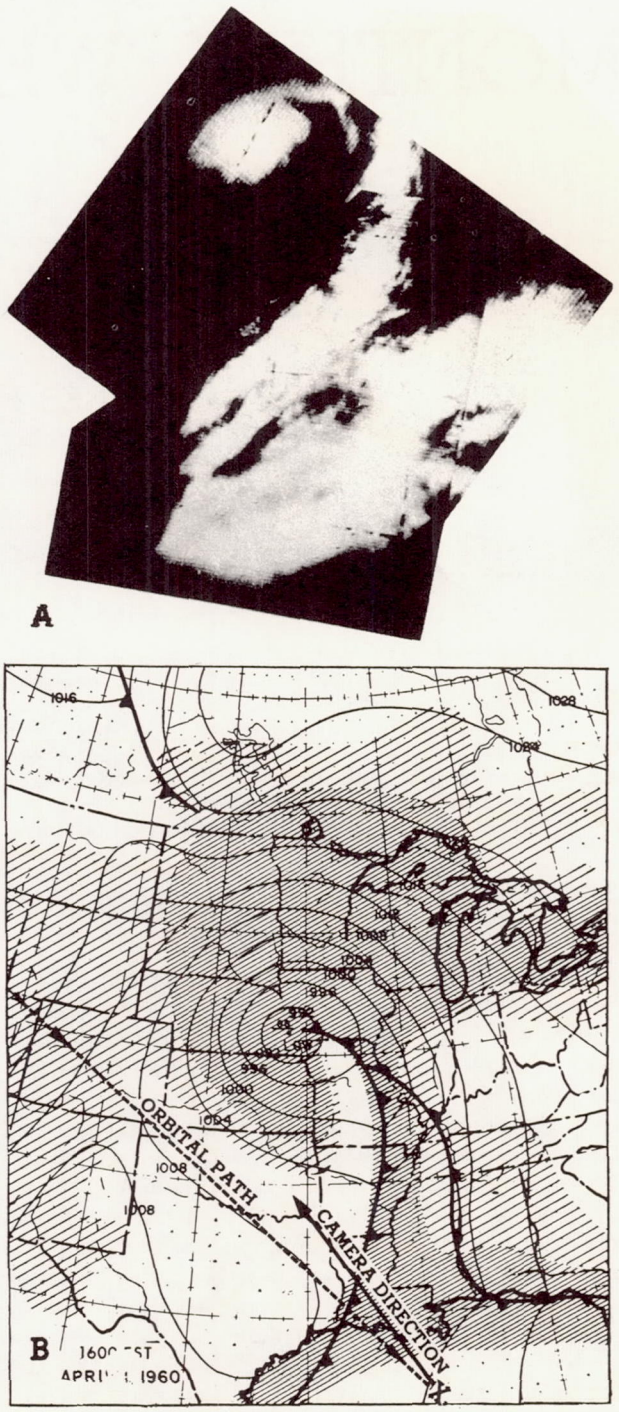

FIGURE 2.—(A) Two overlapping TIROS pictures showing extratropical cyclone centered over southeastern Nebraska, April 1, 1960. (B) Sea level weather map, 1600 EST, April 1, 1960. The key to the cloud cover analysis is given in figure 1B.

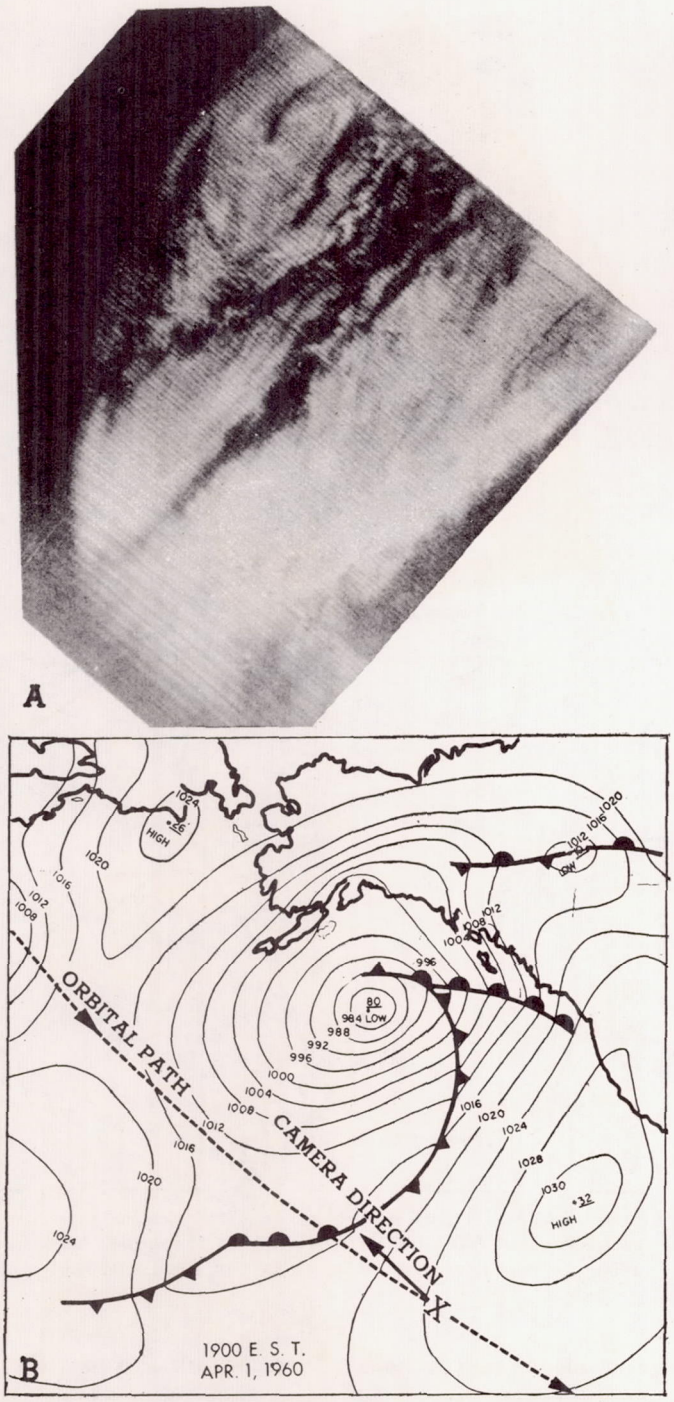

FIGURE 3.—(A) TIROS picture showing extratropical cyclone centered in the Gulf of Alaska about 500 miles southeast of Kodiak Island, April 1, 1960. (B) Sea level weather map, 1900 EST, April 1, 1960.

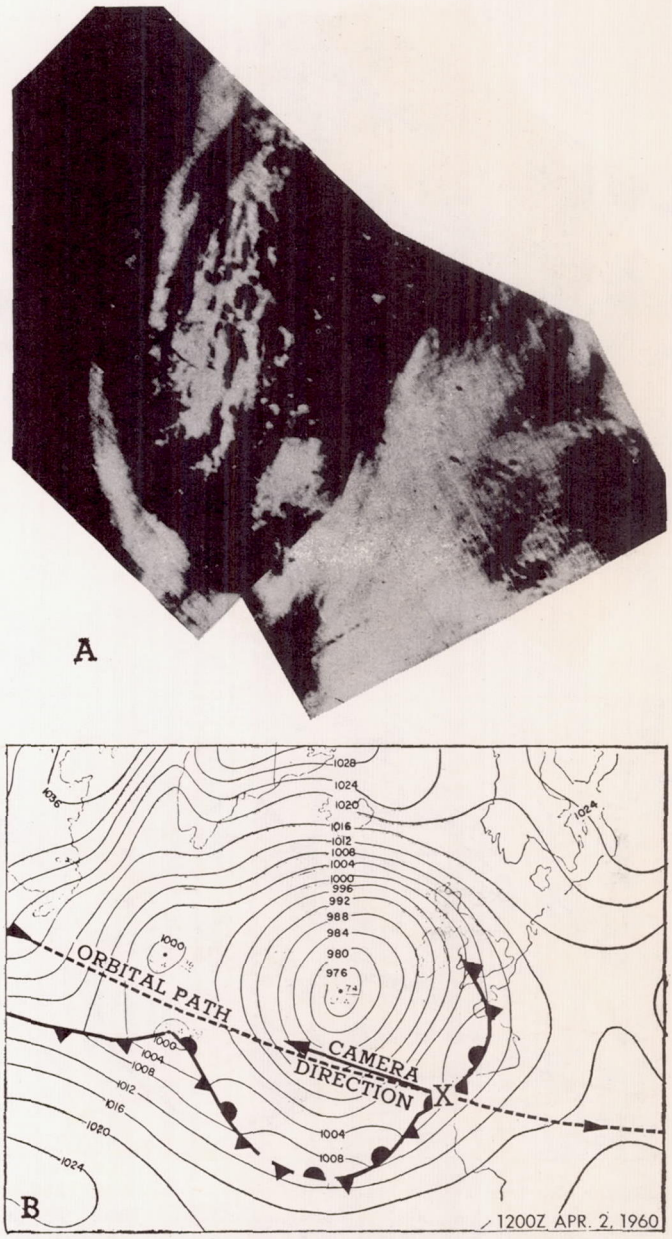

FIGURE 4.—(A) Two overlapping TIROS pictures showing extratropical cyclone centered about 400 miles west of Ireland, April 2, 1960. (B) Sea level weather map, 1200 GMT, April 2, 1960.

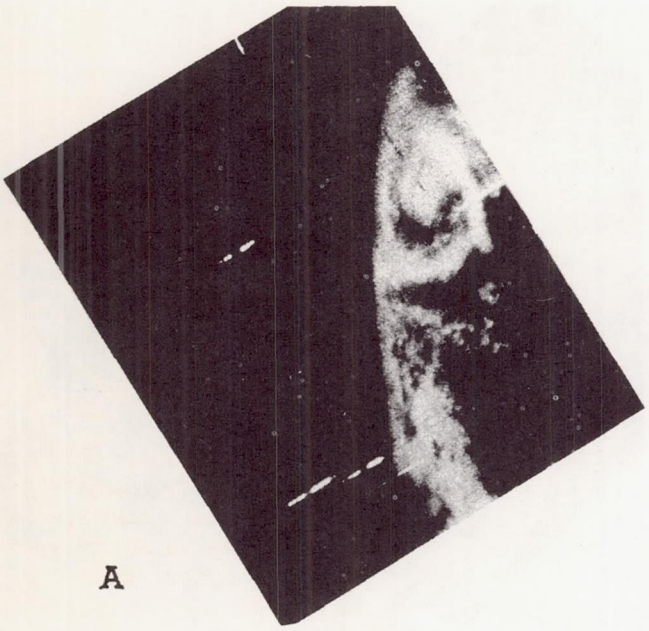

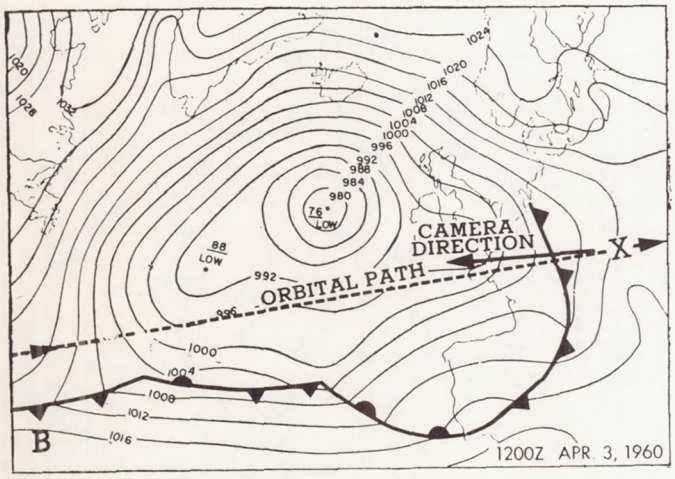

FIGURE 5.—(A) TIROS picture showing extratropical cyclone centered about 400 miles west of Ireland, April 3, 1960. This is the same storm pictured in figure 4A a day earlier. (B) Sea level weather map, 1200 GMT, April 3, 1960.

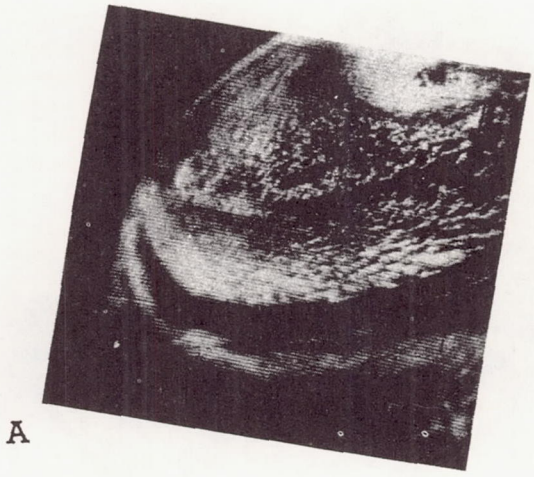

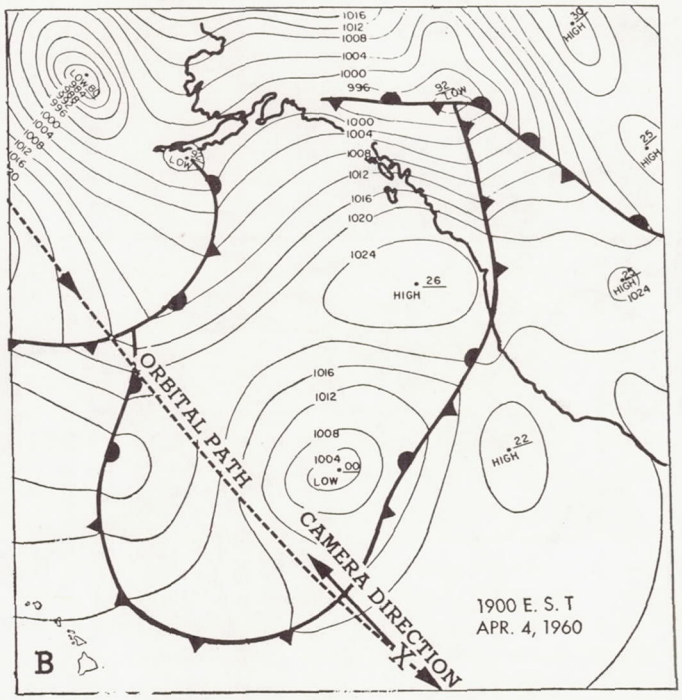

FIGURE 6.—(A) TIROS picture showing extratropical cyclone centered about 800 miles west of southern California, April 4, 1960. (B) Sea level weather map, 1900 EST, April 4, 1960.

early orbits of TIROS on the first day, April 1. The storm was centered 120 miles east of Cape Cod with continental air streaming off the east coast, and moist air over the ocean flowing northward, counterclockwise around the center, producing widespread clouds and precipitation as far north as the Gulf of St. Lawrence. Much of the Gulf of St. Lawrence and the St. Lawrence River was nearly cloudless as is indicated by the dark area near the top of the pictures.

Figure 2 shows a storm in midwestern United States that was also televised on April 1. This rather extensive storm was centered over southeastern Nebraska. Again, we see the clear, cold, dry air (represented by the dark area which is the ground underneath) moving in behind a cold

front. To the east of the front the moist air from the Gulf of Mexico is flowing into the storm center and producing rather widespread cloudiness, shown by the circular cloud near the top of the picture. Near the Gulf of Mexico, where very bright portions of the picture suggest that the clouds are very high, thunderstorms occurred.

Figure 3 shows a third vortex that was observed, also on April 1, in the Gulf of Alaska 500 miles southeast of Kodiak Island. The vortex circulation is clearly portrayed by the clouds which form a spiral array.

The associated weather map of the cyclone is based upon relatively few reports over an area which is larger than the United States; there is therefore opportunity for error because of lack of observations. The paucity of data is even more pronounced in the upper air. In these areas particularly, satellite observations similar to figure 3 will be useful in synoptic scale weather analysis as well as research.

Figure 4 shows a large, mature, occluded cyclone, about 1,000 miles in diameter, centered about 400 miles west of Ireland on April 2. The rather well-marked banded structure of the clouds of this ocean storm is quite different from the more uniform structure of clouds associated with continental and coastal storms whose cold fronts are followed by dry continental air (figs. 1 and 2). The storms over the oceans that TIROS has so far revealed seem to show more of a banded structure; the bands, ranging in width from a few miles to a few hundred miles, appear to spiral cyclonically around the storm center.

Figure 5, showing the same storm west of Ireland a day later, April 3, was photographed from a point farther to the southeast. From this view, in which the storm is near the horizon, there seems to be just one very large band winding around the center. Photogrammetric measurements may reveal the nature of the change in cloud pattern from April 2 to April 3.

Figures 6 and 7 show a cyclone located about 800 miles west of southern California on April 4 in an area where anticyclones are usually found. The storm has a cloud vortex about 1,000 miles in diameter. The cloud picture contains several scales of superimposed bands: first, a series of wide bands in which the clouds seem to start abruptly at a narrow clear zone, sometimes increasing in brightness with distance from the vortex center, only to end abruptly again in a clear zone; second, the individual bands composed of a series of smaller elements, and probably if the resolution were fine enough, there would be smaller elements within those. These are examples of the vast variety of scale of streakiness that characterizes the atmosphere.

The weather map (fig. 6B) associated with this cyclone is based on a few ship reports in the area between Hawaii and California, whereas the TIROS picture (fig. 7) reveals considerably detailed structure of the storm.

Figure 8 shows a vortex in the Southern Hemisphere, where cyclones rotate clockwise instead of counterclockwise. On April 10, this storm was located about 300 miles north of the northern tip of New Zealand. Note the dark, cloudless eye of the storm. The eye and spiral cloud bands of tropical cyclones, such as hurricanes and typhoons, have been studied by means of radar and aircraft photographs, but figure 8 shows the first single picture of a nearly complete typhoon structure as seen from high levels.

The existence of this tropical storm was known to meteorologists in the Southern Hemisphere for several days before TIROS televised it on April 10; after a message was received indicating that a storm was there, the satellite was then programmed to observe it. (TIROS can store pictures taken during only a 16-minute interval; therefore, whenever possible, it is programmed to take pictures of interesting meteorological areas on the daylight side of the earth.) This is one of several pictures taken about 0300 GMT, April 10.

The vortices that have been shown in this section are examples of the most striking phenomena that TIROS has revealed so far. It will now be necessary to study the hydrodynamics and thermodynamics which produce such cloud patterns, to acquire a greater understanding of atmospheric processes, which will then lead to a better interpretation of the cloud pictures.

3. CLOUD PATTERNS OVER EXTENDED AREAS

The second category of cloud information, shown in figures 9 and 10, is the cloud cover and patterns over an extensive area having dimensions far greater than those represented in the individual pictures shown in the preceding section. This different type of cloud information is obtained by overlapping a series of TIROS pictures to make a mosaic (fig. 9) and by deriving a schematic cloud map (fig. 10) from the pictures.

Figure 9 is a mosaic of about 30 pictures taken on orbits 14 and 15 as the satellite moved toward the southeast on April 2. The pictures start about 800 miles west of Ireland to the west of the vortex that was mentioned earlier (fig. 4). On orbit 14, a picture of the vortex was taken and 100 minutes later on orbit 15 another picture of the same storm was taken. The same cloud details can be recognized over the 100-minute interval. The mosaic gives a geographical coverage of cloud patterns beginning in the Atlantic Ocean. They include the vortex west of Ireland and show the extensive cloud area over western Europe, a massive cloud over the Swiss Alps, a general cloud area over Turkey, and a clear area in the Near East, Israel, Egypt, and North Africa.

Figure 10, based on pictures from orbits 28 and 32, on April 3, is a preliminary schematic representation of clouds over an area extending from the west coast of the United States into the Atlantic Ocean, and then from the mid-Atlantic and Europe to the Near East. Selected photographs, from which the schematic array was made, are displayed along the boundaries of the photographed area.

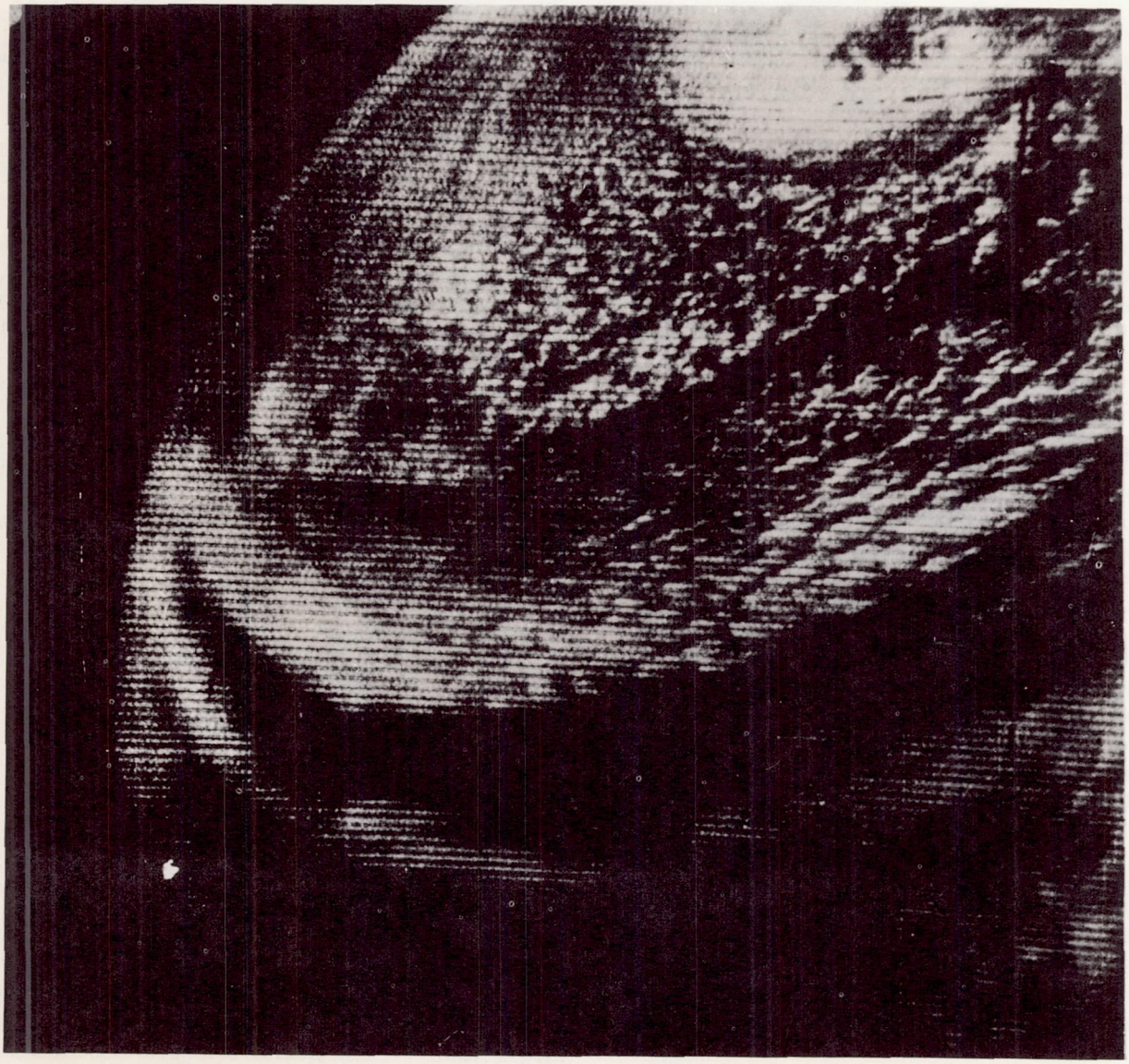

FIGURE 7.—Enlarged TIROS picture of the extratropical cyclone shown in figure 6. Notice the variety of scales shown by cloud patterns.

Some features of the mosaic in figure 9 on the previous day can be seen, as for example the vortex west of Ireland.

4. SUMMARY

TIROS has revealed a large degree of organization in the cloud systems over much of the earth's surface. The most striking patterns are the spiral cloud formations associated with large storms, some as much as 1,500 miles in diameter, observed in such places as the United States, North Atlantic Ocean, North and South Pacific Oceans, and the Indian Ocean (not shown here).

It is well known from radar observations that hurricanes are characterized by bands of clouds which spiral inward around a storm center. Although some suggestions have been made that extratropical cyclones also contain bands, over oceans, now as a direct result of TIROS, we see that the spiral banded cloud structure also exists around well-developed extratropical storms. Compare, for example, figures 7 and 8. In these storms the bands are separated by clear areas and range in width from several miles to a few hundred miles. Also the storm 400 miles west of Ireland (fig. 5), which is not a tropical storm, can be compared with the tropical storm north of New Zealand (fig. 8). In both cases, the cloud bands revealed the circular wind flow around the storm's center. But one of the sig-

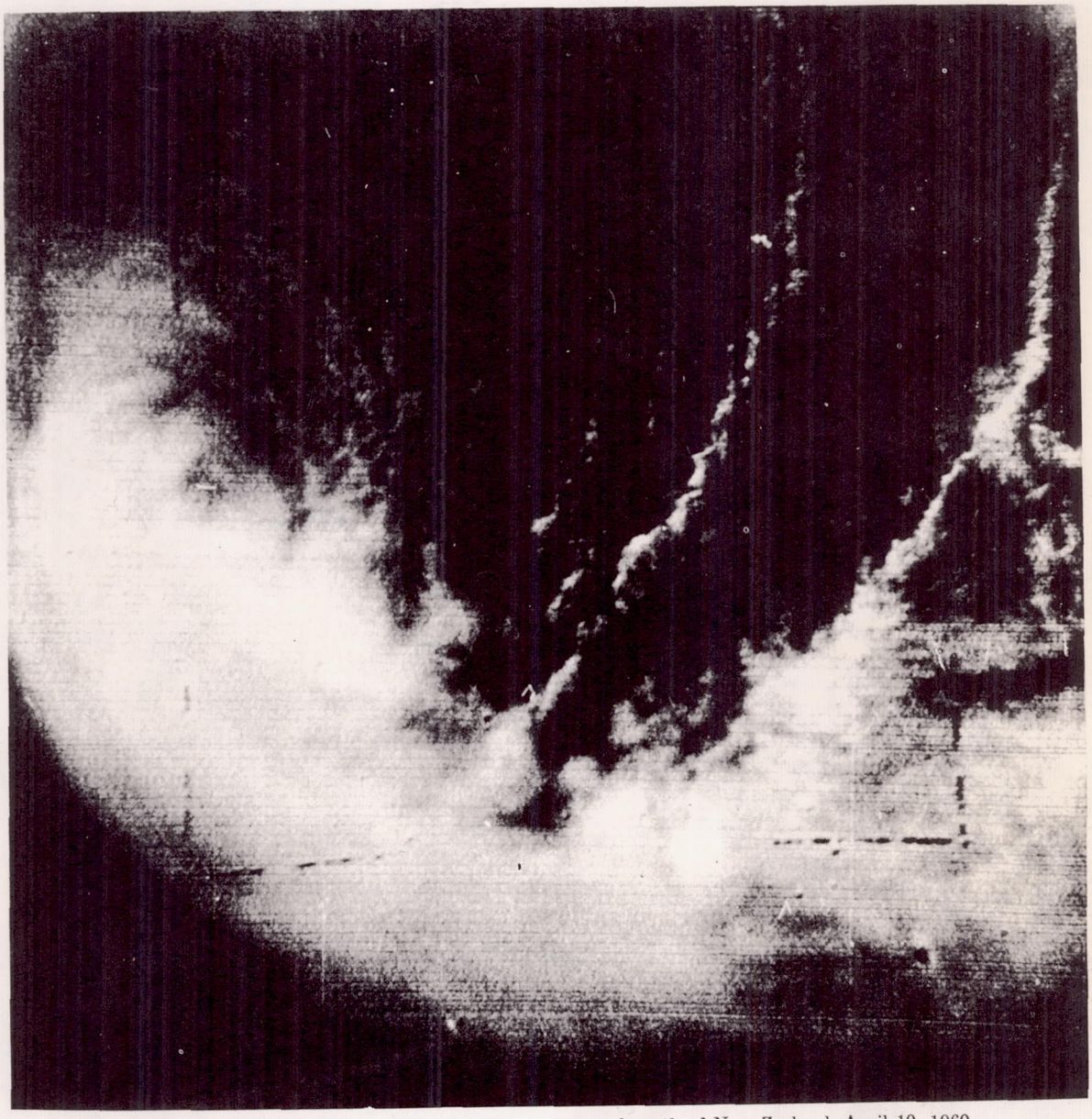

FIGURE 8.—TIROS picture of tropical cyclone centered north of New Zealand, April 10, 1960.

nificant results from TIROS is the clear indication that although storms have similarities, there may also be very marked differences. Study of the causes for these differences should reveal much about atmospheric processes and structures.

Thus far, storms observed over continents have not exhibited such fine banded structure as those over oceans. The continental storms have been associated with general cloud areas with the spaces between the bands either poorly defined or non-existent but the spiral nature of the storm was indicated more by the presence of a wedge of dry, cloudless air curving in toward the storm center behind a cold front, as shown by the Midwest storm of April 1 (fig. 2). A storm photographed on the east coast of the United States on the same day also showed this clearly (fig. 1). It had a similar cloud system without the marked banded structure. However, we do see again the cold cloudless air flowing in behind the cold front. Moreover, both of these storms contained frontal systems.

The photographs shown here are but a few of the more striking examples of cloud pictures revealed by TIROS. A systematic inspection of these cloud pictures is just

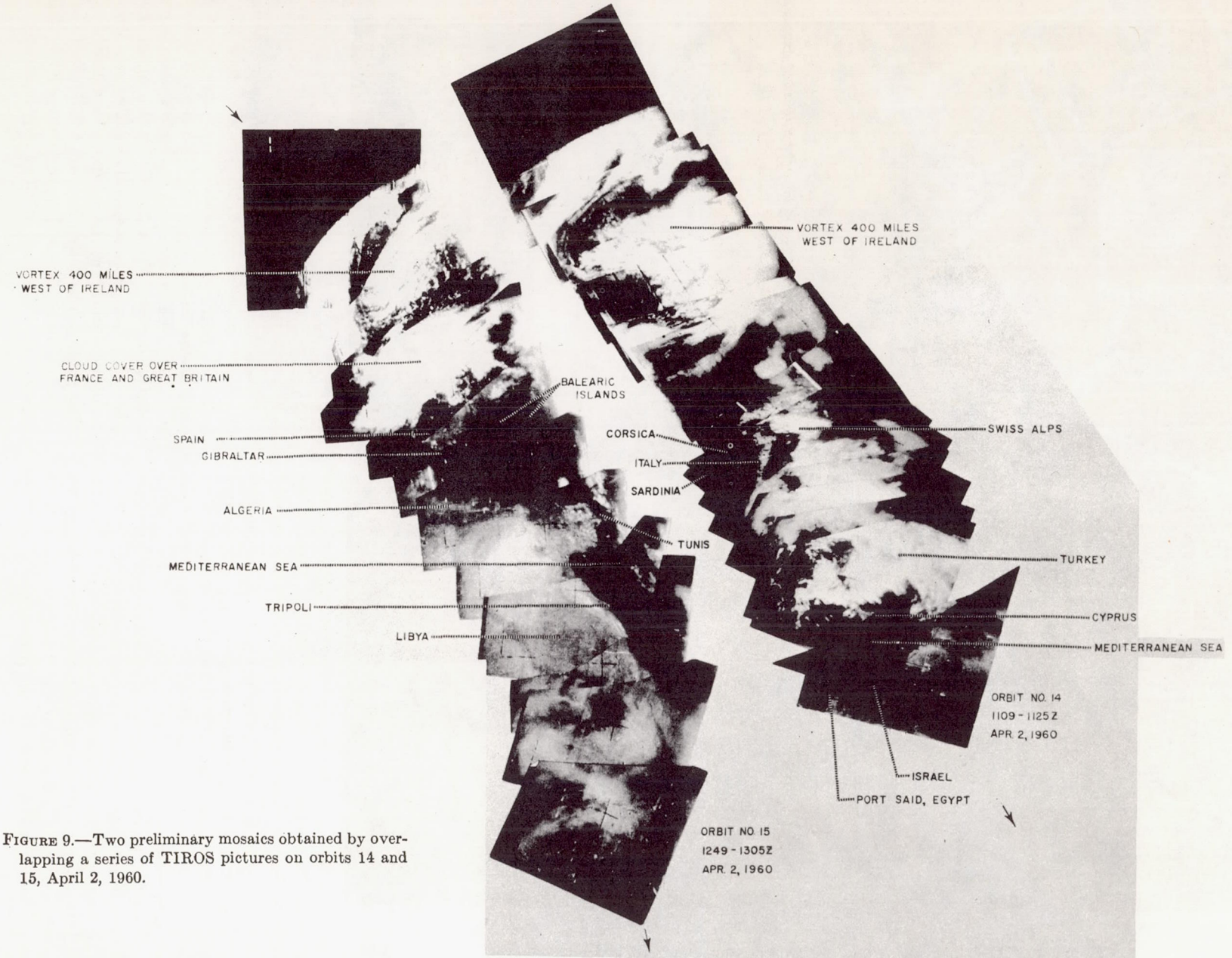

FIGURE 9.—Two preliminary mosaics obtained by overlapping a series of TIROS pictures on orbits 14 and 15, April 2, 1960.

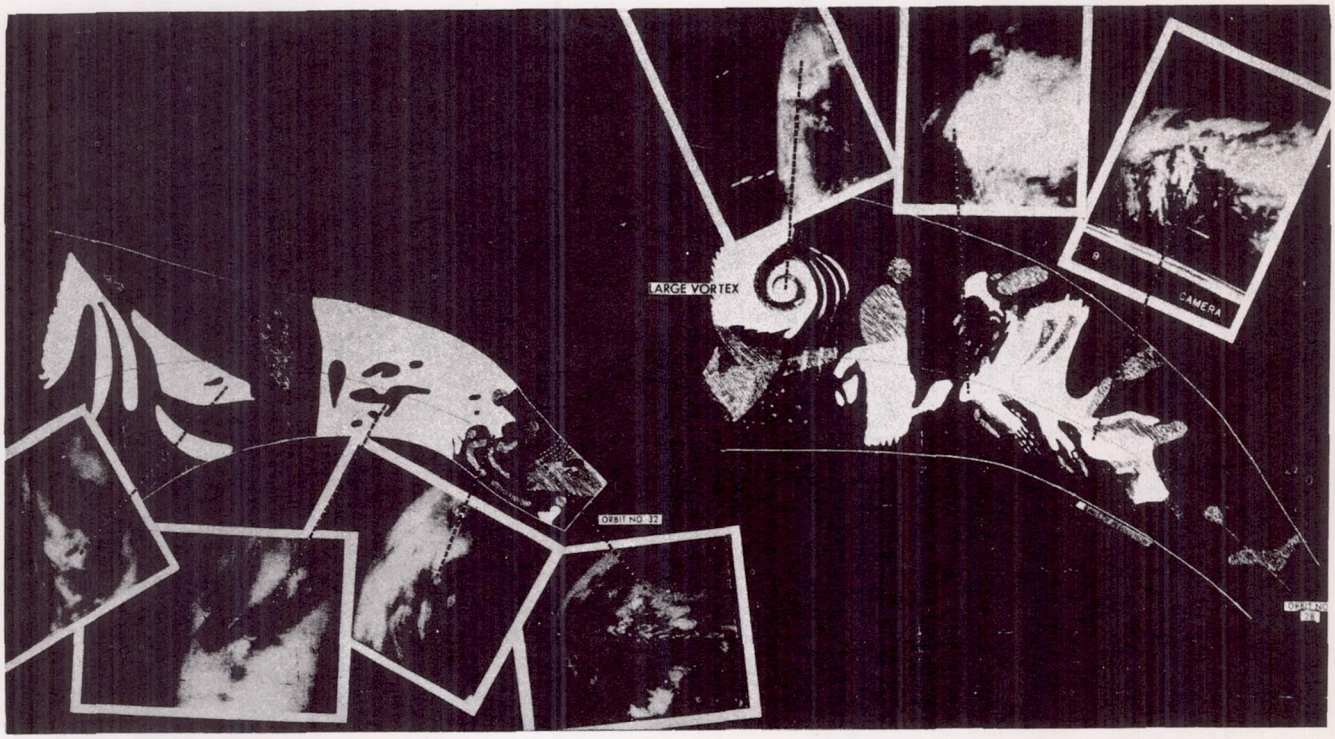

FIGURE 10.—A preliminary schematic representation of cloud patterns revealed by TIROS pictures over an area extending from the west coast of the United States into the Atlantic Ocean (orbit 32) and from the mid-Atlantic to the Near East (orbit 28), April 3, 1960. The solid white lines outline the area covered by pictures on these two orbits. Examples of pictures used in preparing the schematic cloud map are shown along the borders of the area.

getting under way. In the months ahead pictures are expected to reveal much new information about many atmospheric processes—from fair weather situations to incipient storminess to the growth of fully mature storms and their final dissipation.

ACKNOWLEDGMENTS

Thanks are due to L. T. Tourville of the Meteorological Satellite Section who helped with preparation of the photographs for publication; W. H. Hoecker, Jr., of the Office of Meteorological Research who performed the meticulous and laborious work in preparing figure 10 from scores of individual photographs; Marshall Kathan, Chief of the Drafting Section, who supervised and personally assisted in the speedy preparation of illustrations from which the figures were extracted; L. E. Johnson, E. R. Orr, J. H. Morrison, and A. Y. Gardner of the Printing Section who gave excellent service in reproduction of the photographs; James E. Caskey, Jr., the editor, who not only suggested publication of the paper but together with Mrs. Bernice Baddy of his staff assisted greatly in its preparation.

REFERENCES

1. S. Fritz, "On Observing the Atmosphere from Satellites—I. Cloud Observations," *Weatherwise*, vol. 12, No. 4, August 1959, pp. 139–144, 163–165.
2. W. G. Stroud, "Initial Results of the TIROS I Meteorological Satellite," *Journal of Geophysical Research*, vol. 65, No. 5, May 1960, pp. 1643–1644.

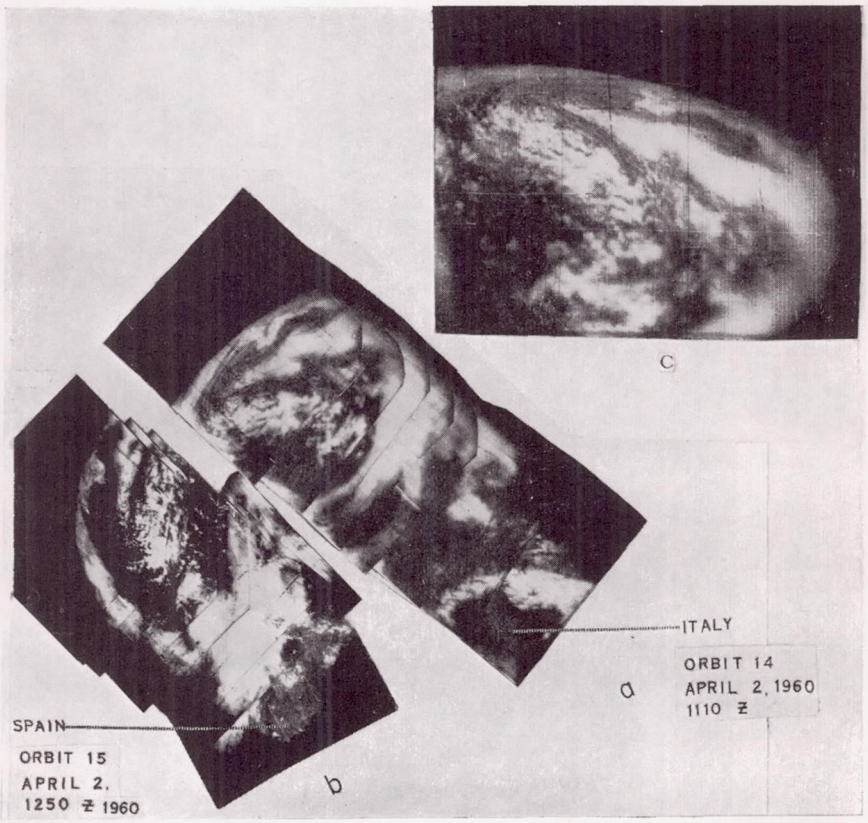

Figure 1. (a) Composite of frames photographed at about 1110 GMT, 2 April 1960, showing stratiform cloud surrounding cumuliform cloud in an Atlantic Ocean vortex. Italy appears just below an extensive bright area in the picture; this bright area is the snow-covered Alps. (b) Composite of frames photographed at about 1250 GMT, 2 April 1960, showing the same Atlantic Ocean storm, 100 min later. The eastern part of Spain is nearly cloudless. (c) Single frame showing continuous stratiform cloud.

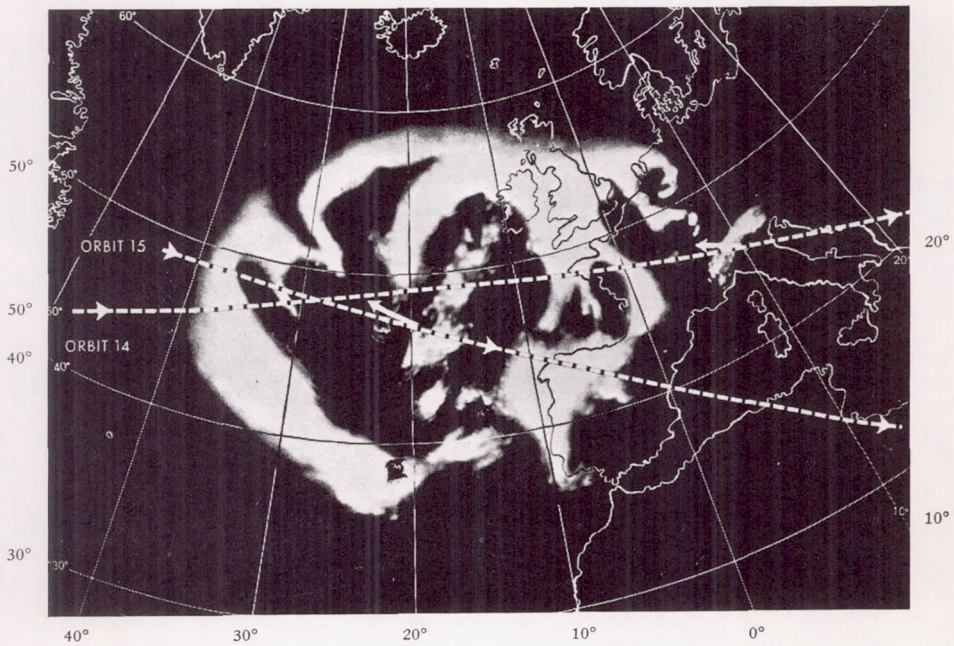

Figure 2. A sketch of the picture in Fig. 1 arranged in proper geographic location.

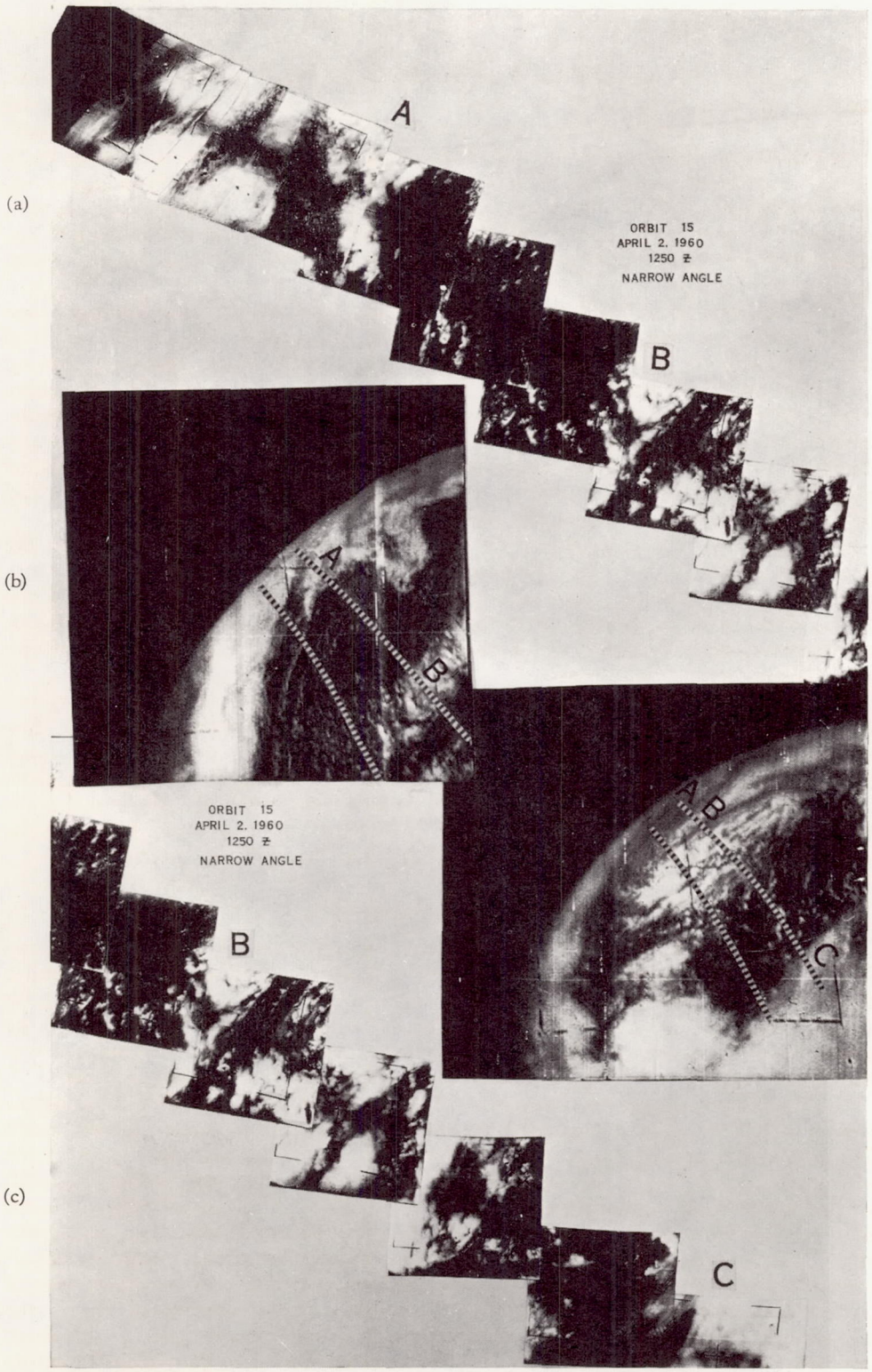

Figure 3. (a, b, c and d) Composite of narrow-angle camera pictures across centre of cloud system shown in Fig. 1 (b), with associated wide-angle pictures (see text).

introduced a means of utilizing the expressions of the homogeneous case in a nonhomogeneous medium. By substituting a proper mean half-width of the spectral lines, the correct transmission can be obtained. *Godson* [1955] later amplified this approach to the problem and *Kaplan* [1959*b*] has discussed it further. If we use

$$\bar{\alpha} = \frac{\int \alpha S \, dm}{\int S \, dm} \tag{9}$$

for α in (5), where $\bar{\alpha}$ is the mean line width over the nonhomogeneous path, and $\int S \, dm$ for Sm in (6), we may obtain τ in the atmosphere.

Line strengths are dependent only on temperature. The strength of a given line is

$$S_l = C_l \frac{\exp(-E_l''/kT)[1-\exp(-hc\nu_l/kT)]}{Q(T)} \tag{10}$$

where C_l is a constant for the line, E_l'' is the energy level of the lower state of the transition, ν_l is the wave number of the line, T is the temperature, and $Q(T)$ is the partition function. Over a limited temperature range, the partition function, evaluated by normal methods [see *Herzberg*, 1945] may be approximated by the quadratic

$$Q(T) = aT^2 + bT + c \tag{11}$$

Within the range of terrestrial temperatures, the coefficients $a = 0.002468$, $b = 0.9607$, and $c = 71.01$ give an excellent fit.

The intensity of upward radiation passing through the 1-mb level of the atmosphere has been calculated, using the above relations. Values of C_l were obtained from the line strengths given by *Yamamoto* [1958]. Equation 9 was written

$$\bar{\alpha} = \frac{\sum \alpha w S \, \Delta p}{\sum w S \, \Delta p} \tag{12}$$

where w is the mass of carbon dioxide in a unit pressure interval. $w = 4.80 \times 10^{-4}$ g/mb cm^2 corresponds to a mixture of 0.0310 per cent of carbon dioxide by volume. The usual relation $\alpha = \alpha_0 p/p_0\sqrt{T_0/T}$ was used, with $\alpha_0 = 0.064$ cm^{-1} at $T_0 = 300$°K and $p_0 = 1013.2$ mb [*Kaplan and Eggers*, 1956; *Yamamoto*, 1958]. The spectral

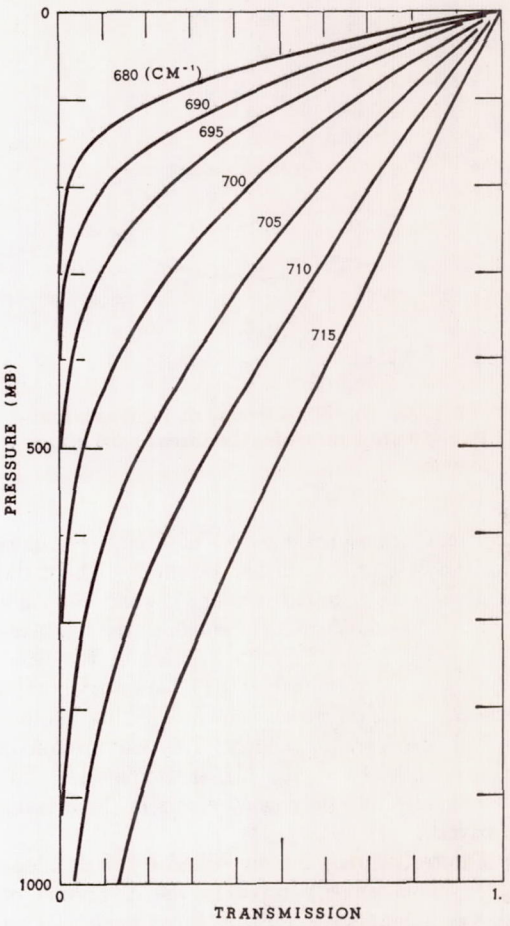

Fig. 2. Transmission between a given pressure and 1 mb plotted versus pressure; values are shown at various wave numbers in the R branch of the ν_2 fundamental.

interval used was the spacing of the lines of the sub-bands. That is, $D \approx 1.6$ cm^{-1}.

Several atmospheric models were used. Figure 1 shows three widely differing models chosen to illustrate the results of the calculations. Temperature versus the logarithm of the pressure is shown.

As might be expected, the calculations show that the transmission in the strongest parts of the P and R branches of the strongest sub-band is very weakly dependent on temperature, while the dependence increases going outward into the wings of the sub-band. Figure 2 shows an example of the transmission versus pressure for several spectral intervals. This result is for

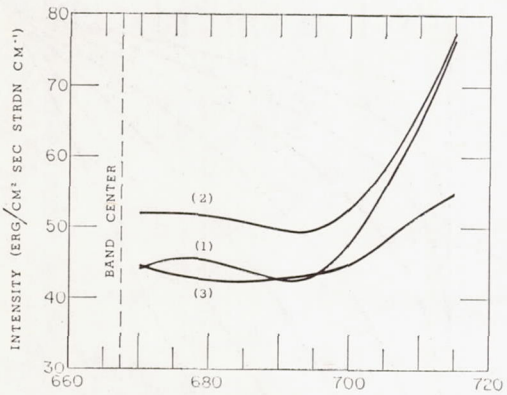

Fig. 3. Upward intensity at 1 mb as a function of wave number for the three model atmospheres.

the first atmospheric model of Figure 1 and is for the case of the vertical beam, $\theta = 0$. In the discussion to follow, the wings beyond 695 cm^{-1} will not be considered. Inasmuch as the temperature effect is small in the portion of the band that will be examined, it will be assumed that the transmission curves shown in Figure 2 apply to all atmospheric models. This assumption is not permissible at the higher frequencies, but it will introduce only small errors in the present analysis.

Figure 3 shows the smoothed spectral intensity versus wave number in the R branch of the ν_2 fundamental for the three models. This figure indicates the 'spectra' of the three atmospheres, within a limited spectral range, as they might appear to a scanning sensor that lacked the resolution required to show individual lines. It should be pointed out that the Q branch contributes significantly to the absorption within about 10cm^{-1} of the band center, and the methods used here must be supplemented by other techniques owing to the quadratic spacing of the lines in the Q branch.

It is now of interest to use the results of the calculations to invert the problem and to try to recover the temperature structure. As was stated earlier, the more simple experiment should be confined to the stratosphere in order to avoid the complications introduced by clouds. As can be seen from Figure 2, radiation from below 400 mb is received at wave numbers beyond 695 cm^{-1}. The tropopause cannot be expected to lie much below 400 mb, and, indeed, is nearer to 100 mb in the tropics. For illustrative purposes only, the spectrum out to 695 cm^{-1} will be used in the following discussion.

Measurements of radiation made from a satellite will be proportional to the specific intensity if the observed solid angle is small. If intensities are obtained in three wavelengths, we can choose to obtain the mean temperatures in three atmospheric layers or the temperatures and mean lapse rates in two layers. The latter approach is somewhat easier.

Equation 1 can be rewritten

$$I' = B_2' + \int_{p_2}^{p_1} \tau' \left[\frac{\partial B'}{\partial(\log p)}\right] d(\log p) + \int_{p_1}^{p_0} \tau' \left[\frac{\partial B'}{\partial(\log p)}\right] d(\log p) \qquad (13)$$

where $p_2 = 1$ mb, p_1 is the pressure dividing the two layers, and p_0 is the bottom of the lower layer ($p_0 = 400$ mb in this case). The prime refers to a given frequency. Two more equations can be written for other frequencies. It is now assumed that within a layer

$$\frac{\partial B}{\partial(\log p)} = \text{constant} = A \qquad (14)$$

At these frequencies this is very nearly the same as saying that

$$\frac{\partial T}{\partial(\log p)} = \text{constant} \qquad (15)$$

Log p, rather than p, is used here in order to conform more nearly to the gradients observed in the atmosphere. Equation 13 can then be written

$$I' = B_2' + A_a \int_{p_2}^{p_1} \tau' \, d(\log p) + A_b \int_{p_1}^{p_0} \tau' \, d(\log p) \qquad (16)$$

where a and b are the two layers. If the transmission is assumed to be independent of temperature, the integrals can be evaluated from the values of the transmission shown in Figure 2. Also, since the range of frequencies is small, one can say that $B_2'' \approx \beta'' B_2'$ and $B_2''' \approx \beta''' B_2'$, where the β's are constants and the A's are independent of frequency. There are now three equations:

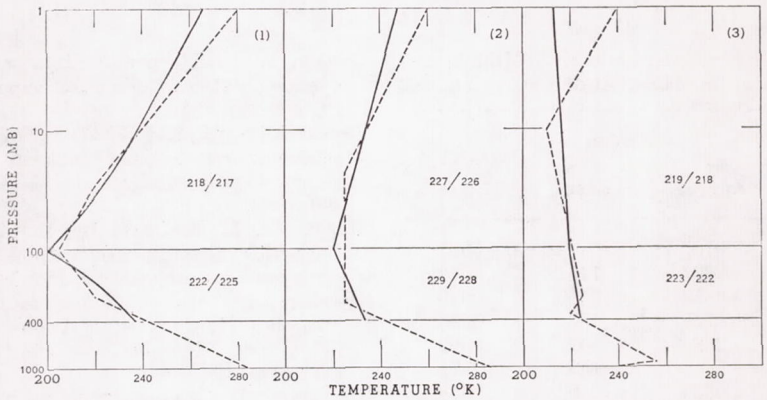

Fig. 4. Temperature structure in two layers derived from calculated intensities. The dashed lines are the original models; the solid lines are the derived structures. Respective mean temperatures in each layer are indicated. The slight curvature in the derived temperature gradients, particularly noticeable in case (1), is due to the fact that assumption (14) is not exactly commensurate with (15).

$$I' = B_2' + A_a D_a' + A_b D_b'$$

$$I'' = \beta'' B_2' + A_a D_a'' + A_b D_b'' \qquad (17)$$

$$I''' = \beta''' B_2' + A_a D_a''' + A_b D_b'''$$

where the D's are the integrals.

The frequencies chosen were $\nu' = 680$ cm^{-1}, $\nu'' = 690$ cm^{-1}, and $\nu''' = 695$ cm^{-1}. The β's were evaluated for $T = 250$°K.

Solving (17), with $p_1 = 100$ mb chosen arbitrarily, the results are shown in Figure 4. The dashed lines are the original models and the solid lines the inverse solutions. Also shown are the mean temperatures of the layers in the two respective cases. Mean temperature is here meant to be the mean by pressure.

There are some remarks that should be added to the foregoing discussion. First, the methods used here are not exact. The results of the calculations of upward intensity are, nevertheless, in very close agreement with those of *Yamamoto and Sasamori* [1960], which do not depend upon the approximation given by equation 8.

Second, other procedures in the inverse solution, such as that of *King* [1959], must be examined. Also, the frequencies chosen here are probably not the optimum. *Yamamoto and Sasamori* [1960] have found that a 5-cm^{-1} spectral interval covering the Q branch is more opaque than intervals in the strongest parts of P and R branches.

Third, the use of the Curtis-Godson approximation over the ranges of pressure in this study should be considered. This has already been discussed by *Godson* [1955], *Kaplan* [1959*b*], and *Yamamoto and Sasamori* [1957], but it was deemed desirable to conduct a test directly applicable to the present work. The transmission was calculated by the approximate method at 680 cm^{-1} for the ν_2 fundamental, using atmosphere (1) of Figure 1; and it was calculated exactly by performing numerically the operation

$$\tau = \frac{2}{D} \int_{\nu_0}^{\nu_0 + D/2} \exp\left[-w \int_{p_2}^{p} k(\nu, p)\, dp \right] d\nu \qquad (18)$$

where, for an Elsasser band,

$$k(\nu) = \frac{S}{D} \frac{\sinh \beta}{\cosh \beta - \cos s} \qquad (19)$$

and

$$s = \frac{2\pi(\nu - \nu_0)}{D} \qquad (20)$$

Results of these calculations are indicated in Table 1, which shows the transmission obtained by the two procedures at several values of p. The errors are seen to be small, being not more than 1 per cent throughout the absorbing layer. Errors of this magnitude will not alter the results of the present study.

Finally, one might ask why the upper level

TABLE 1. Transmission between 1 Millibar and Level p in the ν_2 Fundamental of Carbon Dioxide

p, mb	Transmission		Error
	Approx.	Exact	
11.0	.9102	.9113	.0011
27.2	.7727	.7767	.0040
42.8	.6450	.6520	.0070
65.0	.4758	.4844	.0086
93.0	.2985	.3077	.0092
128.8	.1457	.1531	.0074
173.4	.0509	.0552	.0043

was taken as 1 mb. It was assumed, and with considerable justification, that the absorption (less than 1 per cent) in the top 1 mb of the atmosphere would not significantly influence the results. The departure from thermodynamic equilibrium and the increasing importance of Doppler broadening of the spectral lines at higher levels require a modification of the methods used here. In the Q branch, one must consider these matters, since the absorption in the top 1 mb is about 5 per cent [*Yamamoto and Sasamori*, 1960].

Acknowledgments. I should like to express my appreciation to F. Van Cleef for his efforts in programming this complex problem for the electronic computer.

This work was supported by the National Aeronautics and Space Administration.

References

Curtis, A. R., Discussion of paper by R. M. Goody, 'A statistical model for water-vapour absorption,' *Quart. J. Roy. Meteorol. Soc.*, *78*, 638–640, 1952.

Elsasser, W. M., Heat transfer of infrared radiation in the atmosphere, *Harvard Meteorol. Studies*, no. 6, 1942.

Godson, W. L., The computation of infrared transmission by atmospheric water vapor, *J. Meteorol.*, *12*, 272–284, 1955.

Greenfield, S. M., and W. W. Kellogg, Calculations of atmospheric infrared radiation as seen from a meteorological satellite, *J. Meteorol.*, *17*, 283–290, 1960.

Hagemann, F., J. Gray, Jr., L. Machta, and A. Turkevich, Stratospheric carbon-14, carbon dioxide, and tritium, *Science*, *130*, 542–552, 1959.

Herzberg, G., Molecular Spectra and Molecular Structure II, Infrared and Raman Spectra of Polyatomic Molecules, D. van Nostrand Co., Princeton, 1945, chap. V.

Kaplan, L. D., A quasi-statistical approach to the calculation of atmospheric transmission, *Proc. Toronto Meteorol. Conf.* pp. 43–48, 1953.

Kaplan, L. D., Inference of atmospheric structure from remote radiation measurements, *J. Opt. Soc. Am.*, *49*, 1004–1007, 1959*a*.

Kaplan, L. D., A method for calculation of infrared flux for use in numerical models of atmospheric motions, in *The Atmosphere and the Sea in Motion*, edited by B. Bolin, Rockefeller Inst. Press, New York, 170–177, 1959*b*.

Kaplan, L. D., and D. F. Eggers, Jr., Intensity and line-width of the 15-micron CO_2 band, determined by a curve-of-growth method, *J. Chem. Phys.*, *25*, 876–883, 1956.

King, J. I. F., Deduction of vertical thermal structure of a planetary atmosphere from a satellite, *Aerosciences Lab., Gen. Elec. Co., Tech. Info. ser. R59SD477*, Dec. 1959.

U. S. Weather Bureau, Conference on infrared measurements from satellites, transcript of proceedings, 83 pp., 1959.

Yamamoto, G., Calculations of the absorption of the 15μ carbon dioxide band, Sci. Repts. Tôhoku Univ., Series 5, *10*, 37–57, 1958.

Yamamoto, G., and T. Sasamori, Numerical study of water vapor transmission, Sci. Repts. Tôhoku Univ., Series 5, *8*, 36–45, 1957.

Yamamoto, G., and T. Sasamori, Further studies on the absorption by the 15μ carbon dioxide bands, in preparation, 1960.

(Manuscript received August 11, 1960; revised October 24, 1960.)

taken with the wide-angle camera, as was the original series, also showed the Gulf, but from a greater distance. This time-sequence of pictures over 48 hours has allowed deductions not possible from a single series.

Figure 1 shows a composite of wide-angle photographs taken at about 1500 GMT on April 1. Labrador and Quebec are seen as the gray area in the upper part of the photograph; Newfoundland is on the right; the St. Lawrence River is on the left; the lower part is cloud cover over the southern half of the Gulf. The Gaspé Peninsula and Anticosti Island can be distinguished. The synoptic map at this time showed a large high pressure system in northern Canada centered over Hudson Strait. A frontal system ran south of the High through a weak Low over southeastern Newfoundland, then southwestward through another weak Low off the New England coast. New Brunswick, the lower part of the Gulf, and most of Newfoundland were overcast, while the southern shore of Quebec Province reported mostly scattered clouds. From figure 1 it can be seen that the northern part of the Gulf was clear.

The dark areas are mainly water, while the light areas are mostly land or clouds. In the upper right-hand corner is the Strait of Belle Isle between Labrador and Newfoundland. The grayness in the Strait indicates that it is probably ice-covered. Extending southwestward from the Strait, parallel to but off the coast, is another thin streak of ice which broadens. The main band continues parallel to the coast to the northeastern shore of Anticosti Island, and a branch extends southward between Anticosti Island and Newfoundland to the edge of the clouds. A bright patch can be seen around the eastern end of the island and another just south of the island blends with the clouds. A U-shaped ice pattern can also be readily identified jutting into the St. Lawrence River from the northern coast of the Gaspé Peninsula. Other patterns of ice can be seen just south of the Strait of Belle Isle near Newfoundland.

Figure 2 is a composite of narrow-angle pictures taken at about 1430 GMT on April 2. Newfoundland is on the right; Anticosti Island is in the upper center; the Gaspé Peninsula and the St. Lawrence River are in the lower left. Approximate latitude and longitude lines are shown. The front of the previous day had moved well out to sea, and a high pressure ridge extended southward from the High in northern Canada. The lower St. Lawrence River, the Gulf, and Newfoundland were almost cloudless.

This composite consists of pictures read out directly from the satellite when it was close to the horizon of the monitoring station. The angle of view is quite oblique,

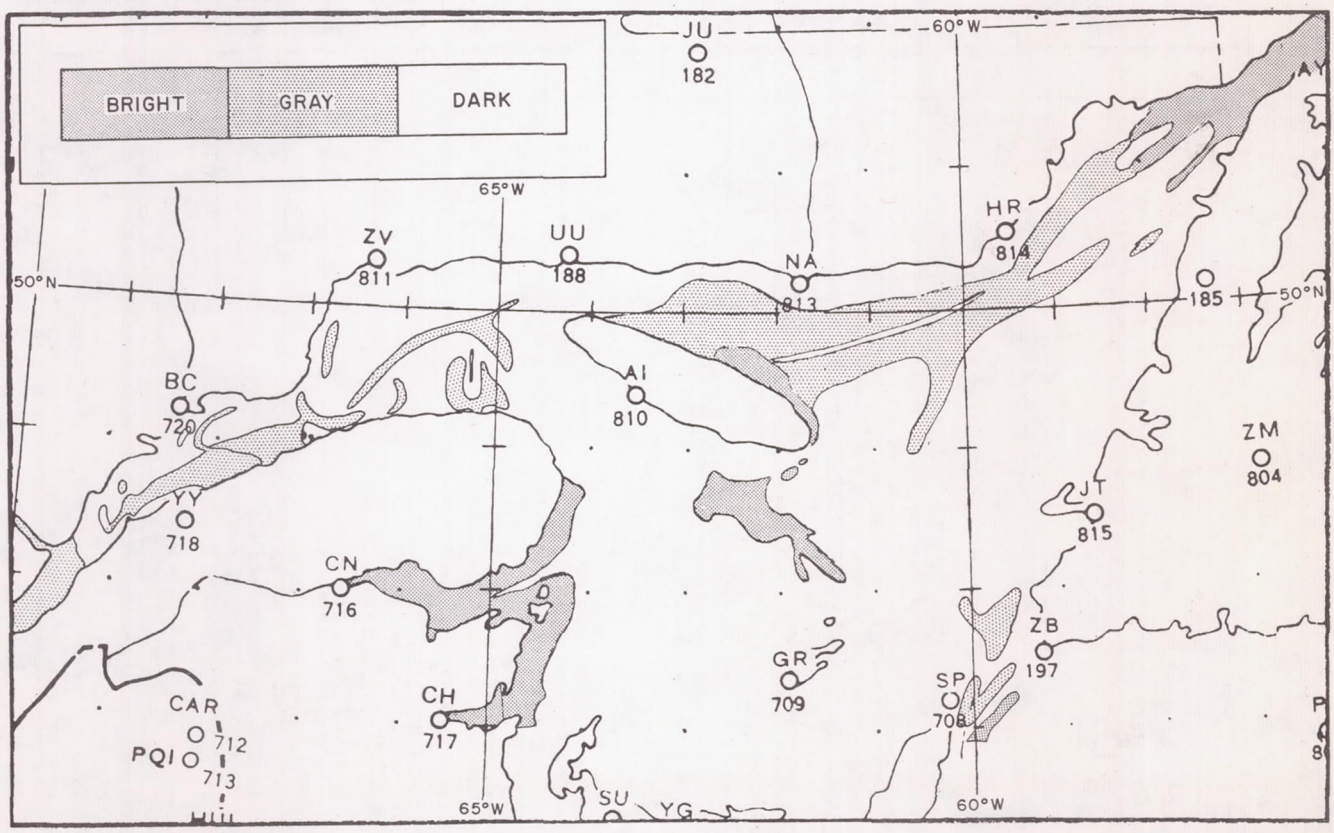

FIGURE 3.—Analysis of ice shown in figures 1 and 2.

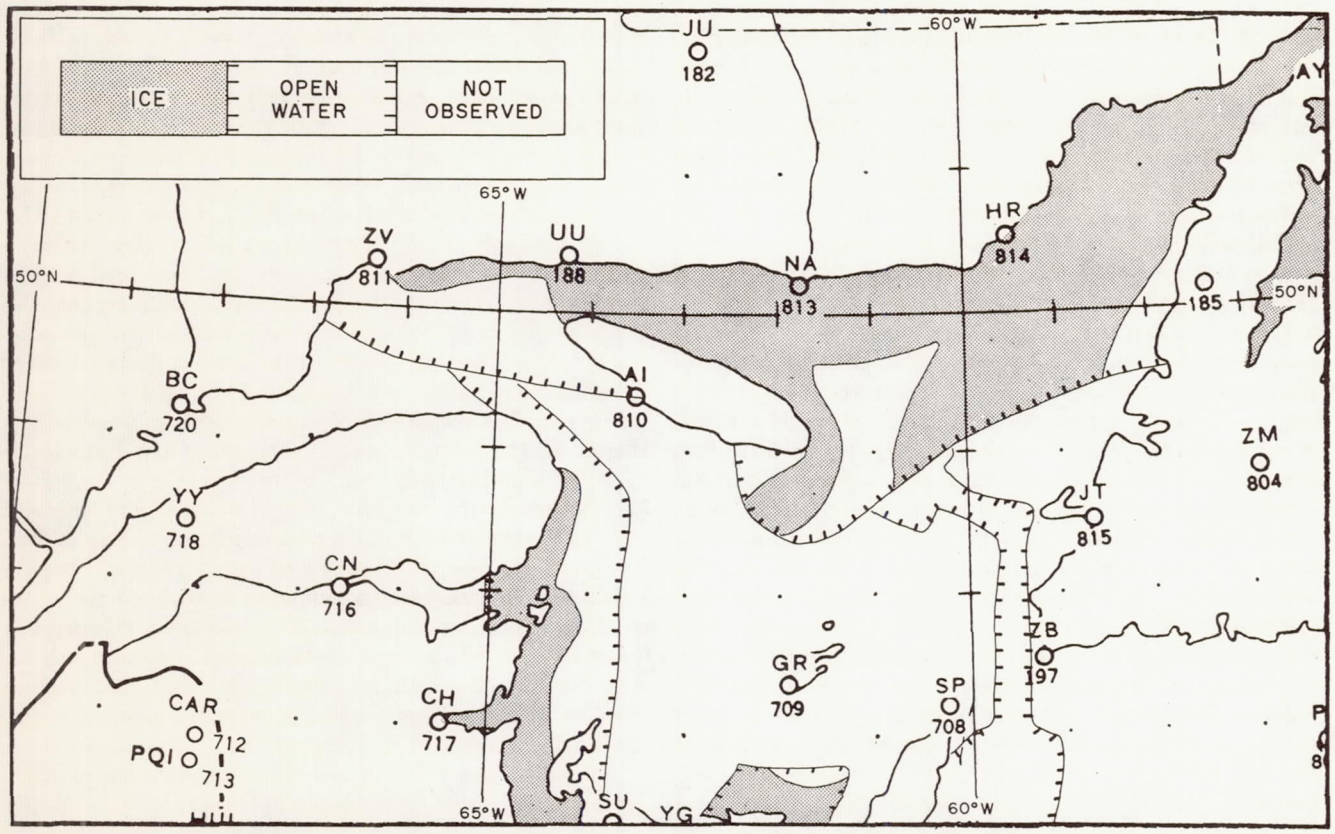

FIGURE 4.—Canadian Meteorological Service aircraft observations of ice on March 23 and 26, 1960.

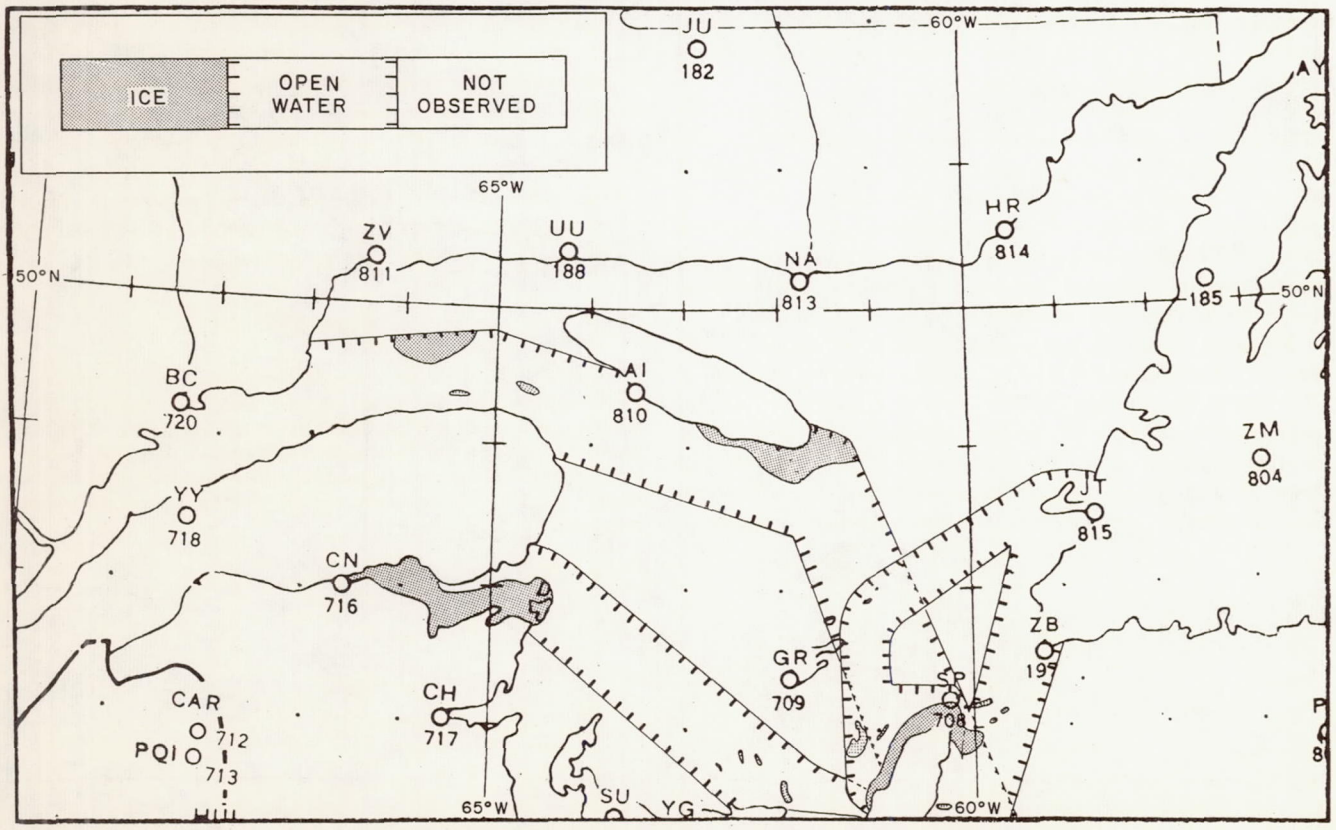

FIGURE 5.—Canadian Meteorological Service aircraft observations of ice on April 6 and 7, 1960.

resulting in considerable foreshortening, as indicated by the shapes of the Gaspé Peninsula and Anticosti Island. One of the most interesting features in this picture is the large bright patch just south of the island, which is believed to be a large ice floe that has broken away from a pack along the island, carried south by the persistent northerly winds. The general configuration of the northern portion of the floe seems to support this hypothesis. Although not so clear as in figure 2, the floe is also evident in figure 1 and on the pictures taken on April 3, not shown here. There appears to be dense, probably pack, ice on the lower northeastern shore of Anticosti Island, while loose ice exists along the upper part of this shore. Near the upper edge of figure 2 at about 60° W., is the southern tip of the band of ice seen in figure 1 to extend southward between Anticosti Island and Newfoundland to the clouded area. The St. Lawrence River from the city of Quebec (not visible, but near the extreme lower left corner) is partially obscured by a thin layer of cirrus clouds, which ends about 80 to 100 miles northeast of Quebec. From there to about 49° N the river is more clearly visible, with loose ice appearing in indistinguishable patterns. Beyond this point and along the northern coast of the Gaspé Peninsula the ice appears in more dense, curved streaks. From Gaspé Bay southward toward Miramichi Bay the shoreline appears highly reflective. Chaleur Bay looks ice-covered, except near the entrance. Part of Gaspé Bay appears to be open water. Some elongated streaks appear off the southwestern tip of Newfoundland, including one bright streak. The rest of the Gulf contains a few less clearly visible, more diffuse patterns.

Figure 3 shows an analysis of the water areas in the Gulf of St. Lawrence, derived from the satellite information contained in figures 1 and 2. The dense dots indicate areas of high reflectance and, presumably of highly reflecting ice; the open dots indicate gray areas, which are presumed to be ice areas of medium reflectance; unmarked areas appear dark and are interpreted as open water or ice areas of very low reflectance.

Figure 4 shows ice conditions as observed on March 23 and 26 from Canadian aircraft. No attempt was made in this figure to distinguish the type or the density of ice; only open water or ice have been shown. The boundaries of the observed areas are indicated. The anvil-shaped area of open water east of Anticosti Island was observed by the satellite, as shown in the analysis and in figure 1. The ice along the southeastern tip of the island may be associated with the floe seen in figure 2. The northern part of the Gulf was almost entirely ice-covered on March 23. Observations on the 26th showed considerable ice along the eastern tip of the Gaspé Peninsula, in Chaleur Bay, and southward along the New Brunswick coast. Open water was indicated off the southwestern part of Newfoundland, then northwestward toward Anticosti Island.

Figure 5 shows aircraft-observed ice conditions on April 6 and 7. Most of the area observed on these days was open water, although some ice still remained in Chaleur Bay, on the southeastern tip of Anticosti Island, and in scattered patches along the path of observation. Much of the area observed on April 7 was outside the satellite photographs.

The sensitivity of the television of TIROS I has been set to render the best reproduction of clouds. It is possible that one might prefer greater sensitivity in order to reveal ice areas which are nearly as dark as the water. In the present case it has been found that the range of grayness extends from white down to the noise level of the system. A greater sensitivity might reveal more of the ice of low reflectance while permitting ice of higher reflectance to appear to be white

On the other hand, these pictures have been taken under unfavorable circumstances, looking at very oblique angles. Pictures taken in the vertical are generally much superior and would reveal more.

It should be mentioned that the problem of distinguishing between ice and clouds is not severe. The existence of pictures on three days has permitted a positive identification of the large floe as ice rather than cloud. A satellite is capable of at least daily observations and only persistent thick clouds should limit knowledge of ice conditions. Ice can definitely be observed in photographs from satellites and it is hoped that in the future satellites can contribute to ice surveys.

ACKNOWLEDGMENT

We thank the Director of the Meteorological Service of Canada for furnishing the ice survey charts, and also members of the Division of Oceanography, U.S. Navy Hydrographic Office, and Mr. A. E. Sik of the Forecasts and Synoptic Reports Division, U.S. Weather Bureau, for assistance in assembling the ice data. We are particularly indebted to H. Wexler for his suggestions and comments.

USCOMM-WB-DC

Reprinted for private circulation from
BULLETIN OF THE ATOMIC SCIENTISTS
Vol. XVII, Nos. 5–6, May–June 1961

Meteorological Satellites

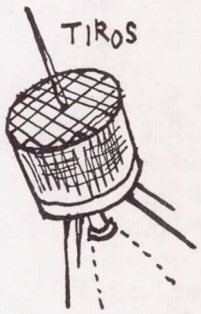

H. WEXLER and D. S. JOHNSON

FOR THE first time in history, there exists an observing platform which can detect atmospheric conditions long before local meteorologists relying on conventional techniques may be aware of them. This platform is the meteorological satellite, which, even in its present primitive stage, has already contributed significantly to meteorological developments through depiction of cloud systems and their interpretation for daily weather prediction, and by collecting basic physical data such as measurements of the radiative exchange between the Earth and Sun and space. Future observations will include the temperatures of cloud tops and the Earth's surface, the average temperatures of layers of the clear atmosphere, concentrations of water vapor, ozone and other properties not yet envisaged.

Man is immersed in a working fluid of a global extension—the Earth's atmosphere—a fluid so massive that there are nearly 2 million tons of it for each person on Earth. From above, it is penetrated by energetic particles and radiations, and from beneath, deformed, restrained, heated and cooled as it passes over the irregular Earth surface in its endless quest to equalize its energy imbalances, thus creating wind and weather. The atmosphere performs countless cycles of interrelated phenomena of every size, from global to microscopic. They are all important. For example, those actions involving water vapor—which comprises only about 0.2 per cent of the total mass of the atmosphere—nevertheless have such a profound effect on our planet's heat balance that without them the mean temperature of the Earth would drop by 40 degrees centigrade.

Harry Wexler is director of meteorological research for the U.S. Weather Bureau. David S. Johnson is chief of the Weather Bureau's meteorological satellite laboratory.

Reprinted from the Bulletin of the Atomic Scientists, May-June 1961, by permission of the Bulletin.
To appear in the Challenges of Space, University of Chicago Press, Spring, 1962.

Meteorologists have traditionally been handicapped by having only fragmentary knowledge of what is going on in the atmosphere at any time. About a century ago, national meteorological services were established to provide forecasts to the public. As observing networks expanded geographically and in altitude, meteorologists continued their audacious attempts to predict the future state of a three-dimensional system whose initial state was inadequately known. Because of insistent public demand, the forecaster makes his daily predictions and up to a certain point is generally successful. His successes, however, are generally limited to forecasts for not more than a few days in the future and for areas in the midst of or close to a fairly dense observing network so that unknown disturbances from distant and sparsely observed regions have not had time to exert significant influence. Even so, disturbances such as tornadoes or severe thunderstorms can develop suddenly or slip through the mesh of observing stations.

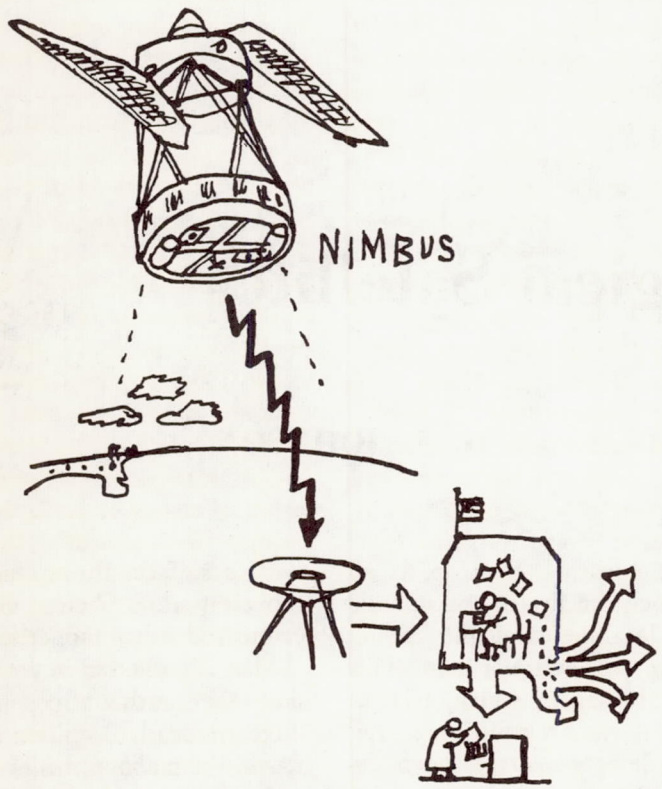

Pictures of such storms, continuous in space and time, can now be provided by the proper distribution of surface radars and meteorological satellites. Radar observations show the three-dimensional array of many cloud types, particularly those with precipitating particles, over limited areas (200–300 kilometer radius) surrounding the radar set. In Earth-orbiting satellites, meteorologists have for the first time an observing platform with a capability commensurate with the global extent of the atmosphere, not only in observing what is going on but in communicating observations and warnings over the entire world.

Until recently, high altitude photographs of large cloud systems for meteorological research have been available as the result of a relatively few rocket flights. The V-2 rocket photographs at White Sands, New Mexico, in 1947 were among the first; then followed the Aerobee photograph of an upper cyclonic vortex over Texas in October 1954. In August 1959, pictures obtained from an Atlas nose cone showed a frontal cloud system 3000 kilometers long, extensive lines of tropical clouds, and cellular cloud patterns over the north Atlantic ocean. In April–June 1960, 14,000 high quality cloud photographs were obtained over the world between 55 degrees north and 55 degrees south latitude by the meteorological satellite Tiros I. These revealed spiral cloud bands associated with cyclonic vortices 800 to 1500 kilometers in diameter, cellular arrangements of cumuliform clouds 50 to 80 kilometers in diameter resembling in appearance the Bénard cells studied in the laboratory, and frontal cloud patterns which confirm in a remarkable manner the classical Norwegian model of cyclone families. In general, the cloud pictures from the Tiros satellites reveal an unexpectedly high degree of organization and unsuspected scales of local activity in atmospheric motions. Full interpretation of these natural "weather maps" will require intensified empirical, laboratory, and theoretical research in the dynamics of convection and vortex flow.

The Tiros I photographs also illustrate in a dramatic way the potential usefulness of satellites in the detection of severe storms by photographing the unique spiral cloud structure of a hurricane near New Zealand and a large cumulonimbus cloud system in the midwestern United States which later produced tornadoes. Snow and ice areas over land and oceans were also observed.

Cloud observations from satellites, once they serve their immediate forecast use, are valuable in meteorological research. They can be used to establish for the first time a truly global cloud census, to draw average charts of world cloud cover by months or other periods, and to note long-time variations in cloud amount and distribution. The world cloud cover is the most important component in determining the Earth's albedo and serves as a natural thermostat to keep the world temperature within narrow limits. A larger than average cloud cover can reflect more solar radiation and cool the Earth, thus reducing the convection currents and cloud cover. A smaller cloud cover will enable more solar radiation to heat the Earth's surface and thus cause more clouds to form.

A second Tiros satellite was successfully placed in orbit on November 23, 1960 and produced useful cloud photographs for more than two months.

In addition to the television cameras identical to those used on Tiros I, Tiros II carries two sets of radiation sensors. One radiation instrument relies on the mo-

tion. The height of the freezing level in the atmosphere could also be inferred from the characteristic radar echo produced when ice and snow begin to melt after falling below the freezing level in the atmosphere. Further engineering development may ultimately permit the use of radar for detection of clouds, including measurements of the height of the bases and tops of various cloud layers beneath the satellite.

Theoretical studies have recently shown that the mean temperature of several layers of the atmosphere in at least the high troposphere and stratosphere can be determined from a series of high resolution spectrometric measurements of the radiation emitted by the Earth's atmosphere in various portions of the 15-micron carbon dioxide band. A spectrometer for this experiment is now under development. The same spectrometer is also being designed to measure the radiation received in a narrow spectral interval centered at 11.1 microns. The gaseous atmosphere is transparent to radiation at this wavelength so that the radiation received by the instrument would be proportional to the temperature of the Earth's surface or cloud tops within the field of view of the instrument.

Great strides have been made in recent years in utilizing digital computers to numerically predict the weather by solving simplified forms of the equations of atmospheric motion. The procedures presently used require quantitative observations as input to the computer. The aforementioned temperature measurements will likely contribute to numerical prediction as will the vertical velocity field as deduced from cloud pictures.

Present numerical prediction models require upper air wind velocities and some parameter directly related to the height of selected constant pressure surfaces in the atmosphere. It has been suggested that balloons be injected into the atmosphere which will move with the wind on surfaces of constant density. A network of balloons circling the globe at three different levels and equipped with temperature sensors would go a long way toward permitting numerical prediction on a global basis. Polar orbiting meteorological satellites might be used for locating the balloons with respect to the Earth's surface and receiving the temperature data from the balloons. The change in the position of a given balloon between observations would yield the mean wind during that period. The observational data could be processed at a central location before international dissemination.

A polar orbiting satellite system of the Nimbus type, while providing rather frequent observations of the whole globe, does not meet the meteorologist's objective of continuously monitoring the world's weather. A satellite in an equatorial orbit and synchronous rotation with the Earth, 35,700 kilometers above the surface, will appear to be stationary. Four such satellites equally spaced about the equator would provide a system of observing platforms capable of viewing all of the Earth's surface continuously in the zone between 60 degrees north and south latitude. The observational coverage of these "stationary" satellites would be complemented in the polar areas by the Nimbus type of satellite.

It only appears feasible to obtain cloud observations from stationary satellites because of their great altitude above the Earth's surface. These satellites might be equipped with low resolution cameras which would provide a new global cloud map (except for polar areas) every few minutes to any station having the proper receiving equipment and located within "line of sight" of one of the four stationary satellites. Other cameras capable of viewing smaller areas in greater detail also might be included in the satellites. The orientation of these cameras could be controlled by regional forecast centers to study critical areas such as developing storms.

International Aspects

It is quite clear from the foregoing that the advent of meteorological satellites will have a strong impact on operational and research meteorology throughout the world. In promoting international cooperation in these areas, it is anticipated that the World Meteorological Organization (WMO) and the Committee on Space Research (COSPAR) will play important roles.

The World Meteorological Organzation, affiliated with UNESCO and in existence since 1950, is the lineal descendant of the International Meteorological Organization, established in 1878. The WMO, composed of 108 members, has these purposes: the facilitation of worldwide cooperation in the establishment of observing networks, the promotion of rapid exchanges of weather information, the encouragement of standardization of meteorological observations, the application of meteorology to transportation, agriculture, etc., and the encouragement of research and training in meteorology.

In this framework of international cooperation in meteorology extending back 83 years, the appearance of meteorological satellites presents some novel aspects and opportunities. First, in contrast to most conventional observing stations, the satellite observatory is not at a fixed location in the home territory or on the high seas. Earth-orbiting satellites are truly global in their range and thus enable the meteorologists of the launching country to observe atmospheric phenomena over their area and outside areas more rapidly and more completely than can be done by local meteorologists and to make some measurements which cannot be done at all by conventional means no matter how dense the station network is. Since some of the phenomena observed by meteorological satellites may have rapid and serious consequences to the safety of the population and to the economy of a nation, it is imperative that meteorological

satellite information be conveyed speedily to all the nations. This can be done in several ways:

—*Read-out of data by the launching country* which relays data summaries on international meteorological circuits by means of coded messages or by facsimile. This system of notification introduces delays of several hours which may seriously limit the value of the information.

—*Read-out of data by individual nations or groups of nations.* This would seem to be the most efficient way of disseminating such information and putting it to immediate use but, as indicated earlier, involves rather expensive equipment of the order of $3 million or more per receiving station and would complicate the satellite instrumentation if all data were to be transmitted in this manner. A more realistic possibility would be the continuous transmission of some of the data (such as cloud pictures over a limited area) with the remaining data being received and processed at a central location before international transmission.

—*Communication satellites.* Here the launching nation could receive the information from its read-out stations and transmit it in digested and analyzed form to other nations via communication satellites. Raw information from meteorological satellites might also be relayed via communication satellites directly to central processing centers not in line of sight of the meteorological satellites.

A small beginning has been made in limited international release of meteorological satellite information from Tiros II. Whenever meaningful data were obtained for the southern hemisphere, these were transmitted by word message to the International Antarctic Analysis Center at Melbourne, Australia where meteorologists of several nations (including the U.S.) are cooperating in studying the meteorology of a major portion of the southern hemisphere. Also daily transmissions of cloud charts by U.S. Navy radio facsimile were beamed abroad for fleet units and received by other nations within range of these transmissions. The WMO informed its member countries of these transmissions and provided pertinent communication information.

WMO can play an important role by keeping its members informed of the launchings of meteorological satellites, their orbits, heights, periods, characteristics of the sensing equipment, frequency and power of the radio transmissions, etc. It could encourage the member countries to participate in the program either by launching meteorological satellites in desirable orbits which supplement those launched by other countries, by assisting in the tracking and receiving of the transmitted data and by taking valuable auxiliary observations such as additional upper air soundings, cloud observations, etc. The WMO could also promote the dissemination of such data and stimulate their use and interpretation by distributing literature and arranging for the visits of meteorologists trained in the new techniques or by sending meteorologists to countries which have launched meteorological satellites.

COSPAR, the nongovernmental Committee on Space Research organized by the International Council of Scientific Unions (ICSU) which sponsored the International Geophysical Year, could encourage and coordinate meteorological satellite experiments and could, because of its broad representation from the international scientific community, draw upon a wealth of knowledge to suggest new meteorological experiments and to promote the design, development and testing of new observing techniques. These techniques, based on developments in the fields of spectroscopy, electro-magnetic radiation, particle dynamics, etc., may depart widely from conventional meteorological instrumentation.

The interplay of the various scientific disciplines engaged in research in space may lead to the unexpected development of valuable new tools and concepts in meteorology. These might include detailed observations of radiations and energetic particles from the Sun and space which affect the Earth's atmosphere, and observations of atmospheric properties of other planets, as discussed previously.

World Data Centers, containing meteorological satellite data for research purposes by all meteorologists, would also be maintained. World Data Center A, Asheville, North Carolina, is now receiving data from U.S. meteorological satellites.

In considering a world system of meteorological satellites for both operational and research use, the question of financial support arises. Who would pay for the satellites? Will this be done by individual countries or will there be a sharing of the costs by many countries, with a few countries designated to do the launching? For the foreseeable future, it is likely that costs of the meteorological satellites will be borne by individual launching countries but other countries might establish their own read-out stations. However, it is interesting that Dr. A. Viaut, president of the WMO, on the occasion of its tenth anniversary, stated; "It would not be realistic to mention—except as an ideal not likely to be attained for a very long time yet— the possibility of a single world meteorological budget." Until this day arrives there is ample opportunity for continued increase of international cooperation in meteorology, and it is expected that meteorological satellites will contribute strongly to this movement.

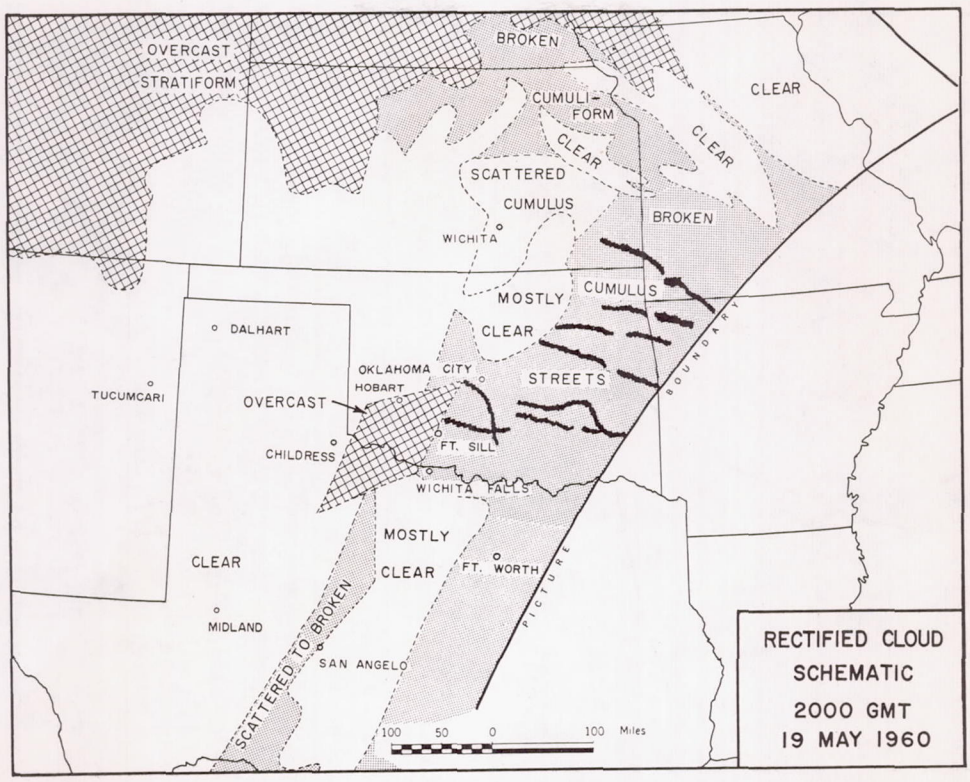

FIG. 2. Schematic geographical location of the cloud features appearing in lower portion of fig. 1. Note that the "square" cloud assumed a rhombic shape after rectification. Cloud amount (scattered, broken, overcast) estimated from cloud picture (fig. 1).

Fig. 2 shows that the bright, isolated cloud assumed a rhombic configuration about 100 miles on a side and was centered along the Texas-Oklahoma border between Childress and Wichita Falls, Texas. This bright cloud area was superimposed on the faint but sharp line separating clear from partly cloudy skies (fig. 1). This line was a synoptic-scale feature, several hundred miles in length, extending south-southwestward from Wichita, Kansas past San Angelo, Texas.

Other cloud features apparent in fig. 1 are also shown in their geographical locations in fig. 2. The extensive cloudiness at the top of fig. 1 covers a large area, the southern part of which encompassed much of the states Colorado, Nebraska, and Kansas. The cloud bands at the bottom right of the picture were oriented east-southeast to west-northwest and lay across eastern Oklahoma and adjoining portions of Missouri, Kansas, and Arkansas. Still other features of the picture such as the relatively dark areas just north and south of the bright, isolated cloud may be located by comparison of figs. 1 and 2.

3. Meteorological analysis

In order to determine the connection between the clouds seen in the picture and the physical state of the atmosphere, hourly surface charts for the period 1900–2200 GMT, 19 May 1960 were analyzed for an area bounded by latitudes 30N and 41N and by longitudes 90W and 105W; accelerated microbarograph traces in the area of the bright cloud mass were also studied. To supplement further this surface information, the Wichita Falls, Texas, radar and the upper-air information were investigated.

The general synoptic situation did not change appreciably over this three-hour period. A frontal system at the forward edge of a continental polar air mass extended southward from a parent low in central Manitoba through a wave in south-central Kansas and thence southwestward as a weak cold front across the Texas Panhandle into New Mexico. Several minor waves moved along the front in the Texas Panhandle over the period (figs. 3–6). A small low pressure area persisted near Tucumcari, New Mexico and Dalhart,

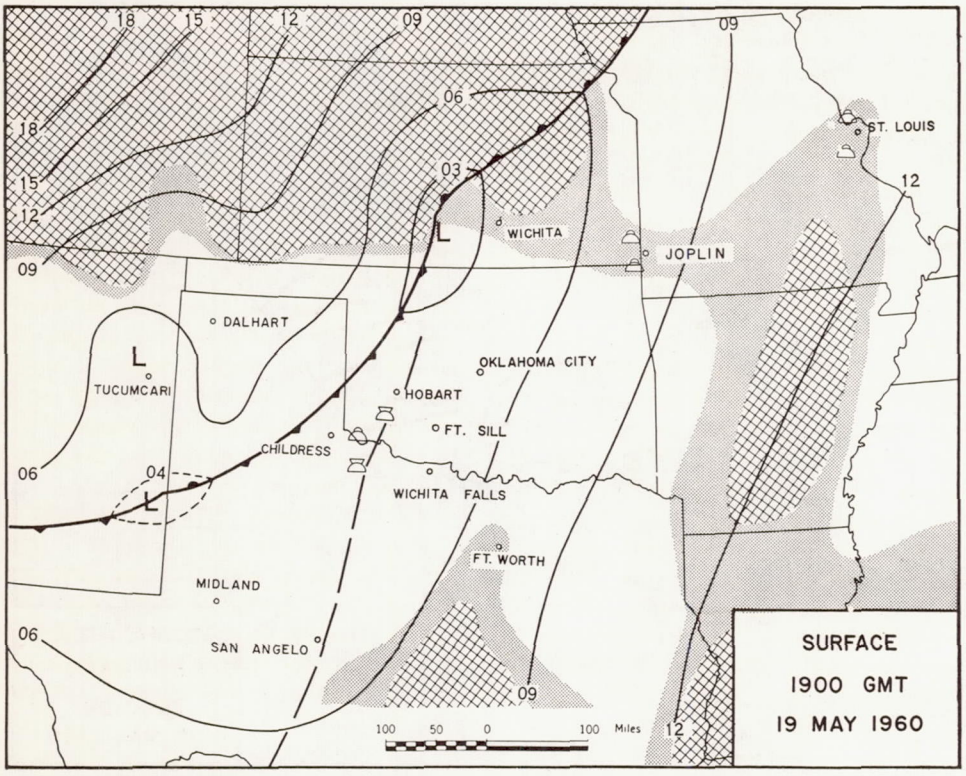

FIG. 3. Surface chart for 1900 GMT, 19 May 1960 showing front, sea level isobars at 3-mb intervals, dewpoint "front" (long dashes), overcast areas from surface observations (heavy cross hatching), broken areas (dotted), and reports of cumulus congestus and/or cumulonimbus clouds (cloud symbols). Clear sky or scattered cloud areas are not shaded.

Texas. Cloudy skies dominated the cold air over Colorado and western Kansas. A line of sharp moisture gradient extended southward from the cold front near Hobart, Oklahoma past San Angelo, Texas, separating a hot, dry, southwesterly flow of air in west Texas from hot, moist air in east Texas—the dewpoints ranged from 19 F to 50 F to the west and from 68 F to 75 F to the east (fig. 4).

Synoptic reports for 1800 GMT (1200 CST) gave no indication of thunderstorm activity or even well developed cumulus clouds within the area of interest. By 1900 GMT (1300 CST), (fig. 3), however, Hobart, Oklahoma and Childress, Texas both reported viewing cumulonimbus and towering cumulus clouds in the direction of the moisture gradient at the Texas-Oklahoma border. Wichita Falls, Texas, though not reporting cumulus congestus clouds visually, did record a line of weak radar echoes to the west in the same area (fig. 7a). There were no other indications of small scale convective activity near the southern Oklahoma border. Overcast skies were primarily restricted to the large cloudy area within the cold air.

At picture time, 2000 GMT, Wichita Falls first reported cumulonimbus clouds to the west (fig. 4), while the line of radar echoes seen the previous hour were closer to the station and more intense (fig. 7b). At Hobart, a thunderstorm was observed south of the station, and Childress continued reporting cumulonimbus and towering cumulus to the east—further evidence of a confined region of strong vertical motion along the moisture gradient line at the Oklahoma border. In general, cloudiness had increased appreciably all along the southern border of Oklahoma. One half hour prior to picture time three jet aircraft were investigating the convective activity reported southwest of Oklahoma City in conjunction with the National Severe Local Storm Research Project. A NASA-instrumented Air Force T-33 jet conducted a survey and preliminary cloud probes in the area of cumulonimbus clouds (fig. 4) in

preparation for penetrations of those clouds by Air Force F102 and F106 jets. Several probes were made at altitudes of about 40,000 feet. The aircraft reported a developing squall line about 40 miles long oriented northeast-southwest and beginning about 80 miles southwest of Oklahoma City. Turbulence was generally reported as ranging from moderate to moderately severe during probes. Occasional heavy, slushy precipitation and some hail were encountered. Cloud tops of major cells reached 42,000 feet and above, while one cell reached to 55,000 feet.

An examination of the two succeeding charts (figs. 5 and 6) shows that the convective activity spread from the dewpoint discontinuity northeastward ahead of the cold front, engulfing Fort Sill and Oklahoma City. During the same two hour period, Wichita Falls noted increasingly stronger and larger radar echoes which appeared to be moving northeastward along the echo line (fig. 7c and d). Hail began shortly before 2200 GMT at Fort Sill (fig. 6), and hail and tornadoes occurred thereafter until 2300 GMT between Fort Sill and Oklahoma City. Those tornadoes and hail storms occurring within one half hour of 2200 GMT are located in fig. 6. A summary of all severe local storm reports in southwestern Oklahoma up to 2300 GMT appears in table 1.

The moisture discontinuity mentioned above is a phenomenon frequently observed in the western plains and has been referred to as the dewpoint "front." Fulks [4] has described in detail a mechanism behind the development of this moisture gradient. Briefly, it occurs when the shallow leading edge of maritime polar air from the Pacific is strongly modified by heating and drying as it moves over the plateau region and the Rockies, and encounters Maritime Tropical air in the western Plains. The mP air by virtue of the modification becomes essentially a continental tropical (cT) air mass.

Three soundings (fig. 8) taken at 1800 GMT, two in the mT air and the other in cT (modified mP) air, clearly illustrate the air-mass difference across the moisture discontinuity. Fort Worth and Oklahoma City, located in the mT air mass, demonstrate the type of sounding frequently found in mT air; that is, a shallow warm, moist surface

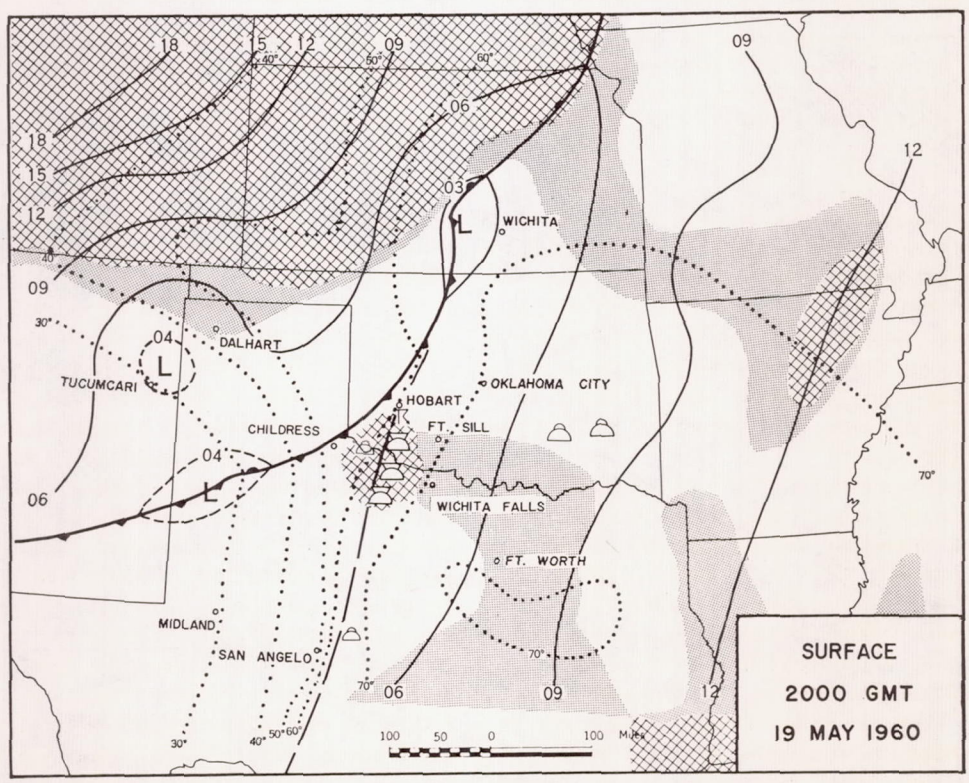

FIG. 4. Surface chart for 2000 GMT, 19 May 1960. Dotted lines are isopleths of dewpoint temperature in deg F. See legend to fig. 3.

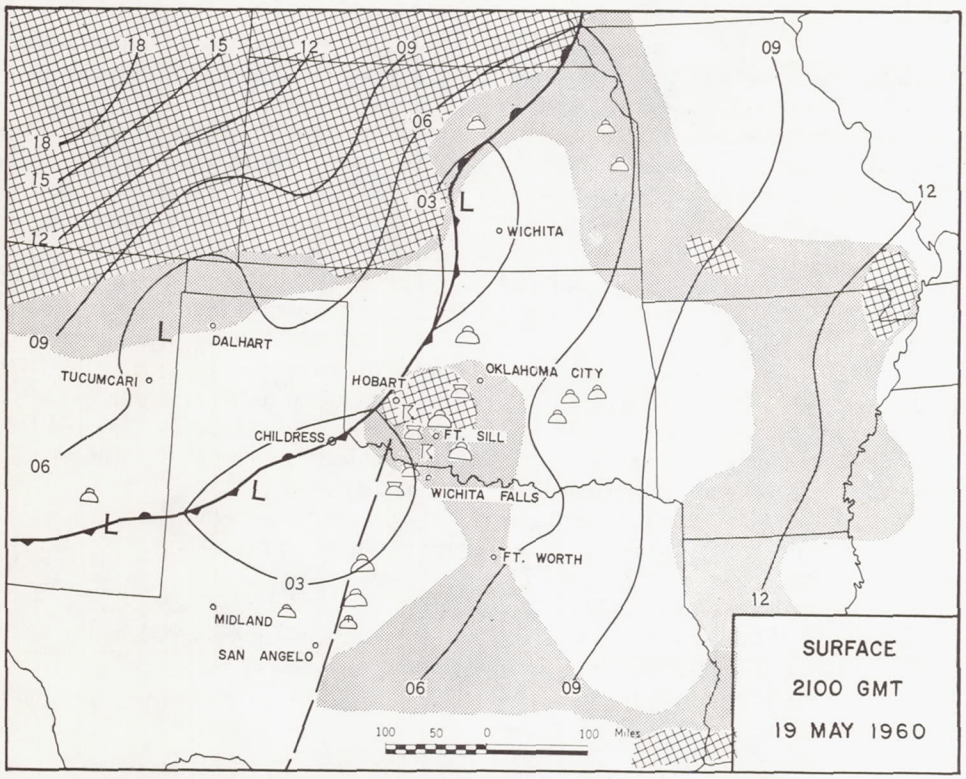

FIG. 5. Surface chart for 2100 GMT, 19 May 1960. See legend to fig. 3.

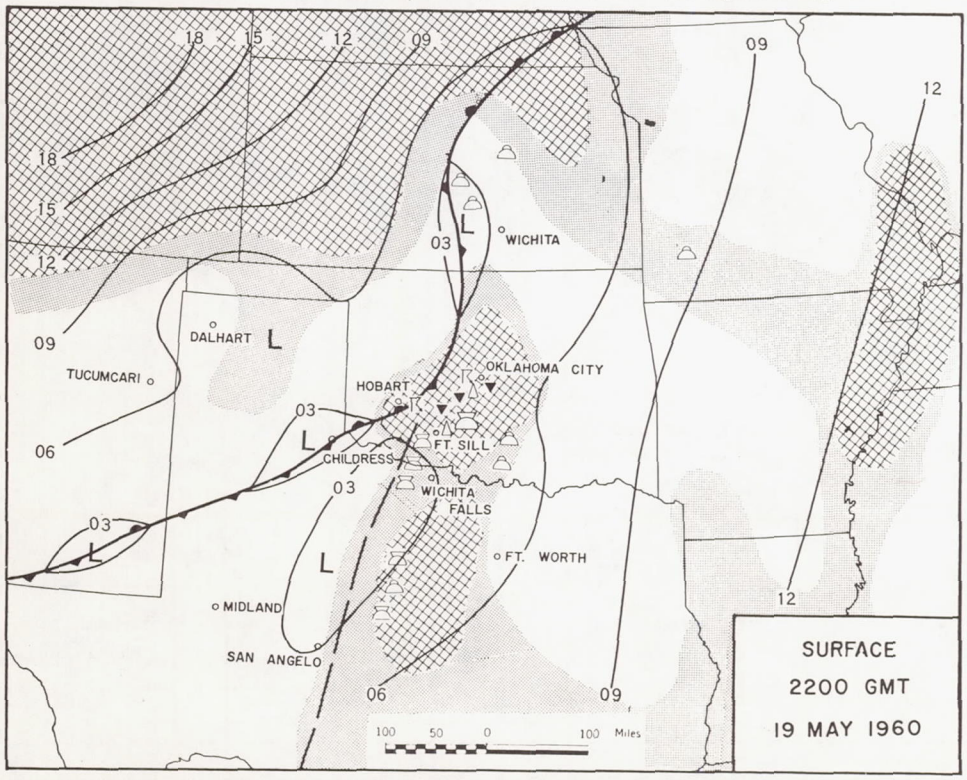

FIG. 6. Surface chart for 2200 GMT, 19 May 1960. Tornado locations are shown by black triangles and hail by the open triangles. See legend to fig. 3.

tions are more favorable, convective activity may be marked."

No detailed mesoanalysis for 19 May 1960 has yet been performed; however, the accelerated microbarograph traces from the dense Severe Local Storms Research Network in Oklahoma, and in particular, those traces near the bright, cloud mass were studied briefly. West of the afternoon position of the dewpoint "front" the pressure traces were very smooth. Quite the opposite situation occurred east of the "front" in Oklahoma and extreme northern Texas. The traces there, though smooth in the morning, became very irregular during the afternoon and night. The first unsteady pressure trace was noted at 1900 GMT at Frederick, Oklahoma (35 miles southwest of Fort Sill) and a second unsteady trace began at Electra, Texas (25 miles west of Wichita Falls) at 1915 GMT. Both locations were beneath the bright cloud mass location of 2000 GMT. During the next few hours, all traces to the east and northeast of Frederick and Electra began showing many short period pressure fluctuations of varying magnitude.

The first abrupt pressure rise of note also occurred at Frederick at 2100 GMT. Thereafter, numerous stations in a "pie shaped" sector northeastward of Frederick recorded strong pressure jumps during at least the following three hours. These stations successively reported the jumps in a manner which indicated the spread of a mesohigh pressure system northeastward from Frederick. The hail and tornado outbreaks appear to have occurred in close association, both in time and space, with the location of the pressure jump line (leading edge of the mesohigh).

Weighing rain-gage records were also available from some of the network stations. Heavy rainfalls occurred to the northeast of the bright cloud mass after picture time, but Frederick, Oklahoma, located very near the center of the isolated cloud mass (of fig. 1) recorded .25 inches of rain during a half-hour period which included the time of the picture, namely 2000 GMT.

Beebe and Bates [8] have discussed the importance of both low-level and high-level jet streams as a factor in the development of tornado activity. In this case, a southwesterly low-level jet stream maximum at 14,000 ft. over Amarillo at 1800 GMT (fig. 9) migrated eastward over Oklahoma City and lowered to 10,000 ft. by 0000 GMT (fig. 10).[2]

[2] Cross-sections through Amarillo and Oklahoma City indicated these levels to be most representative of the altitude of the maximum winds, or jet core, for the two times considered. However it should be mentioned that at 0000 GMT, a second jet core was noted at 7,000 ft. immediately beneath the 10,000 ft. core over Oklahoma City.

The 1800 and 0000 GMT Amarillo RAWIN and the 1800 GMT Oklahoma City RAWIN definitely indicated the presence of a high-level jet in the area of interest. The exact location of the high-level jet [8, 9] at 0000 GMT was hampered by the very brief sounding taken at Oklahoma City at that time; the balloon was forced down by icing conditions after attaining an altitude of only 23,000 ft.

4. Picture content and meteorology

Identification of the 2000 GMT synoptic elements with the features in the photograph were readily established by comparisons made directly with the photograph (fig. 1) and by means of the locations obtained through use of the cloud schematic (fig. 2). For instance, the extensive cloudiness at the top of the photograph (fig. 1) was in part the overcast area over Colorado and western Kansas (fig. 4). The large black areas, one at the right center, and the other, at the lower left of the picture, were the clear areas over northern Missouri and Iowa, and over New Mexico, western Texas and western Oklahoma respectively. These identifications may be made by comparison of relative positions, size and amount of cloud cover of the features in the picture with the nephanalysis (fig. 4), but they are independently corroborated by the rectified schematic diagram (fig. 2) within the accuracy limitations.[3]

Of special interest, however, is the bright isolated cloud mass and the smooth cloud boundary upon which the bright cloud was superposed. It is certain that the location of the sharp cloud boundary, as established earlier, coincided mainly with the surface position of the dewpoint "front" which extended southward from the cold front north of Hobart to the vicinity of San Angelo, Texas (fig. 4). The northern part of the sharp line in fig. 1 may have been associated with the cold front north of Hobart. The surface reports at 2000 GMT clearly indicated that the boundary in fig. 1 separated clear skies to the west from the partly cloudy skies (scattered cumulus humilis) to the east.

With this boundary fixed, the bright "square" cloud mass lay near the dewpoint "front." In

[3] The schematic location of the bright cloud mass is established to be correct to within about ± 30 miles.

fact, this bright cloud represented the concentrated area of heavy convective activity reported by Hobart, Childress, and Wichita Falls at 2000 GMT. It has been mentioned above that rain was falling at the surface in at least one area beneath the bright cloud at picture time.

One other interesting aspect of the picture was the existence of the relatively clear areas immediately to the northeast and south of the bright cloud mass. These two areas suggest that the air was descending perhaps as part of the mesoscale circulation associated with the strong upward motion in the bright cloud mass.

As stated earlier no well defined mesohigh could be detected beneath the cloud mass at the time of the picture though traces in that area became unsteady during the hour preceding 2000 GMT. A significant pressure rise was first noted at this location one hour later.

It is interesting to note from figs. 9 and 10 that the southwest wind direction was more or less perpendicular to the cloud streets in eastern Oklahoma. Since the cloud streets appear in an area with a strong inversion (fig. 8), they may have been associated with Helmholtz waves as discussed by Haurwitz [10]. Moreover the bright isolated cloud was elongated in the direction of the wind. Perhaps in such situations in data-sparse areas, the picture features may offer clues from which one might deduce the wind direction.

The proximity of this cloud and the dewpoint "front" to the low-level and high-level jet maxima are reminiscent of the instability released under such conditions [8]. It will be interesting to examine other cases in which isolated bright cloud masses appear near a sharp boundary like the one in fig. 1, to see whether they are associated with regions of wind maxima.

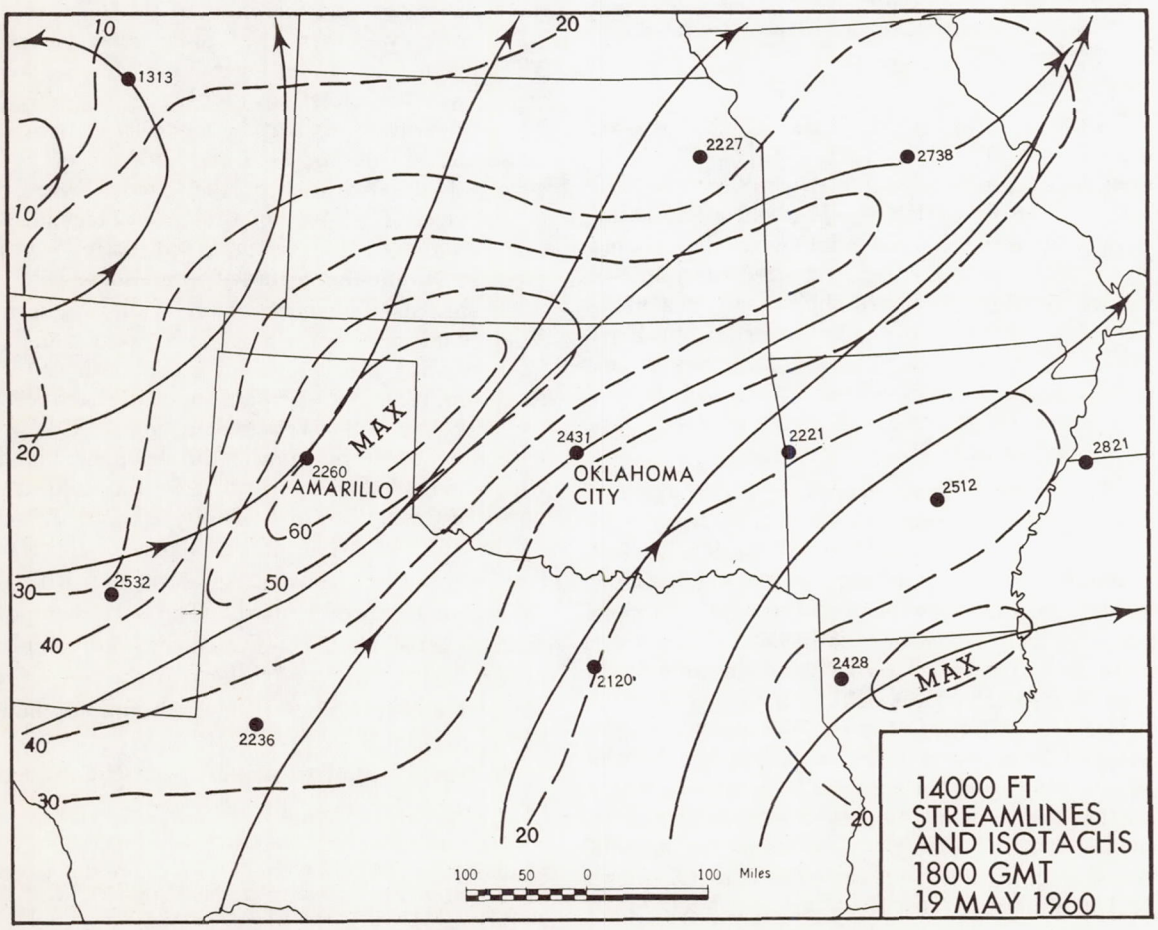

FIG. 9. Streamline chart for 14,000 ft., 1800 GMT, 19 May 1960. Solid lines are streamlines and broken lines are isotachs labeled in knots. Plotted data are wind directions and speeds.

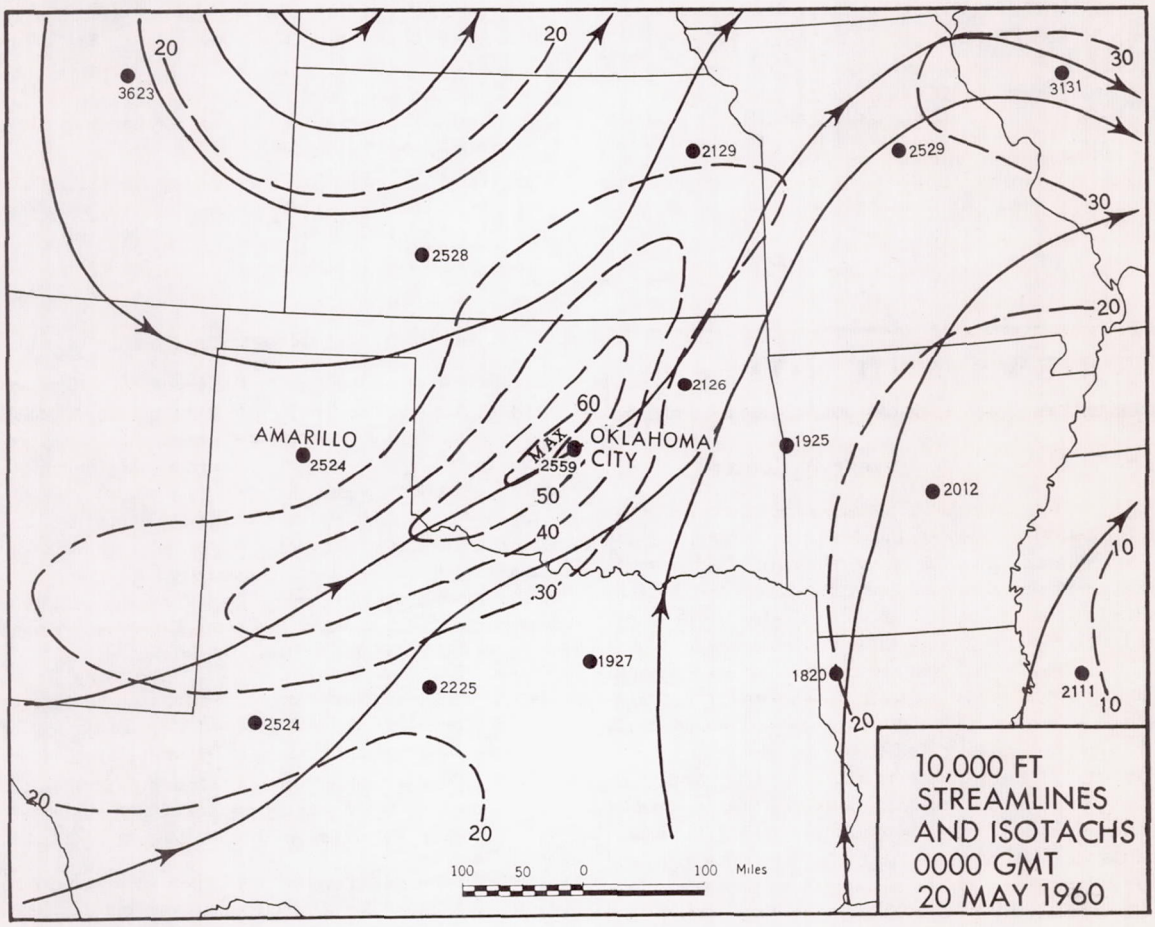

FIG. 10. Streamline chart for 10,000 ft., 0000 GMT, 20 May 1960. See legend to fig. 9.

5. Summary

There is strong evidence (1) that the first intense cumulus convective activity in the Southern Plains on the afternoon of 19 May 1960 was represented by the isolated, bright cloud mass in the picture (fig. 1), (2) that the cloud mass was located in an area possessing characteristics commonly found in tornado development, and (3) that the system represented by the bright cloud mass later expanded and spread northeastward spawning hail and tornadoes in central Oklahoma. It is not the intent here to imply that every bright isolated cloud mass seen from satellite vehicles will be associated with hail and tornadoes. However, such clouds or masses of clouds when considered together with the geographic location, the climatology of the region, and the existing synoptic situation will be subject to close scrutiny as potential producers of severe local storms.

Acknowledgments. The authors wish to express appreciation to Mr. William A. Hass of the U. S. Weather Bureau for making available the microbarograph traces and rain gage traces from the Severe Local Storms Network and to Mr. C. F. Van Thullenar of the U. S. Weather Bureau for providing information obtained on the jet penetrating flights.

REFERENCES

1. Sternberg, S., W. G. Stroud, J. D. Freeman, E. A. Goldberg, V. D. Landon, H. Perkel, M. Ritter, C. A. Osgood, J. E. Keiler, and C. B. Oakley, 1960: Roundup on TIROS I. (A series of articles relating to engineering aspects of TIROS I.) *Astronautics,* **5**, 32–45.
2. Staff Members, Meteorological Satellite Laboratory, U. S. Weather Bureau, 1961: *Some meteorological results from TIROS I* (In report on TIROS I to be published by the National Aeronautics and Space Administration).
3. Hoecker, W. H., Jr., 1960: Characteristics common to several tornado systems. Talk given before the 184th National Meeting of the American Meteorological Society held jointly with the American Geophysical Union at Washington, D. C. Abstract appears in *Bull. Amer. meteor. Soc.,* **41**, 197.

4. Fulks, J. R., 1951: The instability line. *Compendium of Meteorology*. Boston, American Meteorological Society, 647–652.
5. Hanks, Howard H., Jr., and Georgina M. Neubrand, 1957: Tornadoes of April 2 and 3, 1956. *Mon. Wea. Rev.*, **84**, 155–162.
6. Fawbush, E. J., R. C. Miller, and L. G. Starrett, 1951: An empirical method of forecasting tornado development. *Bull. Amer. meteor. Soc.*, **32**, 1–9.
7. Tepper, Morris, 1950: A proposed mechanism of squall lines; the pressure jump line. *J. Meteor.*, **7**, 21–29.
8. Beebe, Robert C., and Ferdinand C. Bates, 1955: A mechanism for assisting in the release of convective instability. *Mon. Wea. Rev.*, **83**, 1–9.
9. Lee, Jean T., and Joseph G. Galway, 1956: Preliminary report on the relationship between the jet at the 200-mb level and tornado occurrence. *Bull. Amer. meteor. Soc.*, **37**, 327–332.
10. Haurwitz, B., 1947: Internal waves in the atmosphere and convective patterns. *Ann. New York Acad. Sci.*, **48**, 727–744.

NEWS AND NOTES

New Space Research Center

The Institute for Space Studies has been established by the theoretical division of the National Aeronautics and Space Administration, crossing standard disciplines to create a new scientific community for space research. The institute is housed in the Interchurch Center at 475 Riverside Drive, New York City, close to the Riverside Church and will have a complement of fifty to sixty people, including about twenty graduate students and fifteen postdoctoral associates. The latter are selected competitively with stipends beginning at $9,500.

Director of the institute is Dr. Robert Jastrow, who has consented to become coeditor of the new *Journal of the Atmospheric Sciences* in association with Dr. Norman Phillips of Massachusetts Institute of Technology and who will thus become increasingly familiar to members of the AMS. Billed as a "New Guide into Space," Dr. Jastrow was the subject of a feature article in the *New York Times* (19 May 1961) which outlined landmarks in his career to date. At the age of 22 he obtained his doctorate in physics at Columbia, and he has subsequently been associated with the University of Leiden in the Netherlands, the Radiation Laboratory of the University of California, and Yale University. As a member of the Institute for Advanced Study at Princeton, he worked under Dr. J. Robert Oppenheimer.

The Exploration of Space (New York: Macmillan Co., 1960), edited by Jastrow and including some of his work, provides a fascinating and highly readable introduction to the field which the new institute will encompass. The institute will not be an experimental center, but will rather generate ideas leading to more imaginative experiments by the rockets and satellites of its parent organization.

Among those expected to work at the institute during the coming academic year are Dr. Jule Charney, professor of meteorology at Massachusetts Institute of Technology; Dr. Harold C. Urey, Nobel Prize Winner and professor of chemistry at the University of California; Bendt G. D. Strömgren, astrophysicist at the Institute for Advanced Study; and Dr. Joseph W. Chamberlain, director of the Yerkes Observatory in Wisconsin.

Geophysics Research Board

The establishment in 1960 of the Geophysics Research Board by Detlev W. Bronk, president of the National Academy-National Research Council, was in part a response to a request from the International Council of Scientific Unions for establishment of a means of cooperation with its International Geophysics Committee, and in part a response to expressions of interest by many members of the geophysical community.

After discussions with many geologists and geophysicists during the past year, President Bronk has defined the basic functions of the Board as follows:

(1) to effect participation by American scientists in the new International Committee on Geophysics of the International Council of Scientific Unions; and
(2) to stimulate and encourage research interest in the United States in geophysics and related fields, particularly those of an interdisciplinary character.

The Board membership consists largely of the chairmen or representatives of existing committees within the Academy, thus serving to bring together the geophysical interests of the Academy and to minimize the burdens on the Board itself. The members and their committee activities are as follows:

Merle A. Tuve, Carnegie Institution of Washington, Chairman
Lloyd V. Berkner, Space Science Board
Henry G. Booker, United States National Committee—International Scientific Radio Union
Harrison Brown, Committee on Oceanography
Michael Ference, Jr., Committee on Atmospheric Sciences
Laurence M. Gould, Committee on Polar Research
Joseph Kaplan, United States National Committee—International Geophysical Year
Martin A. Pomerantz, United States National Committee—International Union of Pure and Applied Physics
Francis W. Reichelderfer, United States Weather Bureau
Walter O. Roberts, United States National Committee—International Astronomical Union
George P. Woollard, United States National Committee—International Union of Geodesy and Geophysics and the American Geophysical Union

The Board has approved the establishment of the fol-

(Continued on page 639)

[Reprinted from BULLETIN OF THE AMERICAN METEOROLOGICAL SOCIETY, Vol. 42, No. 3, March, 1961, pp. 151–165]
Printed in U. S. A.

Cloud Structure of an Occluded Cyclone Over the Gulf of Alaska as Viewed by TIROS I [1]

JAY S. WINSTON AND LLOYD TOURVILLE
U. S. Weather Bureau, Washington, D. C.

(Manuscript received 19 October 1960)

ABSTRACT

The cloud structure of an occluded cyclone and its environs over the Gulf of Alaska is revealed in detail by a series of TIROS pictures. The pictures clearly portray:

(1) the nature and extent of dense cloudiness around the inner core of the cyclone;

(2) a broad band of cloudiness associated with the main polar front;

(3) the pattern of overrunning cloudiness marking a newly developing wave south of the main storm;

(4) a previously undetected, old cyclonic vortex in mid-troposphere; and

(5) the striking cellular arrangement of cumuliform clouds in the cyclonic flow to the rear of the storm.

These features are related to the conventional meteorological data and analyses over this area and are found in many places to corroborate them rather well. On the other hand, there are several places, particularly in view of the sparsity of conventional data, where the cloud pictures suggest that improvements could be made in the map analyses and numerically computed vertical motions on the basis of the TIROS cloud information.

1. Introduction

During its first day of operation, TIROS I photographed portions of an occluded cyclone over the Gulf of Alaska. Wide-angle pictures of this storm and its periphery were obtained on several frames taken at 30-sec intervals starting at 2155GCT 1 April 1960 as the satellite traveled southeastward from south of the Aleutians toward Lower California. The track of the satellite is portrayed in fig. 1, where it is superimposed on the pertinent section of the sea-level analysis of the National Weather Analysis Center

[1] This research has been supported by the National Aeronautics and Space Administration.

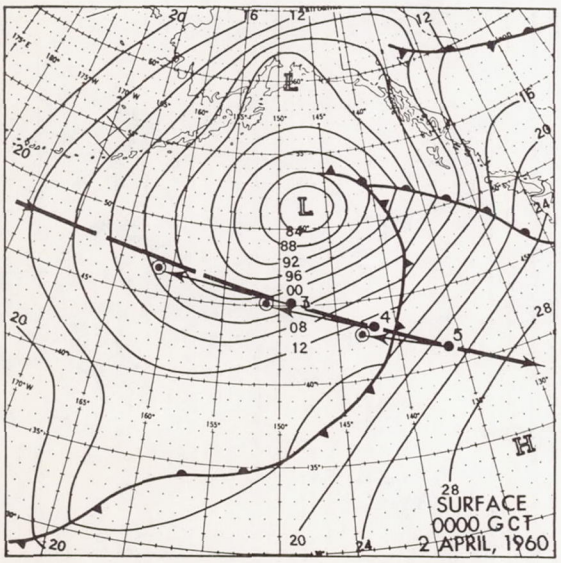

FIG. 1. Sea-level analysis for 0000GCT 2 April 1960 with track of satellite indicated by heavy line. Dots and numbers along path correspond to pictures shown in figs. 3, 4 and 5. Circled dots indicate principal points of pictures, and arrows show orientation of camera for each picture.

(NAWAC) for 0000GCT 2 April (approximately 2 hr after picture time). Since the satellite passed to the south of the Gulf of Alaska low and its camera was pointing generally backward along the track, the pictures obtained portray the cloudiness over mainly the western and southern quadrants of the storm.

This Gulf of Alaska cyclone, as may be seen in the sea-level analysis of fig. 1, was a recently occluded wave of moderate intensity. The center of this storm had moved northeastward into the Gulf of Alaska at an average speed of about 25 to 30 kn during the previous 24 hr and had very nearly reached its minimum central pressure of about 980 mb at this time. Also evident in the analysis of fig. 1 is that the cold front extending from the cyclone center was nearly stationary south of latitude 38N and that a weak frontal wave was indicated near the lower left corner of the map.

An overall view of the cloudiness in the vicinity of this Gulf of Alaska cyclone is afforded by a composite photograph derived from several individual pictures (fig. 2).[2] Of particular interest in this picture are several distinctive cloud features; the cloudiness around the center of the major cyclonic vortex (A), broad, solid cloud bands (BC and DE), cellular cloudiness (F), and the probable remnants of an old cyclonic vortex (G). These features are examined in more detail and are related to information available from standard meteorological observations in the ensuing discussion.

For the purpose of this discussion, three individual pictures have been selected from the group used in making up fig. 2; these are shown in figs. 3a, 4a and 5a. Each of these pictures was taken at the three correspondingly numbered points (*i.e.*, 3, 4 and 5) indicated along the track in fig. 1, where the direction in which the camera was pointed is also shown. Comparison of standard meteorological data and analyses with the pictures has been facilitated by the construction of latitude-longitude grids [1, Appendix 1] for each of these pictures. The gridded pictures with superimposed sea-level data and analyses are shown in figs. 3b, 4b and 5b, and with superimposed 700-mb contours, wind reports at 700 mb, and 600-mb vertical motion[3] in figs. 3c, 4c and 5c.

2. Cloudiness near the vortex center

The inner core of the cyclone over the Gulf of Alaska is clearly identified by dense cloudiness with pronounced cyclonically-shaped streaks (A in fig. 4a). A striking feature of this picture is the pronounced clear "moat" extending outward from near the center of the storm. As may be seen in fig. 5a, where more of this clear area is visible, it appears to be part of a band that spirals into the storm center. Another clear line farther southeastward (figs. 4a and 5a) also seems to spiral into the center and to merge with the first clear "moat".

Examination of fig. 4, b and c, shows that the cyclonically-curved streaks in the vortex clouds generally parallel the sea-level isobars and most of the reported surface winds. They also parallel the 700-mb flow since the latter has virtually the same direction as the surface flow, except to the south of the low center where the upper trough is to the west of the surface trough.

The few ships located within the streaky cloud area near the storm center report stratocumulus clouds in the lower levels with a layer of altostratus clouds above (figs. 4b and 5b). There are no reports of cirriform clouds in the area although they could be present above the layer of altostratus and hence invisible to the ground

[2] In this and subsequent views, the pictures are printed so that north is generally toward the top of the page.

[3] Vertical motion computed by the Joint Numerical Weather Prediction (JNWP) Unit for the initial time of their baroclinic prediction model.

observer. However, the cloudiness (see fig. 4a where the analyses do not obscure the picture) does not have the appearance of a solid cirrostratus overcast. In fact, the streakiness indicates that even the altostratus deck is far from solid, and is probably broken or very thin.

The only sounding in the vicinity of this cyclone is the one at ship "P" (50N–145W), located just southeast of the low center and to the rear of the occlusion (beyond the confines of fig. 4, but just barely at the edge of the picture in fig. 5). This sounding (fig. 6), which is very likely typical of most of the cloud area near the center, reveals a lapse rate that is nearly moist-adiabatic all the way up to 400 mb. The dew-point sounding shows very high relative humidities from the surface up through 700 mb but somewhat lower humidities (about 50 to 60 per cent) from 600 mb on upward. This indicates that the clouds do not extend beyond middle levels (*i.e.*, about 12,000 ft) and thus corroborates the deduction made from the nature of the cloudiness as viewed in area A (fig. 4a). The lack of reports of significant precipitation by ships in area A also lends support to the conclusion that the cloudiness does not extend to high levels.

The vertical-motion field in fig. 4c shows a center of weak downward motion in the vicinity of the cloudiness under discussion. If our deductions about the clouds not extending to 600 mb are correct, this computed downward motion for the 600-mb surface may have some validity. However, it is likely, in view of the extensive cloudiness near this low center, that there is some upward motion between 600 mb and the layers near the surface. In any event, the downward motion computed by the JNWP model, contrary to the assumption inherent in the model, is very likely *not* representative of a deep layer of the middle and lower troposphere. Of course, the sparsity of observations in this region, plus some of the other restrictions of the baroclinic model tend to degrade the accuracy of these computed vertical velocities. The cloudiness revealed in the TIROS pictures may indeed yield the best estimates, albeit only qualitative, of the predominant vertical motions in the lower and middle troposphere.

Estimates of vertical motion from cloudiness of course may be fairly crude since the mere presence of clouds does not necessarily mean that upward motion is instantaneously present. Rather, it is the increase or maintenance of cloudiness over a period of time that is indicative of upward motion; this type of comparison has been cited by Panofsky and Dickey [2]. Thus, only when local-time sequences of satellite pictures become available, will the sign of vertical motion be determinable with more precision. However, pending the availability of better data, it is probably reasonable to assume that upward motion is generally occurring in an extensive cloud mass of the size of the one around this cyclone center.

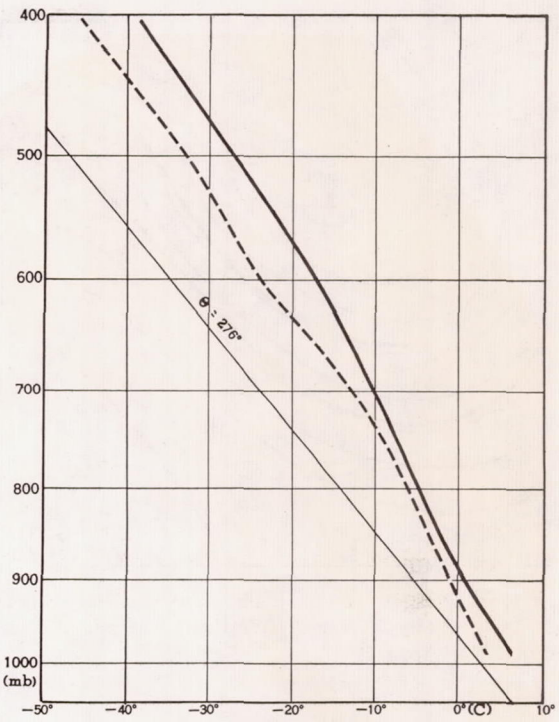

FIG. 6. Sounding at ship P (50N–145W), 0000GCT 2 April 1960. Solid line shows temperature distribution; dashed line, dew point distribution.

3. Frontal cloudiness

The southern and southeastern fringes of the Gulf of Alaska cyclone are dominated by two wide bands of stratiform cloudiness of a more-or-less uniform character (BC in fig. 5a and DE in figs. 4a and 5a). As may be seen immediately in fig. 5b, band BC generally straddles the major cold front associated with this occluded cyclone. Since the frontal position is fixed rather closely by the ship report at 44N-139W, which requires the front to lie to the west of this location, there is little doubt that this stratiform cloudiness does occur on both sides of the front in this case. In general, this cloudiness is continuous, but there is a suggestion of breaks just east of the front northward from latitude 43N.

Fig. 5c shows that this frontal cloudiness is

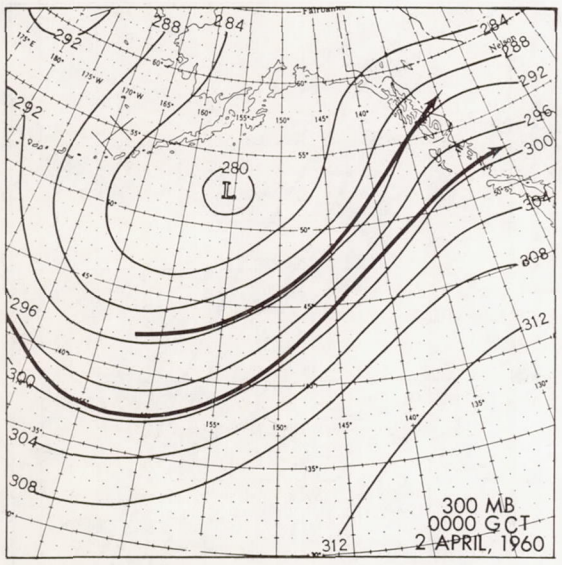

FIG. 7. 300-mb contours and jet axes (heavy lines) as analyzed by National Weather Analysis Center, 0000GCT 2 April 1960.

located in the broad southwesterly current ahead of the trough on the 700-mb chart. The band is elongated at a small angle to the left of the 700-mb contours (looking downstream). Unfortunately, there are no upper-air data within the entire area enclosed by zone BC, but, in view of the strength of the cyclonic system at the surface and of the attendant sea-level pressure gradients, there is little doubt that a broad, vigorous southwesterly flow exists aloft in this zone.

Furthermore, it is obvious that this strong flow in the mid-troposphere is surmounted by a jet stream (or streams) through this area in the upper troposphere. This is indicated by the flow at 300 mb for 0000GCT 2 April (fig. 7), where double jet axes are portrayed in the NAWAC analysis. The more southerly of these jets is actually located beyond the northwestern edge of cloud zone BC, but it is not inconsistent with the displacement of up to 5 deg lat found between the surface front and the jet stream in typical cases [*cf.* 3, 4]. However, credence in the precise jet location in this case can at best be very limited in view of the paucity of upper-air data in this region. (The only report across the entire broad, southwesterly stream is at ship P, which is on the left edge of the current.) In other words, there may be only one jet axis, (or there could even be more than two) and the location(s) in the southwesterly current may be different. If it were known precisely how the jet axis is located relative to the frontal cloudiness, the gridded TIROS pictures (fig. 5, b or c) would readily fix the position of the jet stream. For example, if Conover's [5] suggestion that the jet axis is located along the northern edge of the frontal cloud shield were accepted, the jet axis would be found at the left edge of zone BC in fig. 5.

The other stratiform-cloud zone mentioned earlier (DE in figs. 4a and 5a) seems to be almost entirely separated from zone BC by a narrow, cloudless channel. The northern fringes of this cloudiness seem to consist of streamers which get progressively thinner toward the north. This suggests the leading edge of a cirrostratus or altostratus overcast (note the ship in fig. 4b which reports an altostratus overcast) which is very likely associated with the wave on the polar front located at about 34N–160W on the sea-level chart (fig. 1). Subsequent sea-level maps (not shown here) show that this wave moved northeastward and deepened into another major cyclone in the following 24 hr. Incidentally, the more southerly jet axis analyzed in fig. 7 is located very close to the middle of zone DE.

The vertical-motion field (figs. 4c and 5c) shows upward motion over most of the area occupied by bands BC and DE with a center of maximum upward motion near 39N–147W. Of course, one should be quite satisfied with this crude agreement between the vertical motion and these broad cloud areas in view of the data which were available to the JNWP Unit. If it is assumed that these vertical motions are correct, then the clear area between BC and DE would have to represent a narrow tongue of dry air which has not as yet reached saturation despite a moderate degree of upward motion. However, it seems more likely that the vertical-motion field has two axes of maximum upward motion, one in zone DE where the cloudiness of the incipient wave is spreading northeastward and the other in zone BC where the cloudiness along the cold front is so extensive. It would be of interest to determine how much improvement could be attained in baroclinic numerical prediction of this situation if the initial vertical motion-divergence fields were altered in this direction.

4. Secondary vortex

To the northwest of the main cyclonic vortex is a hook-like cloud (G) which appears to be mainly of a solid, stratiform character (figs. 3a and 4a). From the shape of this "hook" and the adjacent clear area, as well as the synoptic situation, one would deduce that this is a mid-tropo-

spheric remnant of the circulation around an old cyclonic vortex. Fig. 3, b and c, shows rather simple northerly or northwesterly flow at both the surface and 700 mb near G. However, the surface data are quite sparse and the upper-air data non-existent in this area. Thus, it is possible that a center of cyclonic vorticity may still exist near G, at least at the 700-mb level. This could mean that the maximum cyclonic curvature of the 700-mb contours shown at about 1 to 2 deg southeast of the apparent center of the cloud vortex (fig. 3c) may actually belong farther to the northwest. Inspection of both 500- and 700-mb charts for 24 hr earlier (not shown) indicates that a weak cyclonic vortex existed over the eastern Aleutians, just to the southwest of the Alaska Peninsula. It is very likely that the cyclonic cloud pattern at G in fig. 3a does mark the remains of this upper-level vortex which is now drifting southward to the rear of the more vigorous cyclone in the Gulf of Alaska.

It should be noted incidentally that a tongue of positive vertical velocity (fig. 3c) seems to extend from the north in rough coincidence with this vortex cloudiness, which probably means that some elements of this vortex circulation were inherent in the mid-tropospheric analyses at this time.

5. Cellular cloudiness

Much of the region on the western and southwestern side of the Gulf of Alaska cyclone is seen to be occupied by scattered to broken cumuliform cloudiness (area F in figs. 3a and 4a). This cloudiness generally has a definite cellular character to it and is the type discussed in more detail by Krueger and Fritz [6]. The cloud elements are considerably larger on the right side of fig. 3a which means that they are much larger cumulus clouds and/or represent the spreading of the tops of the cumulus clouds into stratiform, middle or low clouds.

The sea-level and 700-mb flow patterns in figs. 3b, 3c, 4b and 4c show that these clouds are found in the cyclonic northwesterly and westerly flow beyond the inner core of the cyclone. The vertical motion is generally downward through most of this area, which is probably consistent with the type of cloudiness (presumably of the low-level instability type) observed here.

6. Summary

The preceding discussion clearly illustrates how satellite cloud pictures can serve as an invaluable analytical tool in regions where conventional meteorological data are sparse. Details of the cloud structure of the occluded cyclone and its periphery, which could never be determined from the available standard observations, have been clearly revealed in the pictures. In particular, the following features have been documented: (1) cyclonically-curved streaks in the dense cloudiness around the inner core of the cyclone which parallel the surface isobars, (2) a "moat" of clear air spiraling into the center of the cyclone from the northeast, (3) the location and extent of broad bands of stratiform cloudiness associated with the main polar front, (4) the pattern of over-running cloudiness associated with a nascent wave cyclone, (5) the previously undetected presence of an old cyclonic vortex in the middle troposphere, and (6) the striking cellular arrangement of cumuliform cloudiness in the cyclonic flow to the rear of the storm.

The clear-cut orientations and arrangements of the cloudiness tend to corroborate the conventional map analyses and computed vertical motions in many places; this is encouraging for the future interpretation of satellite pictures in areas with even sparser data coverage than the Gulf of Alaska. However, there are several places where the cloud pictures intimate that some improvements could be made in these analyses and vertical velocity fields; this emphasizes the complementary role that satellite pictures can play relative to the more conventional data previously available.

Acknowledgments. The assistance of Andrew Timchalk in preparing the pictures with superimposed grids, isopleths and plotted observations and of Mary Ann Ruzecki in fitting latitude-longitude grids to the pictures is sincerely appreciated.

REFERENCES

1. Staff Members, Meteorological Satellite Laboratory, U. S. Weather Bureau, 1960: *Some meteorological results from TIROS I.* To be published as NASA report.
2. Panofsky, H. A., and W. W. Dickey, 1946: Vertical motion and changes of cloudiness. *Bull. Amer. meteor. Soc.*, 27, 312–313.
3. Riehl, H., M. A. Alaka, C. L. Jordan and R. J. Renard, 1954: *The jet stream,* in *Meteorological monographs,* Vol. 2, no. 7. Boston, Amer. meteor. Soc., 100 pp.
4. Vederman, J., 1954: The life cycles of jet streams and extratropical cyclones. *Bull. Amer. meteor. Soc.*, 35, 239–244.
5. Conover, J. H., 1959: *Cloud patterns and related air motions derived by photography.* Final rep., Contract No. AF19(604)-1589, Blue Hill meteor. Observ., Harvard Univ., 268 pp.
6. Krueger, A. F., and S. Fritz, 1961: A cellular cloud pattern revealed by TIROS I. (To be publ. in *Tellus.*)

Reprinted from MONTHLY WEATHER REVIEW, vol. 89, No. 7, July 1961, pp. 229-242.

A SOUTHERN HEMISPHERE CASE STUDY WITH TIROS I DATA

LESTER F. HUBERT

Meteorological Satellite Laboratory, U.S. Weather Bureau, Washington, D.C.

[Manuscript received March 24, 1961; revised April 24, 1961]

ABSTRACT

On April 28, 1960, TIROS I obtained pictures of an exceedingly sharp-edged cloud deck over the Pacific Ocean west of Chile, of cirrus associated with the jet stream on the west coast of South America, and of a mature cyclone in the central South Atlantic. Surface, upper-air, and cross section analyses are presented and compared with pictured cloud features.

Because of the wide spacing of the data, the locations of double jet streams had to be deduced by examining the horizontal temperature gradients associated with Northern Hemisphere jets and assuming that the same general relation holds in the Southern Hemisphere.

An operational surface analysis is shown to be inconsistent with the pictured data in the oceanic region where the analysis was based on a single ship report. A modification of the analysis is suggested to illustrate the potential of meteorological satellite data in data-sparse regions.

1. INTRODUCTION

TIROS I, the meteorological satellite launched on April 1, 1960, photographed interesting cloud patterns over many parts of the earth. From about mid-April until early May 1960 its camera orientation changed in such a manner that pictures of the Southern Hemisphere were obtained. Near the end of April some unusually interesting pictures showed what appeared to be cirrus clouds streaming off the eastern coast of Argentina. Cirrus patterns have been studied in relation to the jet stream in the Northern Hemisphere so these pictures provided an attractive case for comparison. In addition to the cirrus clouds were a sharp-edged cloud deck off the Pacific coast of South America and the classical spiral cloud pattern of a cyclone in the Atlantic east of South America. In order to examine the several interesting features of this sequence, upper-air and surface observations were obtained for a comparison between the standard meteorological data and the picture data.

The Director of the Argentina Servicio Meteorologico kindly furnished plotted and analyzed maps from their files along with some tabulated upper-air data. All observations so collected have been plotted and reanalyzed. There is little difference between the common features of the upper-air analysis furnished by the Argentina Meteorological Service and that shown here—the changes are mainly details added by incorporating the results of the cross-section analysis.

Two versions of the surface analysis are shown—the first is a copy of the operational analysis made by the Argentinian meteorologists (the oceanic portion of which is done on the basis of a single ship report), the second is modified on the basis of picture data. The purpose of the latter is to illustrate how satellite data provide invaluable information where no standard observations are available.

2. PICTURE DATA

Figures 1 through 6 are individual frames on which have been superimposed grids of latitude and longitude, while figure 7 is a schematic nephanalysis showing the major features. In the latter figure the picture outlines are shown with shading inside those boundaries to represent cloudiness. Inspection of the pictures will show that little can be seen near the horizon; consequently the useful part of each picture does not actually extend all the way to the horizon boundaries shown on figure 7. The various cloud patterns are described here briefly for comparison with the nephanalysis, but will be referred to again in more detail in connection with the meteorological analysis, and the analysis superimposed on the pictures will also be deferred to a later section.

Figure 1, viewing toward the western horizon, shows a sharp cloud edge in the Pacific 52° to 48° S. between a stratus deck and cumuliform clouds to the south. The sharp edge of the stratus in the left foreground is along the Andes Mountains, showing the western slopes cloudy and the eastern slopes clear. The breaks in the stratus deck near 40° S. in the Pacific correspond to the limb of the Pacific anticyclone.

Figure 2 shows a bright band across the middle of the picture which is probably cirrus and middle clouds. The stratus clouds on the west coast and the clear downslope area are again visible.

Figures 3 and 4 show the region with few scattered clouds from 40° to 50° W. longitude that is probably associated with a pressure ridge in the low troposphere.

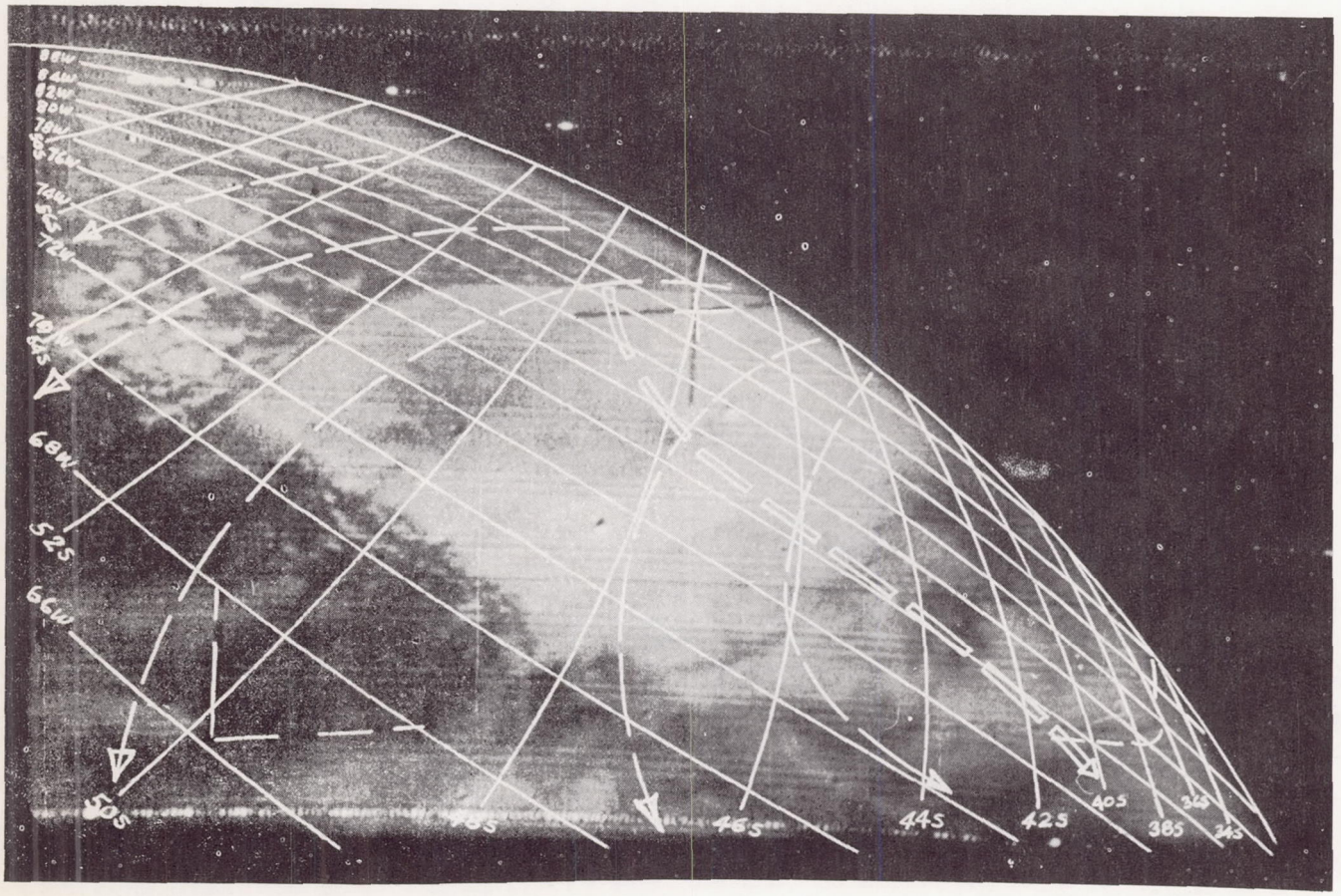

FIGURE 1.—TIROS picture toward the west from above Argentina. Superimposed broken lines are mean streamlines for 700–500-mb. layer; doubled broken line is jet stream axis. 1600 GMT, April 28, 1960.

Figure 5 is a view of the edge of the cyclone where a dry cool air mass has circulated toward the north around the center which is at 17° W.

Figure 6 is nicely centered on the cyclone and shows the dry air completely around the northern (equatorial) side of the cyclone. Of particular interest in this picture are the clouds standing above the lower cloud undercast, near the storm center. The shadows that appear along the eastern edge of each cloud make it clear that these are well above the lower cloud deck and have the appearance of cumulonimbus towers. However, since these elevated features are 30 to 60 miles long, they must represent a combination of cumulus towers and sheared-off cirrus nothus and perhaps some middle clouds.

3. METEOROLOGICAL ANALYSIS

One purpose of this investigation was to determine the location of the jet stream in the pictured area in order to associate it with the cloud features. Data for 1200 GMT April 28 and 29, 1960 were analyzed, but only analyses for April 28, corresponding to the picture time, are shown.

A space cross section approximately normal to the jet in the pictured area proved to be the critical analytical tool for this purpose. The section extended some 1500 n. mi. from northwest to southeast, but incorporated data from only three stations.

In order to estimate the proximity of the jet stream axis to a given station, the horizontal gradient of potential temperature in the various atmospheric layers was computed from 14 winter cases studied by Palmén and Newton [1] and for four autumn cases assembled for this study, all in the Northern Hemisphere. The latter limited sample was computed only for the purpose of estimating any differences that might exist between winter and autumn gradients near and beneath the jet—no claim for statistical significance is made.

The potential temperature gradients shown in figure 8 were derived as follows: temperature gradients (°C. per 60 n. mi.) for various pressure surfaces were measured

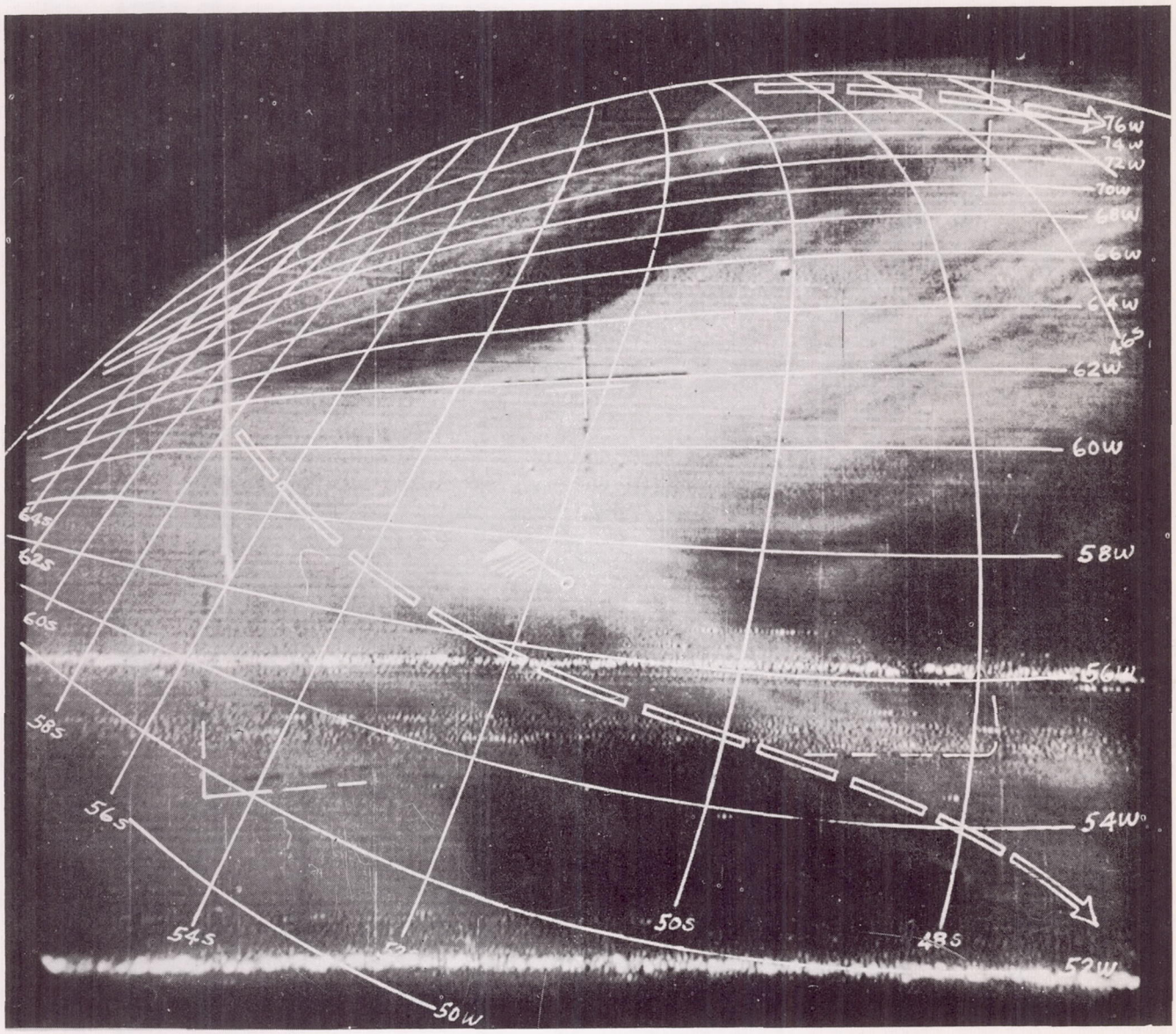

FIGURE 2.—TIROS picture over South Atlantic with South America on horizon. Doubled broken line represents jet stream axis; 200-mb. wind shown from Stanley, Falkland Islands. 1600 GMT, April 28, 1960.

from the mean cross sections of the Northern Hemisphere jets mentioned above. The potential temperature gradients were then approximated by application of equation (1):

$$\frac{\partial\theta}{\partial n}\Big)_p = \frac{\partial}{\partial n}\Big)_p \left[T\left(\frac{1000}{p}\right)^{\kappa}\right] = \frac{\theta}{T}\frac{\partial T}{\partial n} \qquad (1)$$

where the subscript p means differentiation at constant pressure, T is temperature, θ is potential temperature, n is horizontal space coordinate parallel to the pressure gradient, p is pressure in millibars, κ is R/c_p, the universal gas constant R divided by specific heat of air c_p.

Reference to figure 8 shows that the potential temperature gradient maximum is nearly 4° C. per 60 n. mi. The maximum gradient near 700 mb. for the winter cases and near 400 mb. for the autumn cases reflects the intense thermal gradient of frontal regions in the low troposphere during winter contrasted to the maximum gradient occurring high in the troposphere during the warmer season. The feature used here is the value of gradient 100

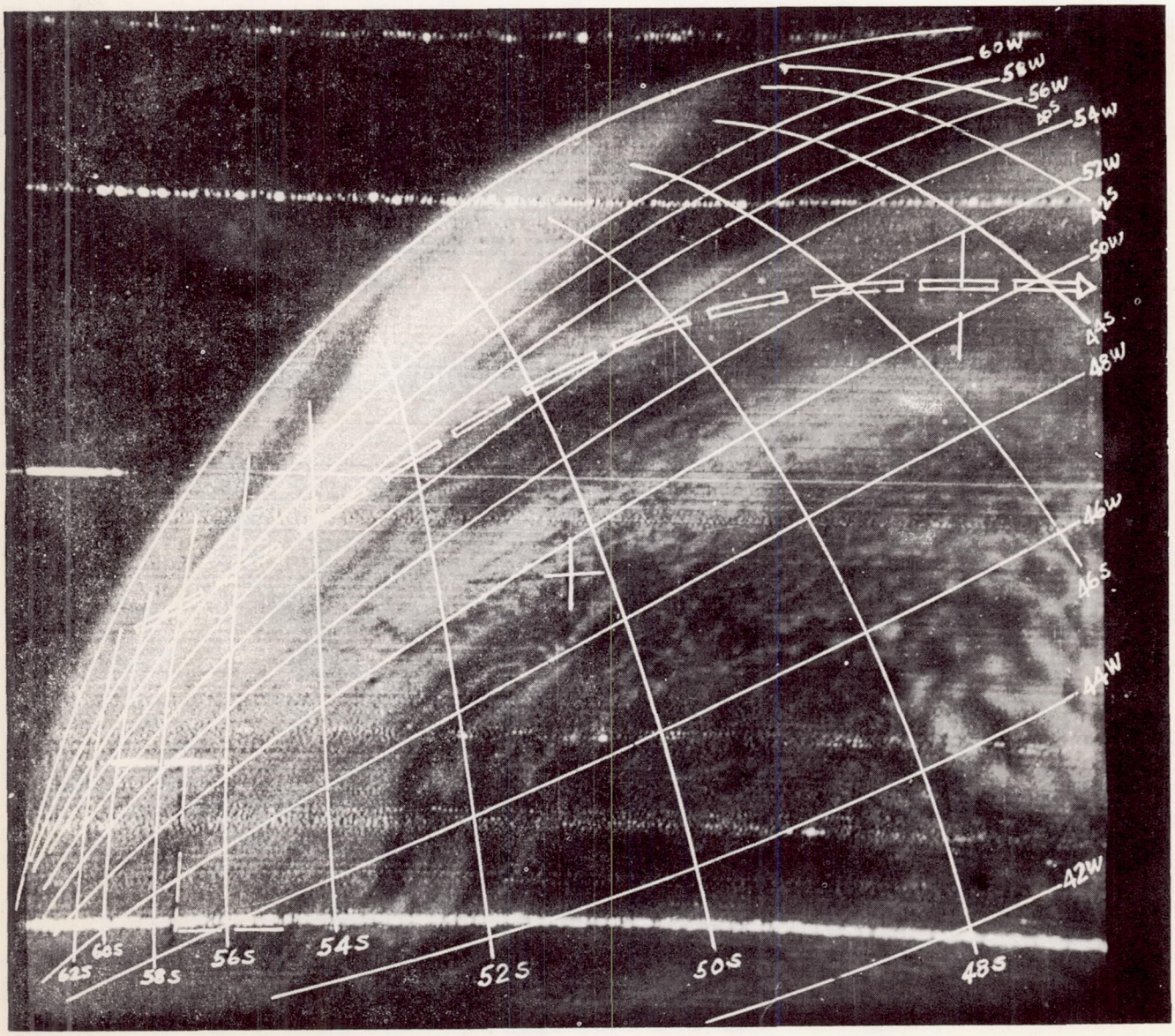

FIGURE 3.—TIROS picture of high pressure area in South Atlantic. Doubled broken line represents jet axis. 1600 GMT, April 28, 1960.

to 200 miles from the jet axis. In both autumn and winter the gradient of 2.0° C. per 60 n. mi. exists no more than 150 to 200 n. mi. from the jet axis and it is this fact that will be applied to the situation under investigation here.

Figure 9 is the space cross section for 1200 GMT April 28, 1960. The line of this section is shown on the 300-mb. map, figure 10, running from Puerto Montt, Chile (41.5° S., 72.8° W.), through Stanley, Falkland Islands (51.7° S., 57.9° W.), to the Naval Observatory at Orcadas, South Orkney Islands (60.7° S., 44.7° W.). The section is plotted with standard radiosonde and wind data. In addition the potential temperatures and potential temperature gradients are shown. The latter were computed by combining the thermal wind equation with equation (1) to give,

$$\frac{\Delta\theta}{\Delta n}\approx\frac{\theta f}{g}\frac{\Delta c}{\Delta z} \tag{2}$$

where f is the Coriolis parameter, g is the acceleration of gravity, and $\Delta c/\Delta z$ is the vertical wind shear.

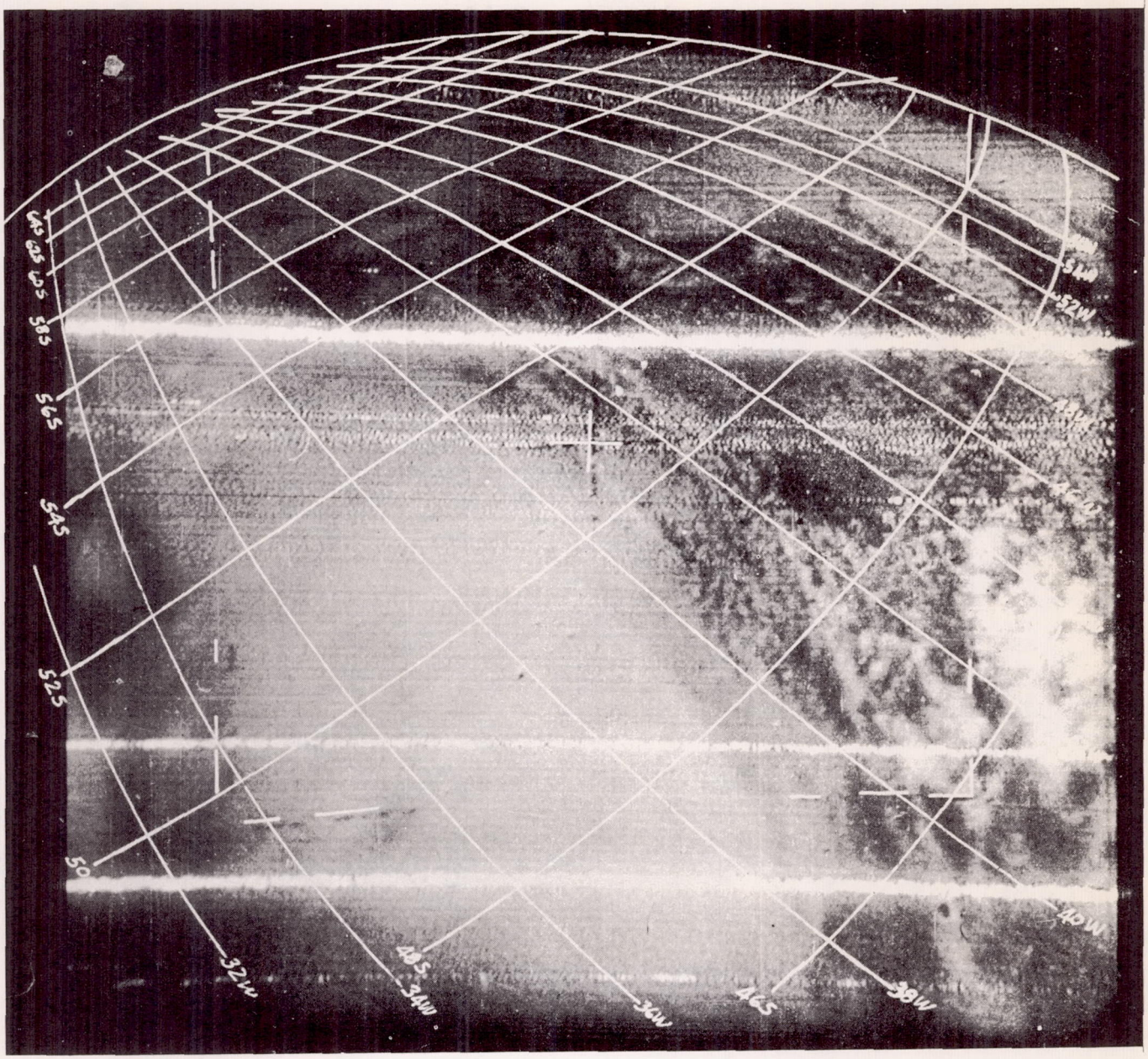

FIGURE 4.—TIROS picture showing transition area between high and low pressure areas in South Atlantic. 1600 GMT, April 28, 1960.

The vertical wind shear was computed for each atmospheric layer reported and the θ-gradient was computed from equation (2) and plotted on the cross section in the same units as those used in figure 8.

Since the cross section is not strictly along the gradients or normal to the mean motion, and because of the probable existence of ageostrophic wind components, absolute consistency cannot be expected between the slope of the isentropes and the plotted gradients. Especially at the northern end of the section the shear vector and wind are not normal to the plane of the section. The analyzed slopes of the isentropes were made consistent with smaller values of $\Delta\theta/\Delta n$ (approximately 60 percent of the plotted values) in figure 9a.

In particular, shear in the layer 300 to 250 mb. over Puerto Montt implies a very large temperature gradient,*

*The gradient of 3.4° C. per 60 n. mi. immediately above a gradient of 0.5° C. per 60 n. mi. hints at an error in the wind report at 300 mb., but even if the two values are averaged, the mean value of 2.0 for the layer 400 to 250 mb. is good evidence for the implication made here.

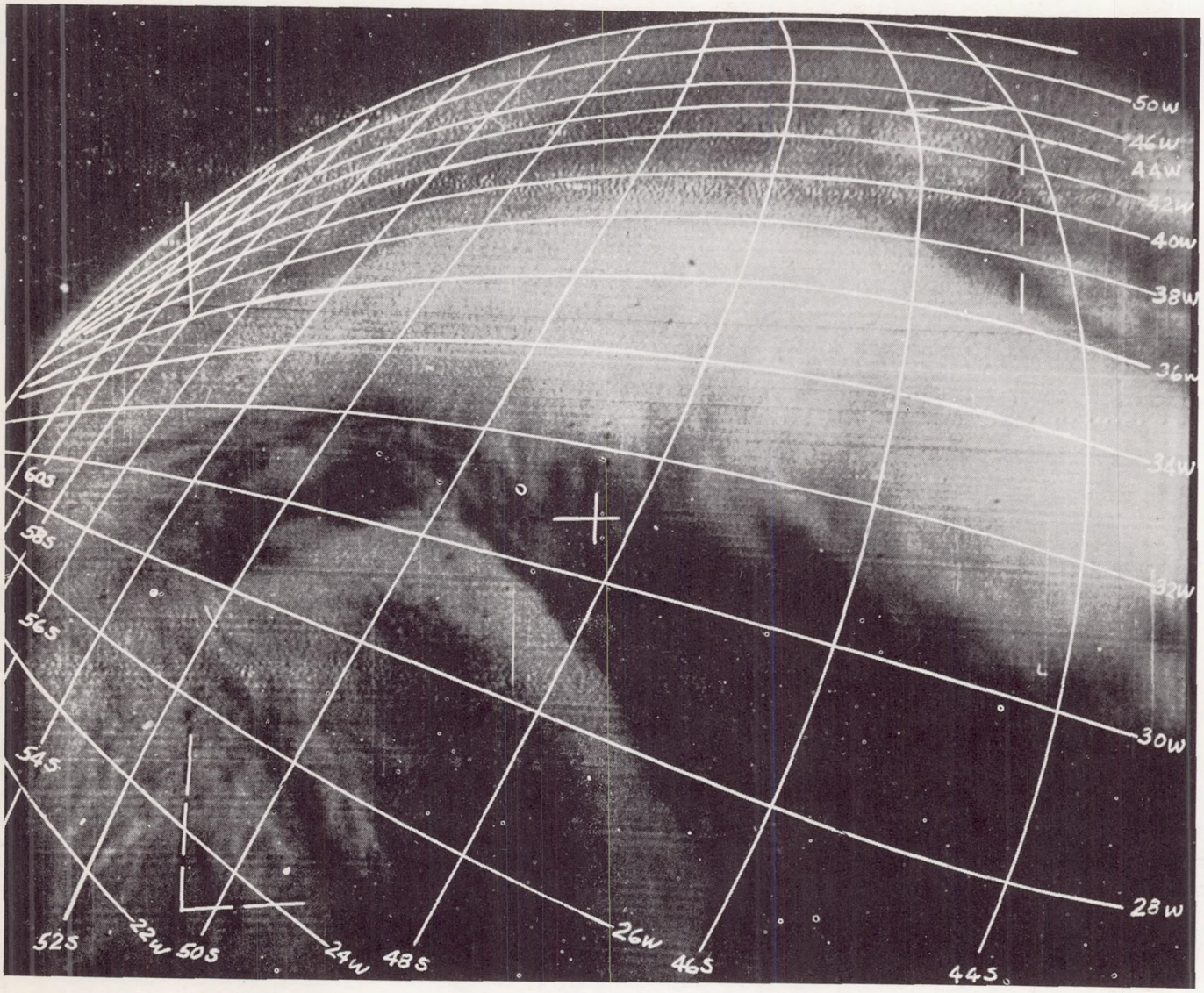

FIGURE 5.—TIROS picture showing curved cloud pattern at edge of cyclone in South Atlantic. 1600 GMT, April 28, 1960.

while the region between that station and Stanley must have a very small gradient in order to retain a reasonable pattern of isentropes. It therefore appears reasonable to postulate the existence of a jet axis northwest of Puerto Montt, and the large gradient indicates the jet axis is probably within 100 to 150 miles of the station. The data from Stanley also indicate a jet axis nearby probably within 150 miles to the southeast since the larger temperature gradients exist southeast of the station.

Figure 9b represents the same cross section but shows the isotach analysis along with lines representing the loci of maximum and minimum temperature gradients. In the low troposphere the maximum gradient is probably associated with a frontal surface and as such is shown sloping poleward. The maximum gradient near Puerto Montt, being high in the troposphere and quite similar to the jet stream gradient found at 400 mb. in figure 8b, may not be directly associated with a frontal surface.

Although it has not been included in the analysis of figure 9b, it appears that the isotach pattern between Stanley and Orcadas might have been more complex than shown here, with a primary speed maximum at the subtropical tropopause and a secondary maximum at about 350 mb., the level of the polar tropopause.

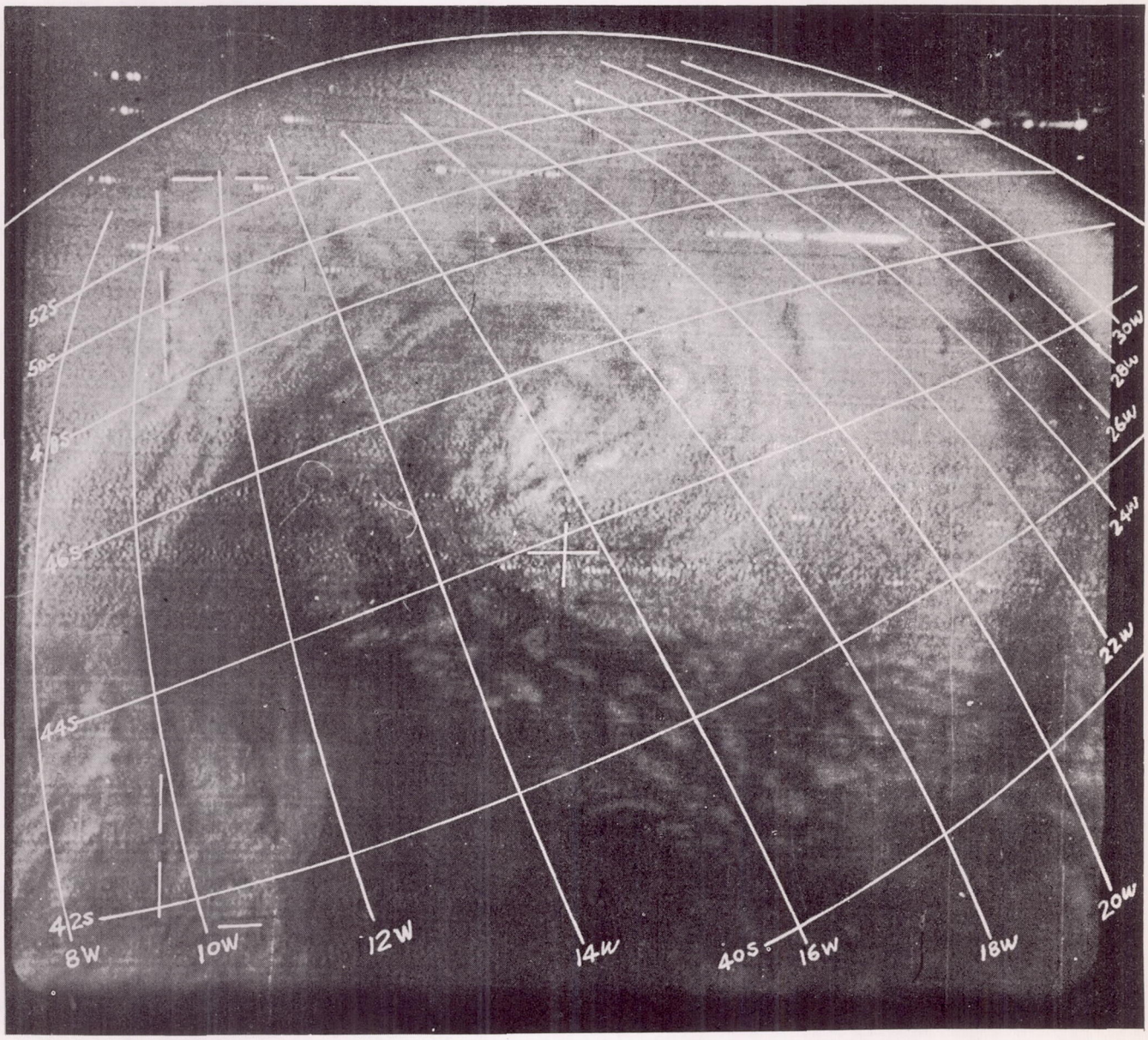

FIGURE 6.—TIROS picture showing cyclone centered at 17° W. in South Atlantic. 1600 GMT, April 28, 1960.

Figure 10 is the 300-mb. analysis for 1200 GMT April 28, 1960 on which the location of both jet axes is shown. Reference to the cross section will show that 300 mb. is not the level of maximum winds, but the general flow pattern for both jet axes is accurately represented by this level.

The closed Low was placed here because such a Low is a frequent feature of the upper flow when a double jet stream appears on Northern Hemisphere maps. The 70-kt. wind at Buenos Aires, 35° S., 59° W., lent credence to the existence of this northern jet axis, and the presence of the closed Low at this time was validated when it moved over that station 24 hours later, producing a wind of 10 kt. from the southwest.

Figure 11 shows three soundings plotted with radiosonde data also used on the cross sections. Both of the soundings over the Atlantic (Stanley and Orcadas) show relatively high moisture content to mid-troposphere, while the upper air over Puerto Montt is extremely dry and shows evidence of subsidence down to the 800-mb. level.

595485—61——4

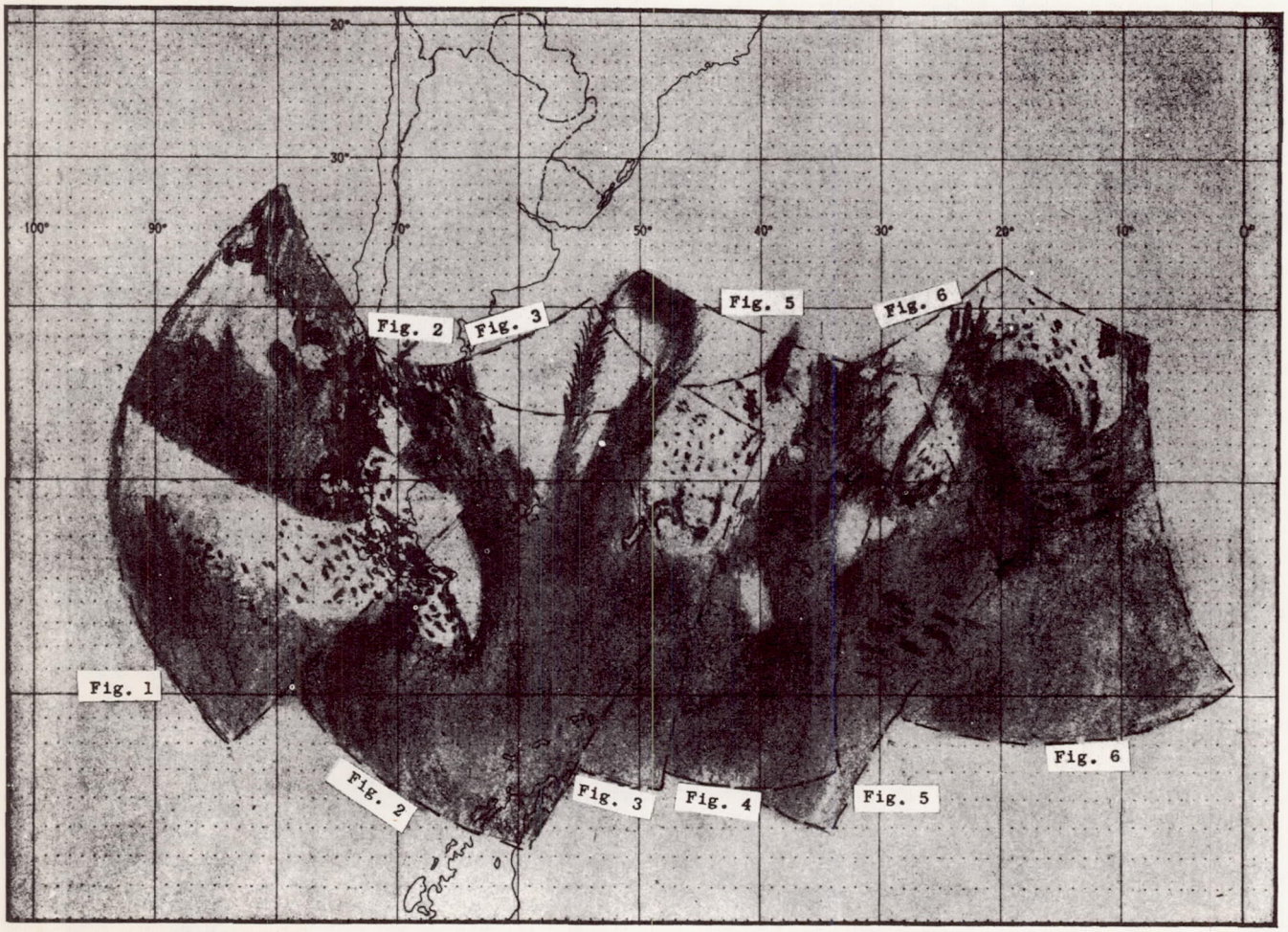

FIGURE 7.—Nephanalysis of clouds visible in TIROS pictures shown in figures 1–6. Broken outlines represent picture boundaries labeled with figures to which they refer.

Figure 12 shows a few of the surface data and analysis furnished by the Argentina Meteorological Service. Data from many continental stations have not been replotted for this illustration, but the isobaric analysis is an accurate copy of that made on April 28 in Argentina.

4. COMPARISON OF ANALYSES WITH PICTURE DATA

It is now possible to associate the analyzed details with the pictures. The overcast cloud deck off the west coast of Chile, shown in figure 1, is clearly below the 800-mb. level because the extreme dryness above that level at Puerto Montt could not support any cloudiness. The overcast deck that ends along the sharp line of figure 1 is a combination of fog and low stratus as shown by the data on figure 12, with the fog probably confined to the coast and the cool coastal waters. South of the 52d parallel in the Pacific the cloudiness is probably stratocumulus giving way to cumulus. The sharp division no doubt represents the boundary between two streams of air that had quite different trajectories—the warmer air from the Pacific anticyclone to the north had been stabilized as it moved over cool water, while the polar air from the south was being made unstable as it moved to lower latitudes. The stratus deck ends along the Andes Mountains in the foreground (along the 71st meridian).

Superimposed on figure 1 is the jet stream axis, representing the jet location at about 250 mb. and streamlines showing motion of the 700- to 500-mb. layer. If there were any high or middle clouds associated with the jet

JOURNAL OF GEOPHYSICAL RESEARCH VOLUME 66, NO. 3 MARCH 1961

A Subtropical Convergence Line of the South Pacific
A Case Study Using Meteorological Satellite Data

LESTER F. HUBERT

U. S. Weather Bureau
Washington, D. C.

Abstract. A subtropical convergence line in the southwest Pacific some 2000 miles long has been recorded by television pictures of Tiros I on May 11 and 12, 1960. The standard meteorological data have been analyzed and compared with the pictorial data. It is shown that although this synoptic system was vigorous and well documented by the pictures, its existence and extent cannot be delineated by standard meteorological observations. The tropical area pictured is shown to contain no vigorous disturbances and the value of such pictures to the tropical analyst is discussed.

INTRODUCTION

The origin, dynamics, and even description of tropical disturbances are incompletely known, but it is generally agreed by tropical meteorologists that lines and areas of convergence lying completely within a homogeneous air mass exist in the lower troposphere. Examples of such systems are the easterly waves studied by *Riehl* [1954], the equatorial waves described by *Palmer* [1952], and the intertropical convergence zone (ITC) which has received continued attention ever since polar front enthusiasts attempted to apply the air mass model at the equator. In addition to the traveling disturbances in the tropics and subtropics, there exists a system variously identified as a convergence line, a shear line, or even a stationary front. Indeed, it is sometimes possible to trace such a line of convergence back to a true polar front from midlatitudes, but having traveled many days over a warm ocean it no longer represents an air mass boundary [see *Riehl*, 1954, chapter 10]. Despite complete frontolysis, a band of cloudiness and frequently an accompanying line of shear retain their identities for several days. Such systems are significant since it is clear they are perpetuated long after the potential energy of the cool air mass has been dissipated, thereby posing the interesting question of the dynamics of its maintenance after the potential energy is consumed. Furthermore, since they often become quasi-stationary, these systems may remain undetected for long periods because they do not sweep across reporting stations as do the waves and vortices, and for that reason have been incompletely described and largely neglected insofar as theoretical study is concerned. The study presented here considers such a quasi-stationary convergence line in the southwest Pacific, studied by use of the television pictures from the meteorological satellite, Tiros I.

TIROS I—METEOROLOGICAL SATELLITE

A satellite carrying two television cameras was launched April 1, 1960, under the auspices of the National Aeronautics and Space Administration. The cameras were mounted so that both their optical axes were parallel to the spin-axis of the vehicle. The payload was spin-stabilized, changing its orientation in space only slowly [*Bandeen and Manger*, 1960]. Since the earth rotates about 25° during the 99-minute satellite period, pictures may be taken along swathes about 1500 nautical miles apart on the northbound or southbound part of a pass. The combination of the earth's rotation rate with the satellite period and the fact that Tiros is spin-stabilized permits photographing the same part of the earth's surface at 24-hour intervals. Such a potential is particularly useful for the application of these data to meteorological analysis because the time change of synoptic systems is an important diagnostic element.

One camera with a wide-angle lens encompassed a field of view just over 100° object space angle while the second camera viewed about 14°. Since the field of view of each camera was scanned by the same number of television raster lines, the 'resolution' of the longer focal length system is an order of magnitude greater than the

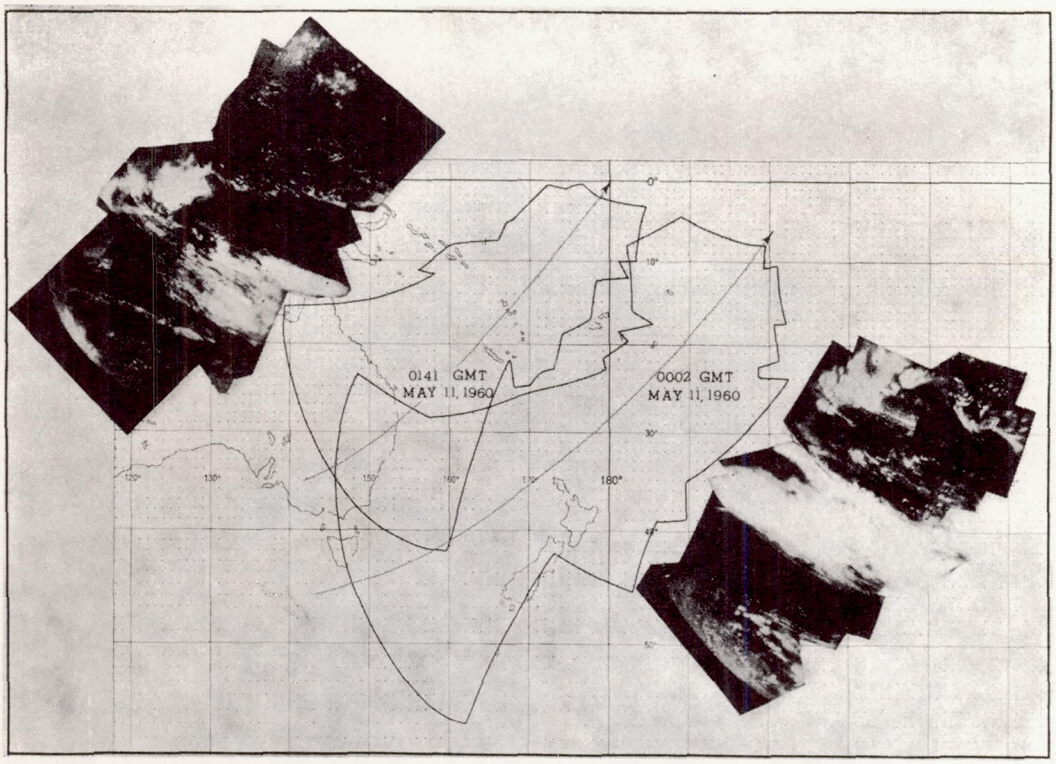

Fig. 1*a*. Composite of pictures taken near 0000 GMT, May 11, 1960. Dotted lines show satellite track; irregular outlines indicate boundary of pictured area.

short focus system. In the mode of operation where pictures are stored on tape for later transmission, both cameras take simultaneous pictures at 30-second intervals.

During the second week of May, Tiros cameras were directed earthward in favorable picture-taking conditions (of angle and illumination) approximately between latitudes 40°S and 20°N. On May 11 and 12 pictures were obtained covering the area shown in Figure 1. Trajectories of the satellite subpoint are shown along with the time of each pass across latitude 25°S. On each pass the satellite was moving toward the northeast and the cameras were viewing back along the track toward the southwest. The strip composites (Fig. 1) represent the photographic coverage obtained on each of the four passes over the area.

Case Study of a Convergence Line

Photographic data. Two frames from each of the four passes (Fig. 1) are shown in Figures 2–9 with geographical grids superimposed. Each picture requires its own grid, which must be computed for that particular camera position in space and orientation of the optical axis. Even small errors in these parameters produce uncertainties in the placement of the grids upon the pictures, so precise location of any detail (within a few miles) cannot be expected. It is estimated that the accuracy of locating features on the pictures by reference to the superimposed grids is ±50 nautical miles at distances halfway to the horizon.

The outstanding synoptic feature that appears in the pictures is a broad, solid band of clouds having an average width of about 300 nautical miles and extending from the Solomon Islands in the southwest Pacific nearly 2000 miles toward the southeast (see Fig. 10). It is not possible, in general, to identify cloud genus (e.g., stratocumulus vs. altocumulus) at great distances on the wide-angle pictures, but the narrow-angle pictures are usually adequate to distinguish between cumuliform and stratiform clouds. Comparison of these higher resolution pictures with simul-

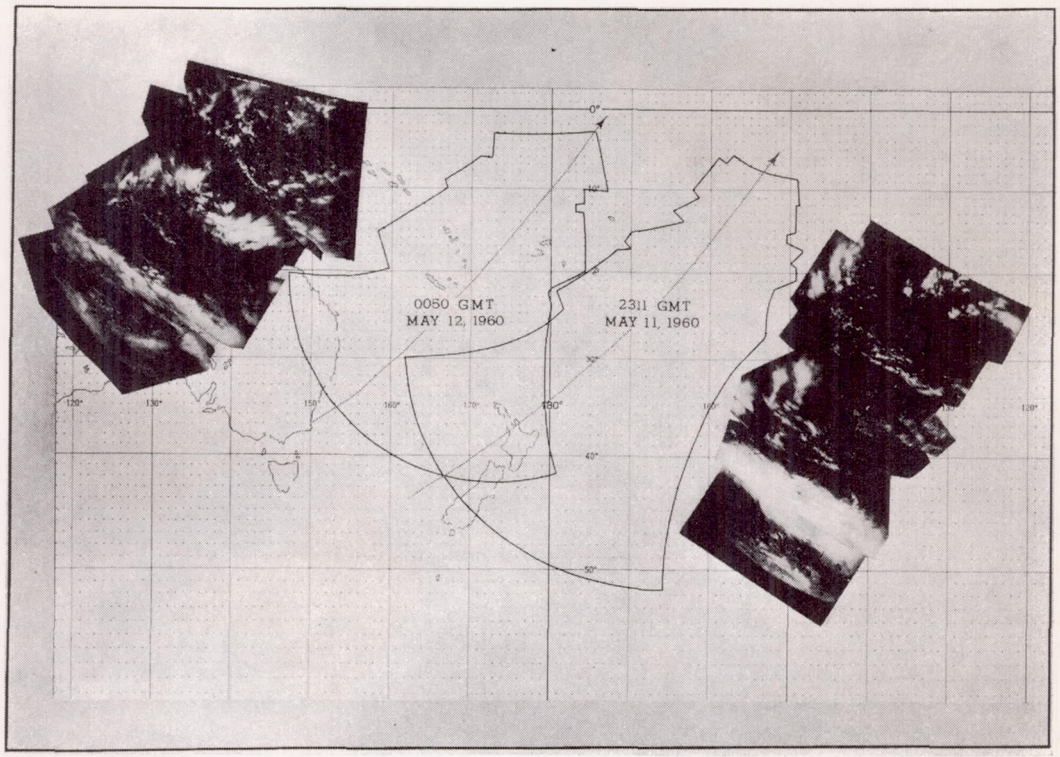

Fig. 1*b*. Composite of pictures taken near 0000 GMT, May 12, 1960. Dotted lines show satellite track; irregular outlines indicate boundary of pictured area.

taneous wide-angle pictures shows that separate elements of cumuliform clouds produce a grey, granulated texture on the wide-angle pictures where the size of the cloud elements and the size of the clear spaces between clouds approach the limit of resolution of the television system. Figure 5 includes a narrow-angle picture illustrating the difference in resolution of the two cameras as well as the relative areas covered. Notice in the lower right portion of the small field picture clouds of cumulus appearance can be distinguished while the same portion of the wide field picture shows only irregular grey shade. Similar areas can be found on most other pictures, for example, Figure 4, in the portion surrounding the intersection 12°S, 170°E. The pictures therefore indicate that the major cloud band is a solid overcast with cumulus clouds on the edges, thereby suggesting that the band is composed of builtup and merged cumulus or multilayered clouds. The surface reports confirm this. It is also clear from surface reports that cirrus clouds existed over portions of the region but, for the most part, they cannot be identified from the wide-angle pictures—see, for example, Figure 8, 13°S, 177°W where cirrus is reported (Fig. 11*b*). On the other hand, the narrow-angle pictures frequently show feather-edged, tenuous patches that might be cirrus, low stratus, or even fog. An example of this is shown in the small field picture of Figure 5. The isolated patch indicated near the center has the tenuous character on its left edge and, occurring as it does in tropical air with cumulus clouds, it is quite probably Cirrus Nothus.

In order to incorporate this type of satellite data into meteorological analysis it is necessary to transpose perspective-distorted cloud pictures onto a map projection similar to that used for mapping and analyzing standard meteorological data. The difficulty of using pictures directly is illustrated by the strip composites of Figure 1. Because of the enormous change of slant range from the horizon to the field directly beneath the camera, the smaller patches of clouds near the camera are exaggerated while the major cloud

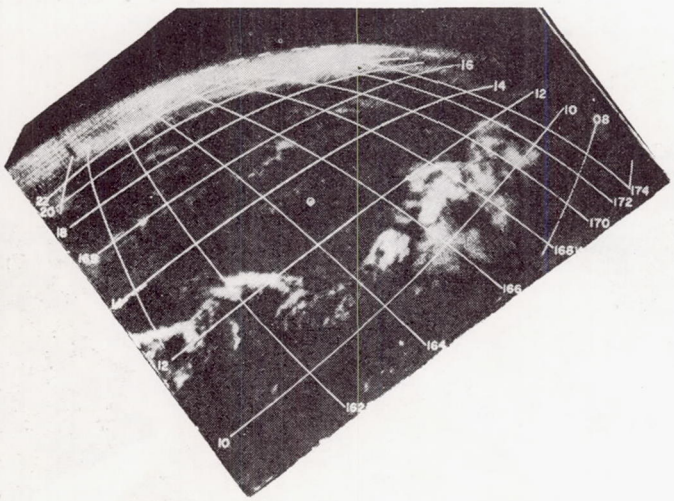

Fig. 2. Individual frame showing weak convergence clouds in tropics and major cloud band on horizon. Picture taken at 0009 GMT, May 11, 1960.

bands at great distance are minimized. Figure 10 is a schematic representation of the pictured clouds from the four passes (Figure 1) in which two shades are used to differentiate the highly reflective clouds from those that are a more dull grey on the photographs. The type of cloud schematic map illustrated here is capable of showing only the large-scale features, and it is obvious that the meteorologist must refer to the photographs to gain a true appreciation of the cloud fields.

Analysis of standard data. In this portion of the South Pacific many surface reports are available, but the tropical analyst must be cautious in evaluating the conflicting evidence of individual observations because the synoptic systems produce subtle changes that are easily masked by local effects and small inaccuracies. For

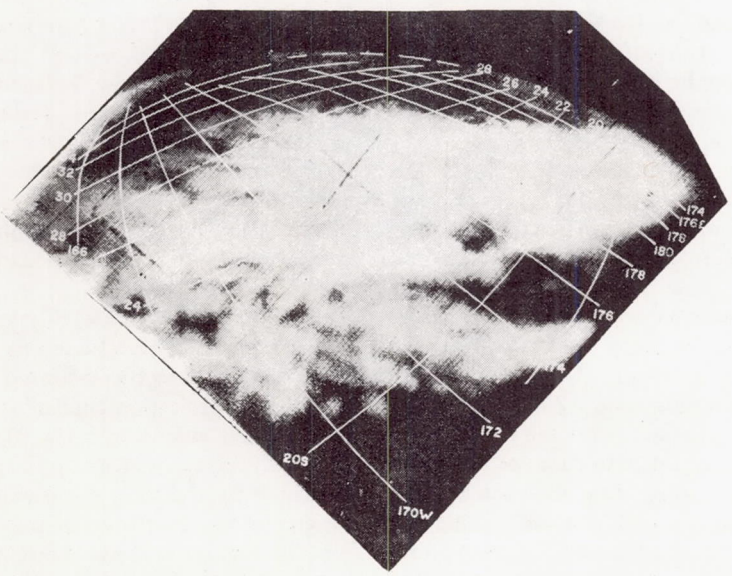

Fig. 3. Individual frame showing cloudless corridor of anticyclone (19°S, 176°W) cutting into northern edge of major cloud band. Picture taken at 0005 GMT, May 11, 1960.

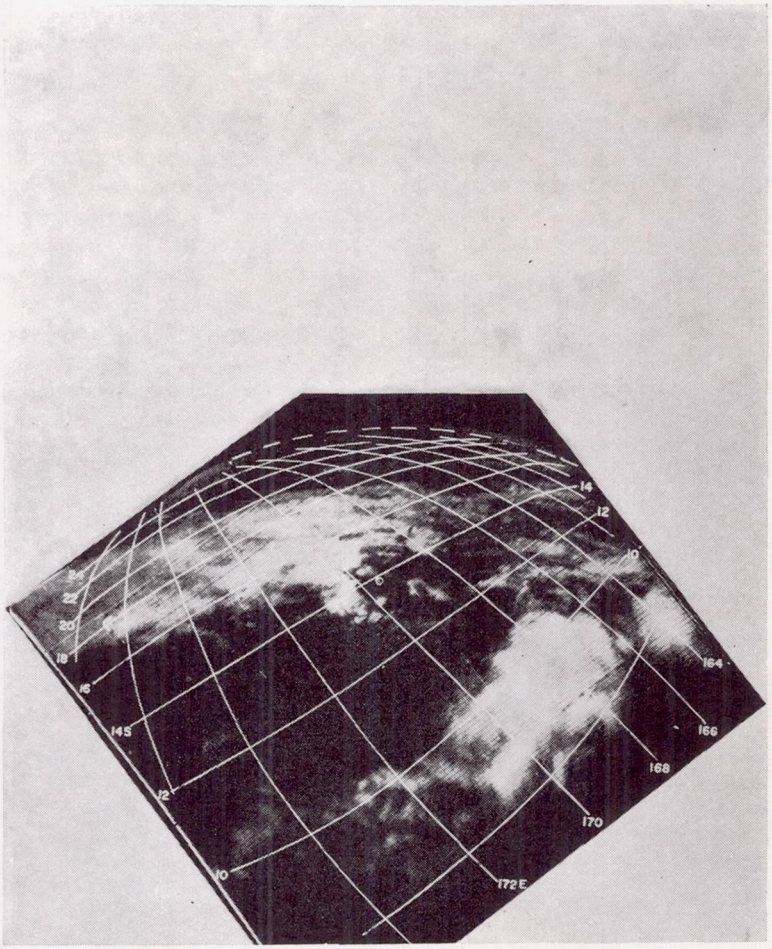

Fig. 4. Individual frame showing western end of major cloud band and weaker convergence clouds at 10°S. Taken at 0150 GMT, May 11, 1960.

example, significant weather-producing systems are often shown only by a small change in wind direction and an increased cloudiness and precipitation, but every sizable island has local and diurnal effects that produce changes of equal magnitude [*Palmer, Wise, Stempson, and Duncan,* 1955]. Ship reports, of course, are not affected by terrain, but small wind changes are not efficiently observed from a moving ship.

The cloud-reporting code is inadequate in the tropics to differentiate local cumulus and showers from those of a disturbed situation. The clue to synoptic disturbances provided by surface observations is a larger-than-normal amount of middle cloudiness at a group of stations. In this event the surface observations do confirm large amounts of middle clouds in the region of the main cloud band, but it is not possible to deduce from those observations that a continuous band existed. Surface pressure analysis by itself is inadequate to delineate synoptic systems before they have reached great intensity, so streamline analyses of the surface wind reports have been made and are shown in Figures 11*a* and 11*b*.

The analyses of Figure 11 were made from surface observations, independent of the photographic data. Six-hourly maps for May 10, 11 and 12, 1960 were analyzed to exploit time continuity, and manuscript maps for this area, furnished by the Weather Bureau Airport Station at Honolulu, Hawaii, were available to show changes over longer periods. Most of the islands

in this region are of rugged volcanic character, and consequently all have local effects that create serious problems in surface streamline analysis. It will be noticed that some of the wind reports do not fit the analyses. In every case where a choice has been made between conflicting evidence, it has been done by reviewing the station's location relative to terrain [*Ramage*, 1959], considering time continuity, and making the most reasonable meteorological choice. For example, the surface west wind reported at Nandi (17.6°S, 177.6°E) appears to be a local wind signifying no large-scale synoptic feature in the low troposphere—an opinion based partly on the fact that this station is downwind from 4000 ft peaks and partly because pilot balloon data show easterlies from 2000 to 9000 ft at the first map time and light and variable winds up to 7000 ft at the second map time.

One of the important uses of streamline analysis in the lower troposphere is to indicate areas of divergence and thereby vertical motion. Divergence is, of course, dependent upon speed as well as directional divergence. Figure 11 shows no speed field because the data are inadequate to yield a definitive isotach analysis. It has been shown, however, that in the tropics frequently there is correlation between directional divergence in the low troposphre and total horizontal divergence [*Palmer, Wise, Stempson, and Duncan,*

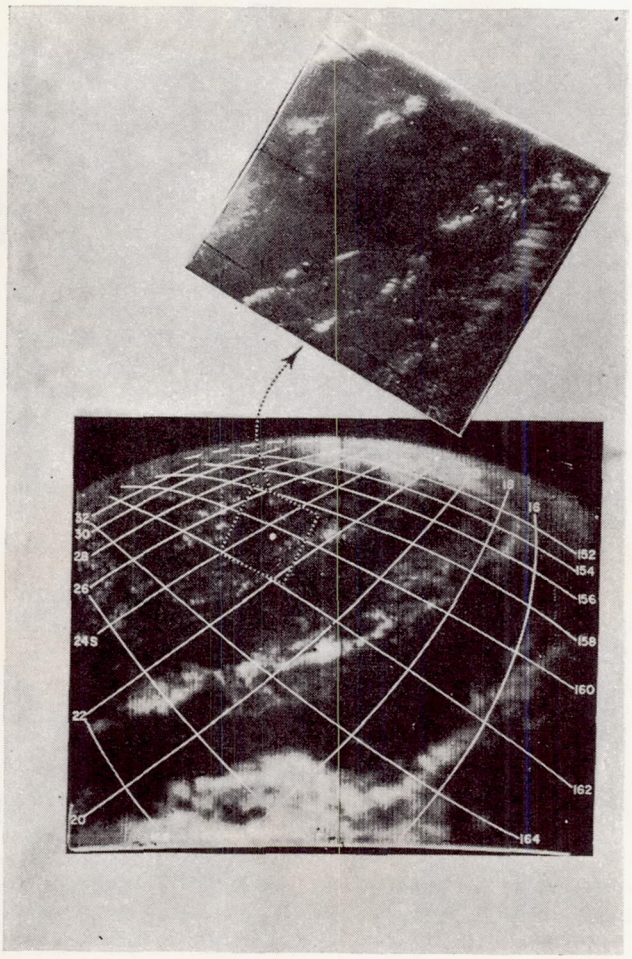

Fig. 5. Individual frame showing cloud pattern in anticyclone from New Caledonia in left foreground to Australia on horizon. Dotted outline in large picture indicates coverage of narrow field picture (above). Pictures taken at 0145 GMT, May 11, 1960.

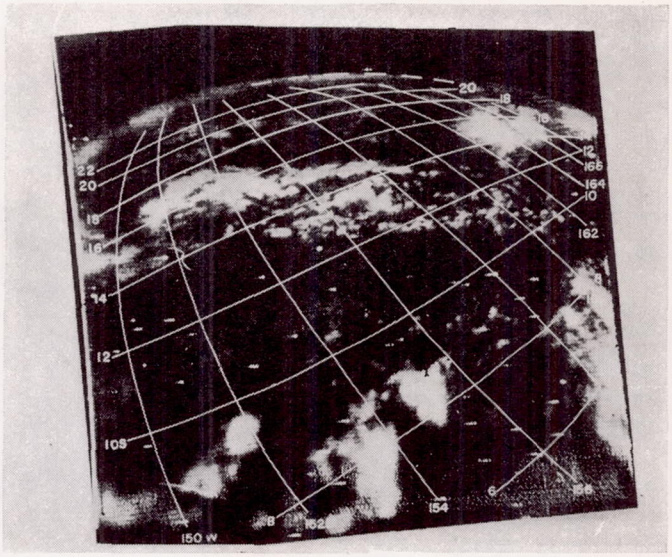

Fig. 6. Individual frame showing weak convergence clouds in tropical South Pacific. Picture taken at 2317 GMT, May 11, 1960.

1955], so that the streamline pattern is of some use by itself in indicating probable lines of convergence for comparison with the pictured cloud band. Directional convergence is implied by the analyses of Figure 11 along the asymptote emanating from the col at 180° longitude. It can be shown that two principal asymptotes must intersect in a col (neutral point), one being the locus of converging streamlines, the other the locus of diverging streamlines [*Palmer, Wisc, Stempson, and Duncan,* 1955]. The convergent asymptote is indicated by the double-weight streamline through the col near the date line in Figures 11*a* and 11*b*, and these asymptotes are

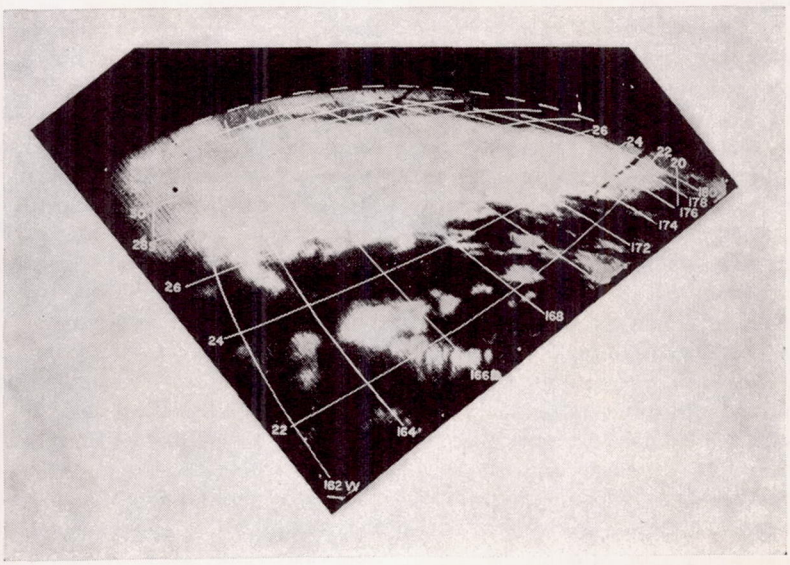

Fig. 7. Individual frame showing western portion of major cloud band. Picture taken at 2313 GMT, May 11, 1960.

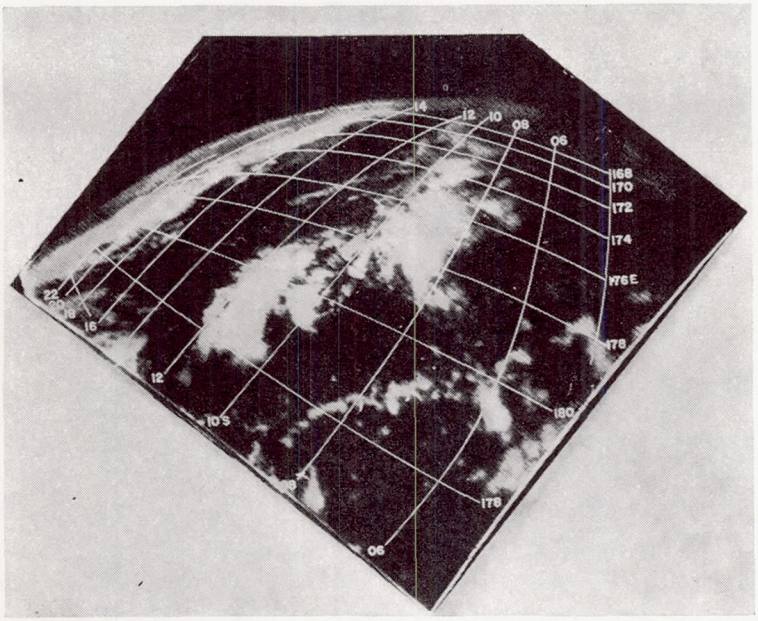

Fig. 8. Individual frame showing tropical convergence line near 10°S and major cloud band on horizon. Picture taken at 0057 GMT, May 12, 1960.

also shown in Figure 10 by the heavy lines through the major cloud band.

If we now examine the pattern of streamline convergence for correlation with the major cloud band, we can see some agreement. In general the cloud band follows the convergence asymptotes emanating from the col at 180°. Furthermore, the portion of that asymptote southeast of the col moved poleward during the 24 hours shown, and the cloud band in that region also moved south. Meanwhile the asymptote extending toward the northwest showed little displacement and the cloud band here was also stationary.

The small anticyclone that moved from 174°W to 180° in this interval is well documented so that it is clear that it moved along the cloud band without any great effect on the total sky cover. Apparently a corridor of little cloudiness extended from the cell center toward the northwest shown by the shading in Figure 10*a* and in the right foreground of Figure 3, and 24 hours later a break is shown in the solid band at 21°S, 178°W in Figure 8. It is significant to notice that this cell *was not* the typical subtropical anticyclone, that is, a slow-moving large-scale high; rather it was small and moved downstream in the trades at a speed typical of disturbances in the easterlies (10 to 12 kt). It is therefore likely that this small cell was quite shallow and produced divergence and downward motion only in the low troposphere. If this were true it would suppress the low cloudiness with little effect on the middle clouds that are seen from above. Indeed, there is a hint of this from the reports in the cell at 0000 GMT, May 11 at 19° and 21°S and at 0000 GMT, May 12 at 21°S, where only one to two-tenths of low clouds are reported beneath the middle clouds. In addition, an upper wind sounding at 21°S, 175°W at 2300 GMT, May 11 shows the wind backing from southwest, through south and east between the surface and 4000 ft, strengthening the deduction that the circulation was very shallow.

During its evolution, if the cloud band was initially associated with a polar front, it was quite likely a line of cyclonic vorticity, because of the shear and sharp cyclonic curvature of the air motion that characterizes frontal zones. The air mass difference across a front decreases and finally disappears during its slow movement over the warm ocean, and in the tropical phase frequently only the cyclonic shear remains, thereby giving rise to its identification as a shear line. Finally even the shear must dissipate; there-

fore it seems reasonable to examine the shear along the cloud band (in so far as it is reflected by surface data), attempting to obtain an estimate of the phase of evolution shown in the pictures from a frontal zone, to a shear line, to a line of weakening convergence.

Were the isotach field available, the vorticity along the cloud band could be computed with reasonable accuracy. In the absence of an adequate speed field, however, the following procedure was adopted in an effort to examine this feature. The surface pressure field was analyzed at intervals of 1 mb (not shown) and the pressure gradient measured on either side of the cloud band at intervals of 180 nautical miles along its length, with the exception of the southeastern extremity where no data were available. Using the relation between average geostrophic and average actual wind speed at low latitudes, after *Jordan*, [1953], the shear across the cloud band was computed and the results are shown in Figure 12. Although the shear above the friction layer thus determined must be regarded only as a crude indication, the similarity between the two curves of Figure 12, representing the beginning and end of a 24-hour period suggests that the sense of the shear may be revealed. Figure 12 shows that not only is the cyclonic shear small—even at its maximum of 7 kt per 180 nautical miles (7 kt per 180 nautical miles = 10^{-5} sec^{-1})—but the sign reverses so that anticyclonic shear extends from the col southeastward.

The point of this is to show there is a suggestion, at least, that this line of convergence retained its vigor for the interval pictured here even though its evolution had passed through the frontal phase and even, perhaps, well through the shear line phase. Further, at this stage it appears to follow the motion of the convergent asymptote between subtropical anticyclones, an indication that its future depends critically upon the convergence between flow in the equatorward limb of the anticyclones and the trade wind easterlies.

Upper air observation. The upper air data are an order of magnitude less dense than the surface coverage so upper air analyses have not been made, but some comment can be made relative to the upper-air circulation in the vicinity of the few reports available. The single wind observation near the small high cell has already been mentioned; no radiosonde observation was taken at this station.

Upper wind observations in the equatorial and tropical regions, at Nauru Island (0.5°S, 167°E) at Guadalcanal (9°S, 170°E) and at Bora Bora

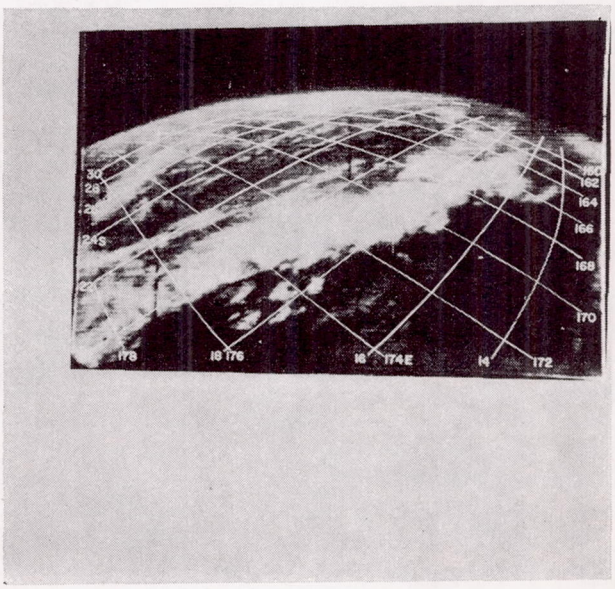

Fig. 9. Individual frame showing western end of major cloud band and cloud covered eastern Australia on horizon. Picture taken at 0054 GMT, May 12, 1960.

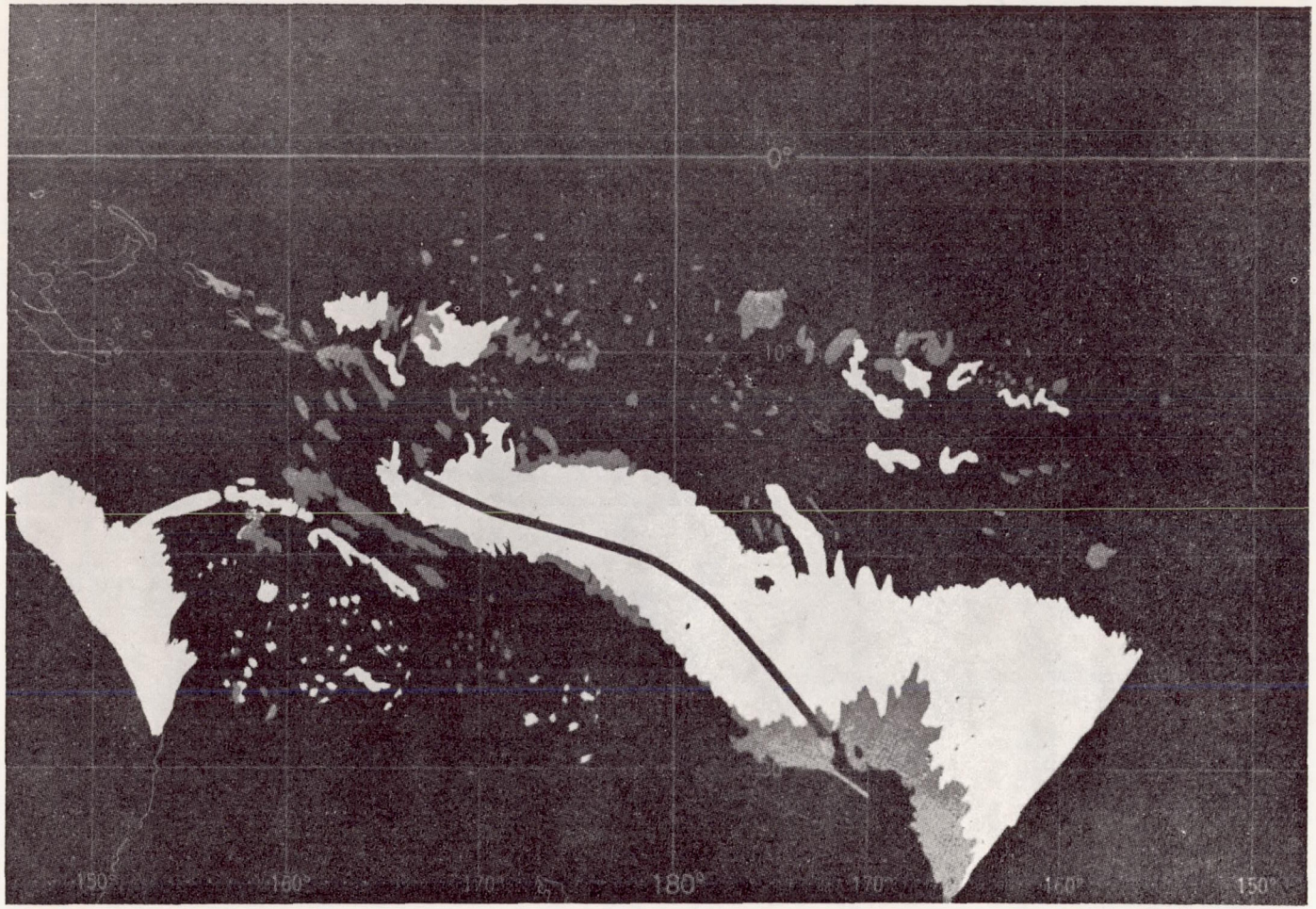

Fig. 10*a*. Schematic representation cloud coverage derived from pictures taken near 0000 GMT, May 11, 1960. Light and dark grey areas represent bright and dull cloud areas of pictures. Heavy dark line in cloud area is the convergence asymptote transferred from Figure 11*a*.

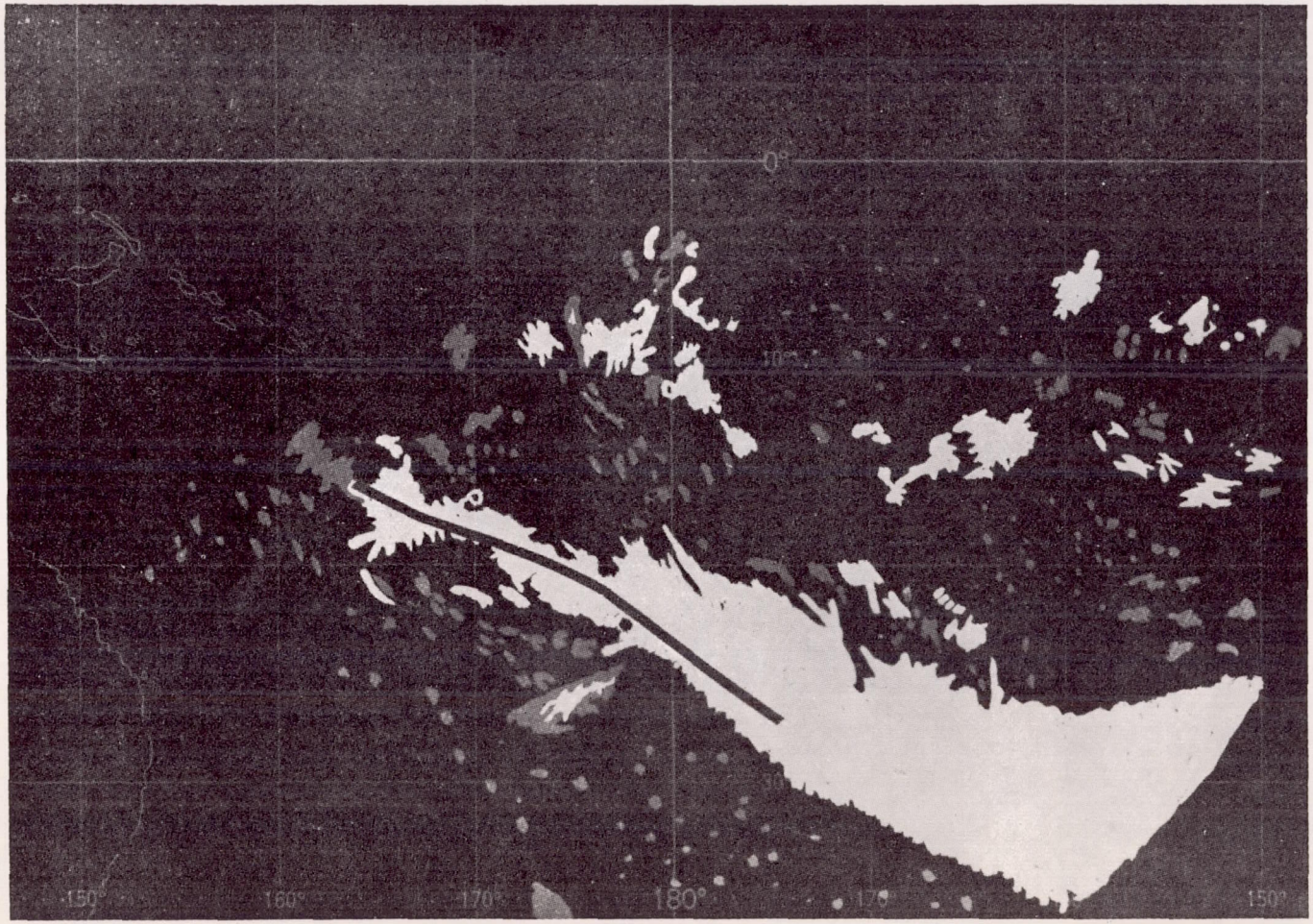

Figure 10*b*. Schematic representation of cloud coverage derived from pictures taken near 0000 GMT, May 12, 1960. Light and dark grey areas represent bright and dull cloud areas of pictures. Heavy dark line in cloud area is the convergence asymptote transferred from Figure 11*b*.

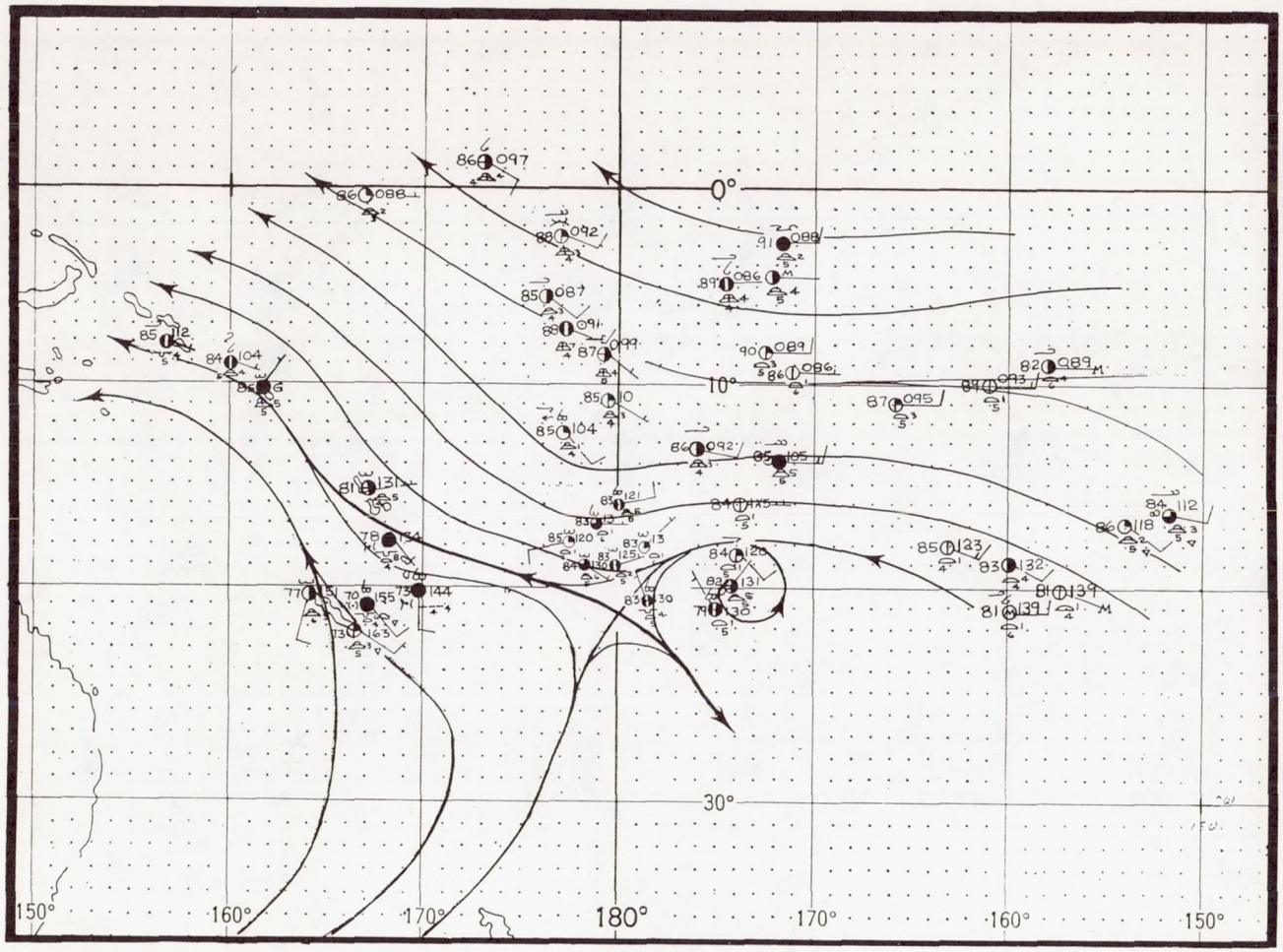

Fig. 11*a*. Surface streamline analysis for 0000 GMT, May 11, 1960.

width from 3 to 10 n.mi.[1] The dimensional spectrum is displayed more graphically in figure 4a by comparison of bands II′ and JJ′. The latter is about 400 n.mi. long and varies from 15 to 60 n.mi. in width. The narrow band at II′, which measures about 2 n.mi. in width, appears to be continuous over a span of about 240 n.mi. It is conceivable that even narrower bands actually existed which are not visible in the photograph due to the limited resolving capability of the vidicon system [5].

In addition to the banded structure apparent in the pictures, another interesting feature is seen in figure 3a along FF′. Here the clouds are arrayed in the form of a chain with the cloud elements which form the links surrounding relatively cloud-free areas. Each link measures approximately 60 n.mi. in diameter with the inner, relatively cloud-free area measuring about 40 n.mi. Patterns similar to this "daisy chain" arrangement have been seen in photographs from the Atlas nose cone on August 11, 1959 [2], and in many pictures taken by TIROS [9]. The significance of this pattern is not immediately apparent though it may suggest the existence of a meso-scale convective regime.

The spiral banded structure of tropical storms has been well documented in the literature [4]. Pictures taken by TIROS I indicate that this banded organization may also be a common feature of the mature extratropical cyclone [7, 15, 6]. The organization apparent in the vigorous extratropical storm (fig. 2a) bears a striking resemblance to that of the typhoon seen near Australia on April 10 by TIROS I [13]. A mirror image of the typhoon is shown in figure 5 to facilitate comparison with the picture in figure 2a. (The mirror image reverses the clockwise sense of the Southern Hemisphere cyclonic circulation.) The relative positions and characteristics of the cloud images seen at A, C, and E as well as the spiral bands are features common to both storms.

SUBJECTIVE INTERPRETATION—CRITERIA AND COMPARISON WITH CONVENTIONAL DATA

Information derived directly from the pictures permits a reasonably accurate and detailed analysis of the organization and distribution of the clouds over most of the viewed area [5]. Information required to complete the description or nephanalysis of the picture—cloud form or type, probable thickness, and probable cloud top heights—must presently be subjectively inferred from the characteristics of the cloud images. Inferences drawn from synoptic models, and from relative brightness,[2] texture, size, shape, and edge characteristics of the cloud images presently form the somewhat tenuous basis for this subjective interpretation [1, 15].

Abbreviated station models showing total sky cover, cloud type, present and past weather, and sferics reports from data available for 0000 GMT on May 6, 8, and 9 are plotted on the appropriate view of the storm in figures 2b, 3b, and 4b for reference in the following interpretation of selected areas of the pictures.

The cloud mass at A in figure 2a, because of its lateral extent and amorphous character is interpreted to be an area of stratiform cloud. The brightness, relative to other cloud images in this picture, and the solid appearance of the area suggest that the clouds are dense, probably overcast and multilayered through the cirrus level. The extreme brightness of the image also suggests the possibility of imbedded convective cloud forms. In contrast, C in figure 2a is a relatively dull, featureless area which gives the impression of rather extensive, thin broken to overcast low stratiform cloud. In general, the spiral bands appear to be composed mainly of cumuliform cloud. This inference is drawn primarily from the small, relatively bright and sharply defined cloud masses within the bands (figs. 3a and 4a) and through reference to cyclone models. The band at JJ′ in figure 4a is reminiscent of the instability lines frequently observed in northwesterly flow to the rear of a cyclone center.

The small, bright, sharply defined cloud masses at E in figure 2a give the impression of strong cumulus activity. This impression is heightened by the thin veil-like cloud at E′ giving the appearance of cirrus spissatus being blown off tops of cumulonimbus.

The scarcity of surface observations from the area of the vortex (figs. 2b, 3b, 4b) prevents a more than superficial comparison of conventional observations and those made by the satellite. The subjective interpretations of cloud form based on criteria mentioned earlier can be neither completely supported nor rejected from the conventional data at hand. Data available in this case tend to show that the relatively brighter areas in the pictures contain clouds and weather generally associated with vertical development or deep cloud layers: (fig. 2a: moderate showers at A, showers and swelling cumulus at B′, showers at D, and towering cumulus below and to the left of E; figure 3a: towering cumulus near F′ and above and to the left of F, towering cumulus and showers at G, squalls at H, and cumulonimbus at H′; figure 4a:

[1] These details, available in the film transparency, may not reproduce clearly in the illustration. Much of the picture is in the local twilight zone resulting in low contrast within the area of the photograph. Local time within the pictured area varies from about 1700 hours on the left to about 1845 on the right where the horizon appears to "melt away" in darkness.

FIGURE 1.—Synoptic history of the west Atlantic vortex. NAWAC surface analyses for (a) 0000 GMT, May 3 1960; (b) 0000 GMT, May 4, 1960; (c) 0000 GMT, May 5, 1960; (d) 0000 GMT, May 6, 1960 with satellite subpoint (●) and picture principal point (+), for the picture in figure 2a; (e) 0000 GMT, May 7, 1960; (f) 0000 GMT, May 8, 1960 with satellite subpoint and picture principal point, for the picture in figure 3a; (g) 0000 GMT, May 9, 1960 with satellite subpoint and picture principal point, for the picture in figure 4a; and (h) 1200 GMT, May 9, 1960.

[2] Relative brightness alone admittedly can be misleading. Neiburger [11] has shown that relatively thin stratus can be highly reflective and Fritz [8] shows that the albedo for a given cloud type can vary over a significant range. On the other hand, preliminary results of investigations by Conover and by member of the Meteorological Satellite Laboratory show that deep cloud masses—large cumuli and cloud masses producing steady rain—frequently correspond to the brighter images in the photograph.

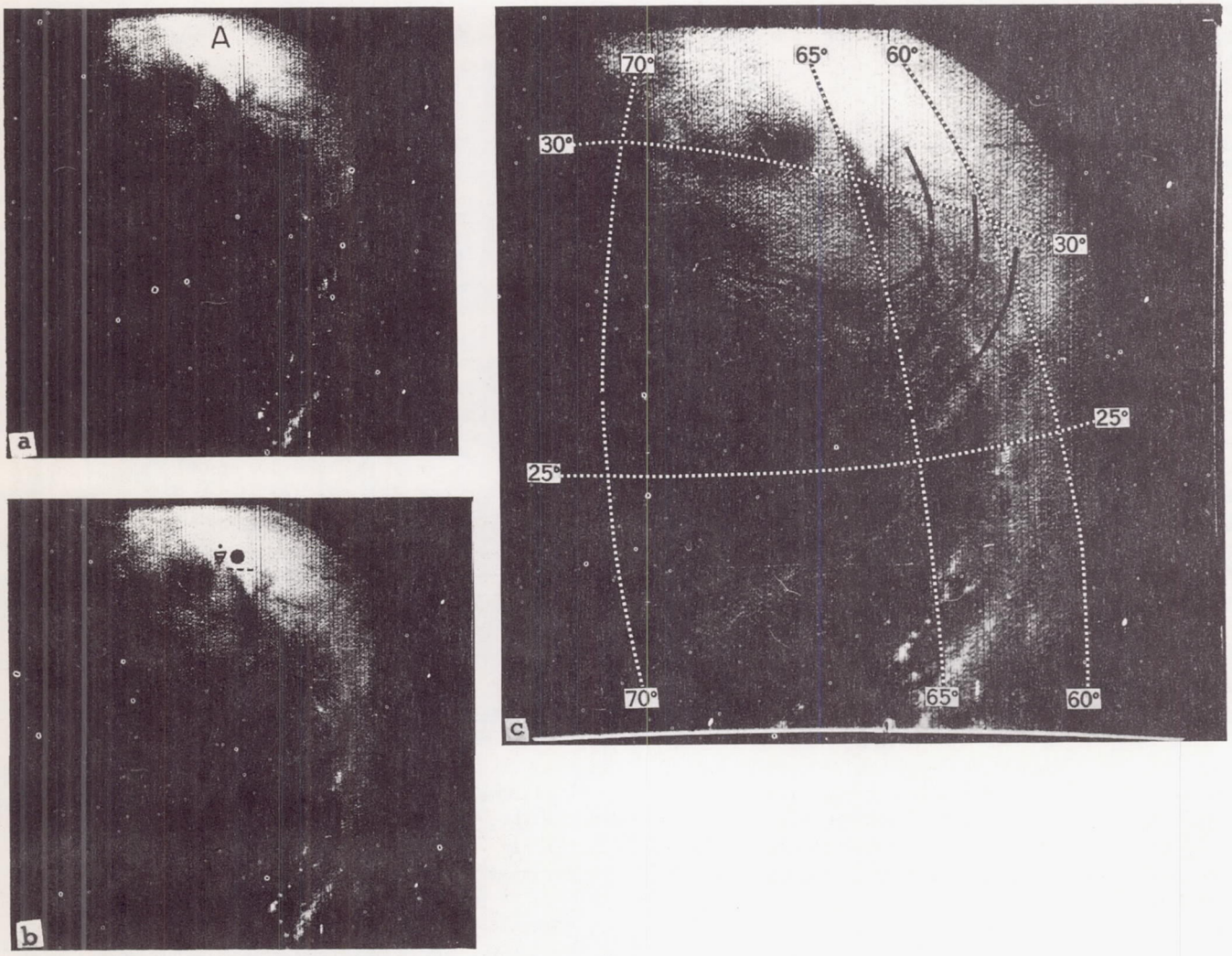

FIGURE 2.—(a) View of the vortex at 2200 GMT, May 5, 1960; (b) Same view with superimposed abbreviated station models from surface data for 0000 GMT, May 6, 1960; (c) Same view with latitude-longitude grid, and 1000–700-mb. mean flow superimposed.

altocumulus—altostratus at A and modreate to strong sferics returns at L). On the other hand, reports of fog, stratus, and stratocumulus—cloud forms and weather indicating little vertical thickness—appear to correspond to the relatively dark, amorphous cloud images in the photographs (fig. 2a: B,D′; fig. 3a: F). The report of clear skies at M in figure 4a corresponds to an area of the picture which is nearly black.[3]

4. RELATIONSHIP TO CONVENTIONAL ANALYSES

Kuettner [10] has shown that under certain conditions of stability and vertical wind distribution, cloud bands tend to parallel the direction of the flow in the convective layer. This relationship, if generally associated with cloud patterns identifiable from a satellite, would obviously enhance the meteorological value of the cloud pictures. For purposes of comparison, the mean flow between 1000 mb. and 700 mb., derived graphically from the surface and 700-mb. analyses prepared in NAWAC, is superimposed on the appropriate picture of the vortex in figures 2c, 3c, and 4c. In addition, latitude-longitude grids are superimposed to provide a familiar frame of reference [3]. Accepting the basic analyses as a good approximation of the flow pattern at the chosen levels—keeping in mind the inherent subjectivity—one finds a fair to good correlation between the orientation of the cloud bands to the south and west of the storm center and the mean contours delineating the flow to the rear of the cyclone within the 1000–700-mb. layer.

[3] Deep water normally appears black to the satellite unless specular reflection is present [8].

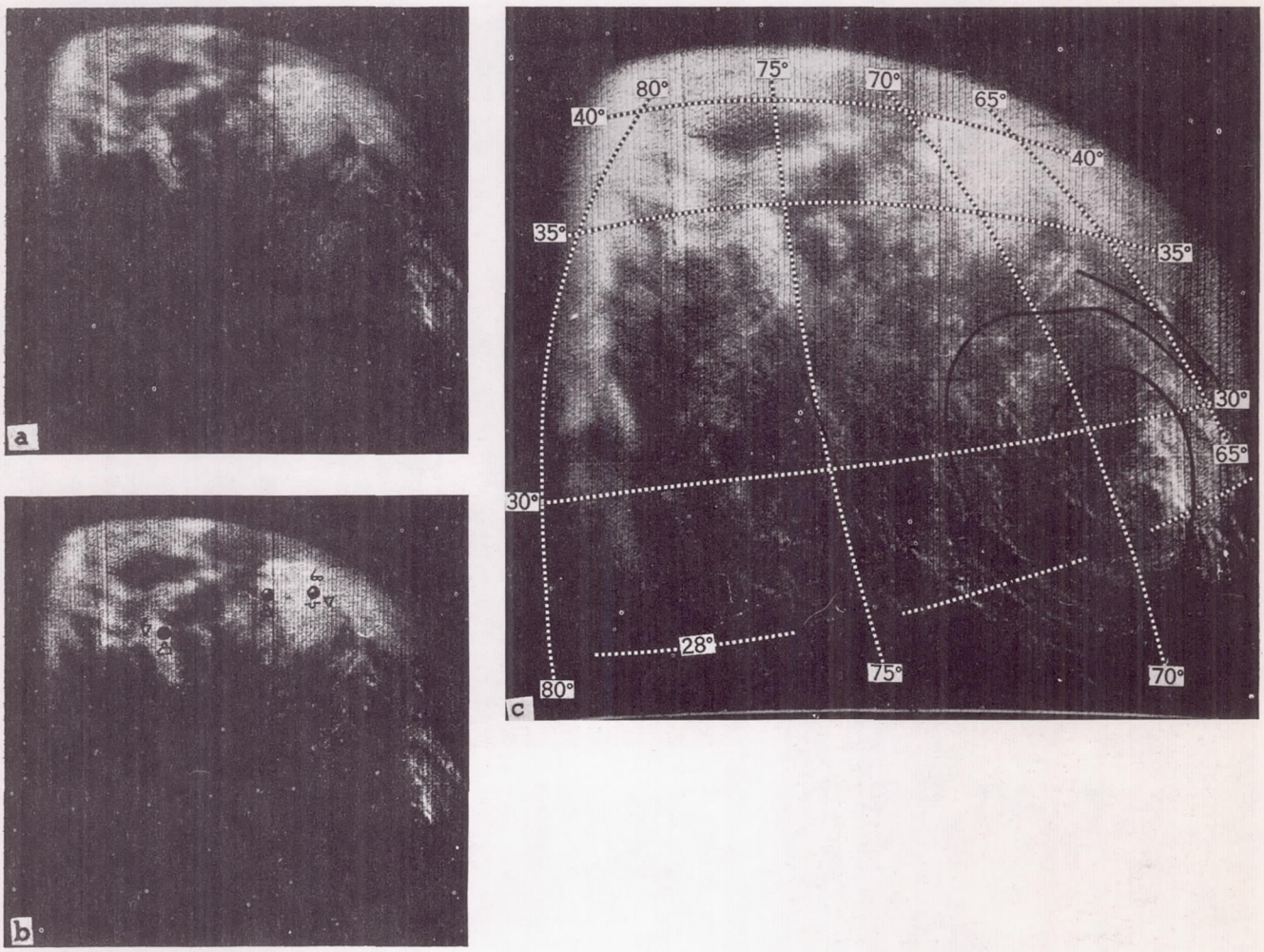

FIGURE 3.—(a) View of the vortex at 2200 GMT, May 7, 1960; (b) Same view with superimposed surface data for 0000 GMT, May 8, 1960; (c) Same view with latitude-longitude grid, and 1000–700-mb. mean flow superimposed.

5. OPERATIONAL UTILITY OF SATELLITE CLOUD PICTURES

The same lack of conventional weather data which frustrates a comprehensive study of this storm emphasizes the potential of a picture-taking satellite to provide useful observational data from areas where meteorological information in any form is either sparse or nonexistent.

The application of satellite cloud pictures to a routine analysis problem is demonstrated in figure 6. The shaded area in figure 6a reproduces an actual analysis of conventional cloud observations in terms of cloudiness significant for air operations in the middle troposphere. The majority of the data considered in this analysis are valid for 0000 GMT, May 9. The schematic nephanalysis from pictures over much of the same area taken approximately 3 hours earlier by TIROS I on pass 543 (fig. 4 represents one picture from this pass) is superimposed on the conventional analysis in figure 6b [14]. The abbreviated station models in figure 6a represent the total conventional data coverage within the area of "No Significant Cloud." It is apparent that an analyst relying solely on these data could not accurately depict the existing cloud distribution observed by TIROS. Yet it is conceivable that the areas of cumuliform cloud and the southward extension of the middle cloud deck at N in figure 6b are significant to the air operations mentioned above.

This series of pictures also provides an opportunity to apply satellite cloud information to the evaluation of a frontal analysis based on a few conventional observations and, of necessity, to a large extent on continuity. The picture in figure 2a represents the cloud pattern over the

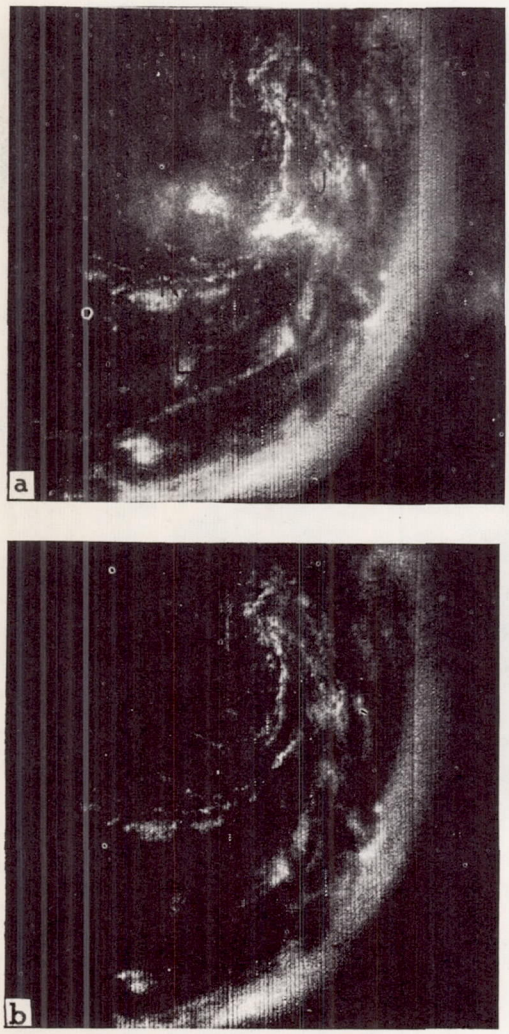

FIGURE 4.—(a) View of the vortex at 2100 GMT, May 8, 1960; (b) Same view with superimposed surface data for 0000 GMT, May 9, 1960; (c) Same view with latitude-longitude grid, and 1000–700-mb. mean flow superimposed.

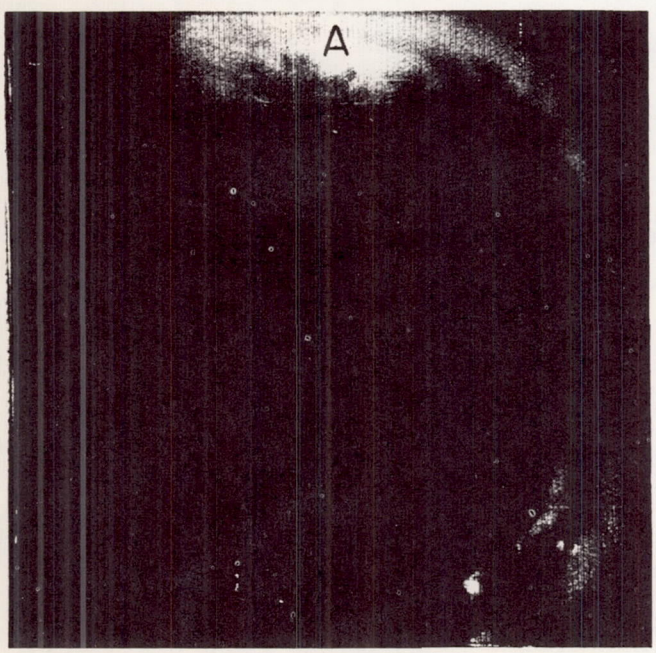

FIGURE 5.—Mirror image of the typhoon viewed by TIROS I near Australia on April 10, 1960 (for comparison of pattern with that of this vortex).

DEPARTMENT OF COMMERCE
LUTHER H. HODGES, Secretary

WEATHER BUREAU
F. W. REICHELDERFER, Chief

MONTHLY WEATHER REVIEW

JAMES E. CASKEY, JR., Editor

Volume 89, Number 9 | Washington, D.C. | September 1961

SOME ASPECTS OF A CYCLE OF AVAILABLE POTENTIAL ENERGY[1]

JAY S. WINSTON AND ARTHUR F. KRUEGER

Meteorological Satellite Laboratory, U.S. Weather Bureau, Washington, D.C.

[Manuscript received April 27, 1961]

ABSTRACT

A large-scale cycle of available potential energy in the Northern Hemisphere over a period of about two weeks during late December 1958 and early January 1959 has been investigated in some detail. During this cycle the zonal available potential energy first built up strongly to a maximum, and then when it began to decline, increases in eddy available and eddy kinetic energy took place. These changes in the energy parameters were well related to variations in the poleward heat transport, large values of which signify substantial conversions from zonal to eddy available potential energy, and to variations in the conversion between potential and kinetic energy. Furthermore some estimates of the generation of available potential energy show good consistency with the available potential energy variations. Examination of this cycle of available potential energy on a regional basis indicates that it was almost completely dominated by developments over North America and vicinity. The synoptic events associated with this energy cycle are also illustrated.

1. INTRODUCTION

Satellite observations of solar and terrestrial radiation will soon be available in sufficient quantity to provide the first direct measurements of the global heat budget. As radiation is measured on a continuing day-by-day basis it will be of great interest to study not only the large-scale spatial and temporal variations in this basic planetary heating, but also the manner in which the atmosphere reacts to it. Since this heating is indeed basic in nature, any clear-cut reactions of the atmosphere to it would most likely be found in some of the more fundamental atmospheric parameters that directly measure the large-scale energetics of the circulation. In particular it seems appropriate to investigate the role of radiational heating with respect to the zonal and eddy components of kinetic and available potential energy as defined, for example, by Lorenz [4].

These various energy components and the typical flow of energy from and to the environment and between various forms are illustrated schematically in figure 1 in the manner presented by Lorenz [3]. Here it is seen that diabatic heating of the atmosphere (actually differential heating between high and low latitudes) builds up the zonal available potential energy, which is basically a function of the latitudinal variance in temperature, or essentially a measure of the strength of latitudinal thermal gradients. As the zonal available energy keeps increasing, the strengthening thermal gradients lead to baroclinic instability and the growth of eddies. Thus eddy available potential energy (increasing thermal differences within latitude circles) increases at the expense of the zonal available energy as northward heat transport increases to relieve the excessive thermal gradients. Some of this increased eddy potential energy is then converted to eddy kinetic energy by means of direct thermal circulations (upward motion in the warm air, downward motion in the cold air) occurring in the eddies, or major cyclone waves. Differential heating relative to these eddies along

[1] This research has been supported by the National Aeronautics and Space Administration.

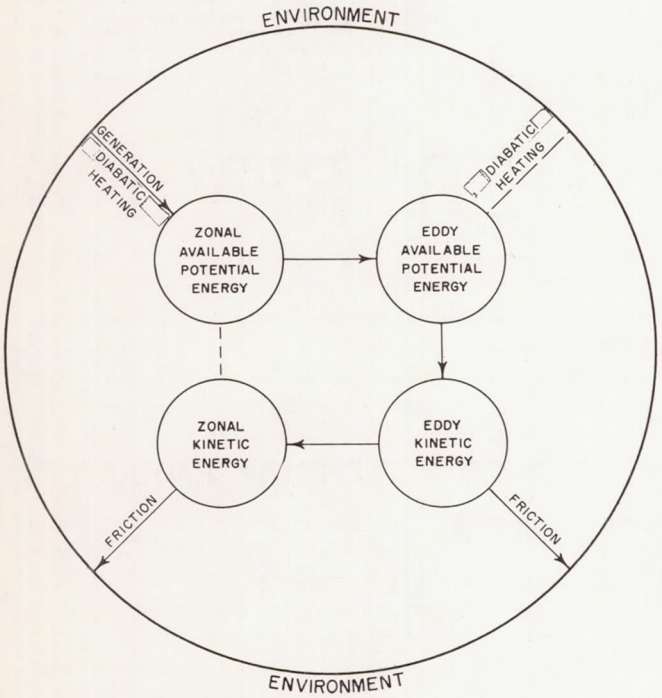

FIGURE 1.—Proposed energy cycle for the earth's atmosphere (after Lorenz [3]). Arrows indicate prevailing directions of energy transformations. Dashed lines indicate that there is apparently no prevailing direction.

latitude circles may either generate or dissipate the eddy available energy—a predominant trend in one direction or the other has not as yet been definitely established. Eddy kinetic energy is partially dissipated by friction and partially converted to zonal kinetic energy (much of the conversion being associated with the poleward transfer of momentum). The zonal kinetic energy is mainly subject to dissipation by friction, but a portion of it may be converted back into zonal available potential energy.

This typical energy flow picture has been generally substantiated by empirical evaluations of energy conversion terms (White and Saltzman [13]; Wiin-Nielsen [14]; Saltzman and Fleisher [10]; Jensen [1]). Although this mode of energy flux is representative of conditions that apparently must prevail on the average, it is realized that the generation and transformation of atmospheric energy may very well vary in both amount and direction at various times. This is the case both in the seasonal sense and also over time periods as short as a week or even a day, particularly when the energy in only one hemisphere or less is considered.

To investigate more closely the behavior of the energy cycle over various time and geographic scales a program for regular daily computation of several atmospheric energy parameters of the Northern Hemisphere has been initiated (Winston [16]). As a substantial sample of such calculations accumulate, it will be possible to document the energy cycle more precisely. Moreover, as radiation data observed by satellites also accumulate, there will be an opportunity to calculate the generation of available potential energy (primarily the zonal component) and to study the reactions of the energy cycle to variations in this radiant energy. These are areas of study for the future, however.

For the present it is of interest to illustrate an actual case of a pronounced cycle of available potential energy which occurred during a pilot period of 42 days of energy computations in the winter of 1958–1959 (Winston [16]). This case seemed to fit the idealized energy flow picture to such a marked degree that it was of interest to examine it in some detail. Presentation of this case is of special significance because it is, to our knowledge, the first time that a cycle of large-scale available potential energy has been investigated for the actual atmosphere. In general circulation model experiments, on the other hand (Phillips [8]; Smagorinsky [12]), there has been extensive "day-by-day" calculation of potential and kinetic energy and energy transformations. Yet it is surprising that there has not been a like body of data computed from the real atmosphere to check similarities of the models and the observed time variations of the atmospheric energetics. Occasionally the energy cycle in the models has been compared to the index cycle of the atmosphere, which was described in detail by Rossby and Willett [9], and indeed the energy cycle and index cycle in a gross sense are often similar phenomena. However, as some experience has been gained with energy parameters, it has been found that the index cycle and the energy cycle do not always occur at the same time and with the same degree of intensity. To a great extent this is due to physically real differences in the behavior of the zonal winds as contrasted with the energetics of the flow. But also it is in part due to the inadequacy of the zonal index as a general circulation parameter. In fact, if one stresses the broader connotation that the term "index cycle" has attained, particularly in terms of cold air penetrations to lower latitudes and expanded circumpolar westerlies (Namias [5]; Rossby and Willett [9]), then it is highly probable that the dynamic and thermodynamic consequences of the energy cycle are truly more descriptive of these typical "index-cycle" phenomena than any index variations themselves. Thus, the expedient of verifying energetics of general circulation models in the real atmosphere by means of the index cycle is a patently crude procedure. It must be pointed out, however, that there have been comparisons of the *average* energetics of models with *average* values of energy transformations computed for the atmosphere.

The first published calculations of available potential energy for the Northern Hemisphere in the actual atmosphere, which were made at about the same time as those calculated by us, are some average values for the month of February 1959 (Saltzman and Fleisher [10]). Their results consist not only of monthly average values of total, zonal, and eddy available potential energy, but also the components of the eddy available energy for individual

wave numbers around latitude circles. It is believed that the present study of one particular energy cycle provides some interesting material which is complementary to that of Saltzman and Fleisher and which also aids in the physical comprehension of the atmospheric energy cycle.

2. DEFINITIONS AND METHODS OF COMPUTATION

The average available potential energy per unit area over the entire earth's atmosphere may be expressed by the following approximate equation, as derived by Lorenz [4]:

$$\overline{A}=\frac{1}{2}\int_0^{\overline{p}_0}(\Gamma_d-\overline{\Gamma})^{-1}\overline{T}^{-1}\overline{(T')^2}dp, \tag{1}$$

where bars within the integral refer to averages over an entire isobaric surface, T is temperature, Γ_d is the dry adiabatic lapse rate, $\overline{\Gamma}$ is the lapse rate, T' is the deviation of the temperature at any given point on the isobaric surface from its average value in that surface, p is pressure, and $\overline{p}_0$ is the average pressure at the surface of the earth. It should be noted that over short time periods (i.e., of the order of days, weeks, or perhaps a month) variations of available potential energy are essentially dependent upon variations in the spatial variance of temperature on isobaric surfaces, $\overline{(T')^2}$, since the mean temperature and mean lapse rates within an isobaric surface are relatively constant with time. In a longer-period sense (e.g., over several months) the time variations in available potential energy are, however, also influenced to a moderate degree by changes in mean lapse rate and to a lesser extent by changes in mean temperature.

Available potential energy may also be expressed in terms of two components, a zonal and an eddy component (Lorenz [4]). The expression for zonal available potential energy is

$$\overline{A}_Z=\frac{1}{2}\int_0^{\overline{p}_0}(\Gamma_d-\overline{\Gamma})^{-1}\overline{T}^{-1}\overline{[T]'^2}dp, \tag{2}$$

where the bracket refers to a latitudinal average and $[T]'$ is the departure of the latitudinal average temperature from the overall mean temperature. The expression for eddy available potential energy is

$$\overline{A}_E=\frac{1}{2}\int_0^{\overline{p}_0}(\Gamma_d-\overline{\Gamma})^{-1}\overline{T}^{-1}\overline{(T^*)^2}dp, \tag{3}$$

where T^* is the departure of the temperature at any point from its latitudinal average value. Thus, zonal available potential energy is mainly dependent upon the variance of the average latitudinal temperatures, or essentially upon the strength of the north-south thermal gradients, while eddy available potential energy is mainly a function of the variance of temperature within latitude circles, having a minimum value when isotherms are parallel to the latitude circles and having maximum values when the isotherms display a wave pattern of large amplitude.

In attempting to calculate available potential energy in the actual atmosphere from synoptic data it is necessary to restrict the computations to a limited area where analyzed temperature data are available. In the calculations presented here, the area considered was the Northern Hemisphere from latitude 30° northward. Temperatures [2] at 700 mb. were used to represent the temperature field in the entire troposphere, and the calculations, which were made by means of a desk computer, were considered to apply to the layer between 1000 and 250 mb. No attempt has been made to weight these energy calculations for pressures less than 250 mb., since the available potential energy would tend to be much smaller in most of the more stable stratospheric layers than in tropospheric layers of comparable pressure intervals. A few tests comparing available potential energy computed from data throughout the troposphere and stratosphere, with values using 700-mb. temperatures only, show that the use of 700-mb. temperatures alone provides a good approximation to the available potential energy through the depth of the atmosphere. Another approximation in these calculations is the use of the standard atmosphere lapse rate for $\overline{\Gamma}$.

The average kinetic energy per unit area over the entire atmosphere may be expressed as follows (cf., Lorenz [4]):

$$\overline{K}=\frac{1}{2}g^{-1}\int_0^{\overline{p}_0}\overline{V^2}dp, \tag{4}$$

where g is the acceleration of gravity, V is the horizontal wind speed, and the bar within the integral again represents averaging over an entire isobaric surface. Kinetic energy may also be expressed in two components, zonal kinetic energy and eddy kinetic energy, the expressions for which are respectively as follows:

$$\overline{K}_Z=\frac{1}{2}g^{-1}\int_0^{\overline{p}_0}\overline{[V]^2}dp, \tag{5}$$

and

$$\overline{K}_E=\frac{1}{2}g^{-1}\int_0^{\overline{p}_0}\overline{(V^*)^2}dp, \tag{6}$$

where $[V]$ is the average wind for each latitude circle and V^* is the deviation of the wind from its latitudinal average value. Kinetic energy and its components were computed by means of a machine program which had previously been devised by C. L. Bristor. This program makes use of 500-mb. geostrophic winds obtained from 500-mb. height data of the Joint Numerical Weather Prediction (JNWP) Unit on their octagonal grid, which fully covers the area between about latitude 20° N. and the pole.

Expressions for time rates of changes of available potential and kinetic energy are also pertinent. Following Lorenz [4] we may write the following expressions for the local changes of energy:

[2] Temperature data recorded at 5° latitude and 10° longitude intervals (diamond grid) by the Extended Forecast Section of the Weather Bureau were used.

$$\frac{\partial \overline{A}}{\partial t}=-C+G \tag{7}$$

and

$$\frac{\partial \overline{K}}{\partial t}=C-D, \tag{8}$$

where

$$C=-Rg^{-1}\int_0^{\overline{p}_0} p^{-1}\overline{T\omega}\,dp, \tag{9}$$

$$G=g^{-1}\int_0^{\overline{p}_0}\Gamma_d(\Gamma_d-\overline{\Gamma})^{-1}\overline{T}^{-1}\overline{T'Q'}\,dp, \tag{10}$$

and

$$D=-g^{-1}\int_0^{\overline{p}_0}\overline{\mathbf{V}\cdot\mathbf{F}}\,dp. \tag{11}$$

In these expressions C represents the conversion between potential and kinetic energy, G is the generation of available potential energy, D is the frictional dissipation of kinetic energy, R is the gas constant for dry air, ω is equal to dp/dt (vertical motion in pressure coordinates), Q is the rate of addition of heat per unit mass, and $\mathbf{F}$ is the frictional force.

Generation of available potential energy is greatest when there is a high positive covariance between heating and temperature (equation (10)). In other words, when the atmosphere is heated where the temperature is high and cooled where the temperature is low there is considerable generation of available potential energy. The energy conversion term appears with opposite sign in equations (7) and (8). Energy is converted from available potential energy to kinetic energy when there is a correlation between vertical motion and temperature such that upward motion occurs in the warm air and downward motion occurs in the cold air (equation (9)). On the other hand, when the vertical motion field is reversed relative to the temperature field, i.e., downward motion in the warm air and upward motion in the cold air, the kinetic energy is converted to available potential energy.

It is obvious from these expressions that the place where radiational heating plays an important role is in the generation of available potential energy (equation (10)). This will be one of the most important terms to evaluate when satellite radiation data become available, and of course, it will be important to compare these evaluations of the generation term with the observed variations in available potential energy. At present, however, some calculations of the energy generation term can be made from indirect estimates of heating on a hemispheric scale (Wiin-Nielsen and Brown [15]).

The conversion term (equation(9)) is also of considerable interest in understanding the time variations of both kinetic and available potential energy. From data kindly provided by A. Wiin-Nielsen, some evaluations of this term have been made. These data are based on initial vertical motions and thicknesses available as a by-product of the operational baroclinic numerical prediction calculations of the JNWP Unit. These data were used by both Wiin-Nielsen [14] and Saltzman and Fleisher [10] to obtain calculations of this energy conversion term.

Expressions for conversion and generation of zonal and eddy components of available potential and kinetic energy are also given by Lorenz [4], but it is beyond the scope of this paper to present all of them here. It is pertinent, however, to write the expression for the conversion between zonal and eddy available potential energy, C_A, which is as follows:

$$C_A=-\frac{R}{g}\int_0^{\overline{p}_0}\frac{\overline{\theta}}{\overline{T}}\overline{\left([T^*v^*]\frac{\partial}{\partial y}+[T^*\omega^*]'\frac{\partial}{\partial p}\right)\left(\frac{\Gamma_d}{\Gamma_d-\overline{\Gamma}}\frac{[T]'}{\theta}\right)}\,dp, \tag{12}$$

where θ is potential temperature, * denotes a deviation from a latitudinal average value, and [ ]′ denotes a deviation of a latitudinal average value from the mean value over the entire isobaric surface. It will be noted that basically this conversion involves the products of the horizontal transport of sensible heat and the north-south temperature gradient and of the vertical transport of heat and the vertical temperature gradient.

In the discussion that follows only the northward heat transport itself is calculated. This transport, H, across a given latitude circle, ϕ_0, in a layer between two constant pressure surfaces, p_1 and p_2, is obtained through the following approximate expression:

$$H=\frac{c_p a\cos\phi_0(p_2-p_1)\Delta\lambda}{g}\sum v^*T^*, \tag{13}$$

where a is the radius of the earth, c_p is the specific heat at constant pressure, v is the meridional wind component, and λ is longitude. In the evaluation of (13), p_2 is taken as 850 mb. and p_1 as 500 mb., v^* and T^* are average values in the layer 850–500 mb., and the summation is over 72 intervals of $\Delta\lambda$, or 5° of longitude, around the latitude circle. Further treatment of the assumptions used in this calculation, including the use of geostrophic flow, has already been given elsewhere (Winston [16]).

3. DESCRIPTION OF THE ENERGY CYCLE AND VARIATIONS IN PARAMETERS ASSOCIATED WITH ENERGY CONVERSIONS

The day-to-day variations of the available potential energy, and its zonal and eddy components for the period of interest are shown in figure 2. It may be seen that the major cycle of buildup and breakdown in the total available potential energy between December 24 and January 7 mainly reflected the variation in the zonal component of the available potential energy. This is essentially indicative of the buildup of strong thermal gradients between latitude circles up to a peak on January 1, which was then followed by a very substantial breakdown in these thermal gradients between January 1 and 10. The eddy available potential energy remained at a nearly

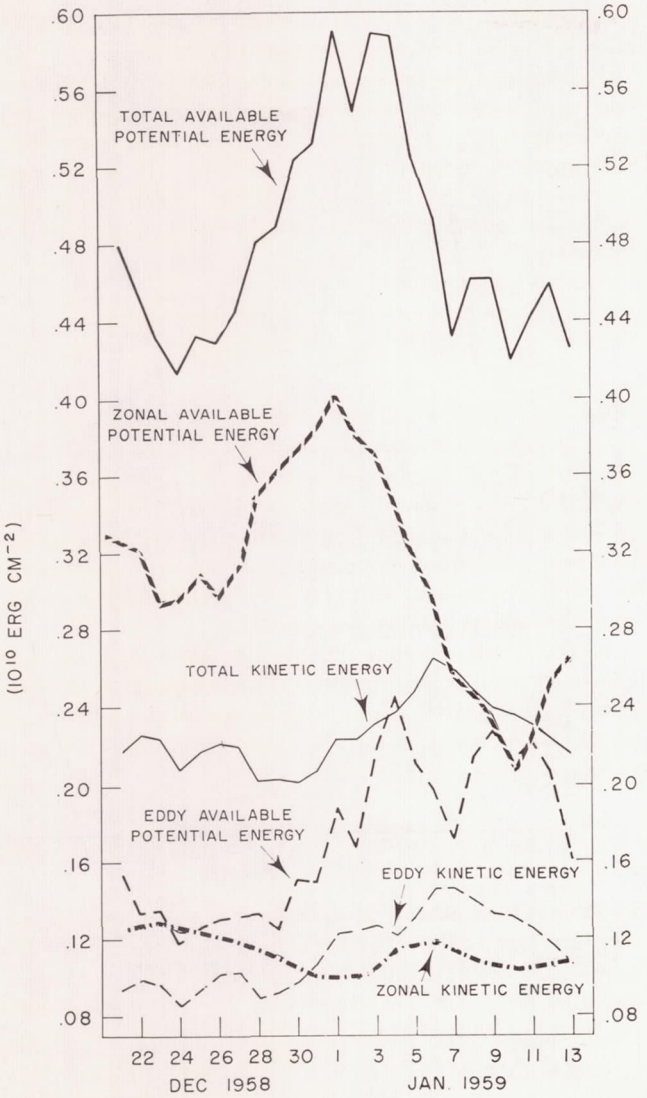

FIGURE 2.—Available potential energy, kinetic energy, and the zonal and eddy components of each for the period December 21, 1958–January 13, 1959. All quantities computed once daily at 0000 GMT.

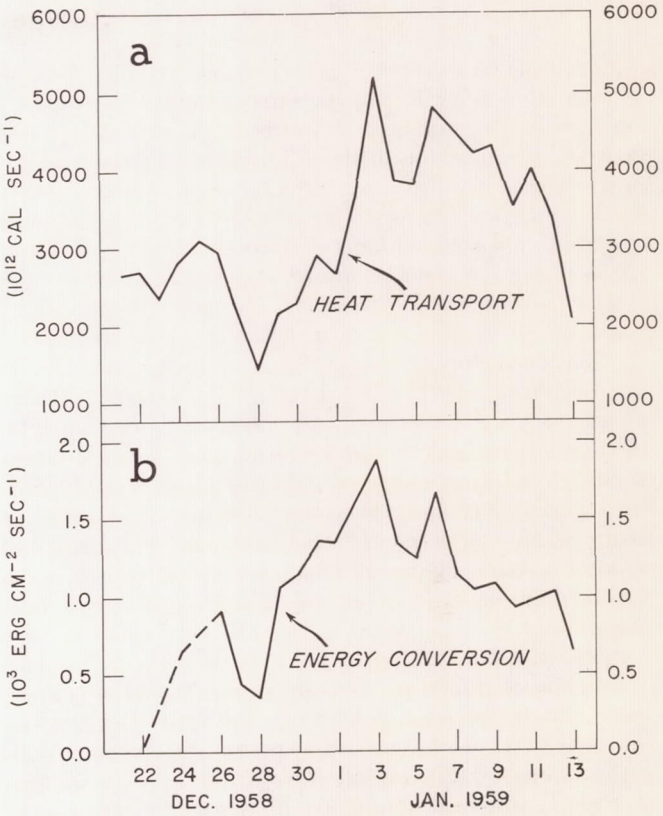

FIGURE 3.—(a) Total heat transport across all latitudes from 20° N. northward, and (b) the conversion between available potential and kinetic energy (positive for conversion to kinetic energy), for the period December 21, 1958–January 13, 1959. Both quantities computed once daily at 0000 GMT. Portion of energy conversion curve prior to December 26 is dashed since conversion data were unavailable for December 23 and 25.

constant, low level until December 29 and then began a general rise culminating in a peak value on January 4, when the zonal available potential energy was falling precipitously. Following this maximum the eddy available energy dropped at a rapid rate to reach a minimum on January 7, but a rapid rebound brought it to values only slightly less than peak values between January 8 and 12, when the zonal component reached its minimum value.

This overall behavior of the eddy relative to the zonal component of the available potential energy suggests very strongly that the increased level of eddy available energy was derived from the zonal available energy. In other words, strong thermal gradients developed *within* latitude circles at the expense of the thermal gradients *between* latitude circles. This is supported by the variation of the total northward heat transport (summed over all latitude circles) which is shown in figure 3. Note that heat transport was at a relatively low level during the buildup of zonal available potential energy, but spurted rapidly upward at the time when the zonal available energy began to decline after January 1. In view of the direct role that heat transport plays in the conversion from zonal to eddy available potential energy (equation (12)) there is little doubt that this increase in heat transport after January 1 signified a marked increase in this energy conversion.

Turning to the kinetic energy variations in figure 2, it is seen that the total kinetic energy also went through a cycle at this time, but it was almost completely dominated by the variations in the eddy kinetic energy. Note that the eddy (and total) kinetic energy generally increased for more than a week before reaching a maximum between about January 6 and 7, more than 2 days later than the peak in the eddy available potential energy. Thus the next step in the energy flow, the transformation from

eddy available to eddy kinetic energy (see fig. 1) evidently occurred.

As for the final step in the typical energy flow, the conversion from eddy kinetic to zonal kinetic energy, there appears to be very little evidence that any appreciable increase in conversion to zonal kinetic energy was realized in this period since the zonal kinetic energy showed rather small time variations. There was, however, a weak maximum in the zonal kinetic energy on January 6, about the same time as the maximum in the eddy kinetic energy.

The conversion between total available potential and total kinetic energy shown in figure 3 generally verifies the increased flow of energy from available potential to kinetic during the first several days of January. Comparison of this conversion with the time changes in total kinetic energy that can be deduced from figure 2 shows that they were generally related in the direction indicated by equation (8); i.e., the conversion term tended to be larger when kinetic energy was markedly increasing and smaller when kinetic energy was markedly decreasing (on the assumption that D always acts to decrease kinetic energy and that it does not vary nearly so much as the conversion term).

It is interesting that the time variation of the conversion term, which is a function of the spatial covariance between vertical motion and temperature, appears to be rather well correlated with the variations in total heat transport, which is a function of the spatial covariance between meridional motion and temperature. This tends to verify the deductions of Kuo [2] that northward heat transport (and hence conversion from zonal to eddy available potential energy) and conversions from potential to kinetic energy must be closely related. However, despite this good correspondence in these quantities, the actual curves of eddy available and eddy kinetic energy (fig. 2) are imperfectly correlated, particularly near the time of maximum values in the two eddy components (January 3–9). In fact, a secondary minimum in eddy available potential energy occurred on January 7, very close to the maximum in eddy kinetic energy. The explanation for this lack of agreement probably lies in the behavior of the generation of eddy available potential energy which apparently was responsible for the downturn in eddy available energy between January 3 and 7. Some evidence for this will be presented in the following sections.

4. THE GENERATION OF AVAILABLE POTENTIAL ENERGY

It was indicated earlier that for a closed region the available potential energy can change due to either a conversion term, depending on a correlation between vertical motion and temperature, or a generation term, depending on a correlation between diabatic heating and temperature (equations (7), (9), (10)). The variations of the conversion term have already been shown (fig. 3) and discussed above. Although readily computed through

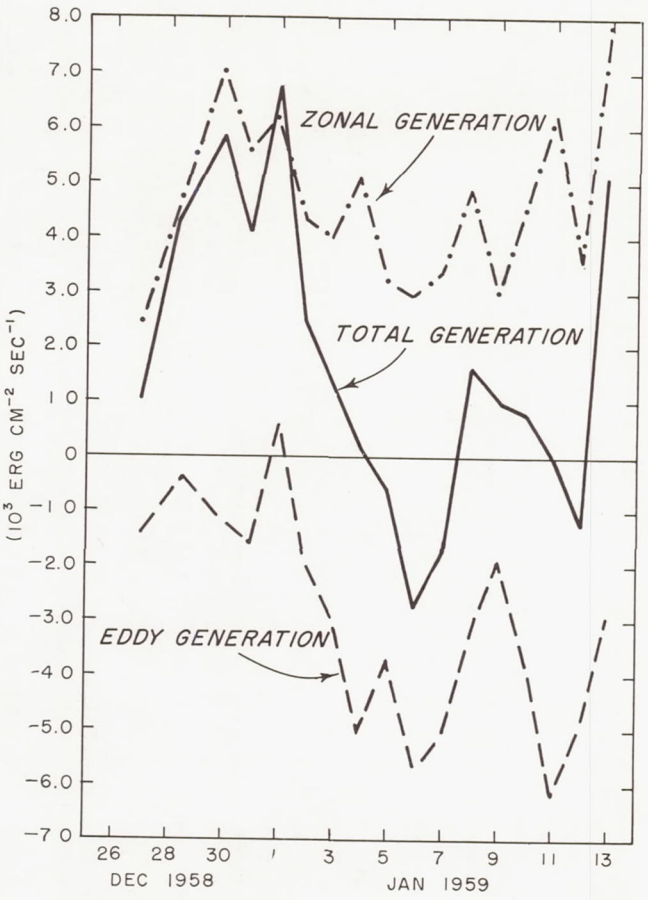

FIGURE 4.—Generation of available potential energy and its zonal and eddy components for the period December 27, 1958–January 13, 1959. Quantities computed once daily at 0000 GMT.

use of numerically calculated vertical motions its accuracy is not readily determinable. The problem of obtaining the diabatic heating, and consequently reliable estimates of the generation term however, is an even more difficult problem. Recently however, Wiin-Nielsen and Brown [15] have devised a method for computing the diabatic heating hemispherically on a daily basis. Their method essentially utilizes an equation derived from the thermodynamic energy equation where the vertical motion is estimated from the vorticity equation.

By utilizing their method it is now possible to estimate the generation of available potential energy from synoptic data, and indeed this was also done by Wiin-Nielsen and Brown. Their computations of the average generation term for the month of January 1959 indicate a value of about 1.5×10^3 ergs cm.$^{-2}$ sec.$^{-1}$, a value comparable to the average conversion from potential to kinetic energy for the same month (Wiin-Nielsen [14]). This represents the sum of 5.0×10^3 ergs cm.$^{-2}$ sec.$^{-1}$ for the zonal component and -3.5×10^3 ergs cm.$^{-2}$ sec.$^{-1}$ for the eddy component. Thus according to these calculations, the only source of available potential energy, at least during

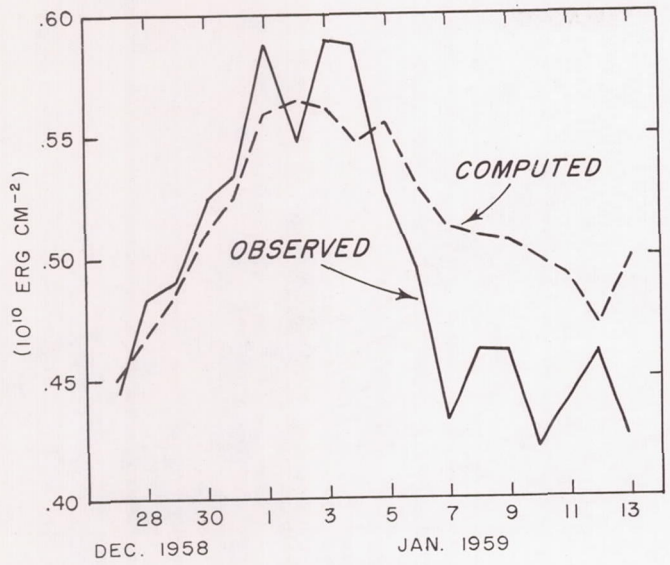

FIGURE 5.—Observed and computed available potential energy for the period December 27, 1958–January 13, 1959.

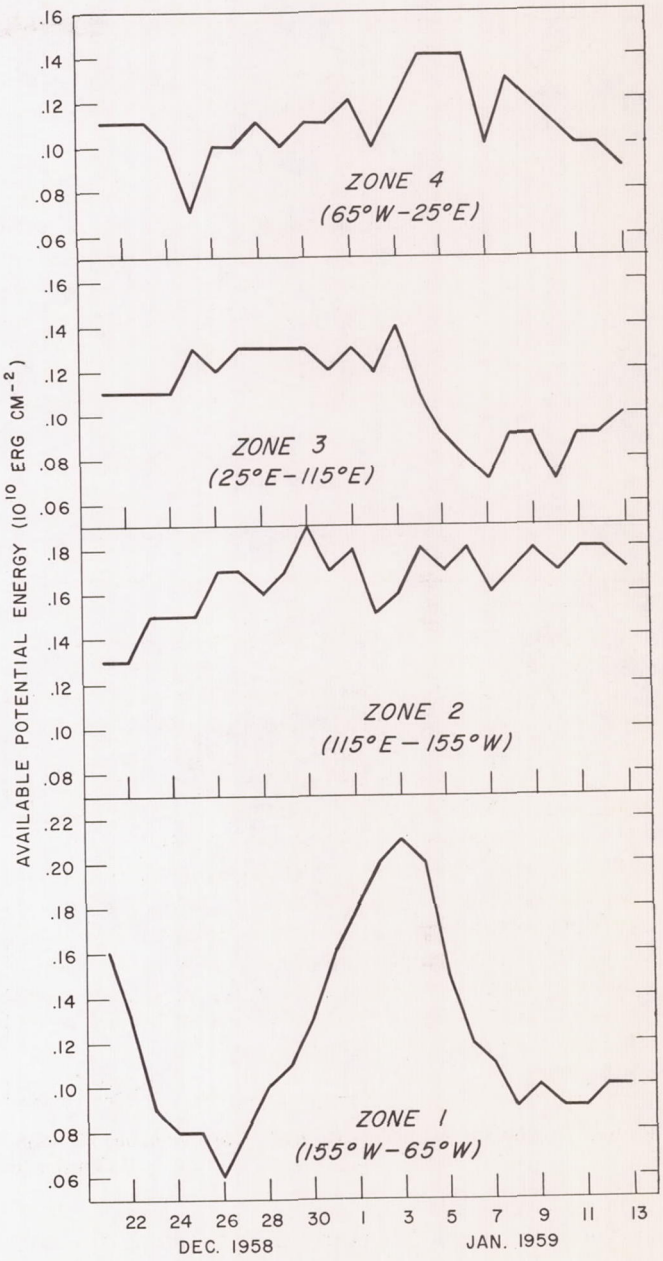

FIGURE 6.—Available potential energy in four zones extending northward from 30° N. within the indicated longitudinal boundaries for the period December 21, 1958–January 13, 1959. Quantities computed once daily at 0000 GMT.

January 1959, was the latitudinal heating gradient. Apparently the heating within latitude circles, which represents the heating associated with the long planetary waves and transient disturbances, served only to reduce the available potential energy.

As part of the study of the cycle in available potential energy treated in this report, it was felt to be of interest to compare the interdiurnal variation of the generation term and its zonal and eddy components with that of the available potential energy. For this purpose Wiin-Nielsen has kindly made his computations for January 1959 available to us and these have been combined with similar computations made in the Meteorological Satellite Laboratory for the period December 27–31, 1958.

The time variations of these energy generation terms are shown in figure 4. As can be seen, the zonal generation was always positive, seldom dropping below 3 units, while the eddy generation was predominantly negative, averaging frequently below −2 units. The total generation, while usually positive, was occasionally negative, particularly between January 4 and 7, indicating that the heating field even in winter can at times act to destroy available potential energy. Of particular interest for this study was the similar behavior of the generation term and the total available potential energy (fig. 2) between December 27 and January 7. Both curves increased very markedly at the beginning of the period with the generation term reaching a maximum of 7×10^3 ergs cm.$^{-2}$ sec.$^{-1}$ about two days prior to the maximum in the available potential energy. At this time the eddy generation was small so that the total was nearly equal to the zonal component, reflecting a predominantly latitudinal heating distribution. Also significant is the fact that the generation term remained above 2 units for about six consecutive days. Considering the magnitude of the energy conversion term (fig. 3) this was sufficient to cause an increase in available potential energy during this period.

After January 1 the intensity of the total generation of available potential energy was drastically reduced and within a few days it had even become negative. Much of this decline was due to the sudden drop in the eddy gen-

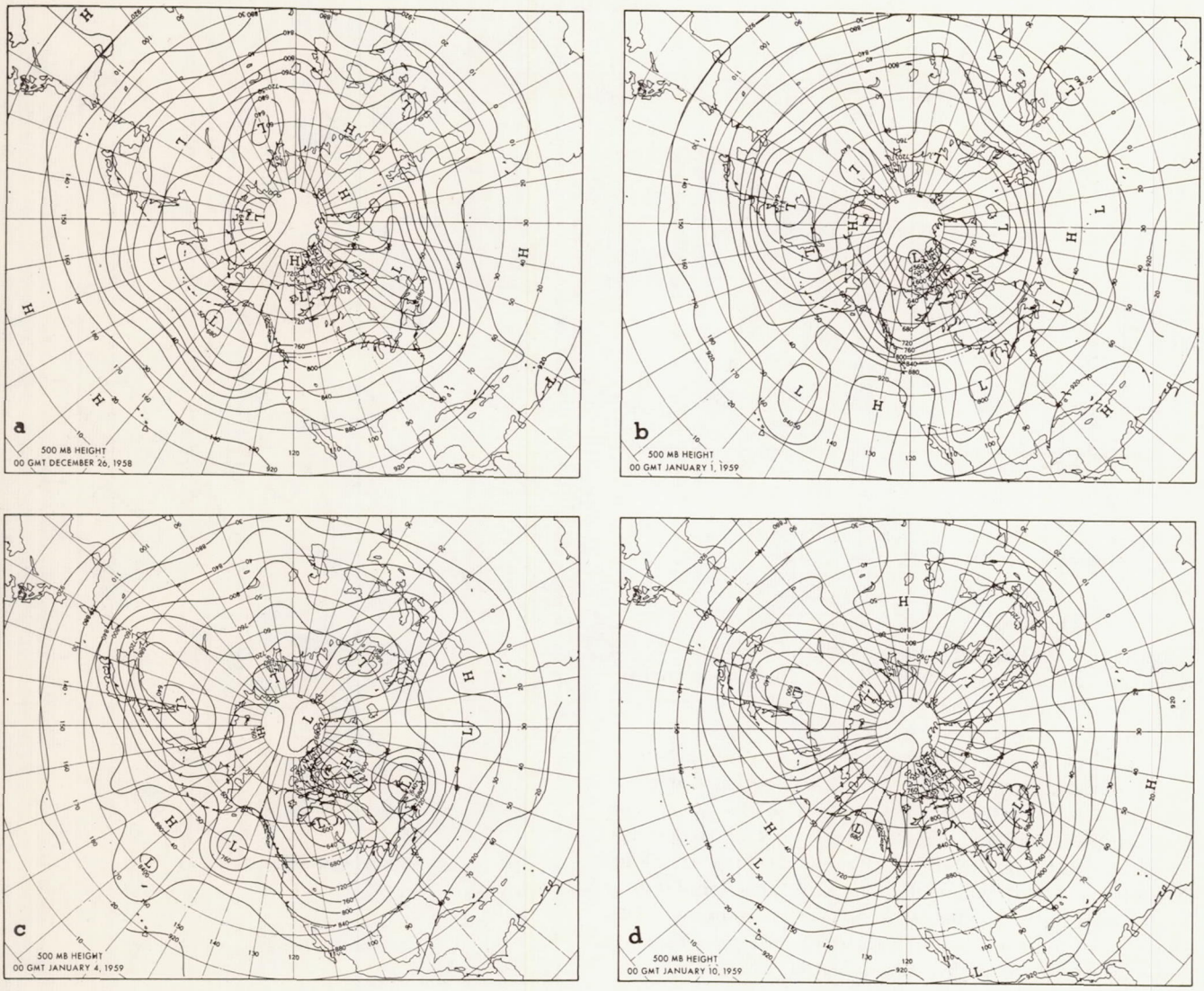

FIGURE 7.—500-mb. contour patterns for (a) December 26, 1958, (b) January 1, 1959, (c) January 4, 1959, and (d) January 10, 1959. Contour interval is 400 ft.

eration term which fell nearly 6 units during the same interval. This was the result of more intense cold air outbreaks and the consequent heating of polar air masses in middle and lower latitudes, as will be illustrated in the next section. The sudden dip in the eddy available potential energy between January 4 and 7 (fig. 2), which was discussed earlier, was probably a response to this strong heating and a direct consequence of the large negative value of the eddy generation. This was a period during which the computed values of both the (total) generation and (total) conversion terms contributed toward a decline in total available potential energy, agreeing with the observed decline. It is of interest in this regard to compare in more detail the computed behavior of the sum of C, the conversion term, and G the generation term, with the observed variation in available potential energy during this period. This will now be considered.

Equation (7) may be integrated to give

$$\overline{A}_n=\overline{A}_{n-1}+(G-C)\delta t, \tag{14}$$

where $\overline{A}_n$ is the value of available potential energy on a given day n, $\overline{A}_{n-1}$ is the value a day earlier, and δt is an interval of 1 day. Specifying the value of $\overline{A}_0$, which has been chosen here to be the observed value of the available potential energy on December 26, one can compute $\overline{A}_1$ and all succeeding values of $\overline{A}_n$ for as many days as one pleases, providing values of $G-C$ are available. These computed values of available potential energy are shown in comparison with the observed values for our period of

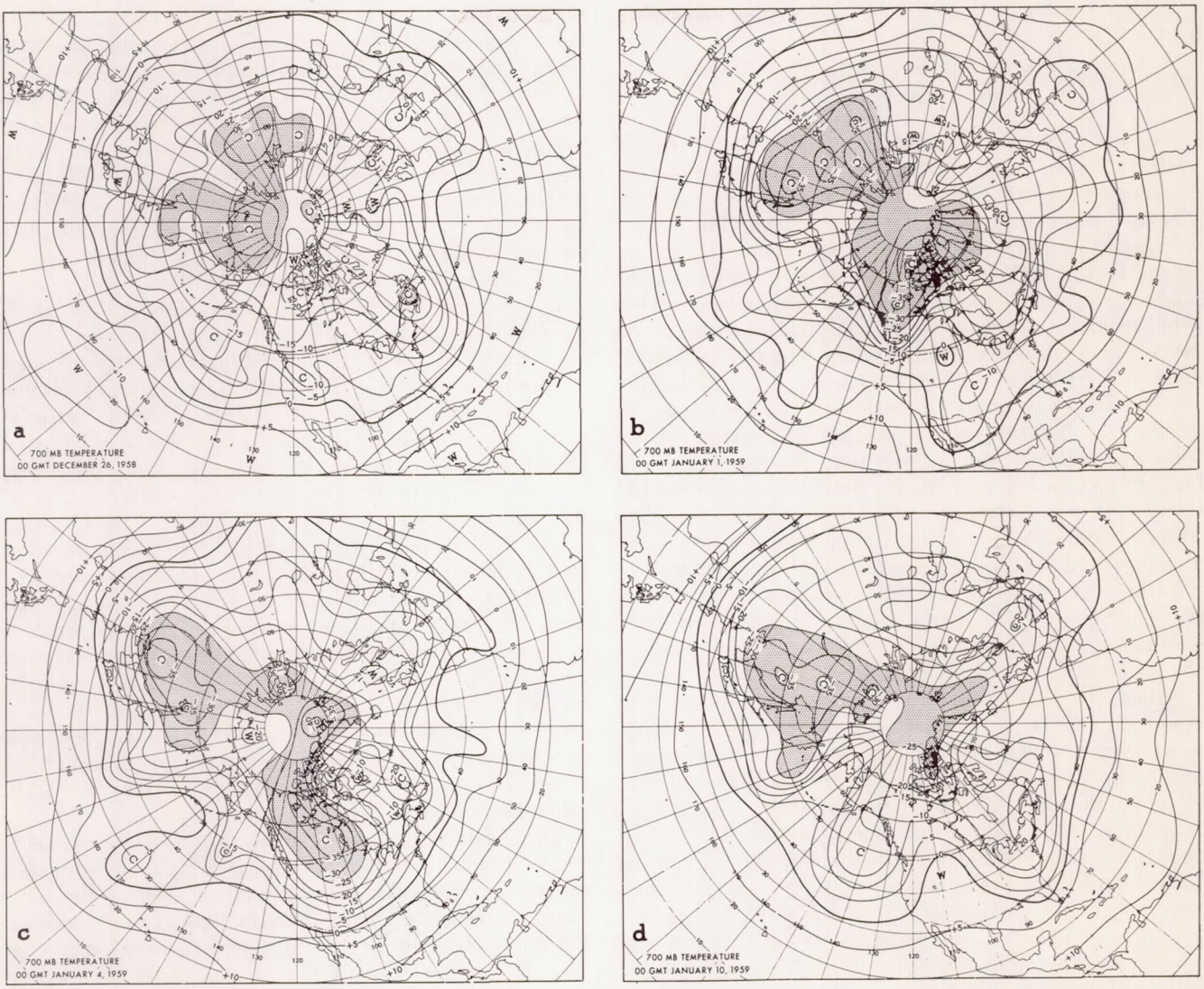

FIGURE 8.—700-mb. isotherms for (a) December 26, 1958, (b) January 1, 1959, (c) January 4, 1959, and (d) January 10, 1959. Interval is 5° C. with area below −25° C. stippled.

interest in figure 5. It is quite clear that the increase in available potential energy between December 27 and January 1 is explained very well by the sum of the generation and conversion terms, although the computed values do not rise to as high a maximum as the observed. The most serious discrepancy between computed and observed values occurred after January 3 during the period of strong decline in available potential energy. This period was represented by only a weak decline in the computed values, which suggests that the computed conversion term particularly after January 1, while indicating the correct trend, was too small. This is most likely attributable to the fact that the vertical velocities used in computing C are too small. Similar conclusions were were reached by Palmén [7], who suggested that the energy conversion computed by this method should be increased by about 40 percent or more. The weak values of the energy conversion probably also reflect the lack of inclusion of moist adiabatic processes in the vertical motion computations. Smagorinsky [11] has indicated that when these are included the upward motions are found to be much larger than those obtained by assuming dry adiabatic motions. Since moist adiabatic effects would be expected to be larger in warm air masses, the conversion from potential to kinetic energy would also be expected to be larger.

Despite these discrepancies, the encouraging fact is that such realistic estimates of the variations in available potential energy were obtained from the generation and conversion terms, particularly since these terms were com-

puted on the basis of rather restrictive and incomplete models of the atmosphere.

5. REGIONAL AND SYNOPTIC FEATURES OF THE ENERGY CYCLE

The variations of total available potential energy shown in figure 2 were also examined from another point of view (as contrasted with the zonal and eddy components previously considered). The available potential energy was partitioned into four regional components representative of sectors 90° of longitude wide, stretching from the pole to 30° N. These four sectors were chosen somewhat arbitrarily, but roughly in such a fashion as to cover the two oceans and two continents. The longitudinal boundaries of each zone and the portion of the available potential energy contributed by each of these zones are shown in figure 6. The most striking feature of the variations of these regional components was that the major cycle of buildup and decline in available potential energy showed up only in the component of energy in Zone 1 (North America and vicinity). Thus the variations in the available potential energy for the whole Northern Hemisphere were basically dependent on the events in only this one particular region. The dominance of one area over another is not too unusual, of course, since differences in the types of flow patterns over various parts of the Northern Hemisphere have frequently been noted (cf., Namias [6]). However the virtually complete absence of an energy cycle at this time in three of the four zones is quite surprising, particularly since the total energy over all longitudes showed such a large variation.

Further insight into this energy cycle is attained through inspection of synoptic charts, which showed some interesting developments over North America and also over other portions of the hemisphere during this period. To illustrate these events, 500-mb. height and 700-mb. temperature fields for four selected days are presented in figures 7 and 8.

Confining our attention at first mainly to the North American area, we see that on December 26, when available potential energy was at a relatively low value, both over North America (Zone 1 in fig. 6) and over the hemisphere as a whole (fig. 2), there was a rather ill-defined circulation pattern (fig. 7a) with weak thermal gradients (fig. 8a). The high values of available potential energy which prevailed by January 1 were characterized by a deep cyclonic vortex over the Canadian Arctic (fig. 7b) with an associated extensive pool of cold air (fig. 8b). By January 4 a cyclonic vortex was located in western Canada, some 20° latitude south of the one in figure 7b, and the broad cyclonic flow to its south dominated most of the United States (fig. 7c). Accompanying these circulation developments, an extensive tongue of cold air covered western Canada and was also invading the United States (fig. 8c). This date marked the beginning of the overall drop in available potential energy over North America (fig. 6) and also the time of the maximum in eddy available potential energy for the hemisphere and of a very rapid drop in the zonal available energy (fig. 2). Thus the southward penetration of cold air over North America was one of the major instrumentalities in the breakdown of the strong supply of available potential energy that had built up over North America and the hemisphere as a whole. Undoubtedly a major part of its contribution to the energy breakdown was in its role in the conversion of zonal available into eddy potential energy and thence into eddy kinetic energy, all of which occurred at this time (fig. 3).

By the final day in this sequence, January 10, when available potential energy over North America (fig. 6) and the zonal available energy for the hemisphere (fig. 2) had dropped to relatively low values again, this cyclonic vortex was located near the Gulf of St. Lawrence with its main trough extending down the east coast of the United States (fig. 7d). The cold air associated with this system was now definitely weaker than before; in fact, most of the colder air (e.g., temperatures below −25° C.) over North America had disappeared (fig. 8d). This warming was undoubtedly reflective of two processes, one the descent of the cold air which contributed to conversion from potential to kinetic energy and the other the heating of the cold air mass as it proceeded off the east coast out over the Atlantic. Very large amounts of heating were computed by Wiin-Nielsen and Brown [15] on the days when the cold air moved off the coast (January 5–6) and it is evident that the strong heating of this cold air contributed to the strong negative values of computed eddy generation on these days (fig. 4).

Turning to other features of the flow and thermal fields it is of interest to note that a considerable amount of cold air was present over eastern Asia on each of the days shown in figure 8. This was very likely associated with the relatively high level of available potential energy in Zone 2 between December 26 and January 10 (fig. 6). Also, while a portion of this cold air was located farther west in Siberia (figs. 8a, 8b), the level of available energy in Zone 3 was fairly high, but as most of it moved east of Lake Baikal (figs. 8c, 8d) a noticeable drop in the energy in Zone 3 occurred. This more narrow longitudinal organization of the cold air near the Asian coast was accompanied by the sharpening of the Asian coastal trough subsequent to January 1 (fig. 7). Although the total energy for Zone 2 remained virtually the same, computations of longitudinal contributions to the northward heat transport (Winston [16]) showed that substantial heat transports were effected by the Asian coastal trough subsequent to January 1. This signified that increased transformations from zonal to eddy available energy occurred in this zone during the period of development of increased eddy energy in January (fig. 2). Thus, despite the lack of a cycle in the overall energy, it appears that eddy Zone 2 (eastern Asia to the east central Pacific) did contribute toward the increase or maintenance of eddy energy.

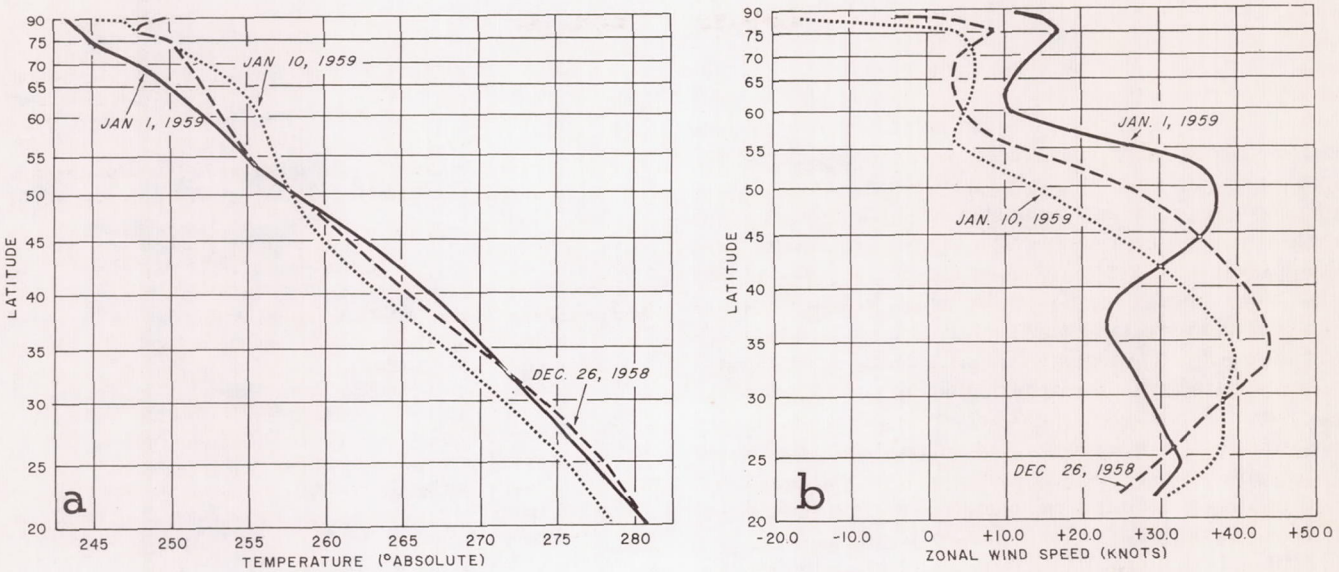

FIGURE 9.—Latitudinal profile of (a) temperature and (b) zonal wind speed for December 26, 1958 (dashed), January 1, 1959 (solid), and January 10, 1959 (dotted).

Finally it is worth noting that the overall hemispheric flow pattern at the end of the energy cycle (January 10, fig. 7d) consisted of four major, large-amplitude waves with large cyclone centers in middle latitudes. As indicated in figure 2, this was a day of minimum zonal available potential energy, but with fairly large eddy available potential energy. This pattern is to be contrasted with (1) the more heterogeneous (although mainly zonal) flow pattern of December 26 (fig. 7a), before zonal available energy started increasing; (2) the zonal flow at higher latitudes surmounting large-amplitude waves at lower latitudes of January 1 (fig. 7b), when zonal available energy was at its peak and eddy available energy was building up; and (3) the pattern of increasing wave amplitudes on January 4 (fig. 7c) when zonal available energy was dropping rapidly and eddy available energy was at a peak.

The latitudinal profiles of zonal wind and temperature for the whole hemisphere for three of these days summarize some of the differences at these different stages further (fig. 9). Note that at the beginning (December 26) and end (January 10) of the cycle there were rather broad zones of westerlies with maximum speeds located near latitude 35°. The flow at the end of the cycle was generally weaker than at the beginning except south of 30°. By way of contrast the westerlies on January 1 were concentrated in a narrow zone in middle latitudes (peak near 50°) with a definite minimum in the flow near 35° and a secondary maximum near 25°. These profiles are roughly characteristic of the zonal wind distributions at various phases of the index cycle (cf., Namias [5]), but it is worth pointing out that the profile for January 1 does not represent a case of extremely high zonal index (in latitudes 35°–55° N.).

The thermal profiles show rather definitely that the peak zonal available energy (January 1) was marked by rather low temperatures north of 55°, a cooling of up to 5° C. from December 26. This high-latitude cooling during a period when the westerlies were strengthening near latitudes 45°–55° was essentially the same type of development which Namias [5] described as containment of cold air in the polar cap during periods of strong westerly flow. By January 10, when the zonal available energy was at its lowest, temperatures were considerably higher north of 50°. The outflow of cold air into middle and lower latitudes in connection with the conversion of zonal available into eddy available energy is strikingly clear. Or putting it another way, the effects of the increased heat transports subsequent to January 1 were quite marked in the reduction of the northward thermal gradient.

6. SUMMARY

This observed cycle of available potential energy for the Northern Hemisphere possessed many characteristics which had been deduced from previous evaluations of some long-period averages of energy parameters and energy conversion terms. The buildup in zonal available energy to a high value and then its subsequent breakdown with the accompanying conversion into eddy available potential and eddy kinetic energy have all been clearly demonstrated. There was, however, little if any reaction to this potential energy cycle in the zonal component of the kinetic energy. The fact that estimates of energy

conversion and energy generation obtained from admittedly crude atmospheric models showed rather good correspondence with the observed short-period variations in the various energy parameters was especially interesting. The partition of available potential energy on a regional (longitudinal) basis showed that this clear-cut cycle in hemispheric available potential energy was dominated to a remarkable extent by events in only about one-quarter of the hemisphere. Investigations of the synoptic aspects of this energy cycle showed that this dominance by one region (North America and vicinity) was associated with the development of cold air over the Canadian Arctic and then the subsequent southward penetration of this large mass of cold air into the United States and out over the Atlantic. Obviously this signifies that studies of atmospheric energetics require close attention to geographical and synoptic-scale influences.

Although this cycle displayed many characteristics of the idealized energy cycle, it should not be concluded that this observed cycle is truly typical of most large-scale energy cycles. Cursory inspection of an accumulating record of available potential energy over more than a year indeed reveals that large-scale variations of the zonal and eddy components of the potential energy occur in a variety of ways. Study of the nature of other large-scale changes in the energy is contemplated, particularly with respect to probable differences in the manner in which the potential energy is generated.

ACKNOWLEDGMENTS

The authors are especially indebted to Dr. A. Wiin-Nielsen for several fruitful discussions concerning the energy problem and also for his generosity in making his data on the conversion and generation of energy readily available to us. Thanks are also due to several members of the Meteorological Satellite Laboratory for assisting in the various computational phases of the work.

REFERENCES

1. C. E. Jensen, "Energy Transformation and Vertical Flux Processes Over the Northern Hemisphere," *Journal of Geophysical Research*, vol. 66, No. 4, April 1961, pp. 1145–1156.
2. H. L. Kuo, "Application of Energy Integrals to Thermally Driven Motions," *Beiträge zur Physik der Atmosphäre*, vol. 31, No. 3/4, 1959, pp. 189–199.
3. E. N. Lorenz, "The Basis for a Theory of the General Circulation," Section IV of "Studies of the Atmospheric General Circulation," ed. by V. P. Starr, *Final Report* Part I, General Circulation Project, Contract AF 19(122)–153, Department of Meteorology, Massachusetts Institute of Technology, May 1954, pp. 522–534.
4. E. N. Lorenz, "Available Potential Energy and the Maintenance of the General Circulation," *Tellus*, vol. 7, No. 2, May 1955, pp. 157–167.
5. J. Namias, "The Index Cycle and Its Role in the General Circulation," *Journal of Meteorology*, vol. 7, No. 2, Apr. 1950, pp. 130–139.
6. J. Namias, "Thirty-Day Forecasting: A Review of a Ten Year Experiment," *Meteorological Monographs*, vol. 2, No. 6, American Meteorological Society, Boston, 1953, 83 pp.
7. E. Palmén, "On Generation and Frictional Dissipation of Kinetic Energy in the Atmosphere," *Societas Scientiarum Fennica, Commentationes Physico-Mathematicae* vol. XXIV, No. 11, 1960, 15 pp.
8. N. A. Phillips, "The General Circulation of the Atmosphere: A Numerical Experiment," *Quarterly Journal of the Royal Meteorological Society*, vol. 82, No. 352, Apr. 1956, pp. 123–164.
9. C. G. Rossby and H. C. Willett, "The Circulation of the Upper Troposphere and Lower Stratosphere, "*Science*, vol. 108, Dec. 10, 1948, pp. 643–652.
10. B. Saltzman and A. Fleisher, "The Modes of Release of Available Potential Energy in the Atmosphere," *Journal of Geophysical Research*, vol. 65, No. 4, Apr. 1960, pp. 1215–1222.
11. J. Smagorinsky, "On the Inclusion of Moist Adiabatic Processes in Numerical Prediction Models," In *Symposium über Numerische Wettervorhersage in Frankfort a.M. vom 23. bis 28. Mai 1956. Berichte des Deutschen Wetterdienstes*, Nr. 38, (Band 5), 1956.
12. J. Smagorinsky, "General Circulation Experiments with the Primitive Equations as a Function of the Parameters," (To be published) Abstract in *Programme of Meetings, International Association of Meteorology and Atmospheric Physics*, XII General Assembly, I.U.G.G., Helsinki, July 26–Aug. 6, 1960. pp. 22–23.
13. R. M. White and B. Saltzman, "On Conversions Between Potential and Kinetic Energy in the Atmosphere," *Tellus*, vol. 8, No. 3, Aug. 1956, pp. 357–363.
14. A. Wiin-Nielsen, "A Study of Energy Conversion and Meridional Circulation for the Large-Scale Motion in the Atmosphere," *Monthly Weather Review*, vol. 87, No. 9, Sept. 1959, pp. 319–332.
15. A. Wiin-Nielsen and J. A. Brown, Jr., "On the Distribution of Heat Sources and Sinks in the Lower Troposphere and the Corresponding Generation of Potential Energy," (To be published in the *Proceedings of the International Symposium on Numerical Weather Prediction, Tokyo, Japan, Nov. 7–13, 1960.*)
16. J. S. Winston, "Preliminary Studies of Atmospheric Energy Parameters," *Meteorological Satellite Laboratory Report to the National Aeronautics and Space Administration, No. 3*, U.S. Weather Bureau, January 1961, 30 pp.

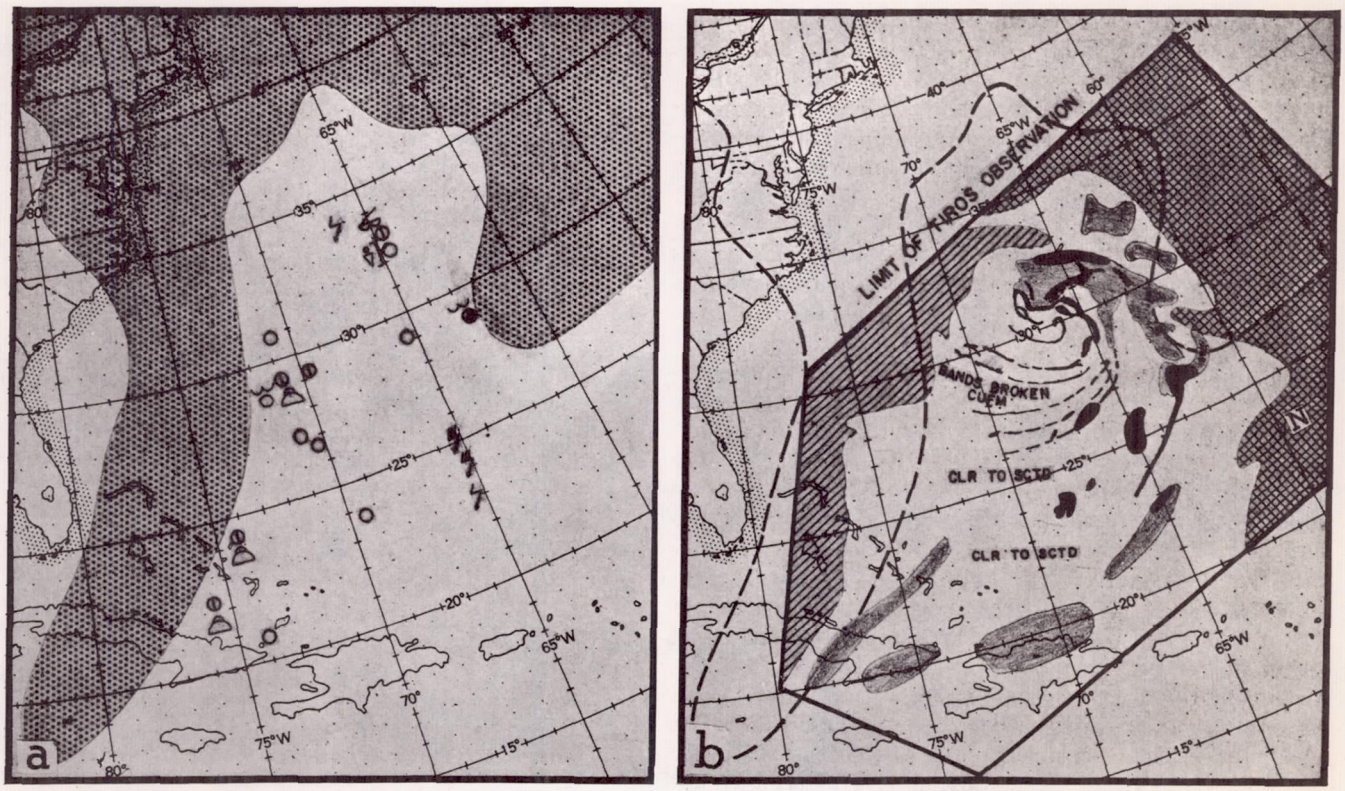

FIGURE 6.—(a) Nephanalysis of conventional cloud observations for 0000 GMT, May 9, 1960. Stippling shows broken to overcast cloud cover between 10,000 and 20,000 ft., no stippling indicates clear sky or scattered cloud between 10,000 and 20,000 ft. Abbreviated station models show conventional data available in the area of no significant cloud. (b) Nephanalysis made from TIROS I pictures for 2100 GMT, May 8, 1960. Dashed line shows extent of broken to overcast cloudiness on conventional nephanalysis of (a). Single-line hatching indicates broken to overcast clouds, type unknown; cross-hatching broken to overcast, probably mid-stratiform; solid shading indicates broken to scattered, probably large cumuliform; light shading broken to scattered, probably stratiform or small cumuliform.

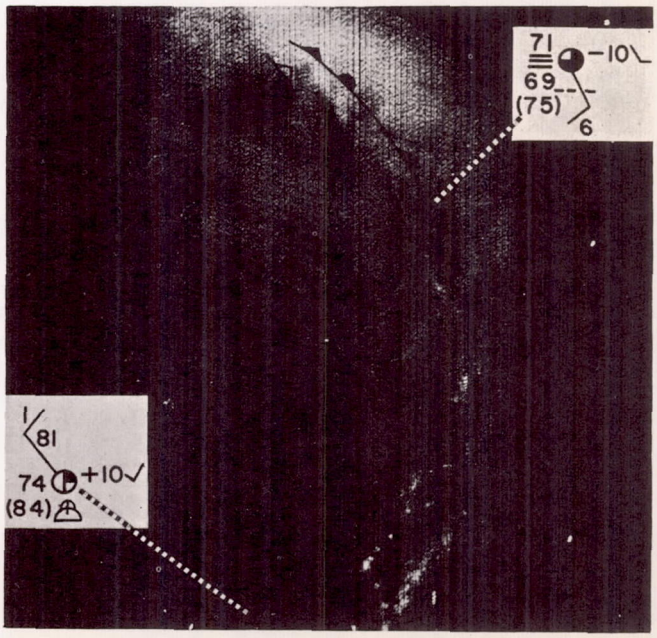

FIGURE 7.—View of the vortex at 2200 GMT, May 5 showing the NAWAC frontal position for 0000 GMT, May 6 (front with open symbols) with the two ship reports available to the analyst, and a proposed reanalysis of the front based on the conventional reports plus the picture data (front with solid symbols.)

region containing the cold front and vortex at the approximate time of the analysis shown in figure 1d. The conventional frontal analysis for 0000 GMT, May 6 relative to the appropriate cloud photograph is shown in figure 7. A revised frontal analysis based on subjective interpretation of the picture is also shown in figure 7. At its mid-point the amended position of the cold front lies approximately 120 n.mi. to the east of the NAWAC position.

The position suggested by the TIROS picture defines a boundary or zone of transition between two apparently different regimes as manifested by the distribution and organization of the clouds. To the west of this line the clouds are arrayed in spiral bands which tend to converge along the proposed frontal boundary. Immediately to the east of the line, generally broken to overcast conditions prevail except for the few parallel lines of apparently heavy cumulus in the lower right portion of the picture which, as mentioned earlier, are suggestive of squall line activity.

Lack of conventional data does not permit an analytical defense of the TIROS frontal position, and for that matter prevents even an analytical defense of the very existence of the front. Assuming, however, that a frontal discontinuity existed in this region, the TIROS position appears to be the more logical one.

6. SUMMARY

The TIROS pictures of the latter four days of this storm revealed a remarkable persistence in the organization of clouds associated with the vortex. The apparent decrease in numbers of spiral bands and the gradual breakup of the "crest" at A in figures 2, 3, 4 suggest that consecutive observations of the cloud patterns associated with a particular system at regular intervals may provide information regarding day-to-day changes of intensity and stage of development.

In discussing the relationship of the images to the conventional cloud observations, the subjectivity of the interpretation and the limitations thus imposed on practical applications are recognized. In spite of this subjectivity, which is also inherent to some degree in conventional weather observations, this study suggests that TIROS observations provide a basis for logical meteorological analysis in areas where conventional data are sparse or nonexistent.

REFERENCES

1. C. L. Bristor and M. A. Ruzecki, "TIROS I Photographs of the Midwest Storm of April 1, 1960", *Monthly Weather Review*, vol. 88, Nos. 9–12, Sept.–Dec. 1960, pp. 315–326.
2. J. H. Conover and J. C. Sadler, "Cloud Patterns as Seen from Altitudes of 250 to 850 Miles—Preliminary Results," *Bulletin of the American Meteorological Society*, vol. 41, No. 6, June 1960, pp. 291–297.
3. R. C. Doolittle, L. Miller, and I. Ruff, "Geographic Location of Cloud Features," Appendix 1 of "Some Meteorological Results from TIROS I," Staff, Meteorological Satellite Laboratory, U.S. Weather Bureau, in a National Aeronautics and Space Agency Report on TIROS I (in press).
4. G. E. Dunn and B. I. Miller, *Atlantic Hurricanes*, Louisiana State University Press, 1960, 326 pp. (pp. 152–173).
5. C. O. Erickson and L. F. Hubert, "The Identification of Cloud Forms from TIROS I Pictures" MSL Report No. 7, June 1961, (U.S. Weather Bureau manuscript).
6. S. Fritz, "'Cyclone-Prints' from Satellite (TIROS I)," *INTERAVIA—World Review of Aviation and Astronautics*, vol. 15, 1960, pp. 1384–1385.
7. S. Fritz, "Satellite Cloud Pictures of a Cyclone Over the Atlantic Ocean," *Quarterly Journal of the Royal Meteorological Society* (in press).
8. S. Fritz, "Solar Radiant Energy and its Modification by the Earth and its Atmosphere," *Compendium of Meteorology*, American Meteorological Society, Boston, 1951, pp. 13–33.
9. A. F. Kreuger and S. Fritz, "Cellular Cloud Patterns Revealed by TIROS I," *Tellus*, (in press).
10. J. Kuettner, "The Band Structure of the Atmosphere," *Tellus*, vol. 11, No. 3, Aug. 1959, pp. 267–294.
11. M. Neiburger, "Reflection, Absorption, and Transmission of Insolation by Stratus Clouds," *Journal of Meteorology*, vol. 6, No. 2, Apr. 1949, pp. 98–104.
12. V. Oliver, "A Comparison of a Satellite Nephanalysis with a Conventional Weather Analysis for a Family of Pacific Frontal Storms," "Some Meteorological Results from TIROS I," Staff, Meteorological Satellite Laboratory, U.S. Weather Bureau, in a National Aeronautics and Space Agency Report on TIROS I (in press).
13. "TIROS I Completes Its Mission: TIROS II Readied," *Weatherwise*, vol. 13, No. 4, Aug. 1960, pp. 158–161.
14. W. K. Widger, Jr., "Examples of Project TIROS Data and Their Practical Use," *GRD Research Notes*, No. 38, July 1960.
15. J. S. Winston, "Satellite Pictures of a Cut-Off Cyclone over the Eastern Pacific," *Monthly Weather Review*, vol. 88, Nos. 9–12, Sept.–Dec. 1960, pp. 295–314.

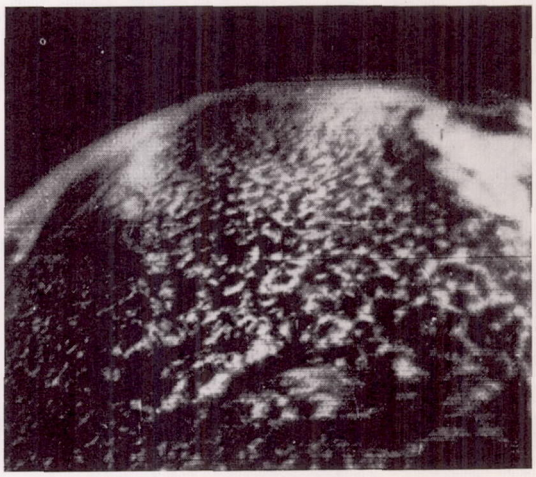

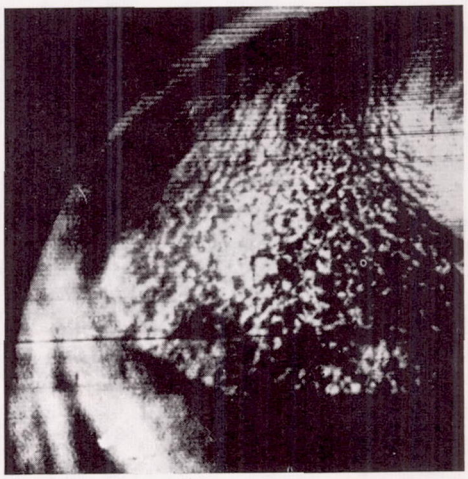

Fig. 1. TIROS I photographs:

a) taken 650 naut mi northeast of Bermuda at 1612 GMT, April 4, 1960.
b) taken over the Pacific looking northwestward at 2341 GMT, April 1, 1960.
c) taken 750 naut mi northeast of Hawaii at 2230 GMT, April 4, 1960.

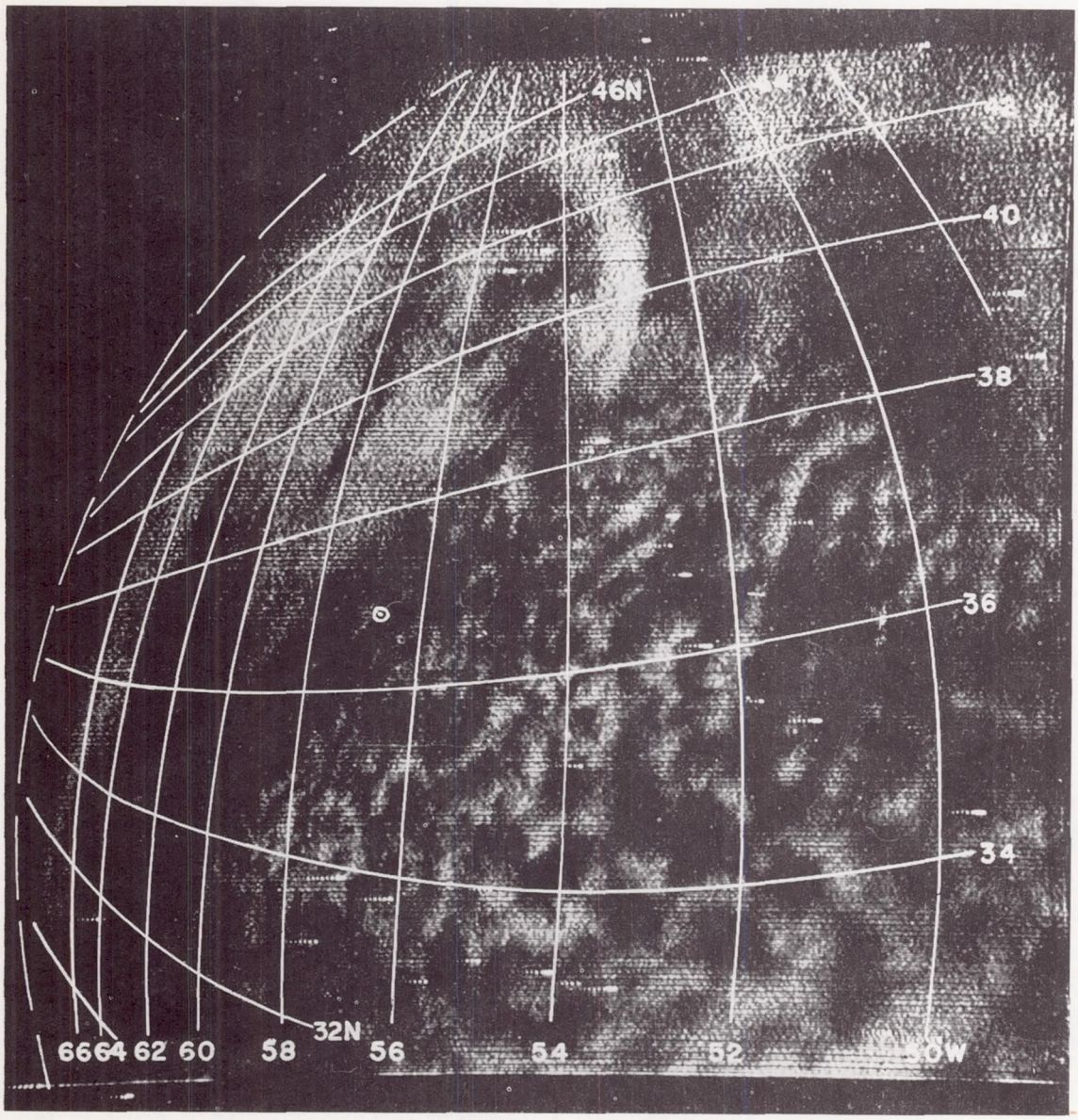

Fig. 2. Same as fig. 1a with 2° latitude-longitude grid superimposed.

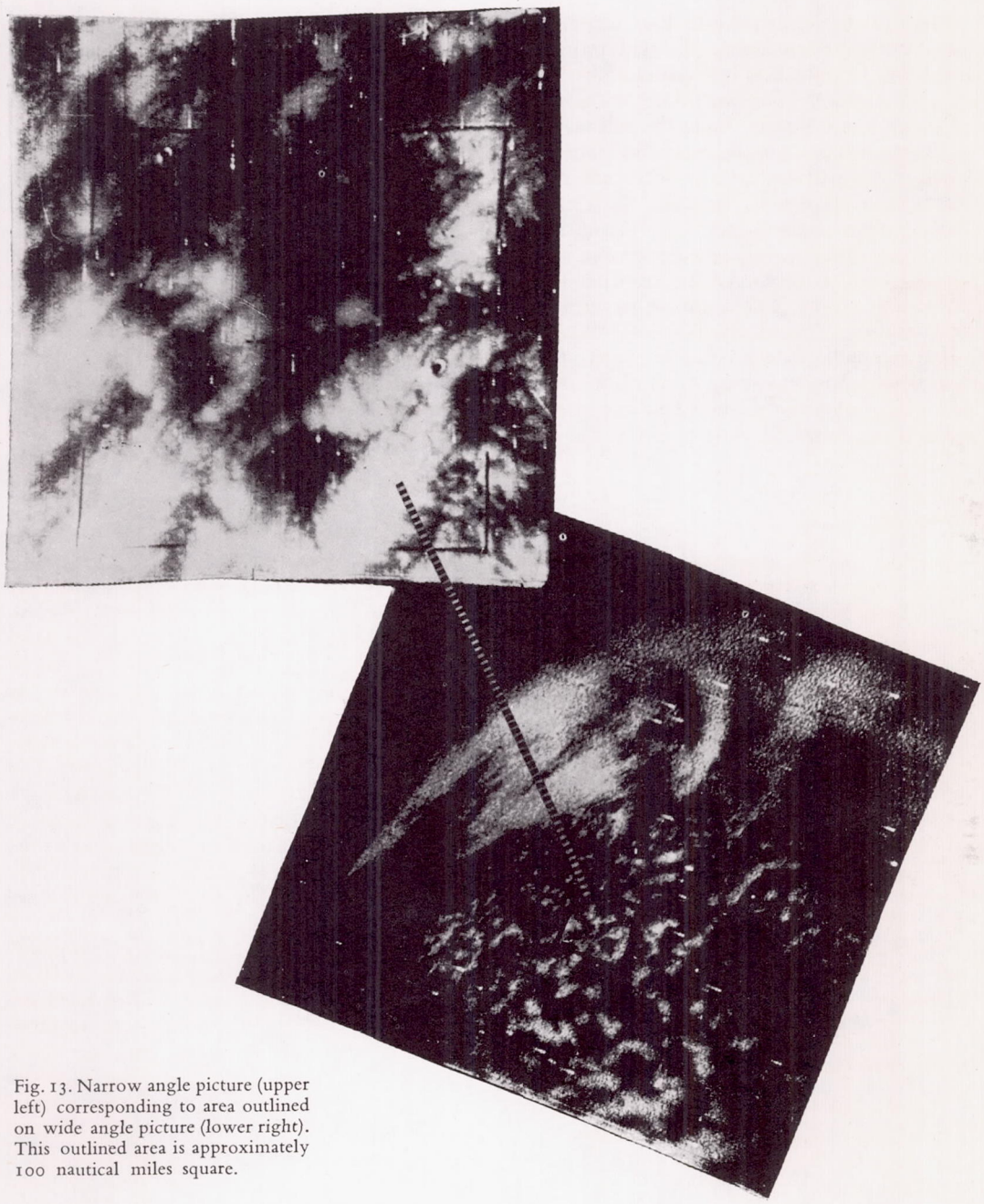

Fig. 13. Narrow angle picture (upper left) corresponding to area outlined on wide angle picture (lower right). This outlined area is approximately 100 nautical miles square.

Another problem is related to the detailed structure of the convection cells. This is apparent from an examination of the narrow angle TIROS I picture corresponding with fig. 1a (fig. 13) where it is seen that the cell walls are often made up of individual cloud elements. This is verified by surface observations of stratocumulus in the area (fig. 4). Thus the TIROS cellular cloud pictures indicate several scales of motion, while in contrast the typical Benard cell as obtained in the laboratory appears to possess a very simple structure and circulation.

Further difficulties involve the treatment of heat conduction and viscosity; for, on the scale of motion in fig. 13, the use of eddy coefficients is required, and these vary widely in space and time. Also, the release of latent heat, compressibility and perhaps the spatial variation of heating should be considered. Some of these problems have been discussed by Malkus (1952) in an interesting review of the convective cloud problem.

The observations presented in this report are but a few examples of cellular convection obtained during the lifetime of TIROS I. Many other examples remain to be studied. For, among its many findings, TIROS I has indicated that cellular convection occurs at a larger scale, and over a greater portion of the Earth's surface, than heretofore realized. These observations should serve to stimulate an increase of interest in this challenging problem.

REFERENCES

Avsec, D., 1939: *Tourbillons thermoconvectifs dans l'air, application à la météorologie.* Théses, Faculté des Sciences de l'Université de Paris, Série A, No. 1910.

Brunt, D., 1951: Experimental cloud formation. *Compendium of Meteorology*, pp. 1255—1262.

Chandra, K., 1938: Instability of fluids heated from below. Proceedings *Royal Society of London*, (A) **164**, pp. 231—242.

Fritz, S. and Wexler, H, 1960: Cloud pictures from satellite TIROS I. *Monthly Weather Review*, **88**, pp. 79—87.

Graham, A., 1933: Shear patterns in an unstable layer of air. *Philosophical Transactions Royal Society of London*, (A) **232**, pp. 285—296.

Malkus, J. S., 1952: Recent advances in the study of convective clouds and their interaction with the environment. *Tellus*, **4**, pp. 71—87.

Nakagawa, Y. and Frenzen, P., 1955: A theoretical and experimental study of cellular convection in rotating fluids. *Tellus*, **7**, pp. 1—21.

Petterssen, S., Knighting, E., James, R. and Herlofson, N., 1946: Convection in theory and practice. *Geofysiske Publikasjoner*, **16**, pp. 44.

Rayleigh, Lord, 1916: On convection currents in a horizontal layer of fluid, when the higher temperature is on the under side. *Philosophical Magazine*, **32**, pp. 529—546.

Staff members, Meteorological Satellite Laboratory, U. S. Weather Bureau, 1961: *Some meteorological results from TIROS I;* in report on TIROS I to be published by the National Aeronautics and Space Administration.

Sternberg, S., Stroud, W. G., Freeman, J. D., Goldberg, E. A., Landon, V. D., Perkel, H., Ritter, M. Osgood, C. C., Keigler, J. E., Oakley, C. B., 1960: Roundup on TIROS I (A collection of papers related to engineering aspects of the Satellite). *Astronautics*, **5**, pp. 32—45.

Wexler, H. and Fritz, S., 1960: TIROS reveals cloud formations. *Science*, **131**, pp. 1708—1710.

Winston, J. S., 1960: Satellite pictures of a cut-off cyclone over the eastern Pacific. *Monthly Weather Review*, **88**, pp. 295—314.

Woodcock, A. H. and Riley. G. A., 1947: Patterns in pond ice. *Journal of Meteorology*, **4**, pp. 100—101.

PRINTED IN SWEDEN
ESSELTE, STHLM 61

DEPARTMENT OF COMMERCE
LUTHER H. HODGES, Secretary

WEATHER BUREAU
F. W. REICHELDERFER, Chief

MONTHLY WEATHER REVIEW

JAMES E. CASKEY, JR., Editor

Volume 89, Number 10 Washington, D.C. October 1961

CLOUD STREETS OVER THE CARIBBEAN SEA[1]

JOHN SCHUETZ AND SIGMUND FRITZ

U.S. Weather Bureau, Washington, D.C.

[Manuscript received June 23, 1961]

ABSTRACT

Bands of cumuliform clouds over the Caribbean Sea as observed by TIROS I are described. The possible relationship between the occurrence of these bands and the vertical structure of the horizontal winds is discussed. The cloud street orientation is compared with the wind direction.

1. INTRODUCTION

The meteorological satellite, TIROS I, [1] presented an opportunity to view the meso-scale structure of cloud systems as well as the large-scale structure [2, 3, 4, 5]. The meso-scale structure is often better shown by the "narrow angle" camera. This camera when pointing vertically downward from a height of 380 n. mi., photographed an area whose diagonal was about 85 miles across. This detail enables one to study several interesting features of "cloud streets."

Such long thin lines of clouds, or cloud streets, occur fairly frequently in the atmosphere. For example, Riehl et al. [6], in a study of cumulus cloud bands in the tropical Pacific, found that the bands were oriented parallel to the low-level wind flow. Kuettner [7] presented several examples in which cumulus cloud streets were parallel to the wind; he also discussed the meteorological conditions under which such cloud bands will align with the wind. He considered mainly cloud streets formed when cold air flows over warm surfaces, although other types were also mentioned.

The TIROS I narrow angle camera also photographed some cumulus cloud streets, and the relationship of the flow patterns to the orientation and other aspects of the streets shown in the pictures will be discussed below.

[1] This research has been supported by the National Aeronautics and Space Administration.

2. THE SATELLITE PICTURES

Figure 1 is a composite assembled from several narrow-angle pictures taken at 10-second intervals between 2030 GMT and 2033 GMT on April 1, 1960. The satellite was traveling from northwest to southeast which is from left to right in the composite. The camera axis was oriented slightly back and to the left at this time.

The white areas in figure 1 are probably all cumuliform clouds. Grand Cayman Island is relatively cloud-free while the western end of Cuba and the Isle of Pines are more cloud covered. The presence of such land features increases the confidence in the location and orientation of the cloud features.

Figure 2 is a schematic representation of the clouds shown in figure 1. The dashed outline defines the areal coverage of figure 1. The track of the satellite is shown by the arrow.

The composite and the schematic diagram indicate a greater concentration of cumulus clouds over the heated land areas of the Isle of Pines and Cuba than over the adjacent ocean areas. This is perhaps better shown by examining figures 3 and 4 which depict the detail of cloud masses over Cuba and over the Isle of Pines, respectively. (The shoreline of the islands is indicated by the white outline.) These figures show much more extensive cumulus activity over the heated islands than over the adjacent ocean areas.

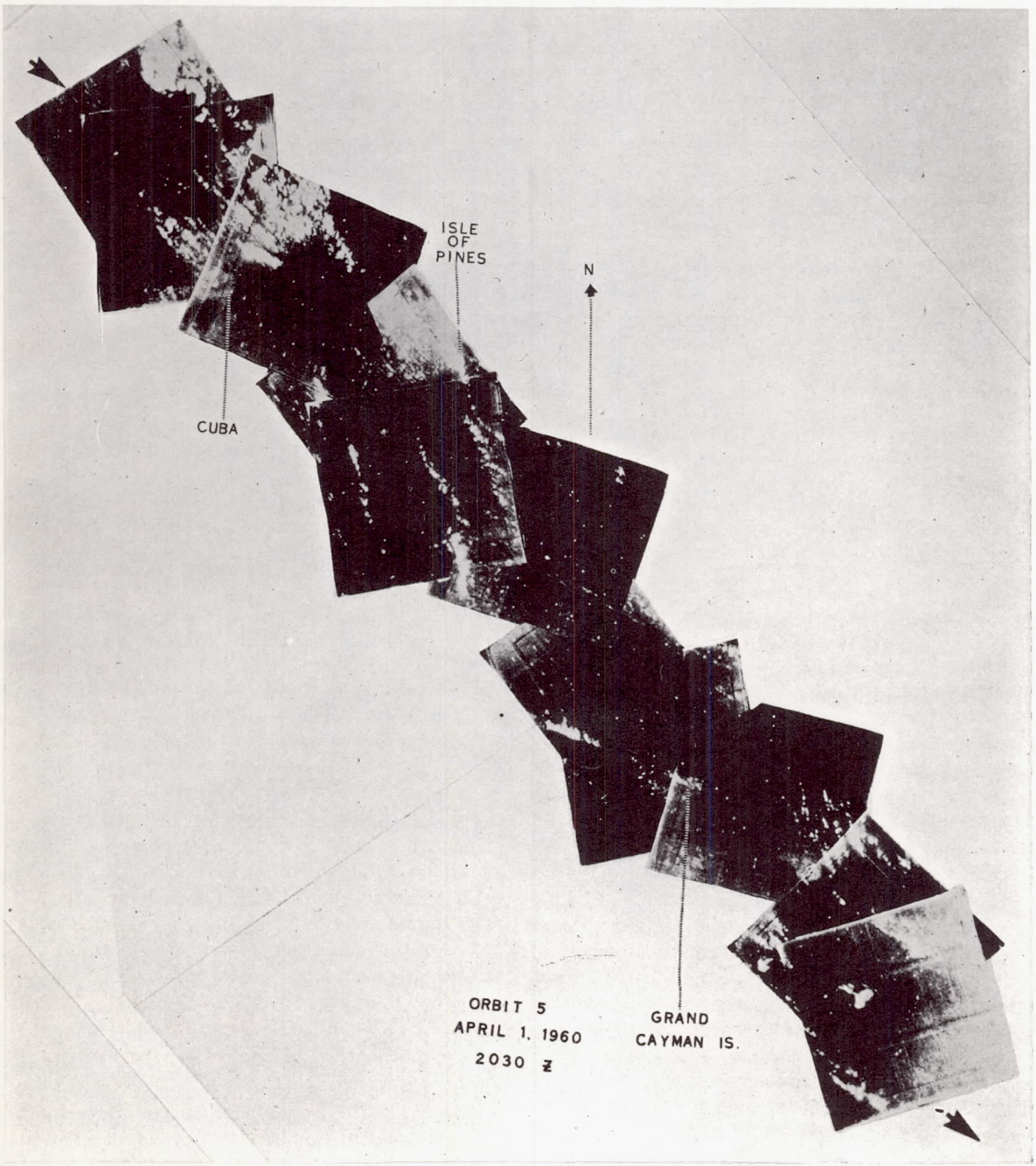

FIGURE 1.—Mosaic of narrow-angle pictures taken at 10-sec. intervals between 2030 and 2033 GMT, April 1, 1960.

This more extensive convective activity is apparently indicative of the greater instability over the islands. In figure 5, comparison of the 0000 GMT, April 2, 1960 radiosonde observations at Havana (considered representative of the heated air over the island of Cuba) with the radiosonde at Grand Cayman (considered representative of the oceanic air) shows the Grand Cayman sounding to be more stable and drier, particularly in the layer from 900 to 800 mb. Differences in heating doubtlessly account for much of this stability difference. An inspection of the sounding for 0000 GMT, April 2 and for 12 hours earlier (not shown here) at Havana (land influence) and at Grand Cayman (oceanic influence) shows that the lower layer at Havana experienced considerably more warming between early morning and evening than did the lower layer at Grand Cayman.

3. CLOUD STREETS IN RELATION TO THE WIND FIELD

The tendency for cumulus clouds to line up in bands or streets under certain conditions has been pointed out [6, 7]. Kuettner [7] discusses some conditions required for the convectively formed clouds to align in bands parallel to the wind. In his observation, the wind direction was fairly constant throughout the convective layer; but a wind-speed maximum also existed within the convective layer giving a negative mean curvature. The important parameter, according to Kuettner [7], in determining whether such bands will align with the wind is the mean curvature of the vertical profile of the horizontal wind speed within the convective layer. He found typical values of this speed-curvature to be of the order of -10^{-7} cm.$^{-1}$ sec.$^{-1}$

Figure 6 shows the wind direction and speed at Havana and at Grand Cayman as a function of height. (Note: The 0000 GMT April 2 wind record for Havana was missing; therefore the 1200 GMT April 1 wind sounding was used. This difference is probably not serious since the synoptic situation in this region was generally unchanged in this 12-hour period.) The Grand Cayman wind profile (fig. 6b) shows a well defined, broad wind speed maximum in the lower layers while Havana (fig. 6a) shows a poorly defined slight maximum at 10,000 feet. Although the wind maximum may not be significant for Havana, computation of the mean curvature in the first 12,000 feet indicated that at both stations the wind profile curvatures were negative, and the curvature had values within an order of magnitude of 10^{-7} cm.$^{-1}$ sec.$^{-1}$

The cloud mosaic (fig. 1) and cloud schematic (fig. 2) show the cloud bands in the vicinity of the Isle of Pines and Cuba oriented at about 140°, and the three cloud bands just southeast of the Isle of Pines oriented at 150°–160°. Referring to figure 6a, it can be seen that the winds at Havana in the first 12,000 feet were within 30° of these orientations. In the layer from 2,000 to 12,000 feet, the wind at Grand Cayman was between 120° and 140°. Thus the cloud streets are aligned quite closely with the wind direction in the convective layer at the two stations.

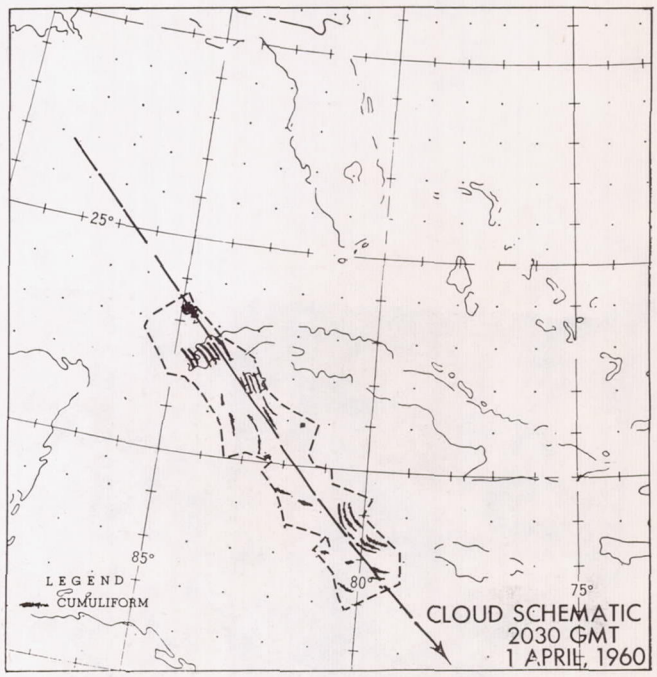

FIGURE 2.—Map showing schematic representations of cloud features appearing on the mosaic of figure 1. The irregular outline delineates geographic coverage of the mosaic. The track of the satellite is indicated by the arrow.

Satellite pictures present an opportunity to observe spacing, shape, and other characteristics of cloud bands. For example, the three cloud bands immediately south and southeast of the Isle of Pines just mentioned (see fig. 1) are interesting because of their length and of the large distances between them. Figure 7 shows these three bands in greater detail. The distance from the easternmost band in figure 7 to the middle one is about 20 miles, and from the middle band to the westernmost one is about 30 miles. The length of the middle band (neglecting the brighter portion in the south which may be part of another cloud band) is about 30 miles, and of the other two about 50 miles.

Noting again figures 3 and 4, one can see that over the heated land masses of the Isle of Pines and Cuba the spacing of the bands is an order of magnitude smaller than the spacing over the ocean. Over Cuba the spacing is about 3 to 4 miles; over the Isle of Pines it is about 2 to 3 miles. Moreover, the length of these lines appears to be related to the distance across the island in the direction of the wind flow. For example, the bands (fig. 3) over extreme western Cuba are shorter than those farther east over Cuba; the bands over the very narrow southwestern portion of the Isle of Pines (fig. 4) are much

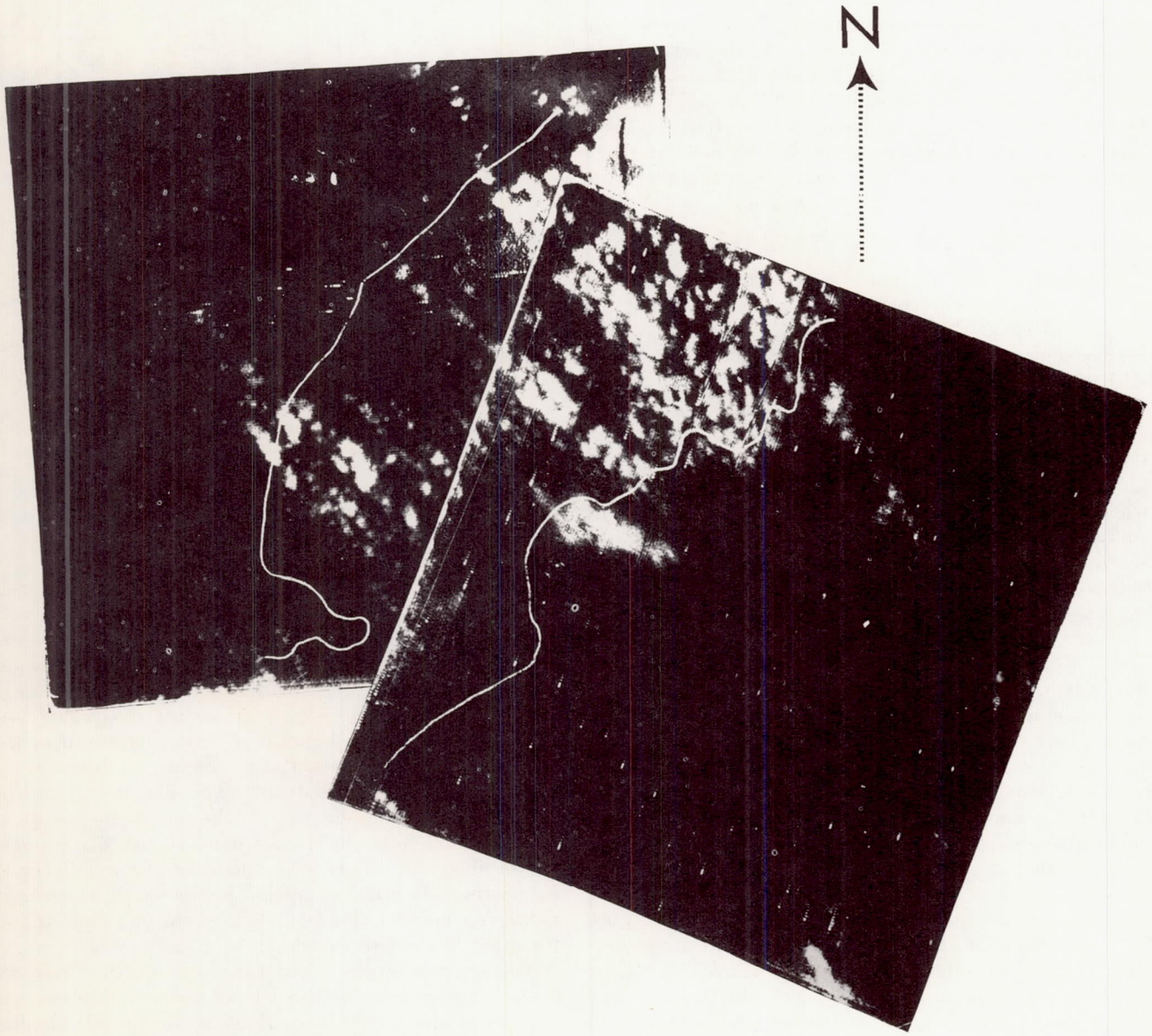

FIGURE 3.—Detailed composite of the portion of the mosaic over Cuba. The Cuban coastline is shown by the white outline.

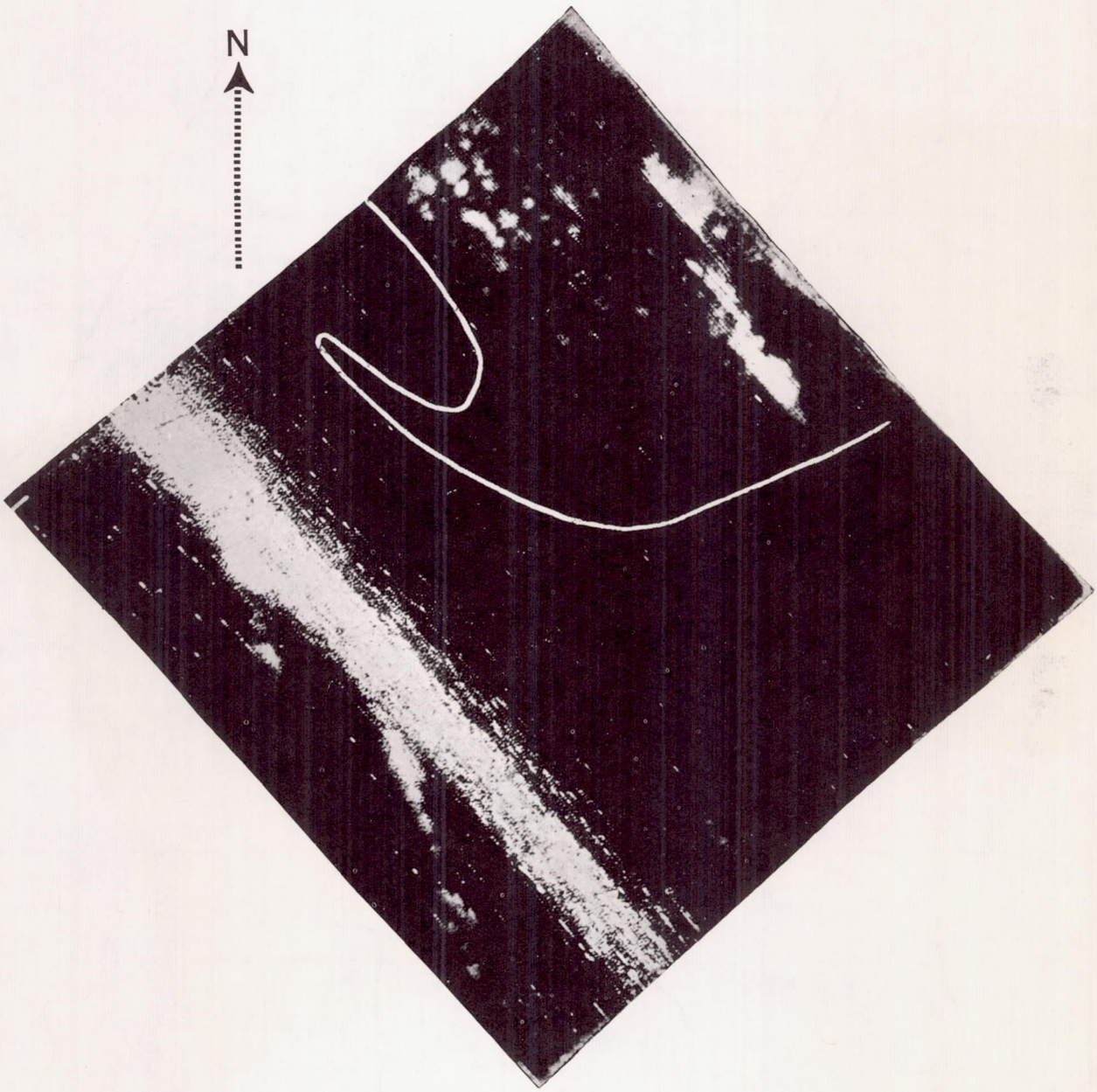

FIGURE 4.—Detailed view of cloud streets over the Isle of Pines. The coastline is depicted by the white outline.

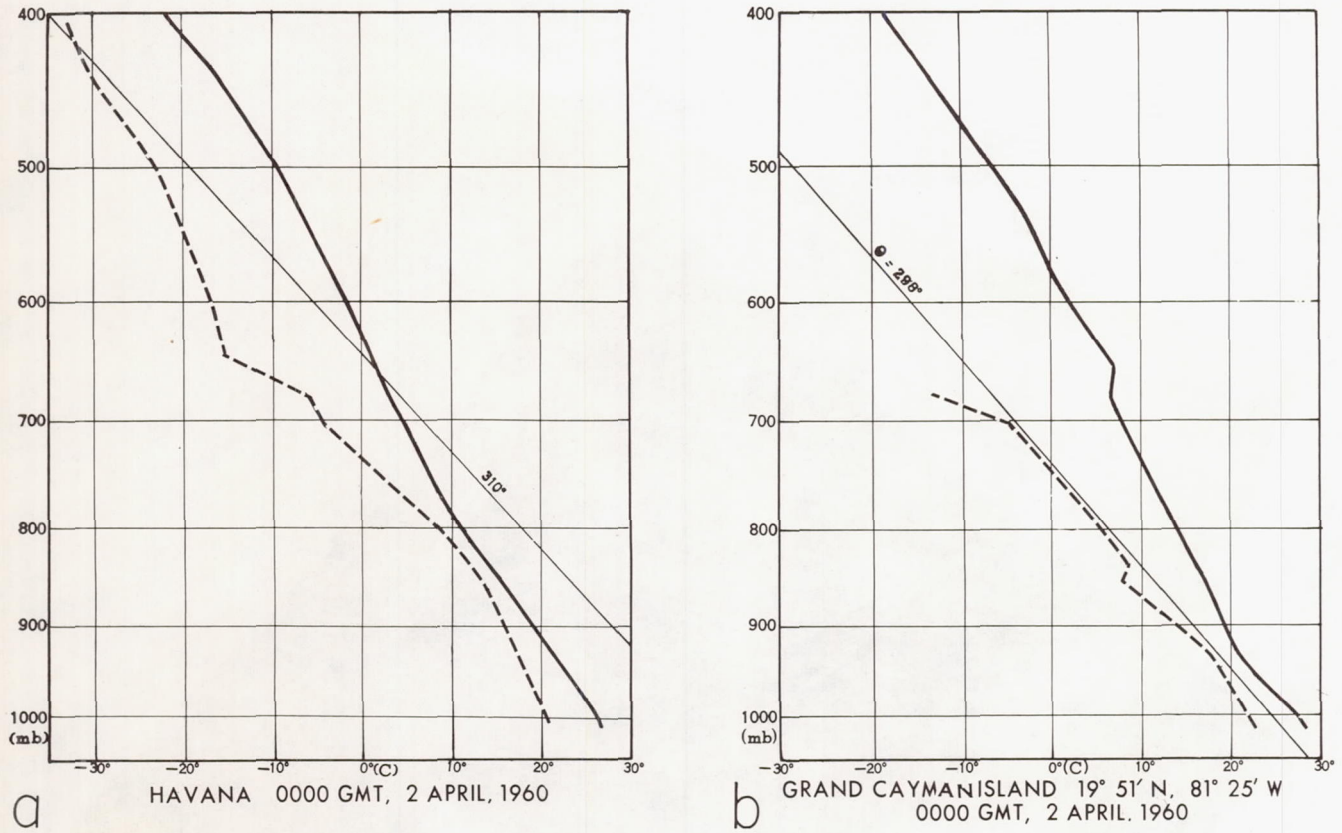

FIGURE 5.—Radiosonde observations for Havana and Grand Cayman Island at 0000 GMT, April 2, 1960.

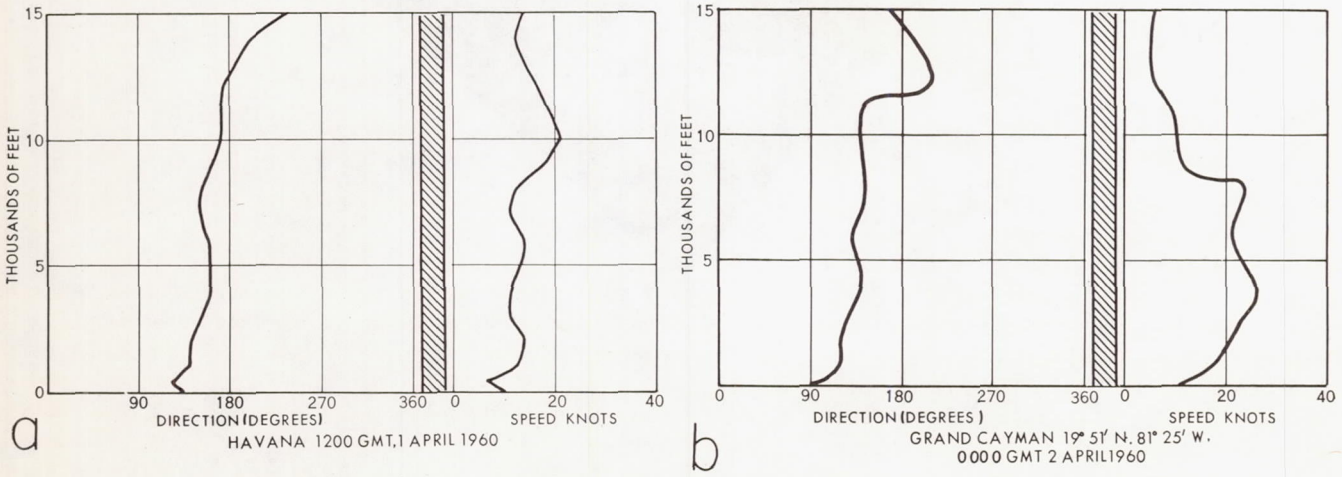

FIGURE 6.—Graph of wind speed and direction as a function of height for Havana at 1200 GMT, April 1, 1960 and Grand Cayman at 0000 GMT, April 2, 1960.

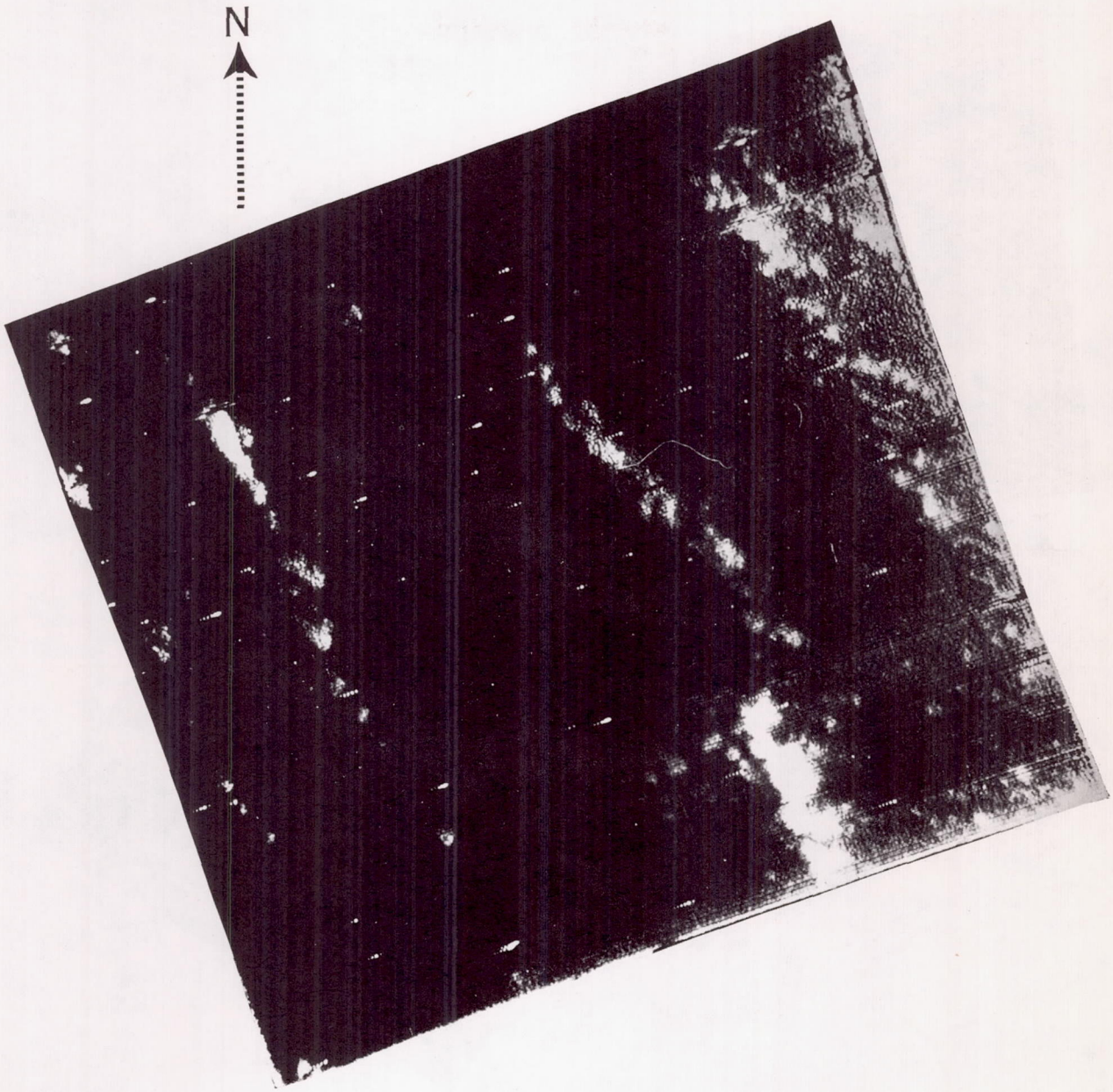

FIGURE 7.—Larger picture of the three oceanic cloud bands in figure 1.

shorter than those over the northeastern portion of the island. The distances across the islands in the direction of the wind flow vary in a similar manner.

In the extreme southeastern end of the picture swath, some anticyclonically (?) curved bands, which were imbedded in the general southeastern flow, were noted (see figs. 1 and 2). These are illustrated more clearly in figure 8. The radius of curvature of these bands is 60 n.mi. and they are spaced at 3 to 4-n.mi. intervals. Meteorological observations in this area were too sparse to determine whether a circulation of such a small scale existed. Nevertheless the curvature in the cloud street suggests that such small undulations in the circulation may have existed.

4. SUMMARY

The TIROS narrow-angle camera presents a means of determining such factors as orientation, spacing, and length of cloud streets. In this study the streets were aligned within 30° of the wind direction in the convective layer. The spacing of the streets over heated land was much less than of those over the ocean. The length of the streets over the larger islands appeared to be related to the distance across the island in the direction of the wind flow.

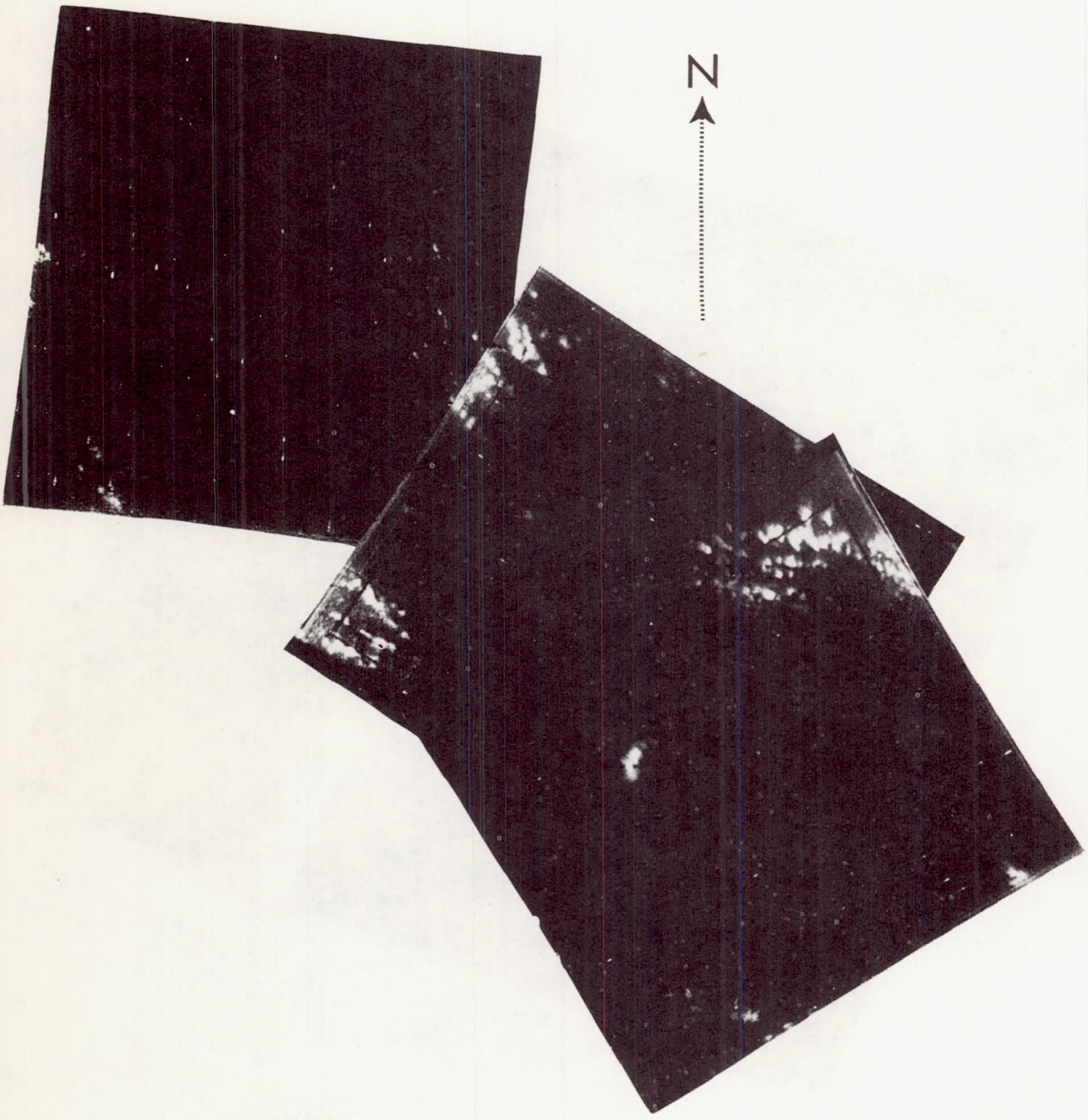

FIGURE 8.—Composite showing greater detail of the curved bands in figure 1.

REFERENCES

1. S. Sternberg et al., "Roundup on TIROS I," *Astronautics*, vol. 5, No. 6, June 1960.
2. S. Fritz and H. Wexler, "Cloud Pictures From Satellite TIROS I," *Monthly Weather Review*, vol. 88, No. 3, Mar. 1960, pp. 79–87.
3. J. S. Winston and L. Tourville, "Cloud Structure of an Occluded Cyclone Over the Gulf of Alaska as Viewed by TIROS I," *Bulletin of the American Meteorological Society*, vol. 42, No. 3, Mar. 1961, pp. 151–166.
4. S. Fritz, "Satellite Cloud Pictures of a Cyclone over the Atlantic Ocean," *Quarterly Journal of the Royal Meteorological Society*, vol. 87, No. 373, July 1961, pp. 314–321.
5. C. L. Bristor and M. A. Ruzecki, "TIROS I Photographs of the Midwest Storm of April 1, 1960," *Monthly Weather Review*, vol. 88, Nos. 9–12, Sept.–Dec. 1960, pp. 315–326.
6. H. Riehl, W. S. Gray, J. S. Malkus, and C. Ronne, "Cloud Structure and Distributions over the Tropical Pacific," Unpublished manuscript, Woods Hole Oceanographic Institution, 66 pp., 1959. Ref. No. 58–62, Technical Report No. 5, ONR Contract Number 1721(00).
7. J. Kuettner, "The Band Structure of the Atmosphere," *Tellus*, vol. 11, No. 3, Aug. 1959, pp. 267–294.

Figures and Legends (Continued):

FIGURE 15: TIROS II Scanning Radiometer Thermal Channel at 8 to 30 Microns, Orbit 88.

The thermal map is quite similar to that from the window (Figure 13). The maximum temperatures were about 15°C lower than those of Channel 2, suggesting that the radiation is emanating from higher levels of the atmosphere. The area to the west of Iberia, which was bright (42 percent albedo) in the albedo channel, is only slightly cooler than the surrounding regions, indicating a low cloud deck.

FIGURE 16: TIROS II Scanning Radiometer Narrow-Band Visible Channel at 0.55 to 0.75 Microns, Orbit 88.

These data are of poorer quality with no strongly identifiable pattern that can be associated with the other channels. It is probably much more susceptible to solar elevation angle corrections.

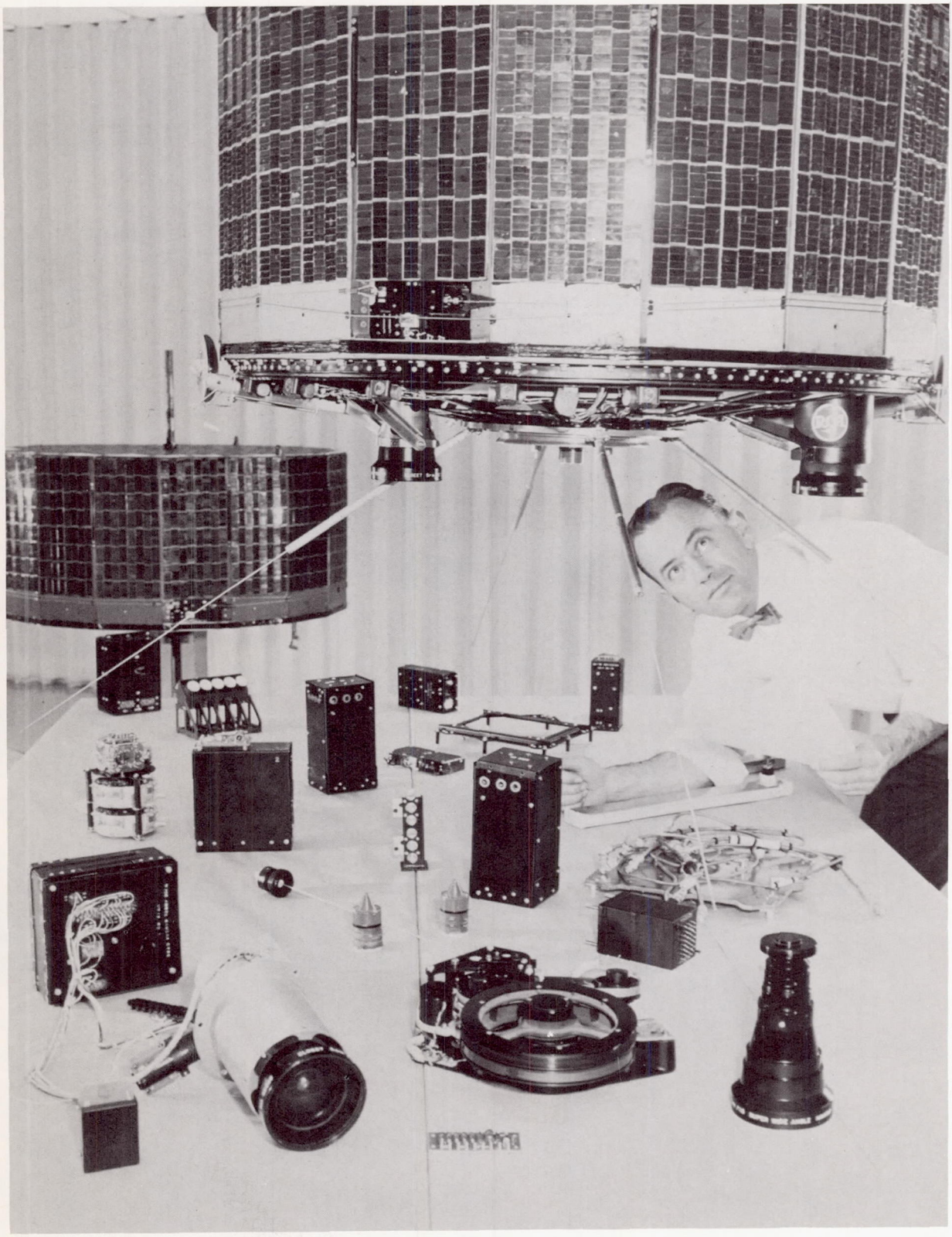

FIGURE 1: The TIROS Satellite and Its Major Components.

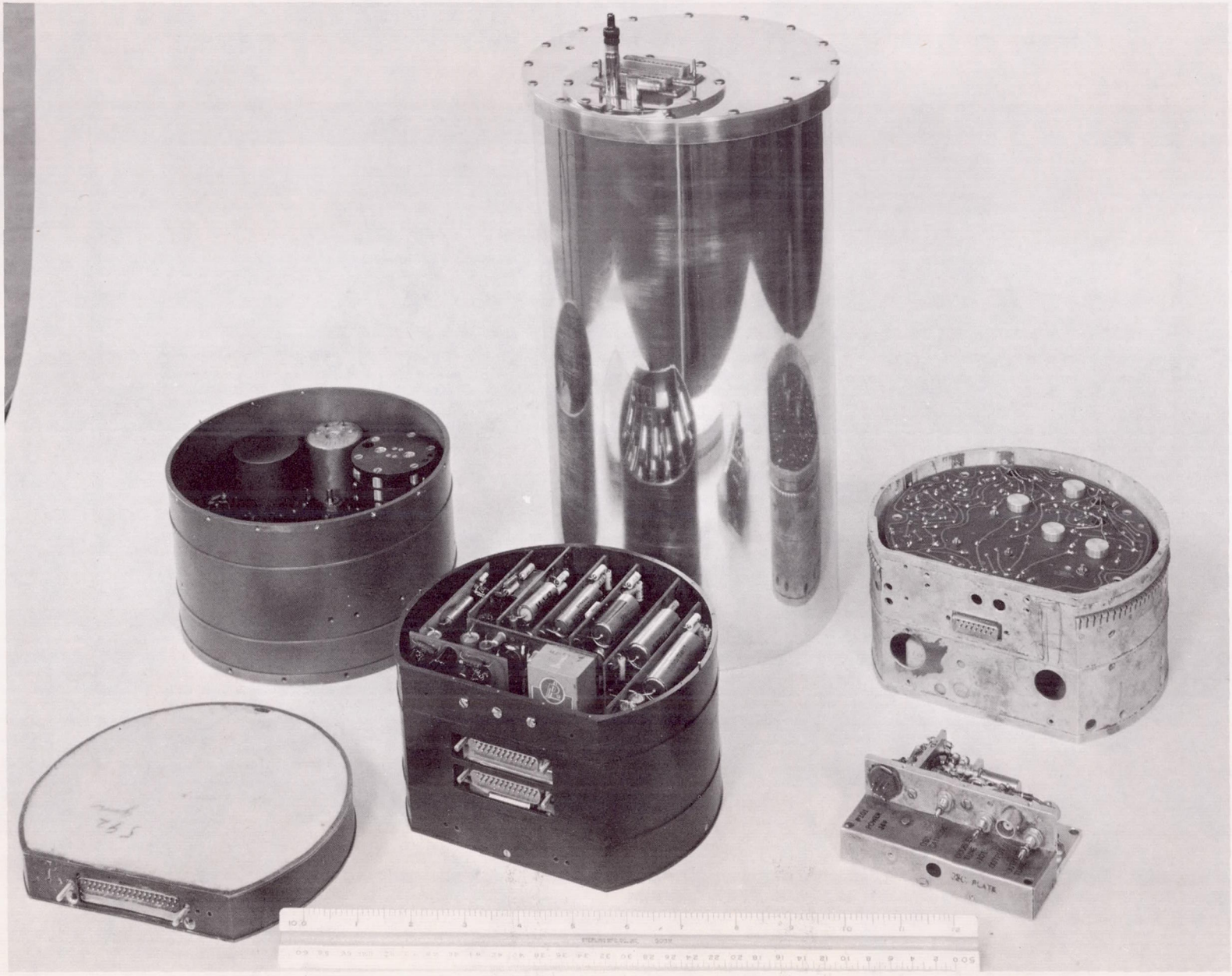

FIGURE 2: The Radiation Subsystem of the TIROS Satellite.

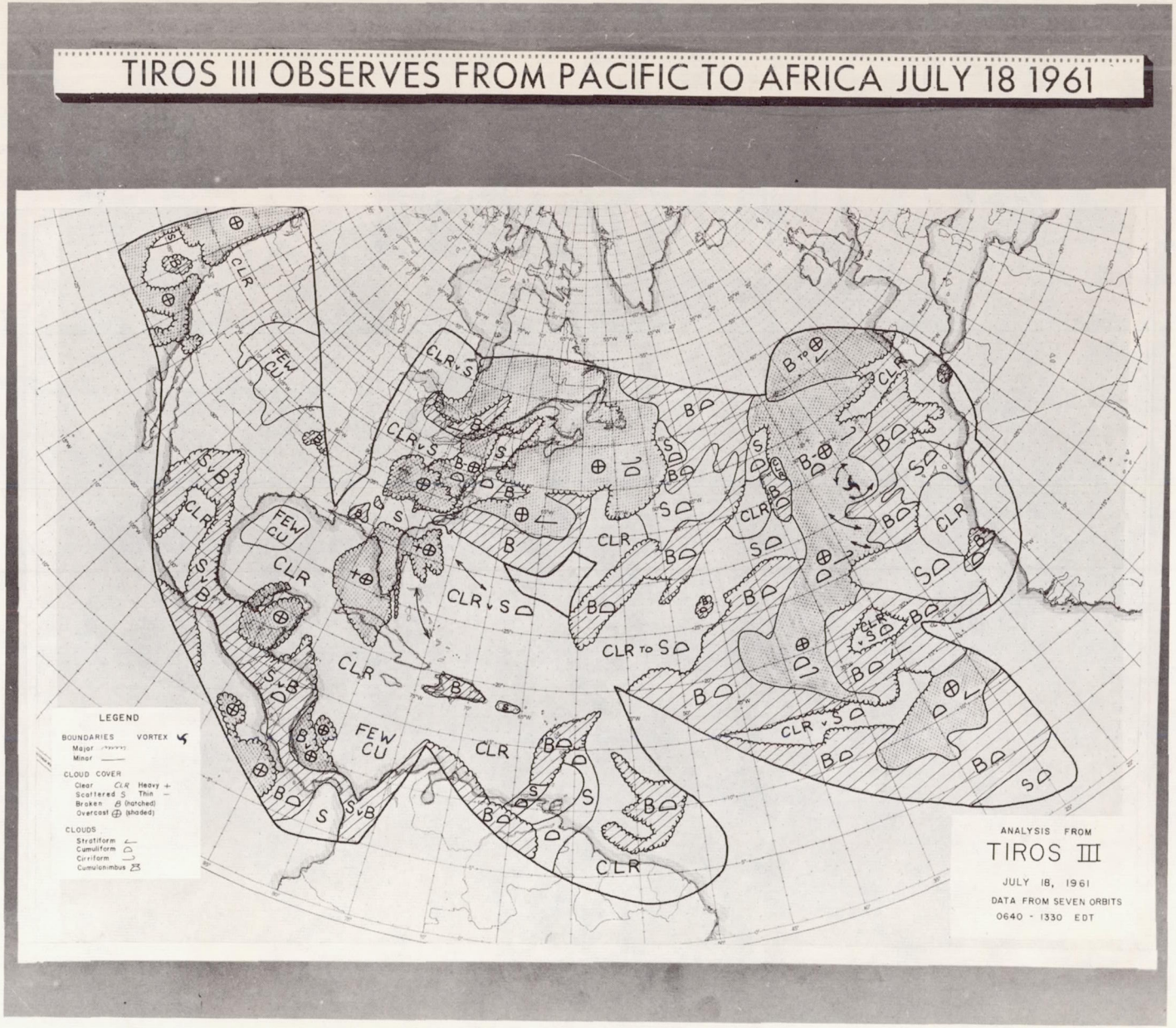

FIGURE 3: The TIROS III Nephanalyses for July 18, 1961 Over the Atlantic-from Seven Orbits.

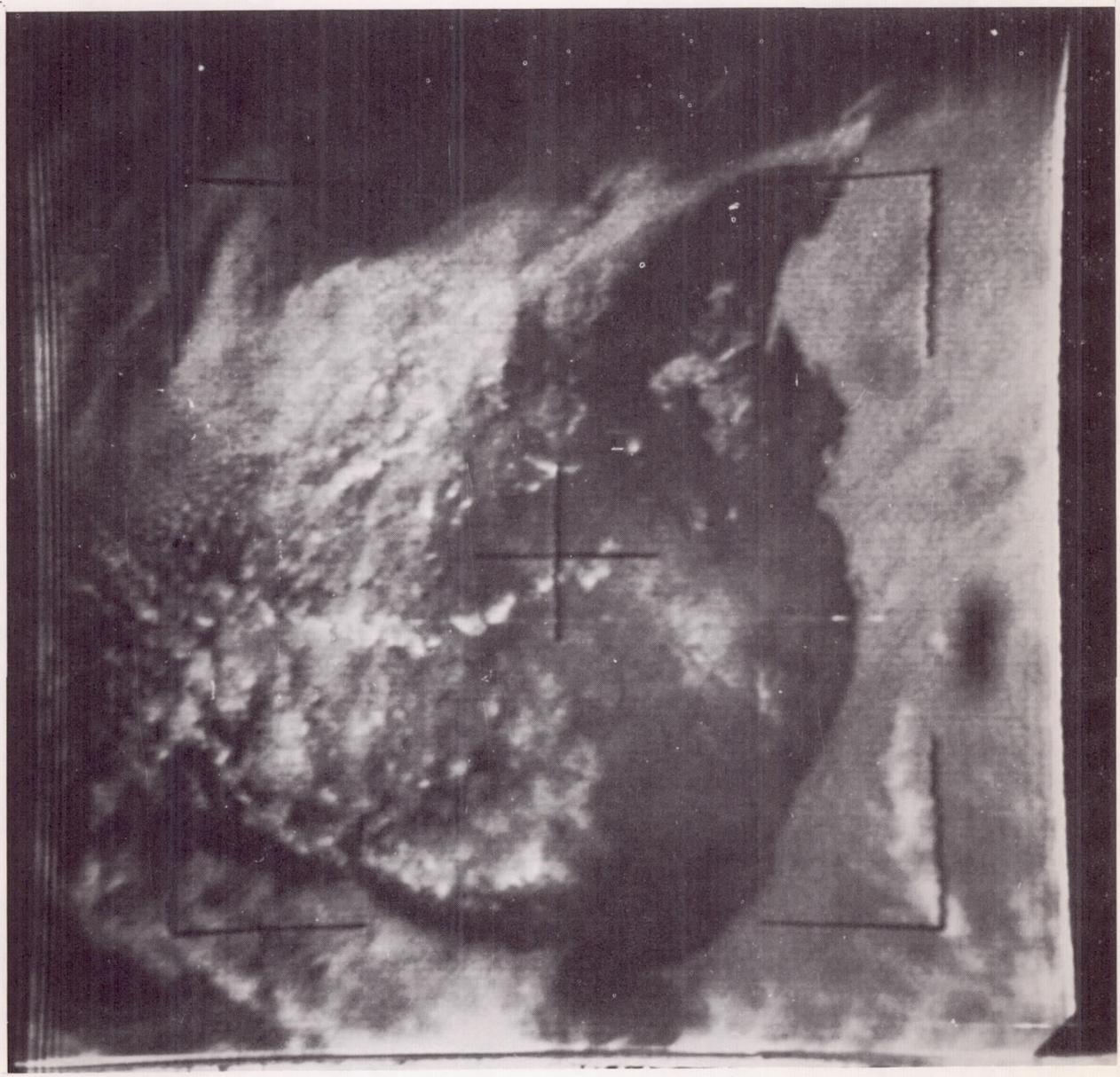

FIGURE 4: An Example of Cloud Photographs Used to Produce Nephanalyses Like Figure 3.

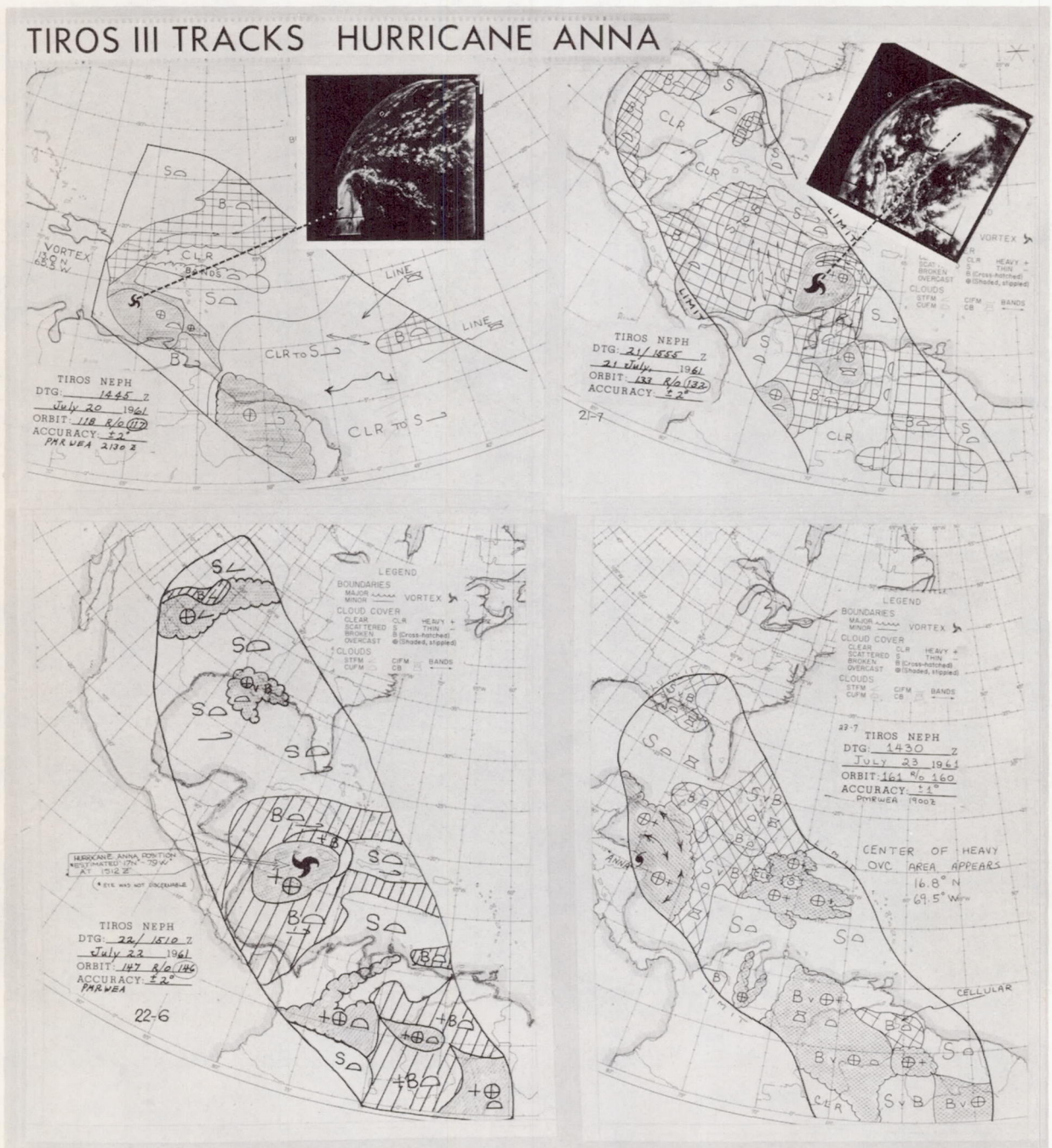

FIGURE 5: Successive Nephanalyses from TIROS III of the Caribbean Area and Hurricane Anna, July 20 through 23, 1961.

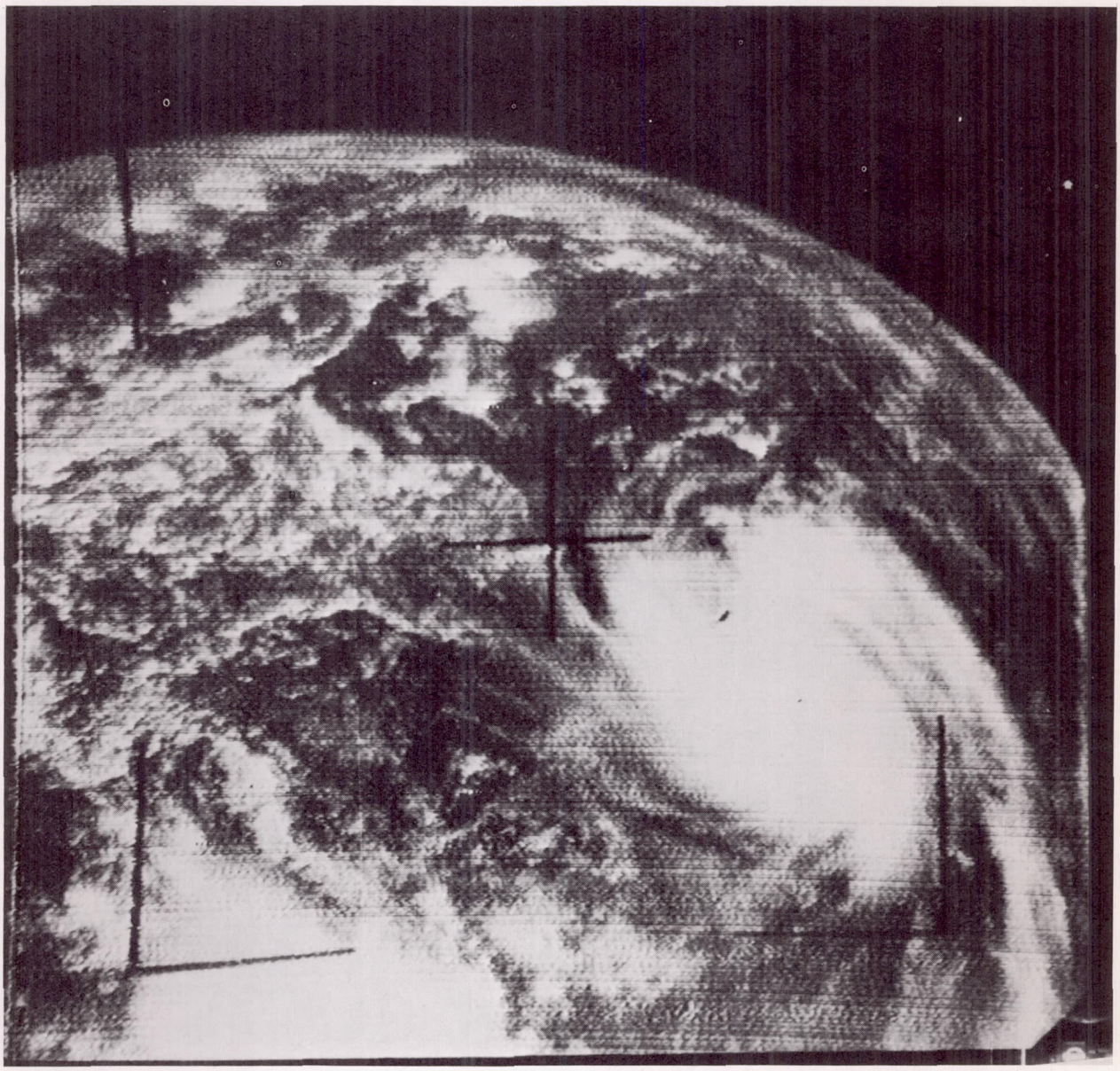

FIGURE 6: Hurricane Anna on July 21, 1961

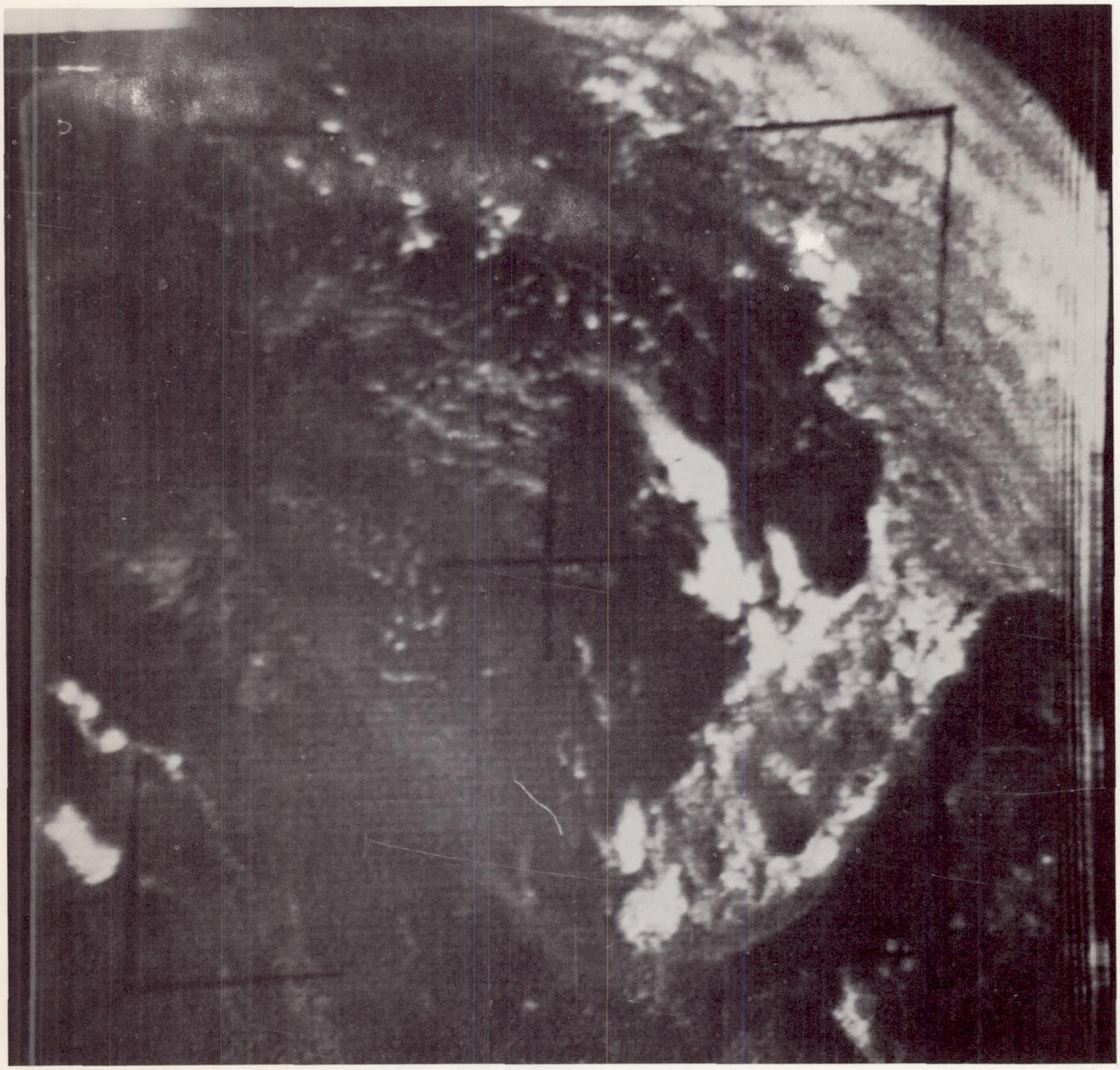

FIGURE 7: TIROS III Photograph of Florida.

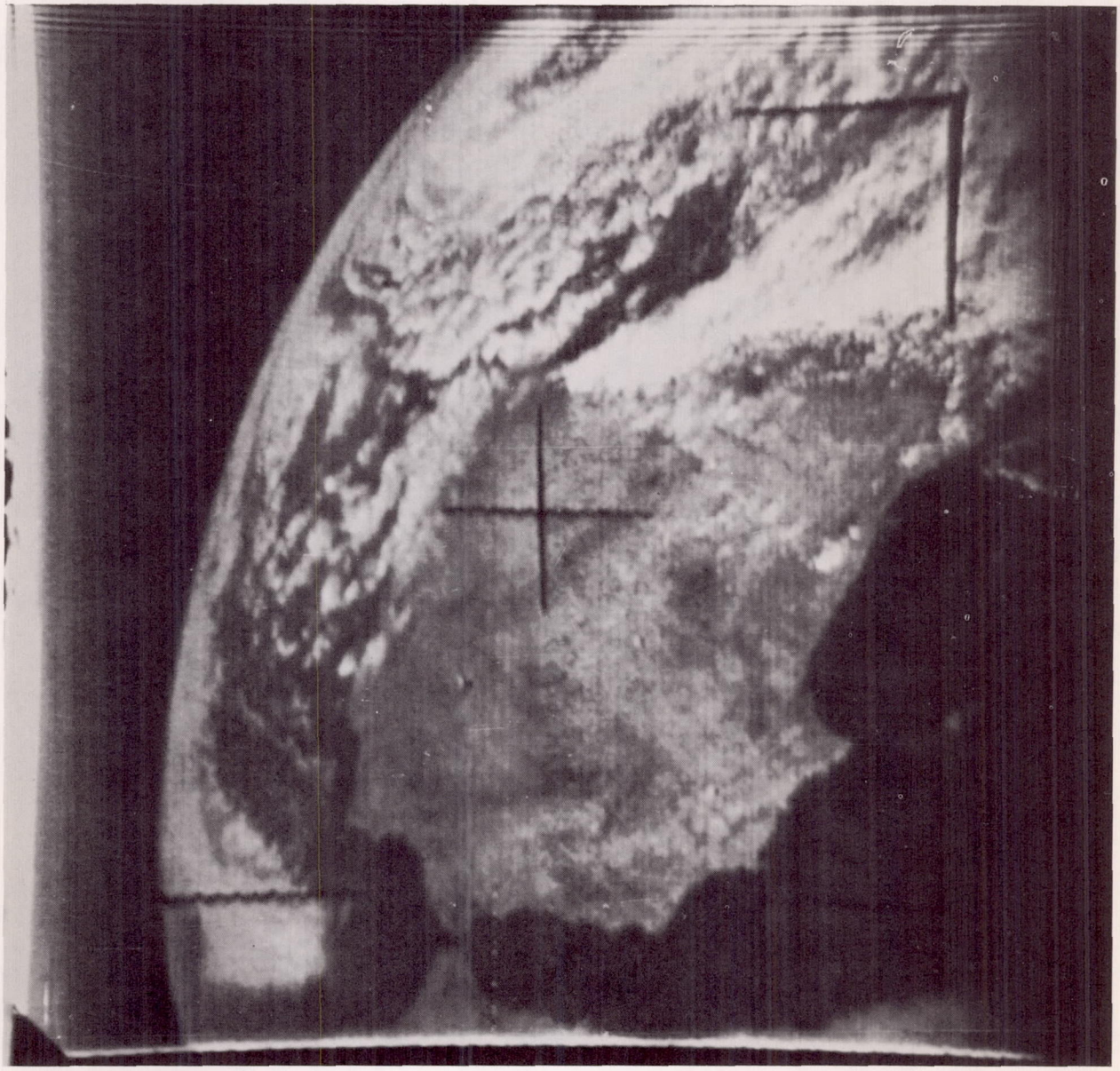

FIGURE 8: The Iberian Peninsula and the Straits of Gibralter, July 15, 1961.

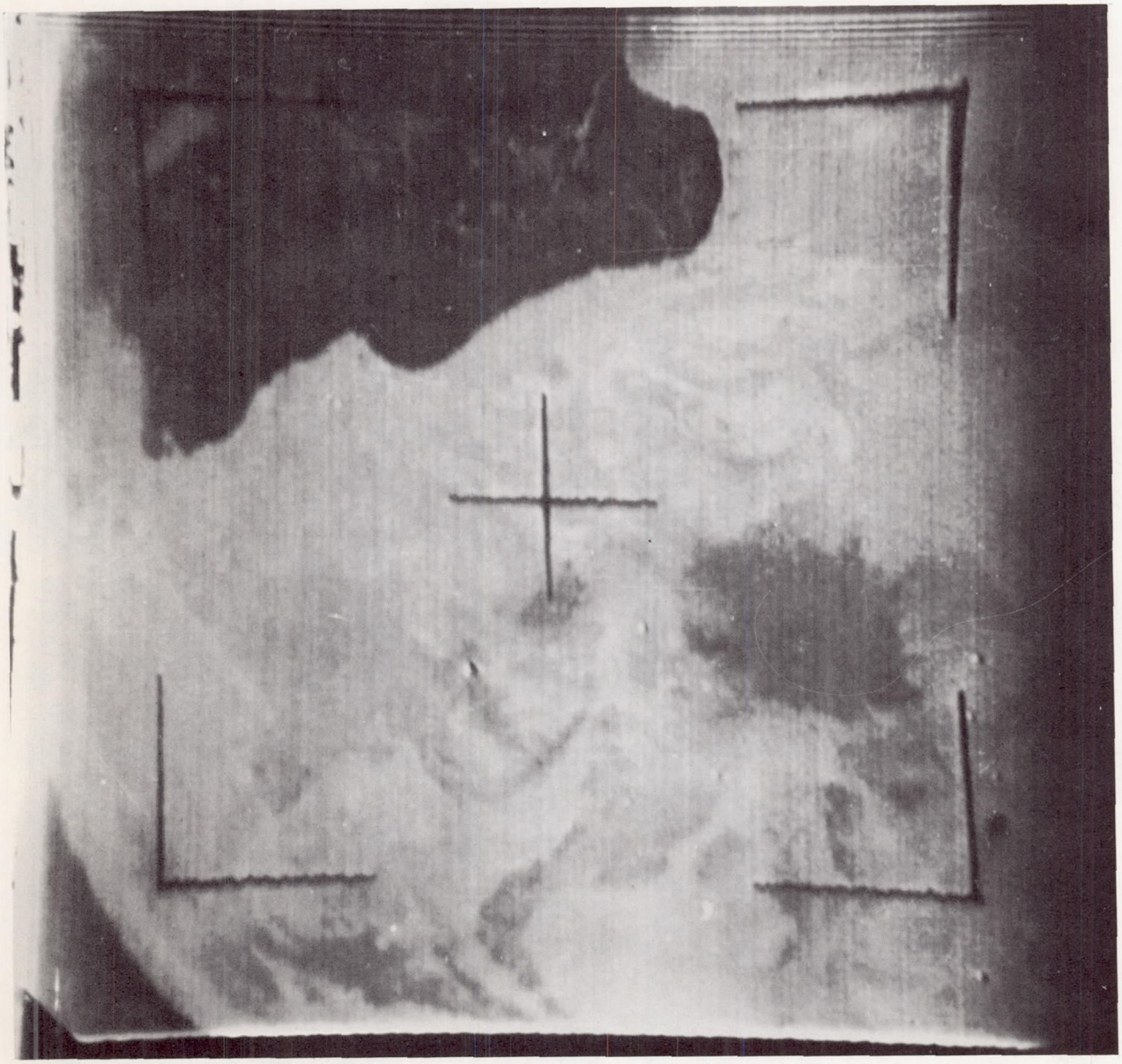

FIGURE 9: The Sahara Desert of North Africa and the Gulf of Sidra, Off Libya.

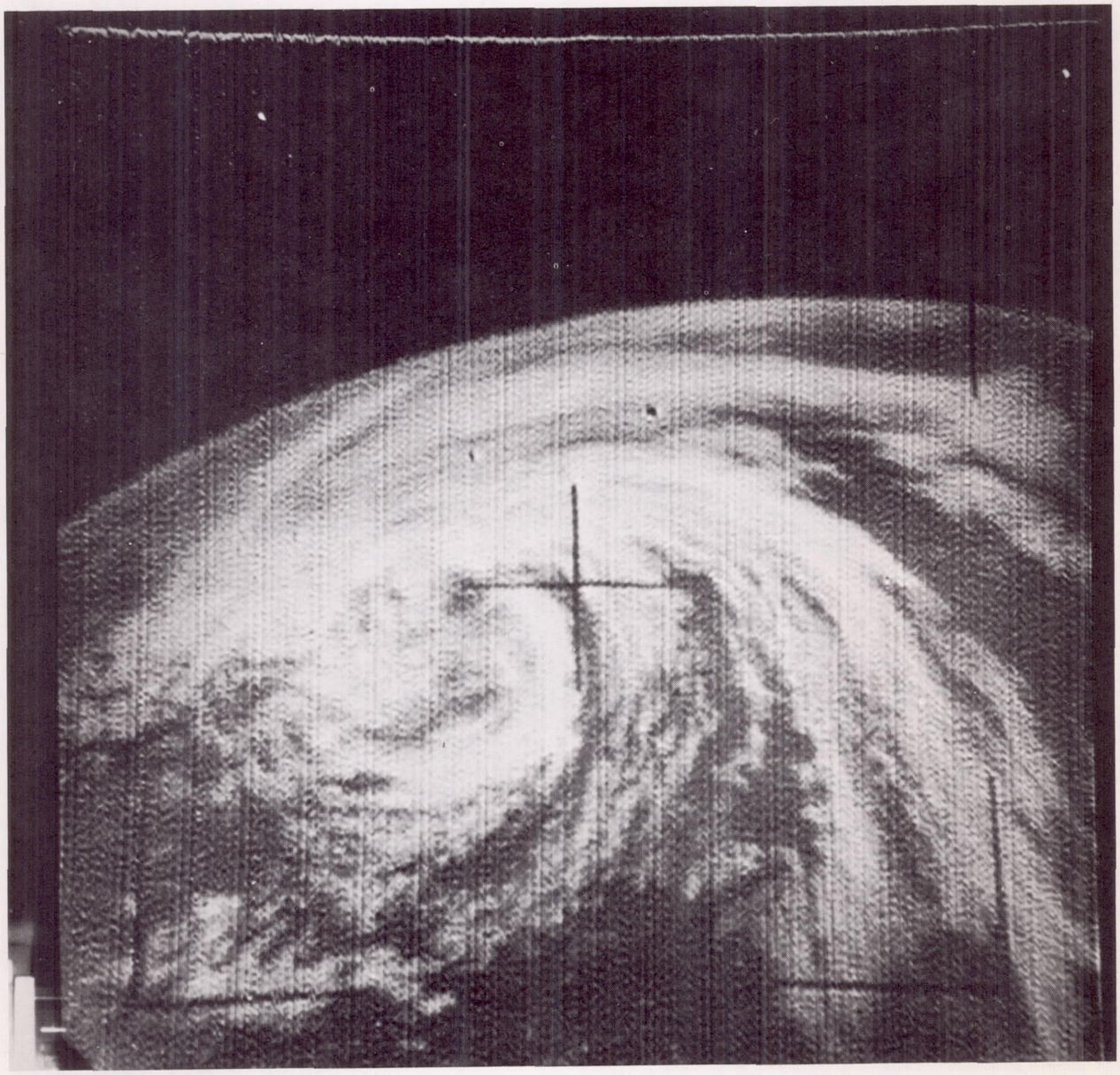

FIGURE 10: A TIROS III-Located Tropical Storm Named Liza.

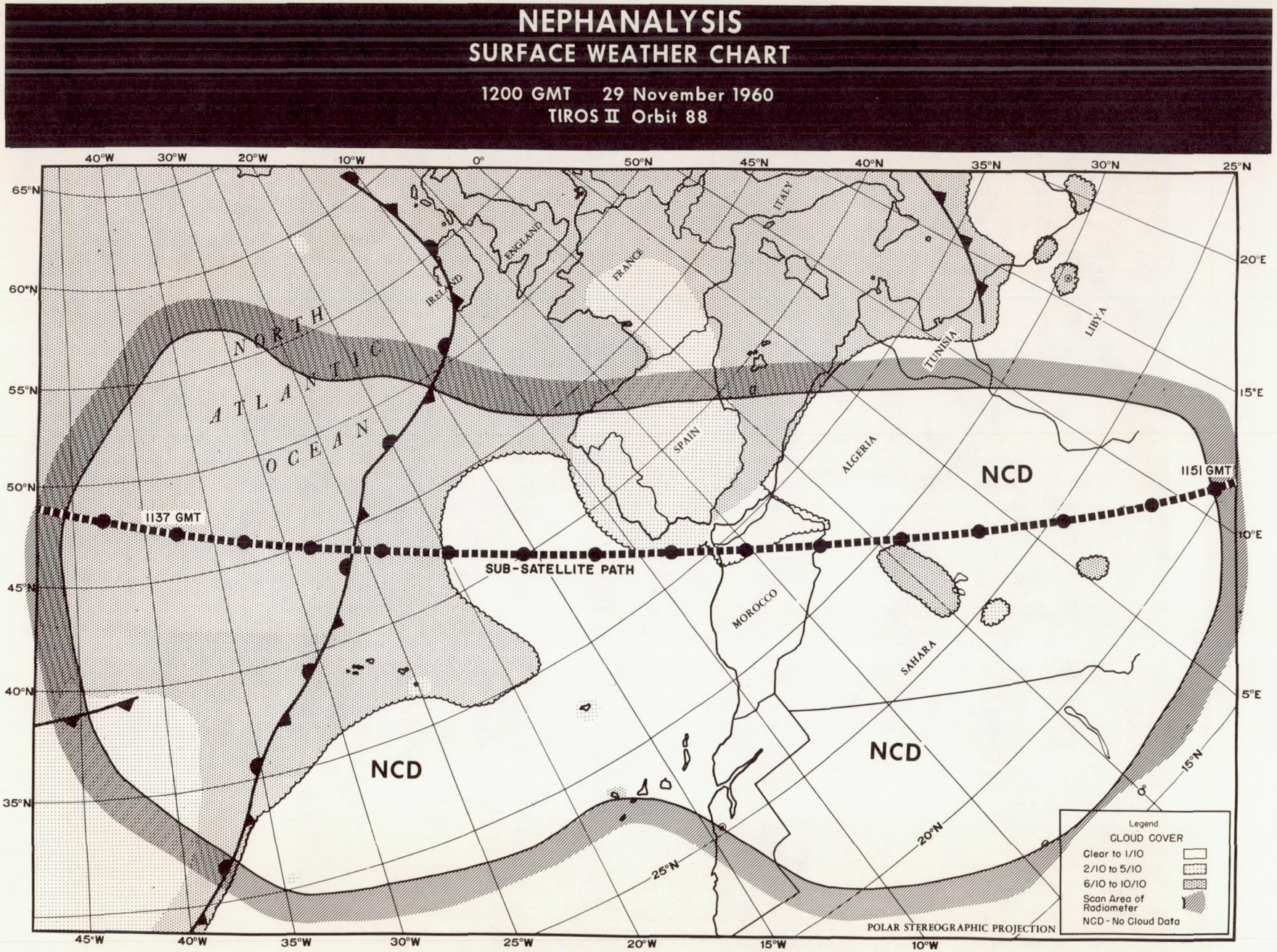

FIGURE 11: A Nephanalysis from Surface Weather Data on TIROS II Orbit 88, Over the Atlantic Ocean and North Africa.

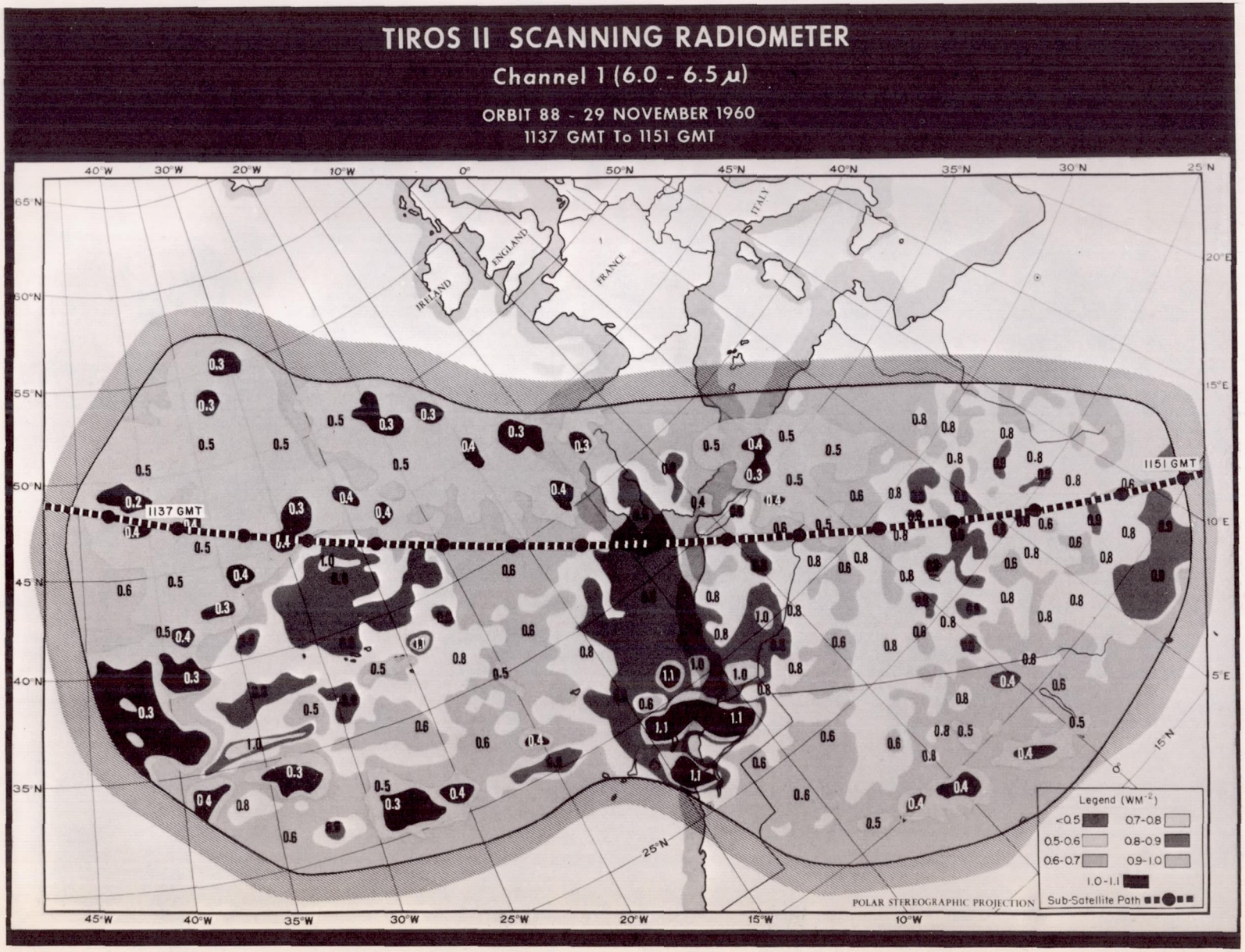

FIGURE 12: TIROS II Scanning Radiometer Water Vapor Channel at 6.0 - 6.5 Microns, Orbit 88.

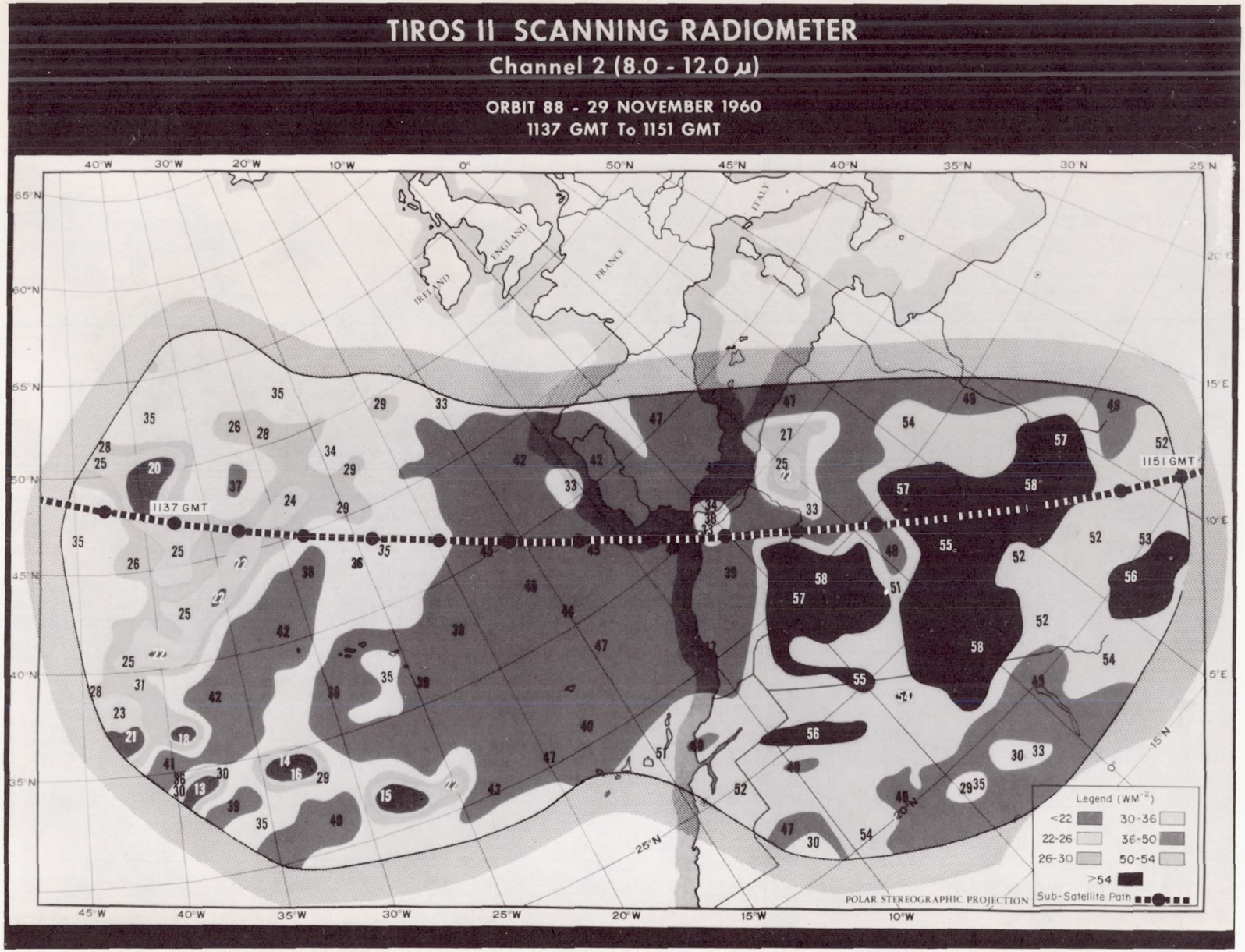

FIGURE 13: TIROS II Scanning Radiometer Atmospheric Window Channel at 8 to 12 Microns, Orbit 88.

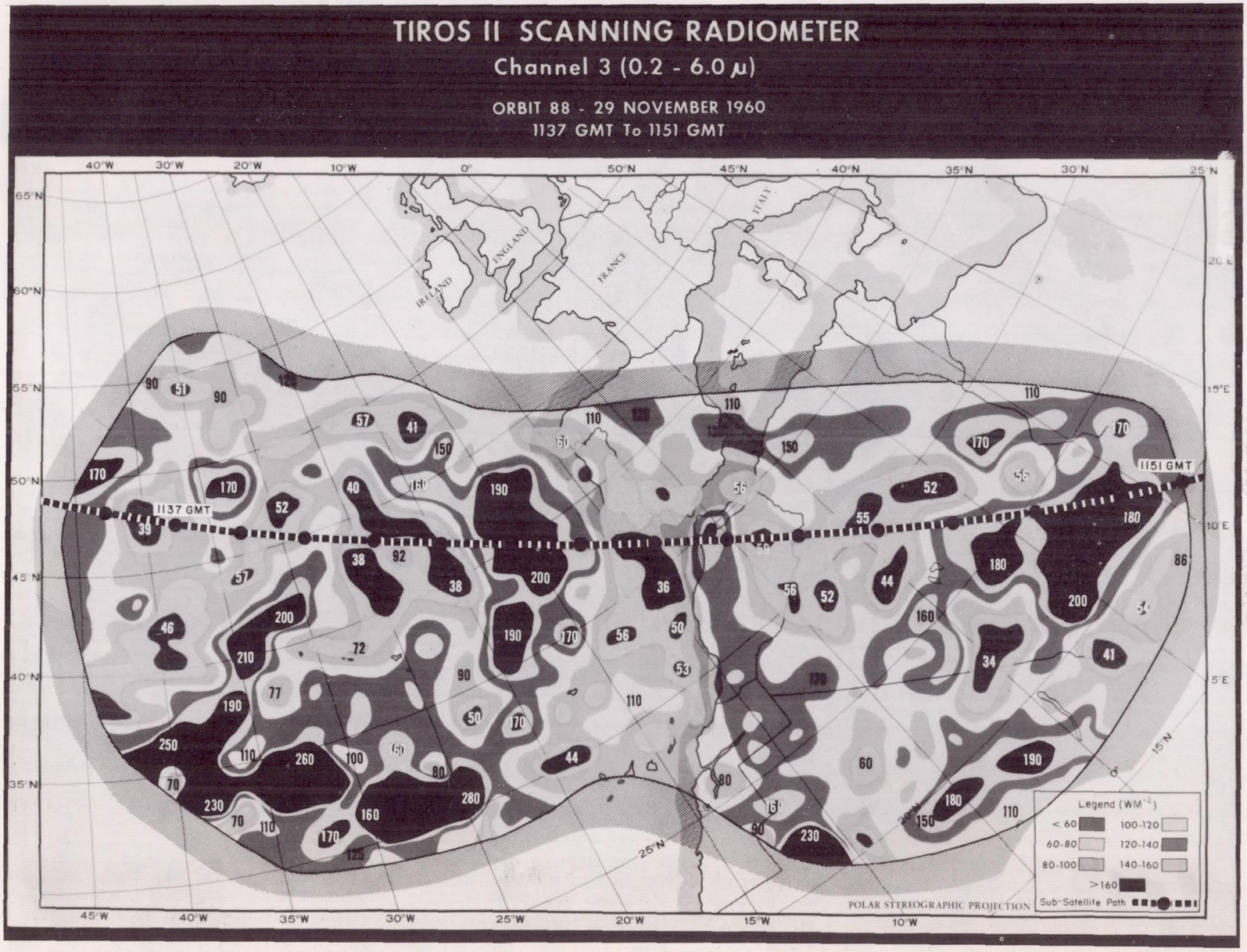

FIGURE 14: TIROS II Scanning Radiometer, Albedo Channel at 0.2 to 6.0 Microns, Orbit 88.

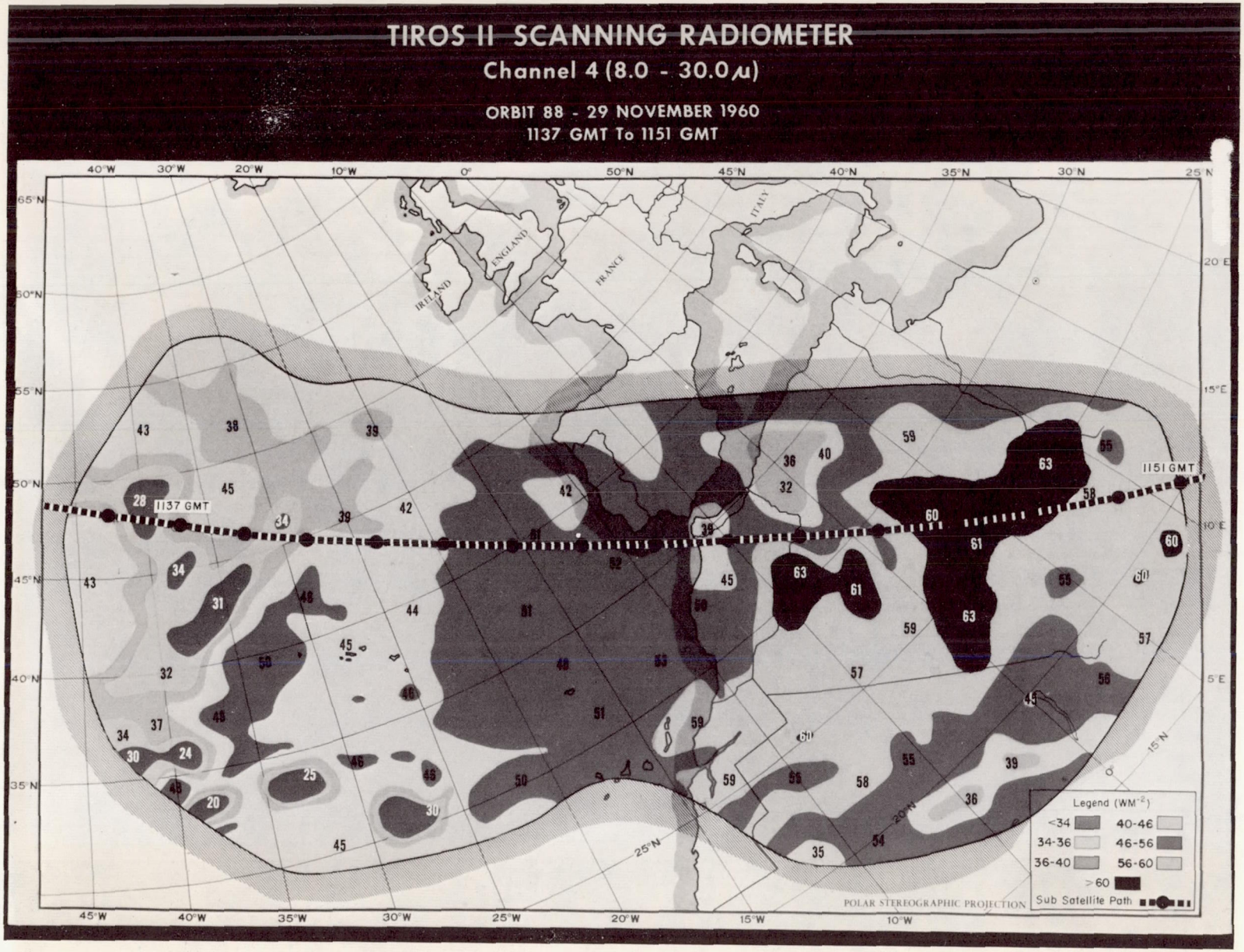

FIGURE 15: TIROS II Scanning Radiometer Thermal Channel at 8 to 30 Microns, Orbit 88.

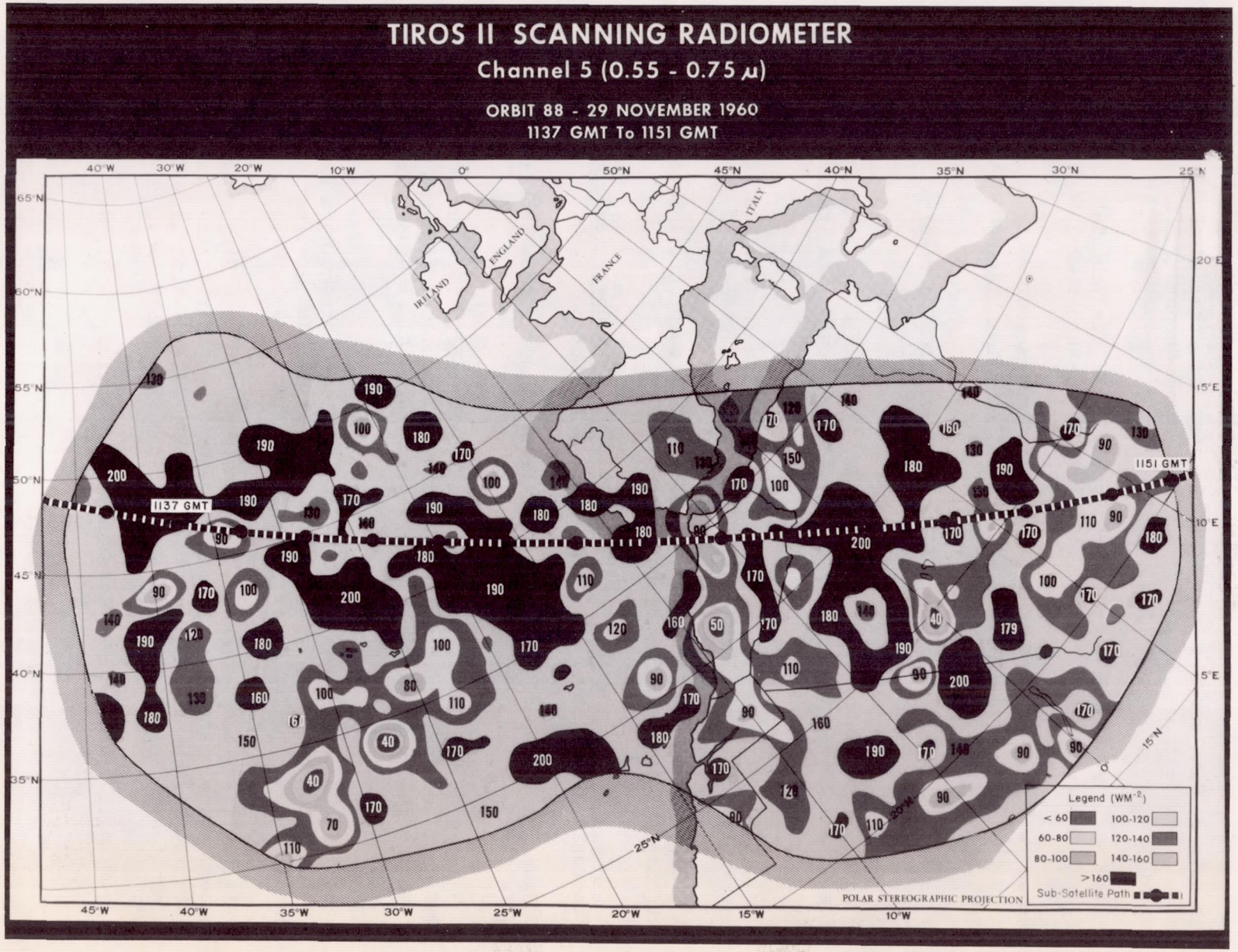

FIGURE 16: TIROS II Scanning Radiometer Narrow-Band Visible Channel at 0.55 to 0.75 Microns, Orbit 88.

REFERENCES

1. Greenfield, S.M. and Kellogg, W.W. "Inquiry into the Feasibility of Weather Reconnaissance from a Satellite Vehicle", Rand Corporation Report R-365, August 1960.

2. Wexler, H., "Observing the Weather from a Satellite Vehicle", Journal of the British Interplanetary Society, 13(5):269-276, September 1954.

3. Stroud, W.G. and Nordberg, W., "Meteorological Measurements from a Satellite Vehicle", Chap. 13 Scientific Uses of Earth Satellites, James A. Van Allen, Editor, Ann Arbor, U. of Mich. Press 1956.

4. a) Hubert, L.F. and Berg, O., "A Rocket Portrait of a Tropical Storm", Monthly Review 83(6): 119-124, June 1955.

   b) Hanel, R.A., Licht, J., Nordberg, W., Stampfl, R.A., and Stroud, W.G., "The Satellite Vanguard II: Cloud Cover Experiment", IRE Transactions, Vol. MIL-4, Nos. 2 and 3, April - June 1960.

5. Suomi, V.E., Parent, R.J., and Swift, W.B., "The Thermal Radiation Balance Experiment on Board Explorer VII, N-85910, U. of Wisc. 1960.

6. a) Sternberg, S. and Stroud, W.G., "TIROS I Meteorological Satellite", Astronautics 5(6): 32-34, 84-86, June 1960.

   b) TIROS I Meteorological Satellite System, Final Operational Report, Astro-Electronics Division of RCA, Princeton, N.J., October 1960.

7. a) Hanel, R.A., and Stroud, W.G., "Infrared Imaging from Satellites", Journal SMPTE 69:25-26, January 1960.

   b) Bandeen, W.R., Hanel, R.A., Licht, J., Stampfl, R.A. and Stroud, W.G., "Infrared and Reflection Solar Radiation Measurements from the TIROS II Meteorological Satellite". In publication: Journal of Geophysical Research, October 1961.

8. Bandeen, W.R., and Manger, W.P. ="Angular Motion of the Spin Axis of the TIROS I Meteorological Satellite Due to Magnetic and Gravitational Torque", Journal of Geophysical Research, Vol. 65, No. 9, 2992-2995, September, 1960.

9. Staff, Aeronomy & Meteorology Division, Goddard Space Flight Center, and Meteorological Satellite Laboratory of U. S. Weather Bureau: (a) TIROS II Radiation Data Users' Manual, and (b) TIROS II Radiation Data Catalogue. In publication as NASA Technical Memoranda, September 1961.

10. Tepper, M., "TIROS Program Results", Astronautics, p. 61, May 1961.

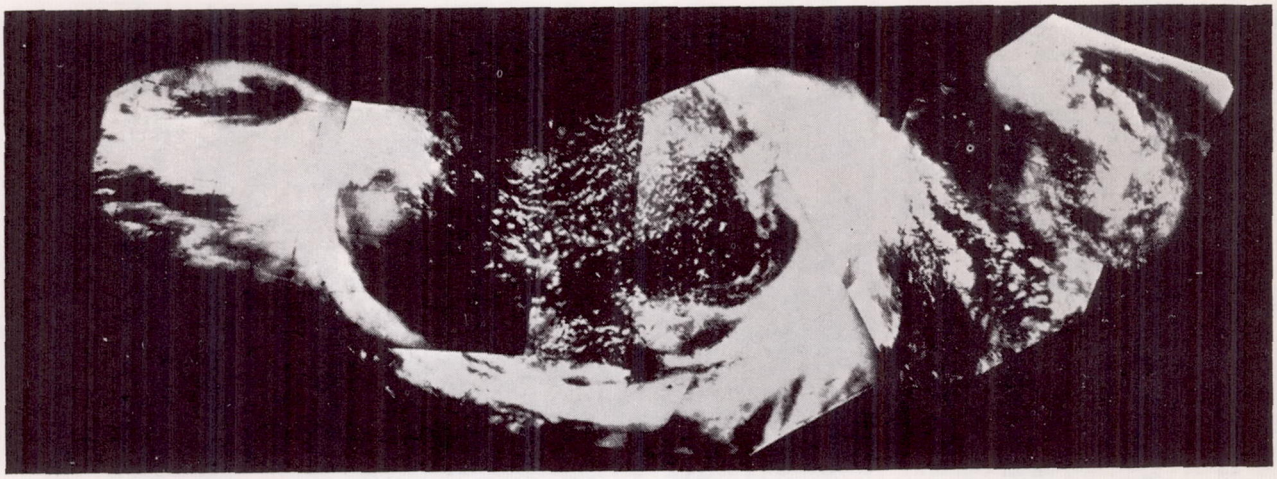

Tiros program results

Two history-making Tiros shots showed that satellite data can be extracted and transmitted to weather stations fast enough to profit forecasting and warrant advanced systems

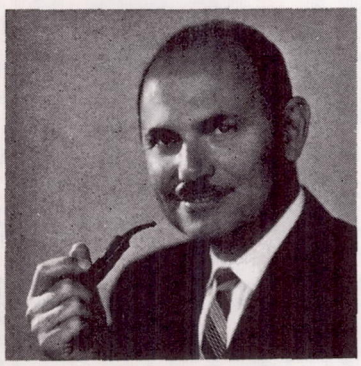

By Morris Tepper

NATIONAL AERONAUTICS AND SPACE ADMINISTRATION, WASHINGTON, D.C.

Morris Tepper is chief of the Meteorological Satellite Program at NASA and chairman of its joint meteorological satellite advisory committee, as well as a member of other key panels and advisory groups in this field. A member of the staff of the U.S. Weather Bureau previously, since 1946, he was chief of its Severe Local Storms Research Unit when he joined NASA in 1959. In 1950, the American Meteorological Society gave him the Meissinger Award (jointly with John C. Freeman Jr.), and in 1952 Johns Hopkins Univ. conferred his Ph.D. in fluid mechanics. Besides his important contributions to the Tiros program, Dr. Tepper is known for proposing a theory on squall-line formation, based on the analogy to fluid flow in an open channel, and for his many papers on weather research.

TIROS I was launched into orbit on April 1, 1960, and had a useful operating lifetime of 78 days. Tiros II was launched into orbit on Nov. 23, 1960, and at the time of this writing is still transmitting useful data. Without doubt, the year 1960 will go down in both space and meteorological history for introducing the world to these first two experimental meteorological satellites.

It is fitting, near the first anniversary of the Tiros I launch, to evaluate the results of the Tiros experiments and to interpret their immediate and future significance. I shall try to be brief and to concentrate on the more significant features.

Both Tiros satellites had essentially the same configuration. Tiros I weighed 270 lb, Tiros II 280 lb. Each was launched into a nearly circular orbit slightly in excess of 400 mi. They were both shaped like a hat box 19 in. high and 42 in. across. The top and sides were covered with solar cells, the primary source of power. The main sensors were two TV camera systems for photographing the earth's cloud cover. When viewing the earth vertically, one camera took pictures covering about 700 mi on a side, while the other took more detailed pictures, about 70 mi on a side. Tiros II, in addition, had nonscanning and scanning IR equipment to provide measurements of the atmospheric heat budget. The satellites were spin-stabilized, so the TV cameras and the nonscanning radiometers could view the earth only part of each orbit. Tape recorders stored pictures taken over areas distant from the U.S. and then read them out over the two command and data-acquisition stations.

(*Reprinted from* ASTRONAUTICS, *May, 1961*)

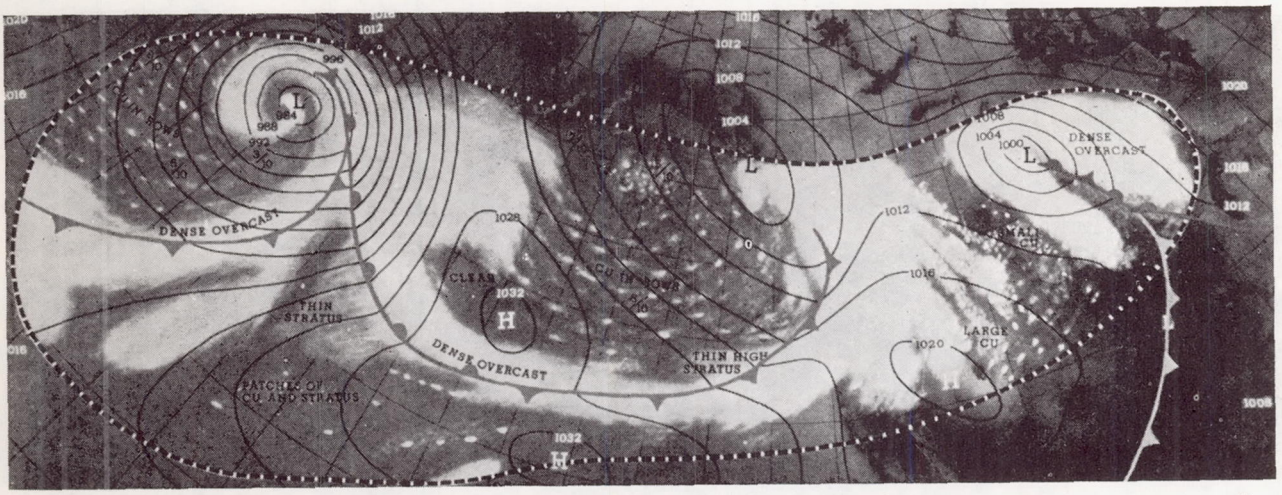

At the left is a mosaic of several Tiros I photographs, and above is a map of the area containing a corresponding meteorological frontal analysis. The clouds from the left figure have been drawn at the right in proper geographic location (after V. J. Oliver in the Oct. 1960 *Weatherwise*). Below is operational weather data—a nephanalysis—done on this mosaic. This analysis was transmitted in facsimile by the meteorological team at a data-acquisition station to the National Meteorological Center of the U.S. Weather Bureau at Suitland, Md. The cloudy areas are clearly depicted, as are the cloud bands themselves. The storm center south of the Aleutian Islands is outlined by the spiraling arrows.

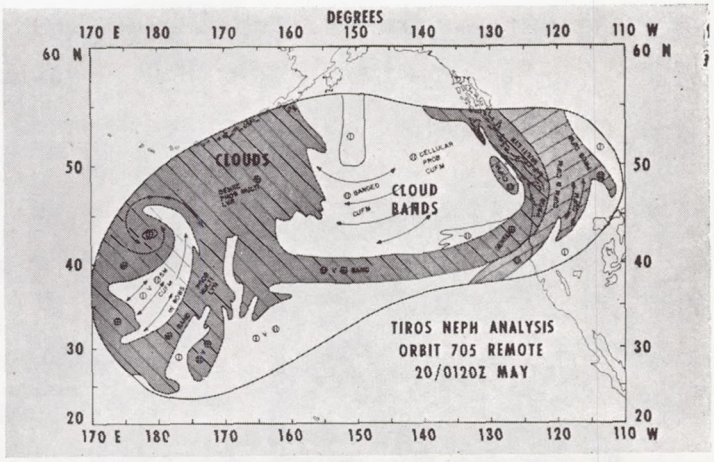

Tiros was in effect a multiphased experiment. Over and above the more general problems and uncertainties underlying launch-vehicle development, launch operations, payload injection, and tracking—there were three basic questions which the Tiros experiments were designed to answer.

1. *Could a satellite system be developed around TV cameras and IR radiation detectors to transmit with satisfactory fidelity the measurements of these sensors to the earth?*

This question can be answered without hesitation with an unqualified YES. In the last analysis, the almost 23,000 pictures acquired by Tiros I and the similar number acquired by Tiros II to date, as well as the considerable volume of IR data, all provide the most convincing testimonial of successful satellite system operation. The brilliance of this performance is only slightly dulled by the fact that the wide-angle camera in Tiros II was somehow defocused during launch. The resulting pictures, although not of the same quality as those from Tiros I, still show clearly the larger cloud and land areas, and lack only detail.

Success by Interdependence

This remarkable performance required the successful operation of many interdependent and delicate subsystems, components, and electronics. Most of these are fully described in seven papers in the June 1960 issue of *Astronautics* and in a report on Tiros I to be issued shortly by Goddard Space Flight Center of NASA. In (CONTINUED ON PAGE 63)

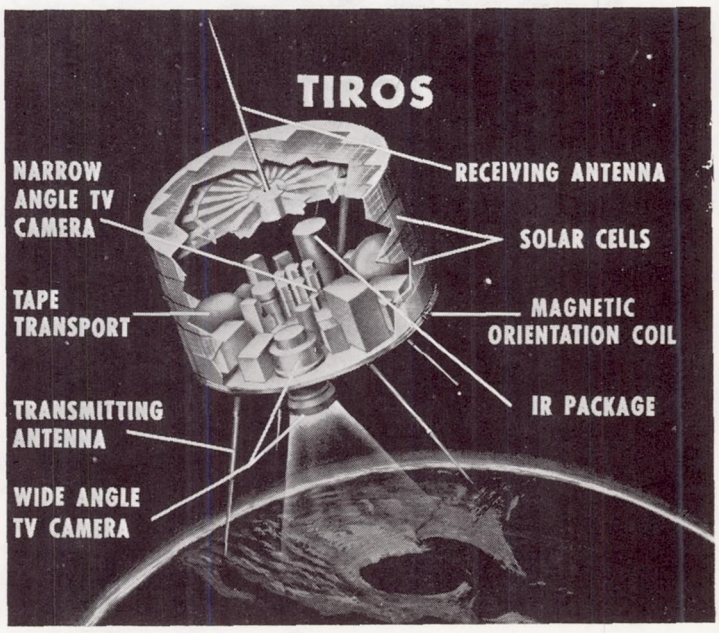

Reprinted from Monthly Weather Review, vol. 88, No. 5, May 1960, pp. 182-186.

TIROS I OBSERVATIONS OF ICE IN THE GULF OF ST. LAWRENCE*

D. Q. WARK AND R. W. POPHAM

U.S. Weather Bureau, Washington, D.C.

[Manuscript received June 7, 1960; revised June 21, 1960]

ABSTRACT

TIROS I pictures of the Gulf of St. Lawrence, taken during the first days after launch, have clearly revealed areas of ice. The ice patterns found in two series of pictures are mapped. Also shown are aircraft observations of ice made a week earlier and a week later. The results indicate that observations from satellites might contribute to ice surveys.

The first series of photographs taken by TIROS I on April 1, 1960, showed the Gulf of St. Lawrence and its environs. H. Wexler noted gray areas in the Gulf and in the St. Lawrence River which appeared to be ice. At his suggestion an investigation of satellite pictures of this area has been conducted to map the ice and to compare the results with observations made from aircraft by the Canadian Meteorological Service. It was hoped that the results of this study might form the basis for further investigation of the feasibility of utilizing pictures taken from satellites for ice surveys over the water areas of the world.

On April 2 a sequence of narrow-angle pictures was obtained which showed most of the Gulf. A third series,

*This work was supported by the National Aeronautics and Space Administration.

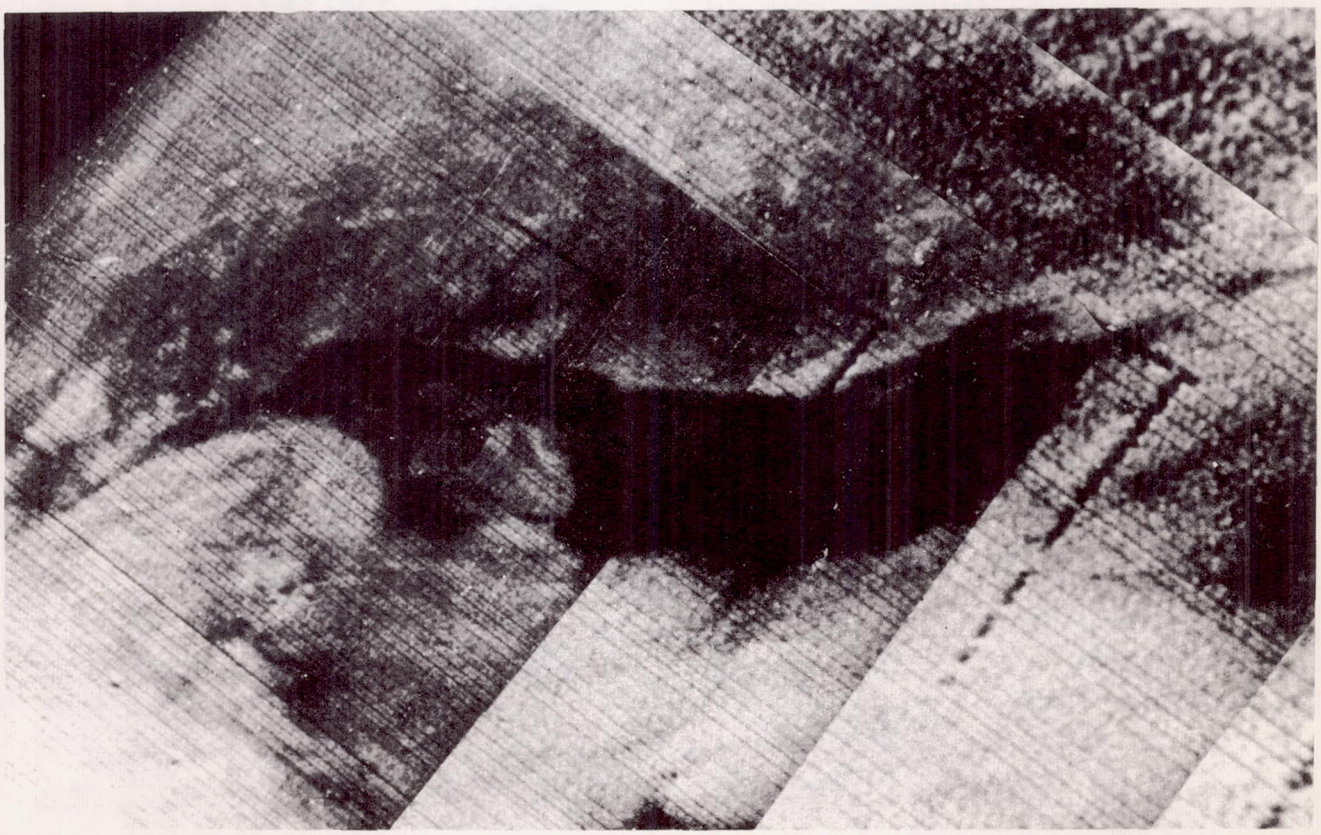

FIGURE 1.—A composite of TIROS I wide-angle photographs taken on April 1, 1960, showing the Gulf of St. Lawrence and environs.

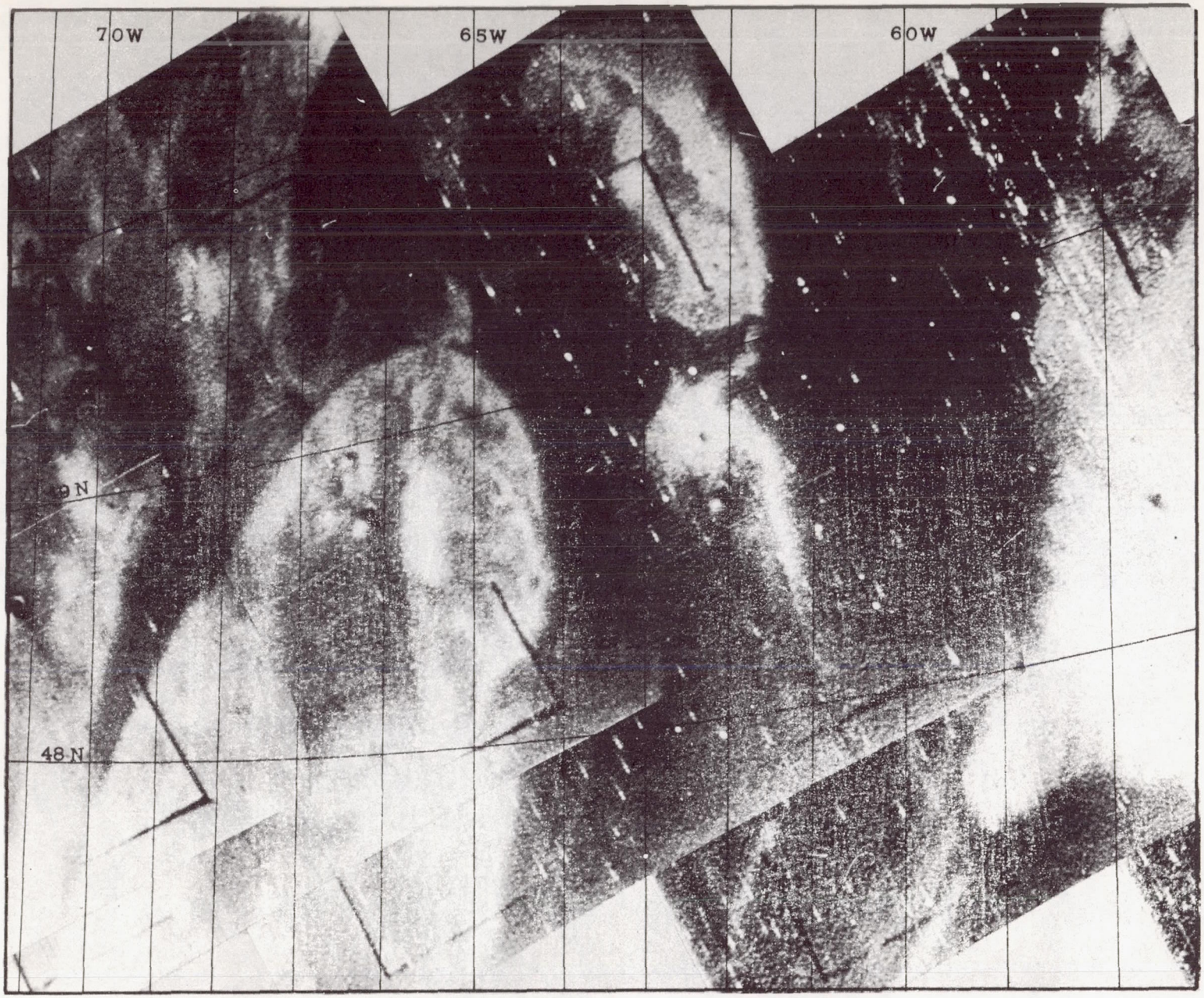

FIGURE 2.—A composite of TIROS I narrow-angle photographs taken on April 2, 1960, showing portions of the Gulf of St. Lawrence and environs.

tion of the satellite to scan the Earth with five sensors having a spatial resolution of about 50 kilometers and designed to measure reflected solar radiation from the Earth and hence the albedo; infrared radiation from the Earth; emission of the atmosphere in the 6.3 micron water vapor band; temperature of the Earth's surface or the cloud tops; low resolution cloud cover in visible light for comparison.

In the second experiment, two sensors, having a resolution of about 800 kilometers, view a portion of the Earth in the center of the area depicted by the wide angle television camera. One sensor responds to the terrestrial radiation emitted by the Earth and atmosphere while the other measures the radiation as well as the reflected and scattered solar radiation.

Observations from these radiation sensors are still under study but a preliminary analysis indicates that much of the data are of excellent quality and should reveal useful information concerning the radiative sources and sinks in the atmosphere, the surface and cloud temperatures and thus the approximate heights of cloud tops. The radiation sensors on Tiros II represent a continuation and extension of the low resolution solar and terrestrial radiation measurements made from the Explorer VII satellite which was launched on October 13, 1959. The data for Explorer VII are still in process of analysis, but some interesting preliminary charts of outgoing radiation from the Earth to space have already been drawn.

These satellite observations of radiation will be used to study weather developments and motions of atmospheric disturbances as related to the radiation balance, and to compute net radiation gains and losses over the Earth—a possible aid to long range weather prediction. It is known that poleward transport of excess energy from the tropics can vary considerably. When winds are blowing mostly from the west or east, the energy flow away from the tropics is inhibited. But when the flow pattern changes from this "high index" condition to meridional or "low index" flow pattern (typically characterized by large quasi-stationary anticyclonic and cyclonic vortices), poleward energy flow is promoted, giving rise to rather prolonged spells of the same general weather type—fair weather, droughts, floods, storms—depending on geographic location with respect to the stalled weather pattern.

Observations of unusual solar radiations, energetic particles, and meteoric dust from space should be readily available from satellites for correlation with unusual weather behavior. World weather charts should make it possible to study contrasts and similarities in northern and southern hemispheric circulation patterns, and to see whether one hemisphere precedes the other in assuming anomalous patterns or whether both react simultaneously to a common external excitation such as unusual solar radiations or meteoric dust. Also, observation of compositions and circulations of atmospheres of other planets by space probes, planetary satellites and landings, will permit comparisons with the terrestrial atmosphere and will assist in the separating out of phenomena common to all planetary atmospheres from those characteristic of a particular planet.

Climatic Changes

Much climatic warming, which has attracted considerable attention in recent years, is confined to rather restricted areas of the Earth, particularly to the north Atlantic subarctic region and the eastern and central United States. Other regions, such as the northwestern United States and parts of central Canada, have cooled appreciably during the past 40 or 50 years. But whether the Earth as a whole is warming or cooling cannot be determined from the present inadequate observation networks. Measurements over periods of a year or longer of the incoming solar radiation and the fraction that is reflected by the atmosphere, clouds, and Earth's surface (Earth albedo), as well as the outgoing infrared radiation from the Earth and the atmosphere should enable us to learn whether the Earth is receiving more energy than it returns to space or vice versa.

The difficulties of detecting changes in energy budget of some of these components by conventional means are illustrated by the following. On the average, each square centimeter of the Earth's surface and the atmospheric column above annually receives from the Sun about 175,000 gram calories. If there were complete radiative balance (as most textbooks in meteorology assume) there should be an equal return of energy to space. But if, averaged over a year, there were a one per cent excess of energy received by the Earth, what would this mean in terms of heating the oceans, melting the glaciers, and warming the atmosphere? If all the extra energy were concentrated in heating the oceans and nothing else, this would raise their average temperature by 0.006 degrees centigrade, which could not be detected by present observing techniques.

Imagine that the excess energy resulting from the imbalance of incoming and outgoing energy streams were concentrated in the atmosphere. This would raise the average atmospheric temperature by seven degrees centigrade—an amount believed to be the difference in world air temperature between that of the last ice age and the present time—a difference readily detectable even by our present observation networks.

Actually the excess (or deficit) of energy would be partitioned among atmosphere, oceans, glaciers and land in some unknown manner. Determination of the overall global energy budget plus that of such individual components as the atmosphere and glaciers (with the aid of greatly expanded observation networks) would permit determination of the energy budget changes of oceans and land masses. Thus the advent of satellites will unveil a new tool by which meteorologists may soon learn

more about the energy exchanges of the planet Earth with Sun and space, and how the exchanges, in turn, may be translated into the climate trends on which man's existence depends so crucially.

Operational Use of Satallite Data

Although significant improvements in meteorological analysis and forecasting will most likely result from a broad research program to which meteorological satellite data will contribute, it has already been possible to utilize cloud data from the Tiros satellites to a limited degree in meteorological operations. While operational use of data is considered to be experimental, it has already indicated the potential of even such simple analyses as cloud maps. They are particularly valuable in filling in the vast distances on weather maps between existing conventional observing stations, particularly over the oceans and other data-sparse areas of the world.

While the radiation data from the Tiros II satellite are not yet being used in meteorological operations, preliminary study of these data indicates they will be operationally useful as soon as rapid processing and analysis techniques are established. For example, the radiation measurements made in the eight to 12 micron water vapor "window" show promise of indicating in a gross sense the world's cloud distribution at night, complementing the existing daytime cloud observations obtained by the vidicon type television cameras. The correlation between the various radiation temperatures and weather patterns indicates that these data will be operationally useful in an empirical sense even though much research is required before the full import of these data in a quantitative, physical sense will be known.

The nature of the orbit and type of stabilization of the Tiros satellites do not permit the observation of the whole globe on a daily basis. The Nimbus satellite now under development by the National Aeronautics and Space Administration is designed to overcome these limitations in observational coverage inherent in the Tiros satellite. The quasi-polar orbit planned for Nimbus will bring the entire Earth into its view twice each day—a great impetus to the operational use of satellite data. By an active stabilization system, one axis of the satellite will always be normal to the Earth's surface.

Operational Meteorological Satellite System

The initial operational system might utilize a single Nimbus-type satellite launched so that on each orbit the satellite will cross the equator at the ascending node (northbound) at local noon and again at the descending node at local midnight. Presently available television cameras could produce cloud pictures over the entire solar illuminated portion of the Earth once each day with a resolution of about 0.8 to 2.4 kilometers. The cloud distribution over the portion of Earth in darkness could be determined by a scanning infrared radiometer.

A second Nimbus satellite might be launched so that one satellite crosses the equator at the ascending node at 9 a.m. local solar time and the second at 3 p.m. Thus each point on the Earth's surface would be viewed at least once every six hours, twice in daylight (except for the winter polar regions) and twice in darkness (except for the summer polar regions).

The complexity and tremendous volume of data expected from even the early experimental Nimbus satellities will require the use of a costly ground station for satellite control and data reception. Only one such station would be required if it were located at a point poleward of about 80 degrees latitude. Initially, two or more ground stations probably will be used, utilizing existing facilities as much as possible. Wide bandwidth communications will be required to speed all of the data to a central analysis facility, such as the National Meteorological Center in Washington, D.C. Meteorologists, assisted by high-speed data processing equipment, would reduce the observational data and prepare analyses for both national and international use. The analyzed satellite observations would be distributed to field forecast centers by teletypewriter and high quality facsimile equipment.

While limited amounts of satellite data could be transmitted to other nations of the world via existing teletypewriter circuits, the global nature of satellite observations indicates the need for more adequate global meteorological communications. Indeed the large volume of data expected from meteorological satellites, when added to the ever increasing number of conventional meteorological observations, sharply emphasizes the urgency of providing greatly improved communications in support of meteorology. Communication satellites now under development offer promise of providing a means for the worldwide dissemination of meteorological data for the benefit of all mankind.

It also appears feasible to measure the vertical distribution of precipitation beneath the satellite by use of radar carried by polar orbiting satellites. Such data would greatly enhance the value of the cloud pictures because of the added knowledge of vertical distribution of cloud layers not obtainable from the cloud pictures alone and the ability to determine something of the intensity of storm systems as indicated by the intensity of precipita-

A Tornado-Producing Cloud Pattern Seen from Tiros I[1]

LINWOOD F. WHITNEY, JR. AND SIGMUND FRITZ

Meteorological Satellite Laboratory, U. S. Weather Bureau

(Manuscript received 11 November 1960)

ABSTRACT

A small, bright, isolated cloud mass was observed by TIROS I over the Central Plains near an area of known tornado activity. The rectification of the TIROS picture is shown; the meteorological situation is presented; and a comparison of the picture content is made with the synoptic events. Evidence is presented indicating that (1) the first intense convective activity was associated with the isolated cloud mass in the picture, (2) the cloud mass was located in an area possessing characteristics found in tornado development situations, and (3) the cloud mass later expanded and spread northeastward spawning hail and tornadoes in central Oklahoma.

Several other significant features were seen in the satellite picture; included among these was a prominent boundary separating a very dark area from a somewhat brighter area. This boundary corresponded to a dewpoint "front" or strong moisture gradient separating very dry air from moister air.

1. Introduction

TIROS I, the first meteorological television satellite [1], was launched 1 April 1960, by the National Aeronautics and Space Administration. From that date through 15 June 1960, the satellite televised picture sequences of many sectors of the earth between the latitudes of about 55N and 55S. A wide range of cloud patterns and scales of patterns have been observed by the satellite's narrow and wide angle cameras from an altitude of about 450 statute miles. The Meteorological Satellite Laboratory of the U. S. Weather Bureau has undertaken case studies of some of those cloud patterns [2]. The following presentation represents one such study.

Several tornadoes were reported in Oklahoma and Kansas during the afternoon of 19 May 1960. On the same afternoon, TIROS I photographed a series of pictures over the central United States. Those pictures were examined for any unusual cloud formations which might be associated with severe local storm activity. One striking and unusual cloud pattern, photographed at 2000 GMT, was immediately discovered (fig. 1). A small, isolated cloud appeared as a very bright square astraddle a faint but sharp, smooth line. Hoecker [3] has pointed out that, in many cases, tornado clouds have, at least on one side, been surrounded by cloudless areas. Since it was known that tornadoes and hailstorms had broken out on a line between Fort Sill and Oklahoma City within two hours following the time of the TIROS picture, it seemed logical to investigate the possibility that the "square" cloud mass represented the incipient stages of a severe weather system.

2. Discussion and rectification of picture

In order to examine the picture in more detail and to compare it with the meteorological analysis, it was necessary that the cloud features be defined as to size and geographical location. To accomplish such a picture rectification, a latitude-longitude grid was prepared by means of the technique described in the Appendix 1 of a forthcoming NASA report [2]. A schematic cloud analysis based on the gridded picture is illustrated in fig. 2.

At picture time it was determined that TIROS I was over extreme southeastern Iowa looking obliquely back along its southwest-to-northeast trajectory. Only those portions of the picture which are discernible and essential to this investigation are shown in the schematic diagram (fig. 2).

[1] This work has been supported by the National Aeronautics and Space Administration.

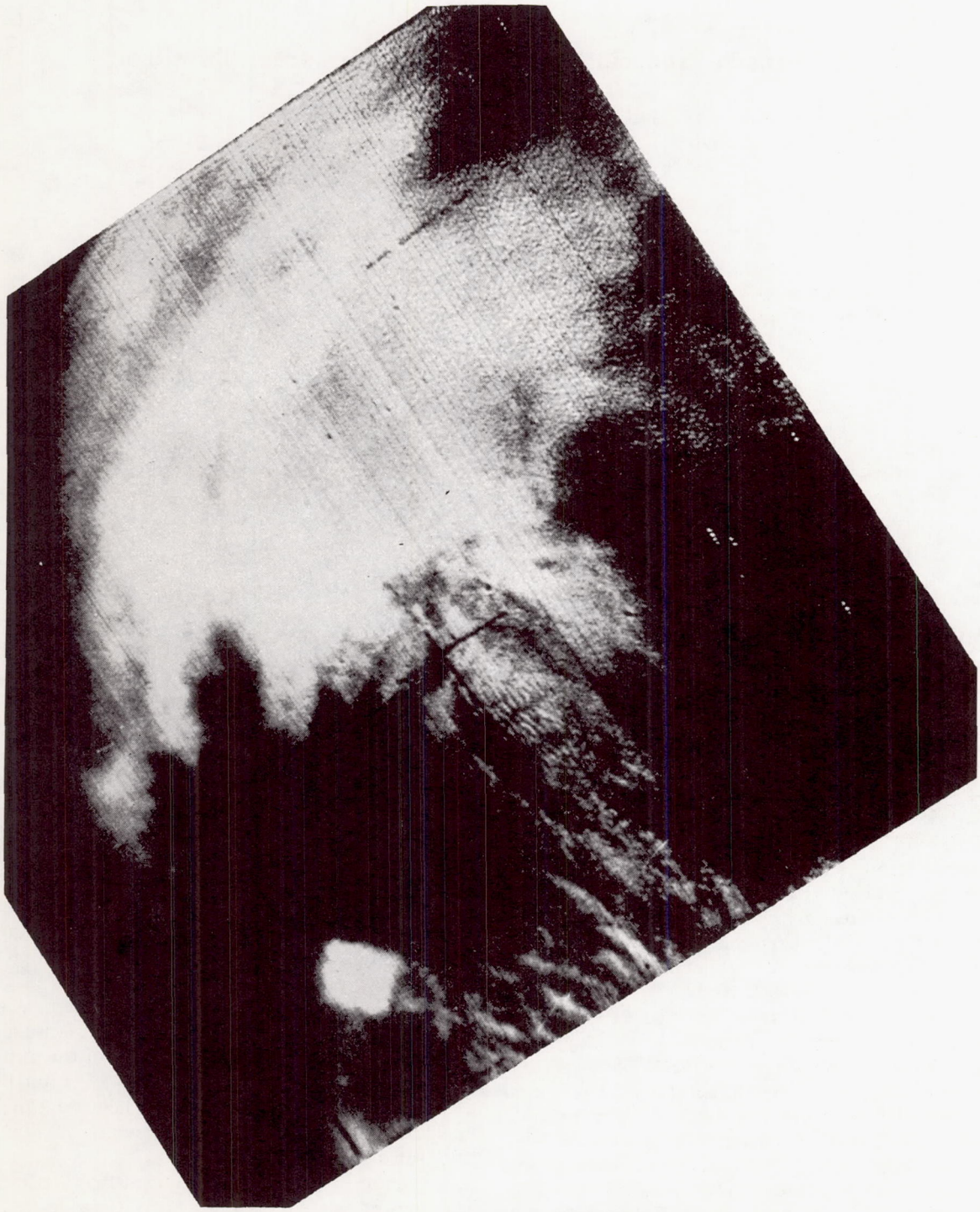

FIG. 1. TIROS I photograph taken at 2000 GMT, 19 May 1960. The satellite was over extreme southeastern Iowa with the TV camera aimed obliquely toward the southwest and overlooking much of the Central and Southern Plains. The picture is oriented with north approximately at the top. The "square" cloud mass is at the bottom center of the picture.

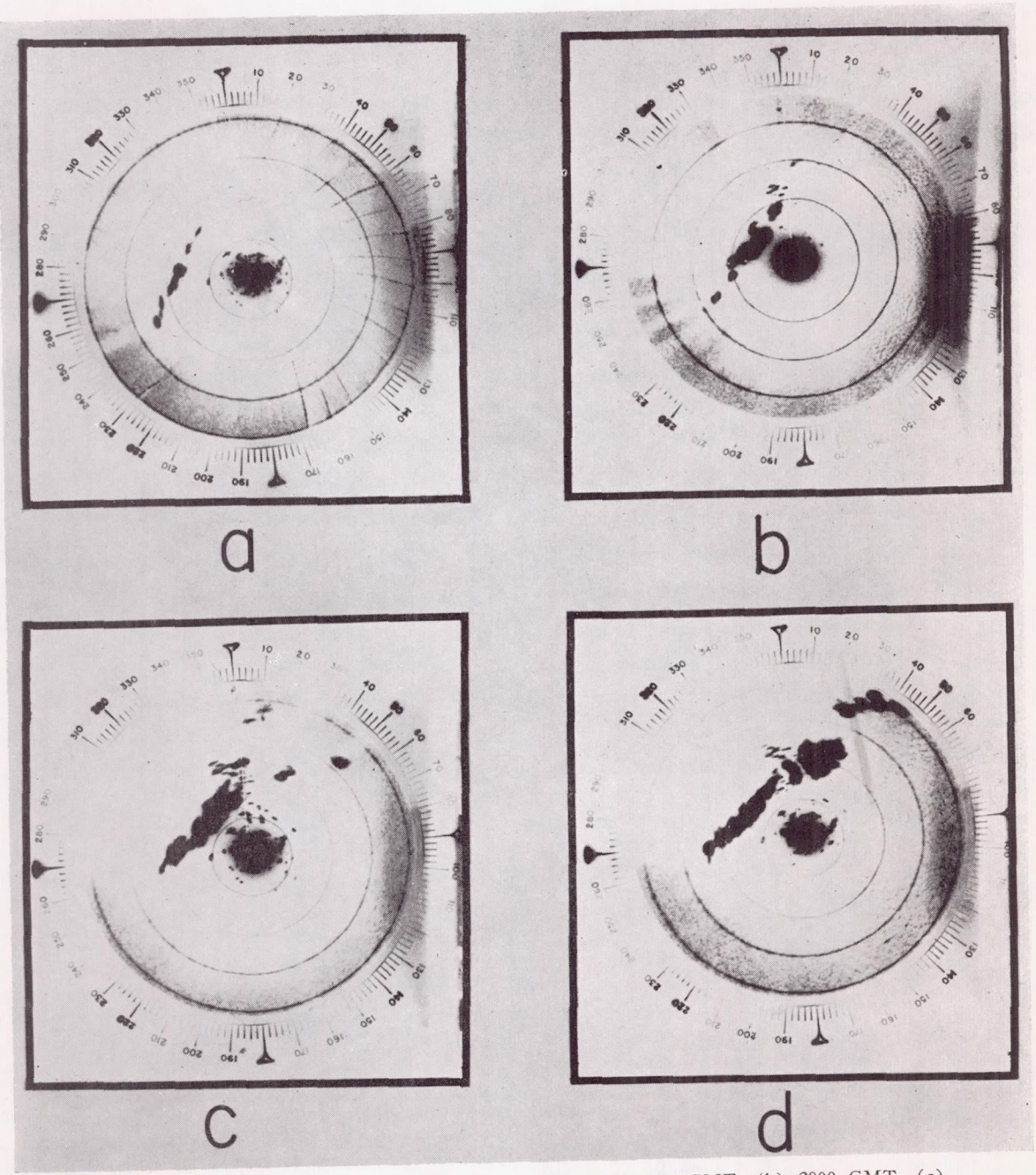

FIG. 7. Wichita Falls radarscope photographs for (a) 1900 GMT, (b) 2000 GMT, (c) 2100 GMT, and (d) 2200 GMT, 19 May 1960. Range marks are at 20 naut. mi. for all four photographs even though the sweep length was altered in fig. (b) giving a slightly smaller scale size.

TABLE 1. Severe local storm reports for southwestern Oklahoma during the period 1800 GMT–2300 GMT 19 May 1960 (taken from the Operational Log of the Severe Local Storms Center at Kansas City and *Storm Data*, Vol. 2, No. 6 published by U. S. Weather Bureau).

Time	Type	Location	Remarks
Unknown	Hail	Hobart	Up to 90 per cent wheat damage southwest of Hobart.
2145 GMT	Hail	Fort Sill	Golf-ball-size hail.
2200 GMT	Two tornadoes	50 mi. SW of Oklahoma City	Both tornadoes on the ground.
2206 GMT	Tornado	235°, 28 mi. from Oklahoma City	Minor tree damage.
2215 GMT	Funnel aloft and hail	18 mi. SSW of Oklahoma City	$\frac{1}{4}$-in. hail covered the ground.
2225 GMT	Tornado	125°, 7 mi. from Oklahoma City	House top lifted; looked like a large dust devil.
2250 GMT	Tornado	70 mi. SSW of Oklahoma City	
2300 GMT	Unconfirmed tornado	202°, 48 mi. from Oklahoma City	From Oklahoma City Radar.

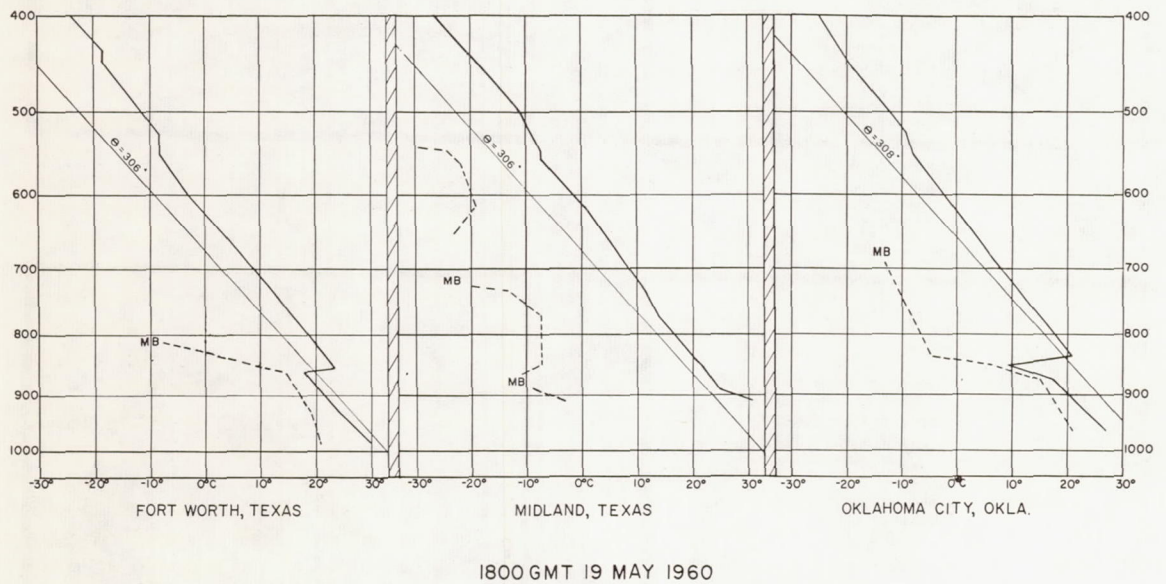

FIG. 8. Soundings for 1800 GMT, 19 May 1960. Solid lines show temperature distribution; dashed lines show dewpoint distribution. MB indicates radiosonde "motorboating" (low humidity).

layer topped by an inversion. Midland, Texas, on the other hand, was in the cT air mass and characteristically was warm, with no inversion in the troposphere, and extremely dry. By comparison, one can see that Midland was potentially warmer below 850 mb than was Fort Worth, while above that level there was little difference.

The moisture gradient or dewpoint "front" is of particular interest here since the convective activity appears to have developed near it. This "front," and moisture gradients in general, have been mentioned or implied in the literature as a factor in tornado development in the Plains. Hanks and Neubrand [5] for instance found that the tornado producing squall line of 2 April 1956 formed along a dewpoint "front." Provided that all their criteria are fulfilled, Fawbush, Miller, and Starrett [6] state that tornadoes should first develop on the windward border of the moisture wedge. Also Tepper [7] in presenting the pressure jump theory, stated "a pressure jump propagating into a region where the atmosphere is dry may not set off any shower activity; yet if that same jump enters into a region where condi-

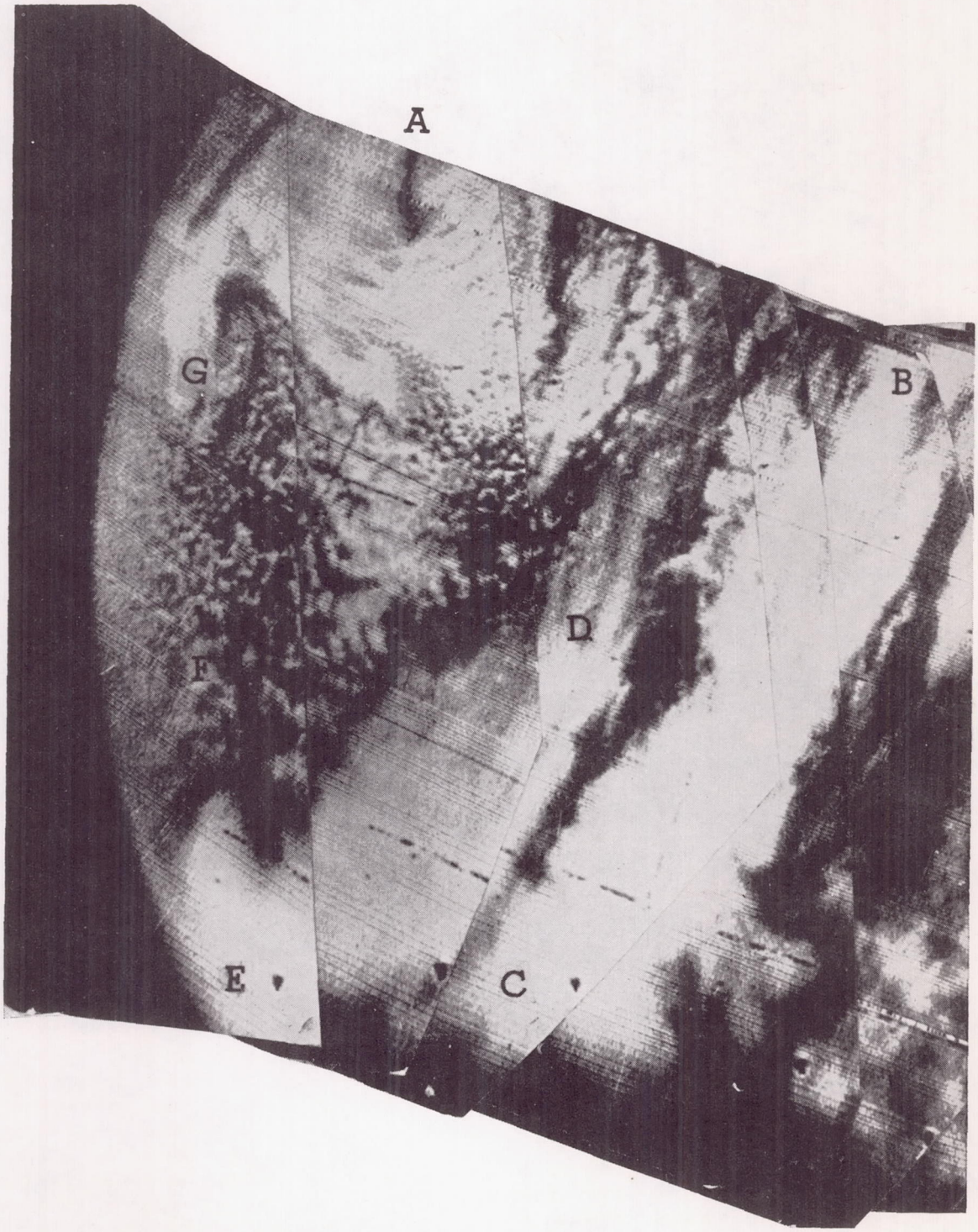

FIG. 2. Composite picture of the Gulf of Alaska storm and adjacent synoptic features. Pictures were taken at approximately 2200GCT 1 April 1960.

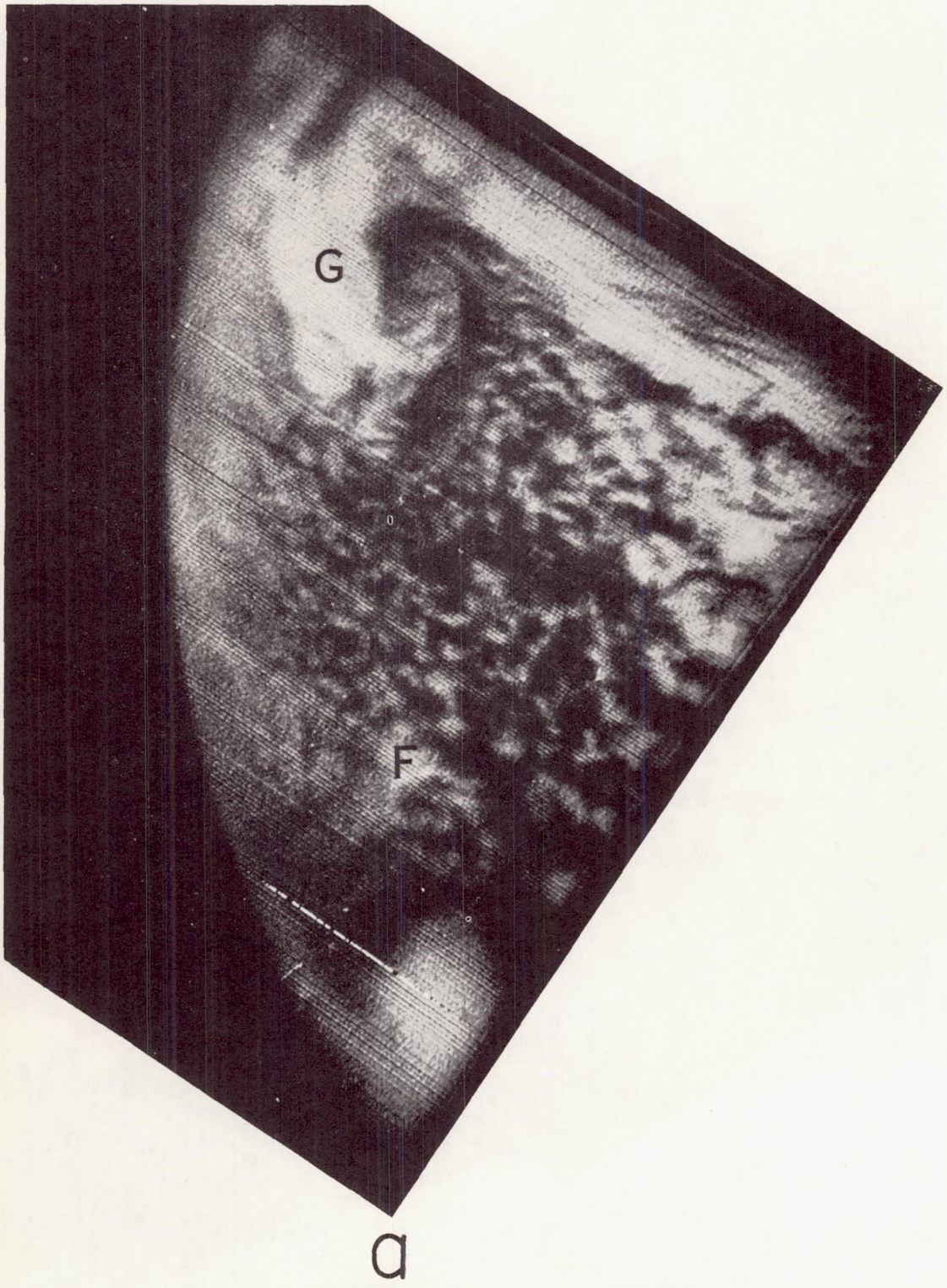

FIG. 3a. Picture of the clouds west and southwest of the main cyclone in the Gulf of Alaska showing probable old cyclonic vortex (G) and cellular cloud structure to the rear of the storm (F).

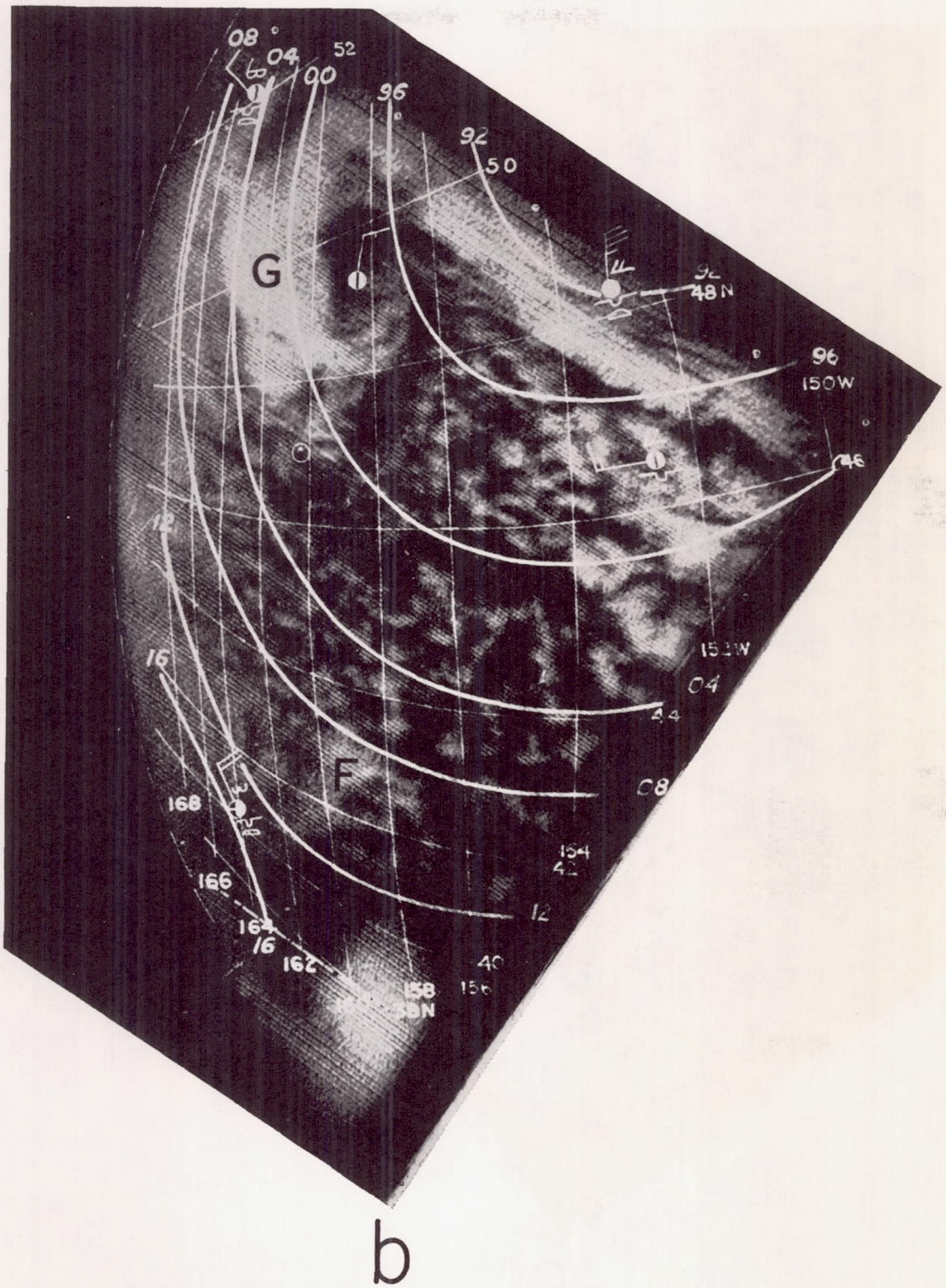

b

FIG. 3b. Same picture as in (a) with superimposed 2-deg latitude-longitude grid; principal point of picture (circled dot); sea-level isobars at 4-mb intervals; and abbreviated surface reports showing sky cover, cloud types, present weather and winds. Solid white circles denote overcast. Surface data and analyses for 0000GCT 2 April 1960.

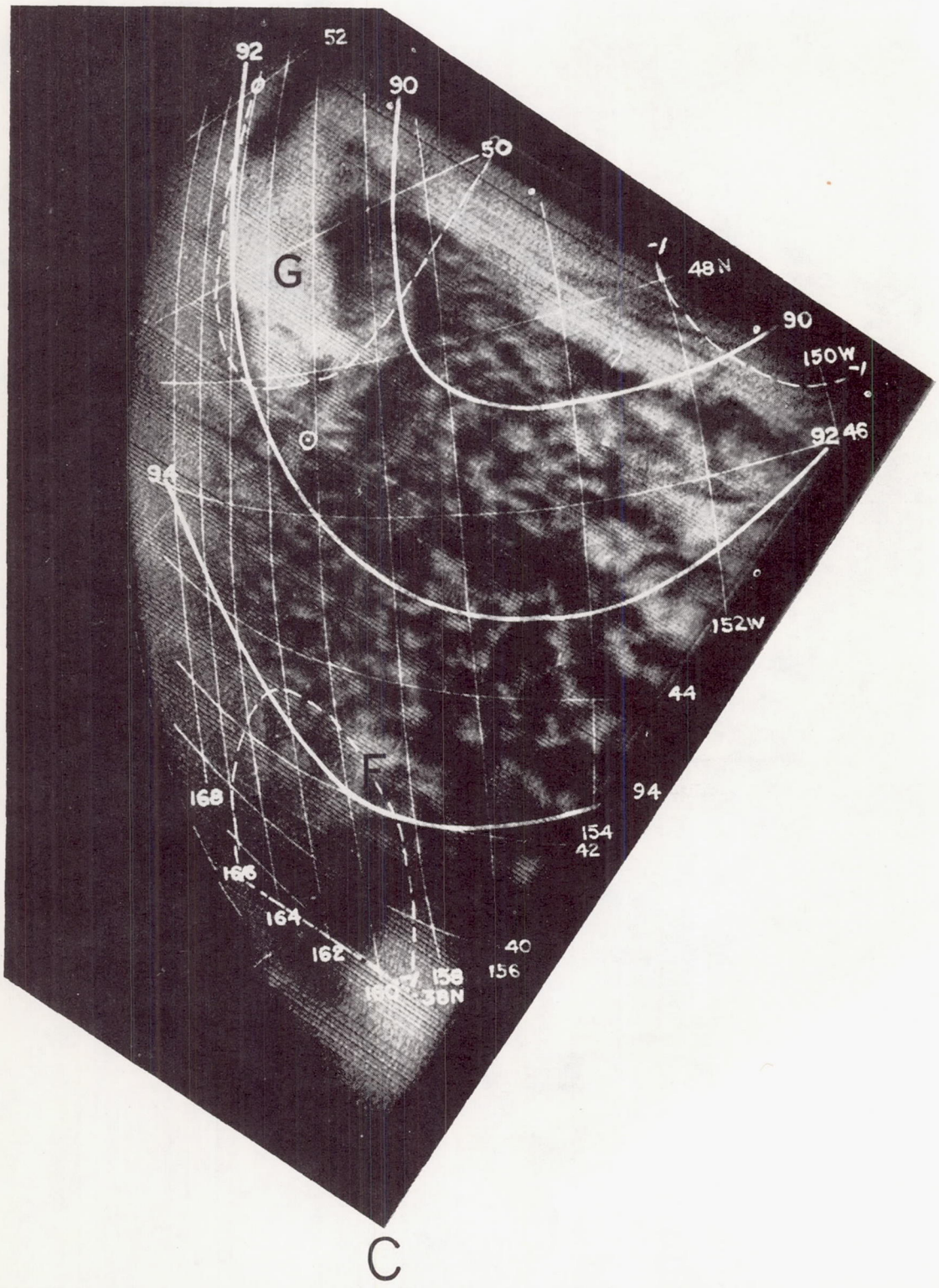

FIG. 3c. Same picture as in (a) with superimposed grid; 700-mb contours at 200-ft intervals; and 600-mb vertical motion (dashed) in cm sec^{-1} as computed by the Joint Numerical Weather Prediction Unit. Superimposed data for 0000GCT 2 April 1960.

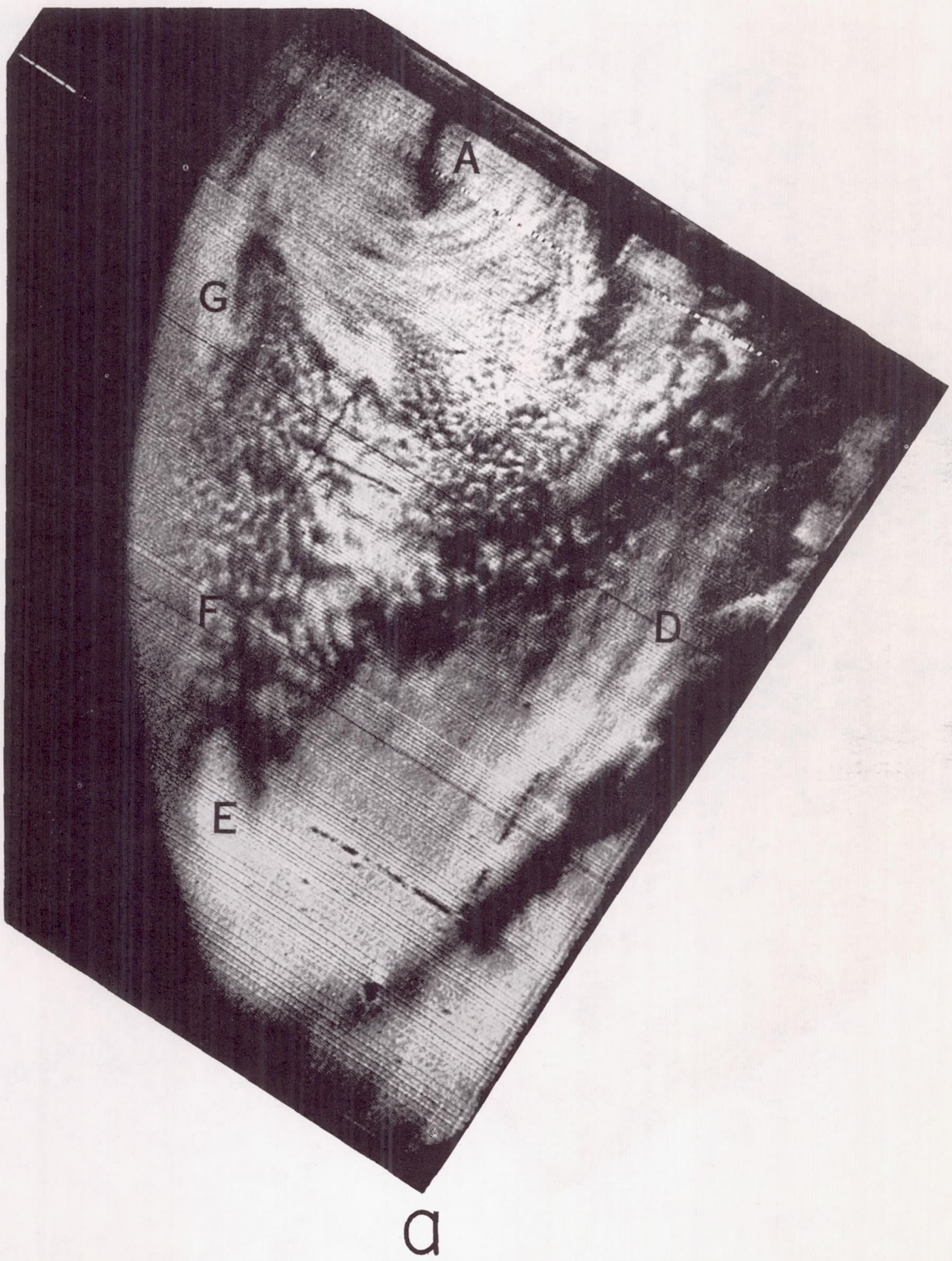

FIG. 4a. Picture of cloudiness south and southwest of the Gulf of Alaska cyclone showing cloud structure near the vortex center (A), over-running cloud system associated with new wave on polar front (DE), cellular cloudiness (F), and probable old cyclonic vortex (G).

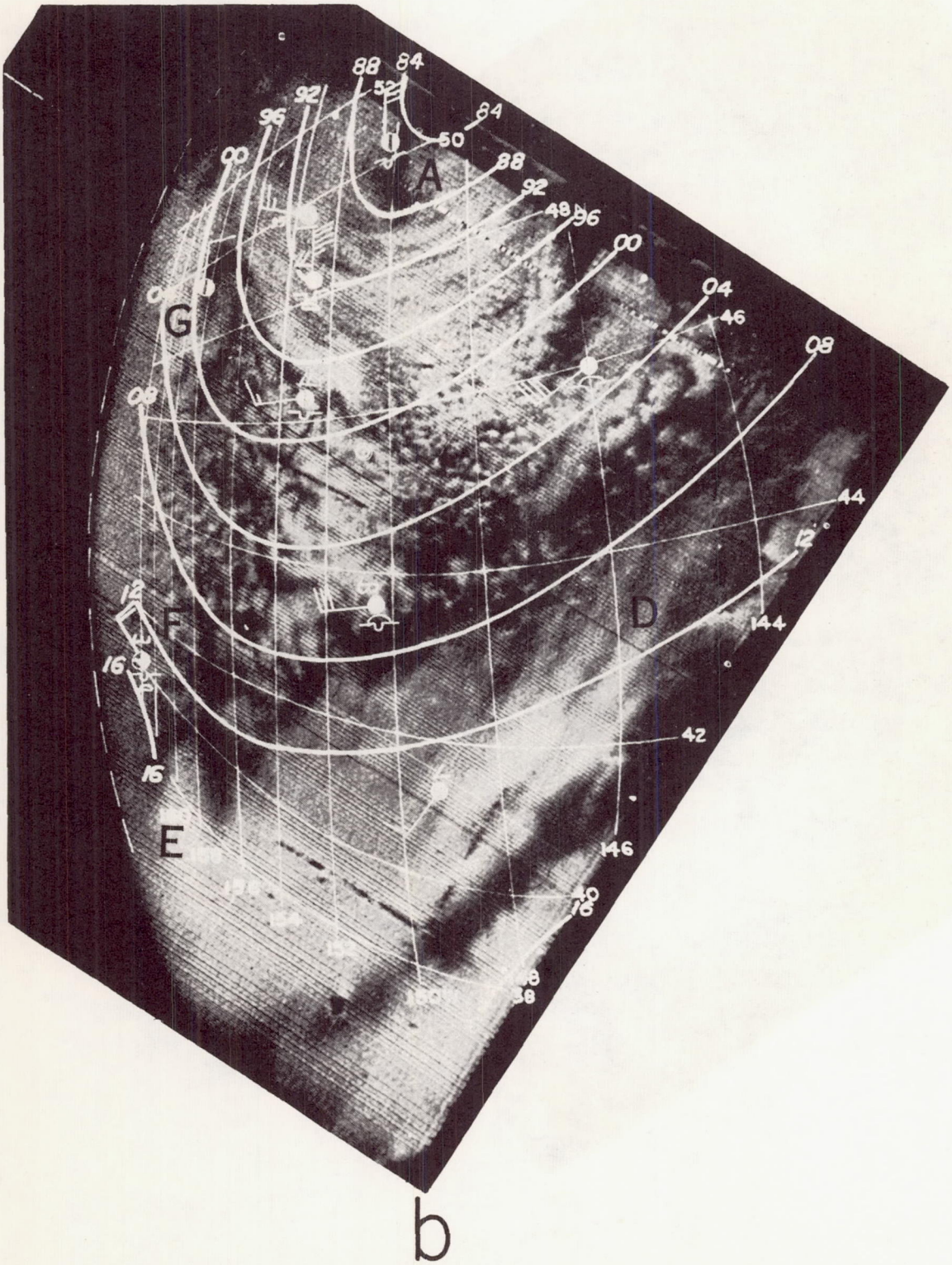

FIG. 4b. Same picture as in (a) with superimposed grid and other items as in fig. 3b.

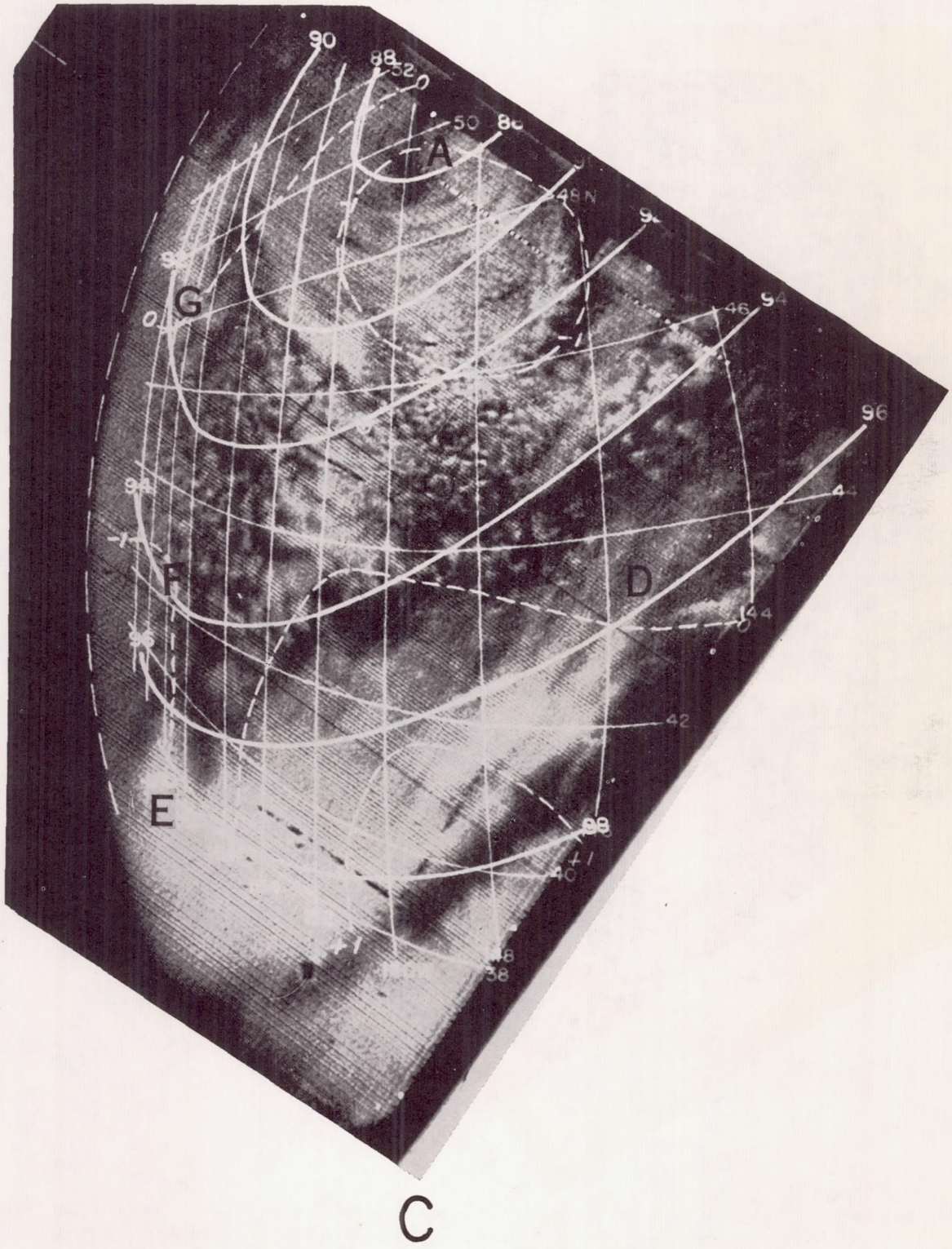

FIG. 4c. Same picture as in (a) with superimposed grid and other items as in fig. 3c.

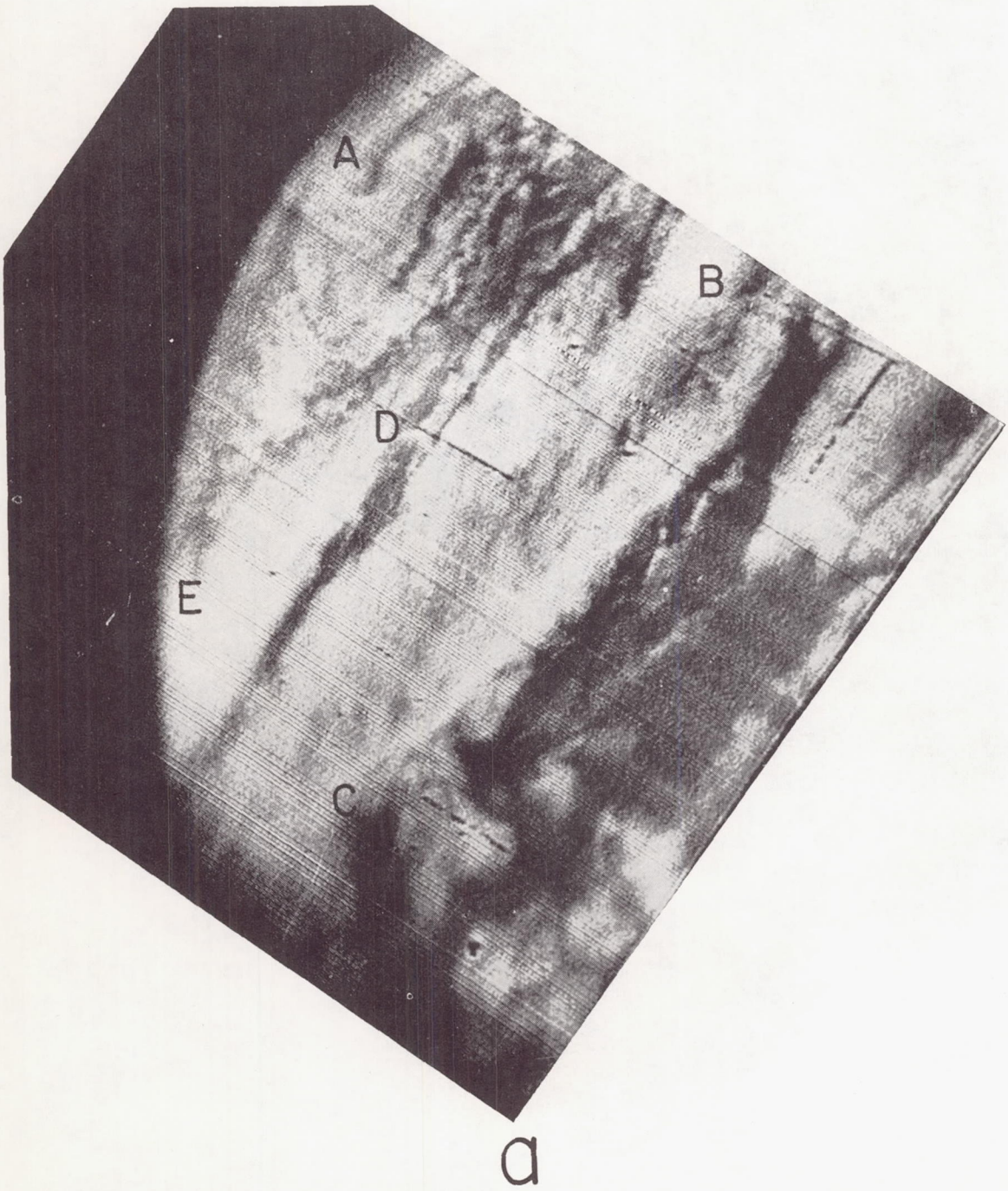

FIG. 5a. Picture of cloudiness south and southeast of the Gulf of Alaska cyclone showing zone of frontal clouds (BC), cloud system associated with new wave on polar front (DE), and clouds around vortex center (A).

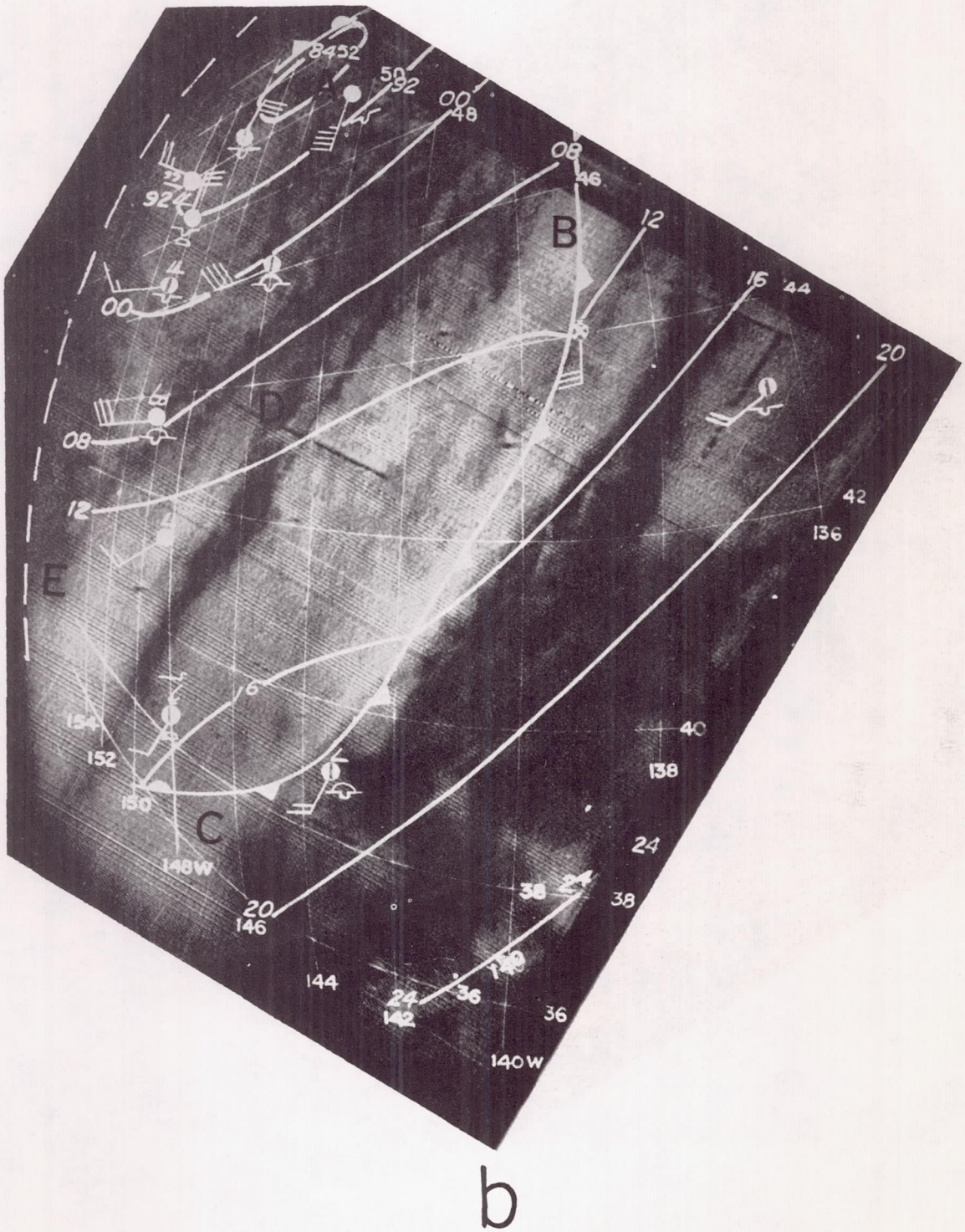

FIG. 5b. Same picture as in (a) with grid and other items as in fig. 3b except isobaric interval is 8 mb for pressures below 1008 mb.

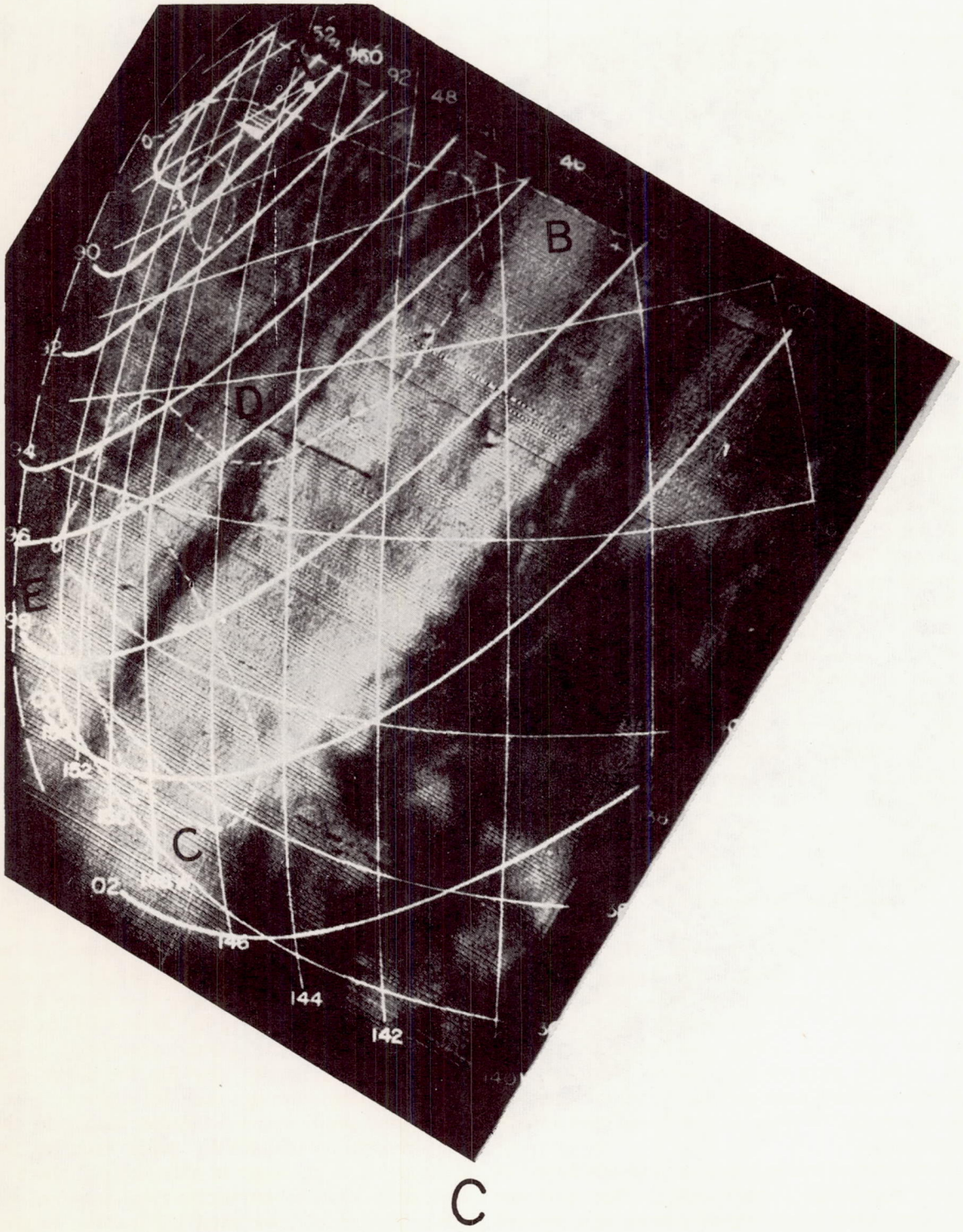

FIG. 5c. Same picture as in (a) with grid and other items as in fig. 3c, except that 700-mb wind at ship P is plotted on this picture.

DEPARTMENT OF COMMERCE
FREDERICK H. MUELLER, Secretary

WEATHER BUREAU
F. W. REICHELDERFER, Chief

MONTHLY WEATHER REVIEW

JAMES E. CASKEY, JR., Editor

Volume 88
Numbers 9-12

SEPTEMBER—DECEMBER 1960

Closed November 15, 1960
Issued December 15, 1960

SATELLITE PICTURES OF A CUT-OFF CYCLONE OVER THE EASTERN PACIFIC*

JAY S. WINSTON

Meteorological Satellite Laboratory, U.S. Weather Bureau, Washington, D.C

[Manuscript received October 10, 1960; revised October 24, 1960]

ABSTRACT

TIROS I photographs taken near the most intense stage of a cut-off cyclone over the eastern Pacific are examined relative to the standard observations and analyses in the area. Broad cloud bands seen in the southwestern portions of the cyclone have been found to be nearly perpendicular to the wind direction at both the surface and aloft, and to consist mainly of cumuliform cloudiness whose tops did not extend more than about 5,000 ft. above the sea surface. Examination of the photographs relative to the conventional frontal analysis and to vertical motions computed by a numerical prediction model suggests that satellite cloud pictures can lead to improvements in the standard analyses of surface and upper-air charts.

1. INTRODUCTION

On two successive days early in April 1960 the experimental meteorological satellite, TIROS I, photographed portions of a cut-off cyclone in the eastern Pacific between Hawaii and California. One of the pictures (fig. 2) taken on the first of these days was so striking in its portrayal of broad, cyclonically curved, cloud bands, with superimposed smaller-scale cloud patterns, that it has already been illustrated several times in the early literature on the TIROS I pictures [1, 2, 3]. In the present paper this picture and several others taken on the same orbital pass and on another orbital pass over the storm about 23 hours later are examined in some detail. The cloud structure portrayed in these pictures is also interpreted in relation to the conventional synoptic observations and analyses, computed vertical motion fields, and the synoptic history of the storm.

2. DESCRIPTION OF PICTURES

Three photographs taken with the wide-angle camera on the first of the two days, April 4, 1960, at intervals of one minute starting at about 2250 GMT, are shown chronologically in figures 1–3. Each picture was obtained when the satellite was above the correspondingly numbered point in figure 8d, where isobars and fronts of the sea level analysis for 0000 GMT, April 5 by the National Weather Analysis Center (NAWAC) are shown. As is evident from the arrows in figure 8d between the subsatellite points and the locations of the optical centers (principal points) of the pictures, figures 1–3 give views of the cloudiness in principally the western and southern quadrants of the storm.

The cloudiness illustrated in figure 2 (as well as in figs. 1 and 3) is remarkable for its broad, banded structure with narrow, relatively clear bands in between. The forward edges of these bands are generally quite sharp, whereas the rear edges tend to be diffuse. Note that the cloudiness behind lines AA and BB (figs. 1 and 2) appears to be predominantly of the cumuliform type, much of it with very interesting cellular structure (cf. Krueger and Fritz [4]).

A narrow-angle picture (fig. 4), encompassing the approximately square area outlined in figure 2, and taken 30 sec. after that picture, reveals very interesting details of the cloud structure straddling line BB. Note that the portion of line BB visible in figure 4 is quite clear-cut

*This research has been supported by the National Aeronautics and Space Administration.

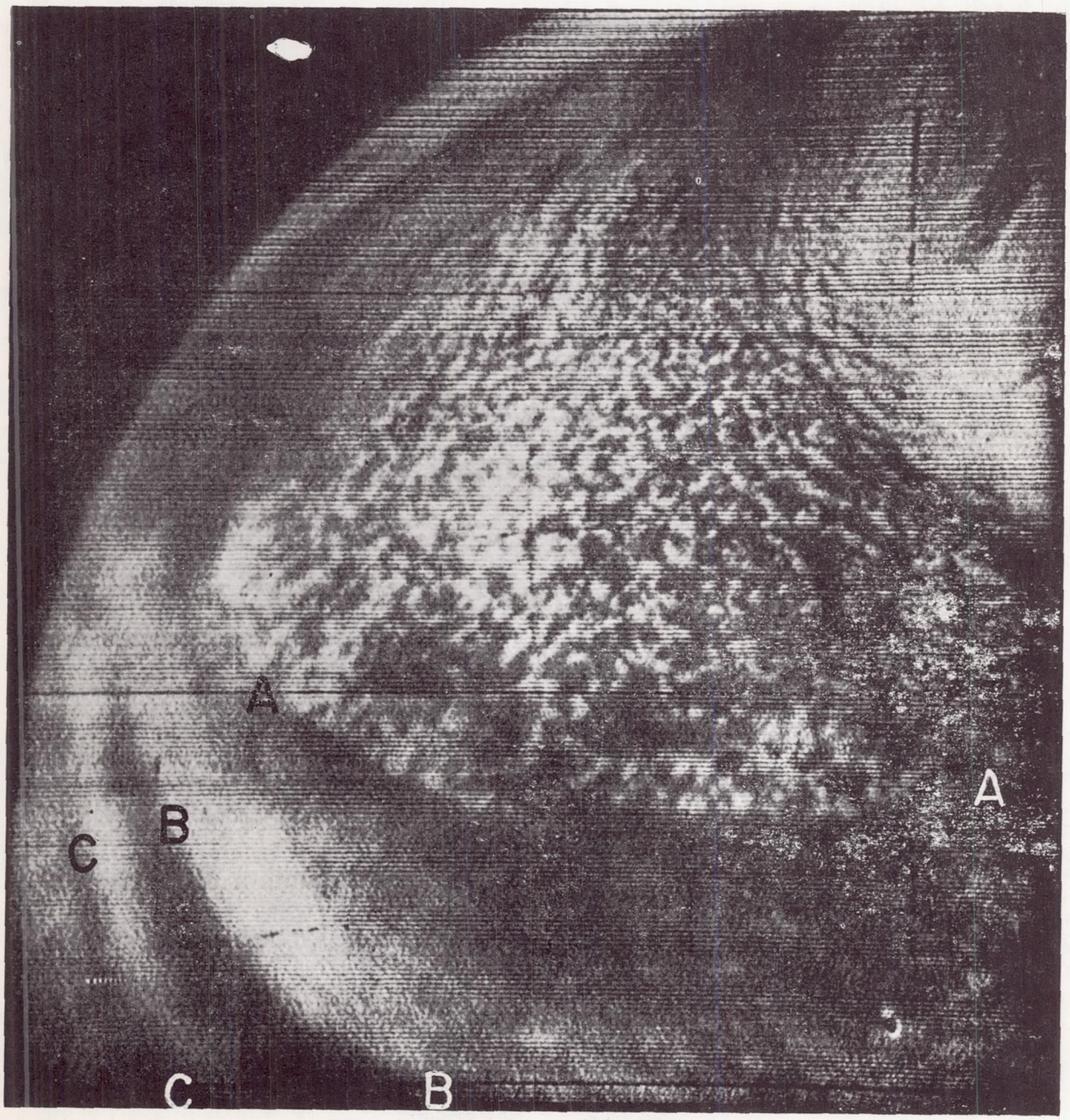

FIGURE 1.—Photograph of cloudiness west and southwest of cut-off cyclone in eastern Pacific showing principally cellular cumuliform cloudiness with sharp edge along line AA. Picture was taken at about 2251 GMT, April 4, 1960 when TIROS I was located above point 1 in figure 8d.

although it does not mark the edge of a solid wall of clouds. (Of course, this could also be determined to some degree from figure 2.) The cumuliform cloud elements which cover much of the area to the rear of this line appear to have a variety of sizes ranging from approximately 1 to 15 n. mi. in diameter. (The area visible in figure 4 is approximately 100 n. mi. on a side.) The cells in the upper right of this picture seem to merge together so that it is difficult to distinguish individual cells within these brighter cloud masses, which have a breadth of 20 n. mi. or more. When the wide-angle view (fig. 2) of this area seen in figure 4 is studied carefully (at least in a photo-print, if not in the printed reproduction available to the reader), some of these elements are barely discernible, but for the most part the clusters appear to be the basic cloud elements and one would on the average have to infer that they were composed of smaller-sized cumuliform cells. The area immediately ahead of line BB in figure 4 appears to be predominantly clear, but small, faint cumuliform cells with diameters of about 1 to 2 n. mi. cover much of the

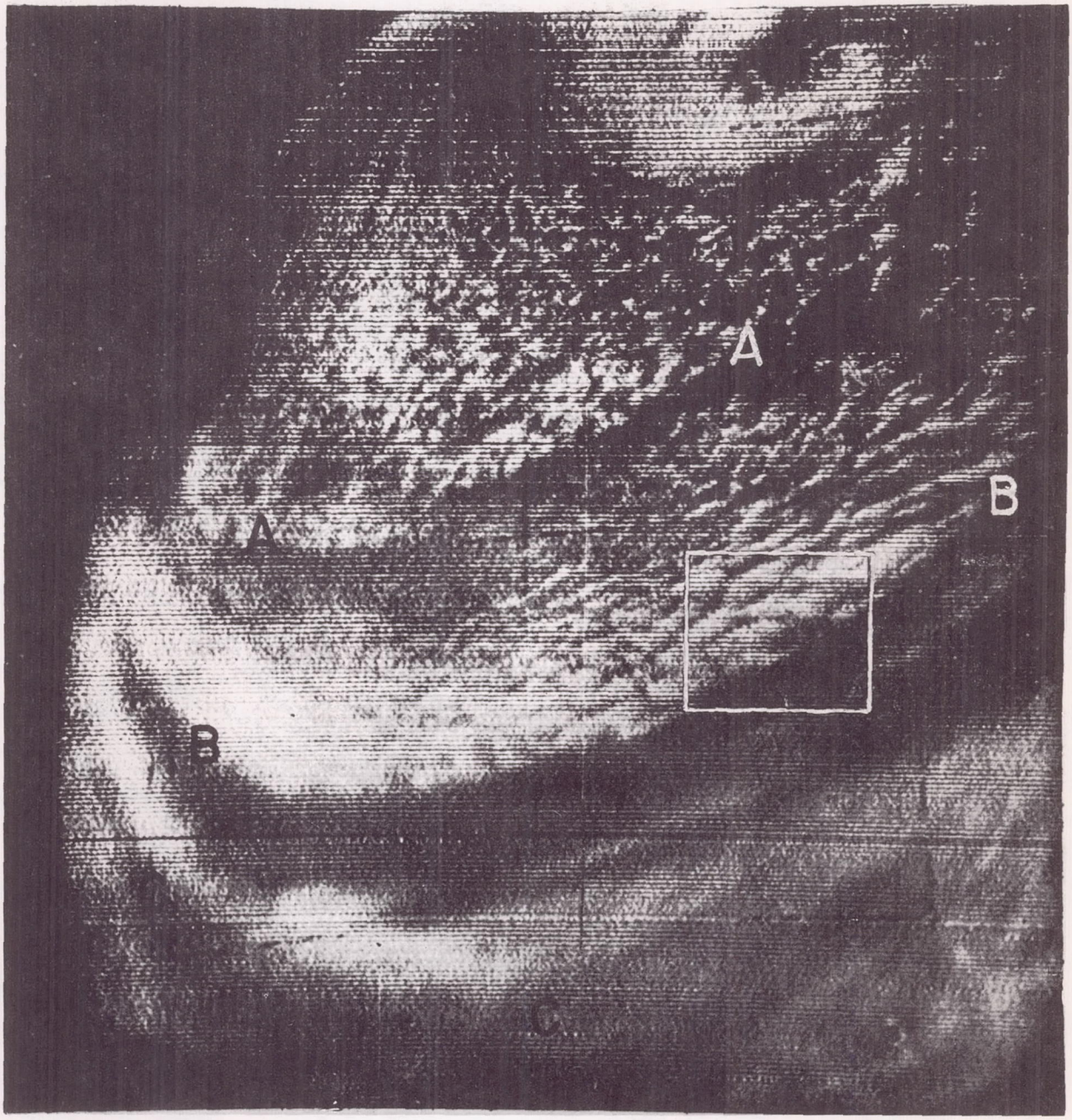

FIGURE 2.—Photograph of cloudiness southwest and south of cut-off cyclone in eastern Pacific showing pronounced lines, AA and BB, at forward edges of cumuliform cloud fields. Picture was taken at about 2252 GMT, April 4, 1960 when TIROS I was located above point 2 in figure 8d. The nearly square area outlined on the right side of the picture indicates the region viewed in a narrow-angle photograph shown in figure 4.

bottom and lower right portions of the picture. This structure is beyond recognition in figure 2, where only a wispy, gray shading is discernible.

The broad band of cloudiness behind line DD toward the upper right of figure 3 appears to have a more stratiform character than the cloudiness behind lines AA and BB. Very likely this represents the altostratus or cirrostratus tops of a cloud system rather extensive both horizontally and vertically. Toward the lower left the cloudiness in this band becomes more broken, and farther on a broad area of little cloudiness is found ahead of the relatively diffuse line designated as CC. The forward edge of the clouds along line DD is very sharp except where it is almost lost in some electronic "noise" toward the bottom of the picture. The line seems to have a more wavy character than lines AA and BB. This is portrayed in more detail in the narrow-angle picture (fig. 5) which gives a view 30 sec. later of the approxi-

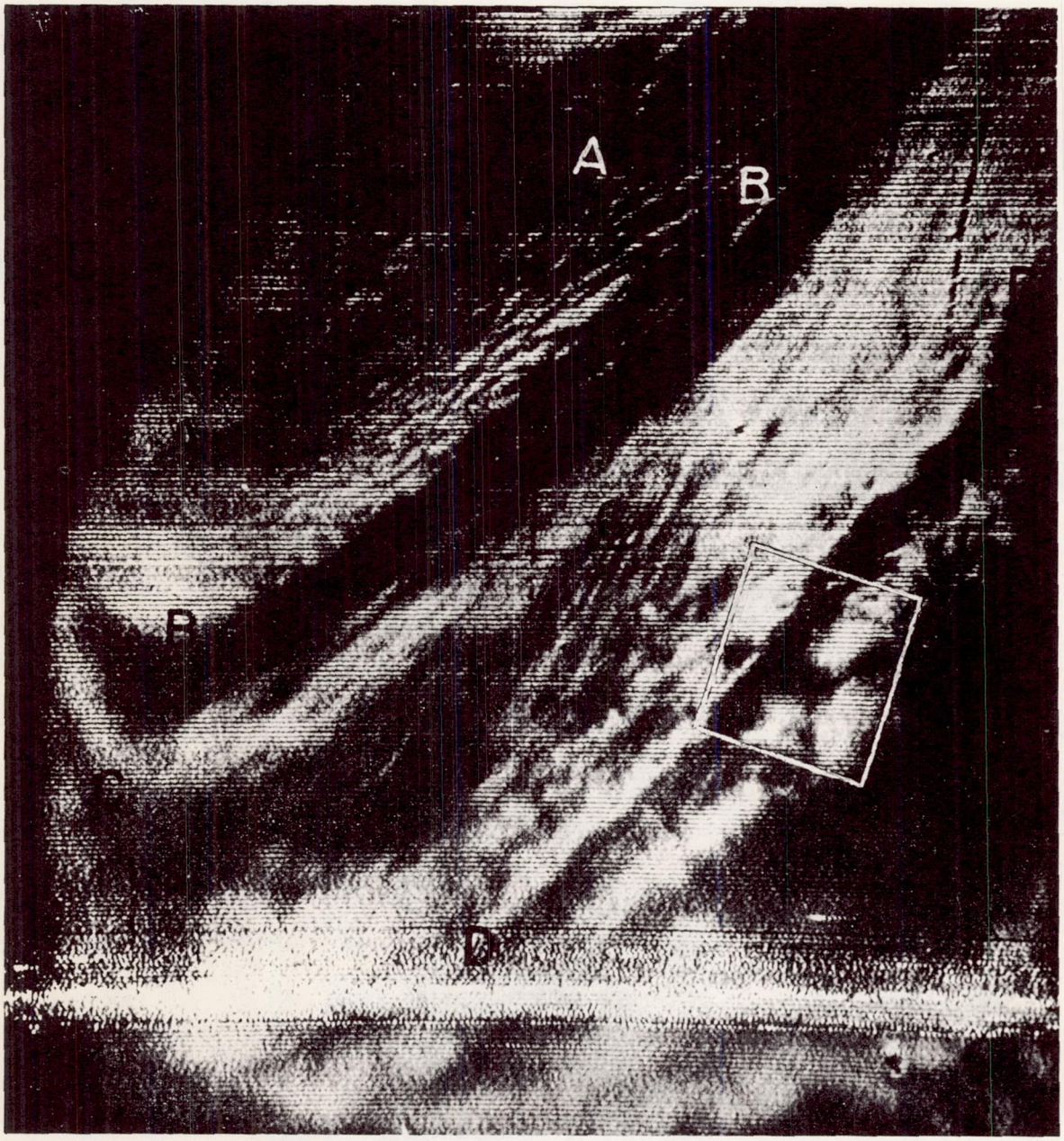

FIGURE 3.—Photograph of cloudiness southeast through southwest of cut-off cyclone in eastern Pacific showing frontal cloudiness with sharp forward edge along line DD. Other pronounced lines along forward edges of clouds are the two seen more prominently in figures 1 and 2 (AA and BB) and the one along CC. Picture was taken at about 2253 GMT, April 4, 1960 when TIROS I was located above point 3 in figure 8d. The nearly square area outlined on the lower right side of the picture indicates the region viewed in a narrow-angle photograph shown in figure 5.

mately square area outlined in figure 3. This shows not only the larger-scale meanderings which can be perceived in figure 3, but also detailed scalloped cloud edges which convey the impression of a wall of cumuliform clouds typical of the leading edge of a pronounced cold front or squall line. Individual cellular elements are not distinguishable along this cloud line (as they are in fig. 4), which leads one to suspect that whatever cumulus clouds were present along this line were surmounted by a shield of middle or thick upper clouds. The other clouds visible in figure 5, to the right of the section of line DD just discussed, have outlines which are much more amorphous and are therefore suggestive of thick cirrostratus or altostratus cloud sheets.

Two wide-angle photographs of the storm on the second day, April 5, taken one and a half minutes apart ending at 2200 GMT, are shown in figures 6 and 7. The satellite path, sub-satellite points, principal points of the pictures,

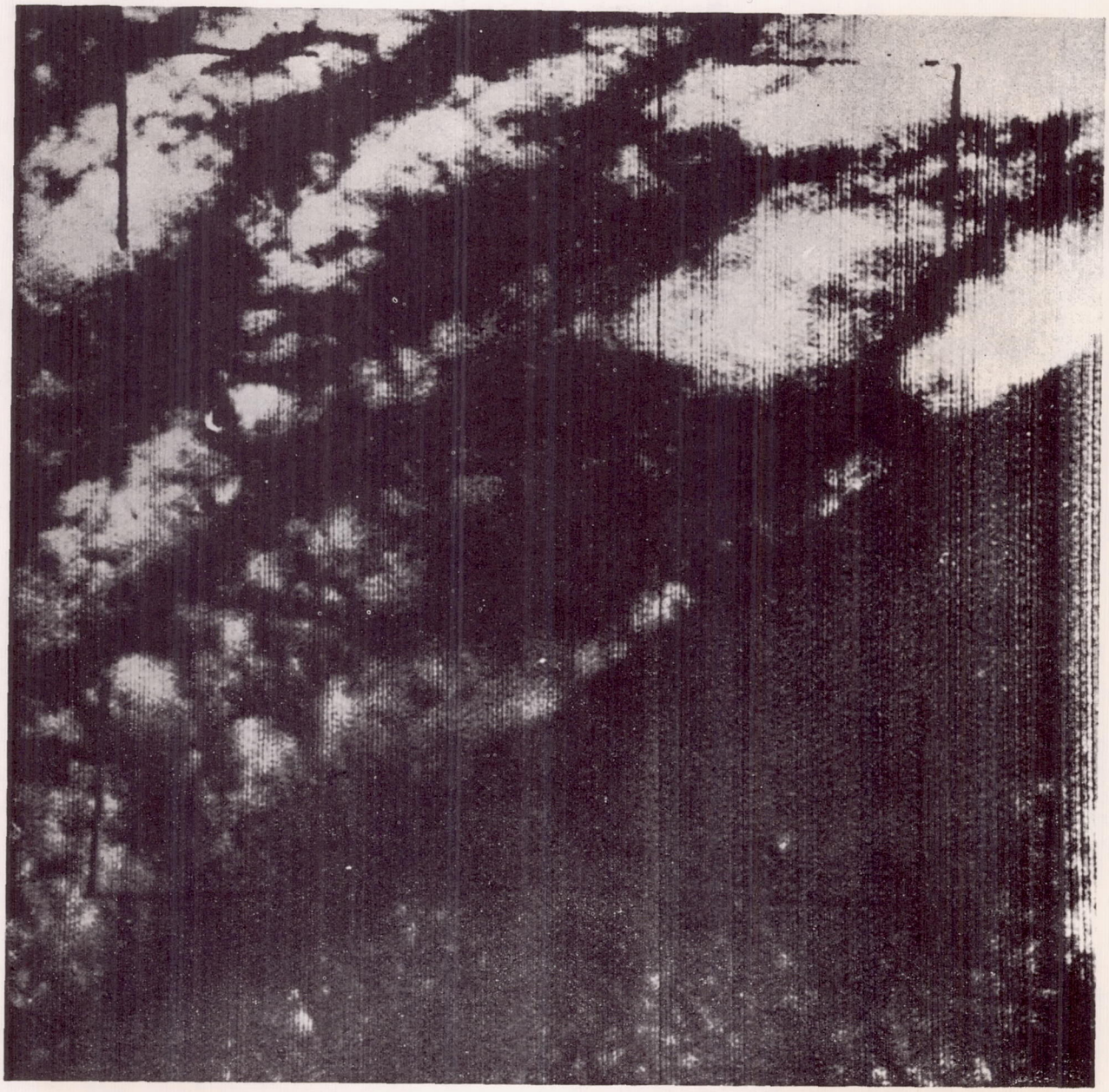

FIGURE 4.—Narrow-angle photograph showing details of cloudiness along a portion of line BB as indicated by the nearly square area outlined in figure 2. Picture was taken 30 sec. after wide-angle photo in figure 2. Several black dots (surrounded by bright white areas) in the middle left and lower right portions of the picture are due to flaws in the vidicon tube of the narrow-angle camera. Also, all pictures from this camera have a spurious darker swath running vertically through much of the middle of the picture.

and the NAWAC sea level chart for 0000 GMT, April 6 are illustrated in figure 8f. The pictures are oriented in approximately the same direction as before and therefore mainly cover the western and southern portions of the cyclone, but there is a better view in figure 7 of the central part of the storm than on the preceding day The broad bands of cloudiness and alternating cloudlessness spiraling into the cyclone center are especially outstanding and resemble strongly the classical cyclonic spial as observed in the laboratory (cf. [5], [6]) and in tropical storms with radar [7]. Although a fair degree of cellular structure is still evident in these two pictures, the areas of cellular cloudiness on the west and south sides of the cyclone center have generally diminished, as compared with the preceding day.

3. SYNOPTIC HISTORY OF THE STORM

The evolution of this major cyclone is illustrated by a series of NAWAC sea level analyses at 12-hr. intervals (fig. 8). On April 3 at 1200 GMT (fig. 8a) a broad cyclonic

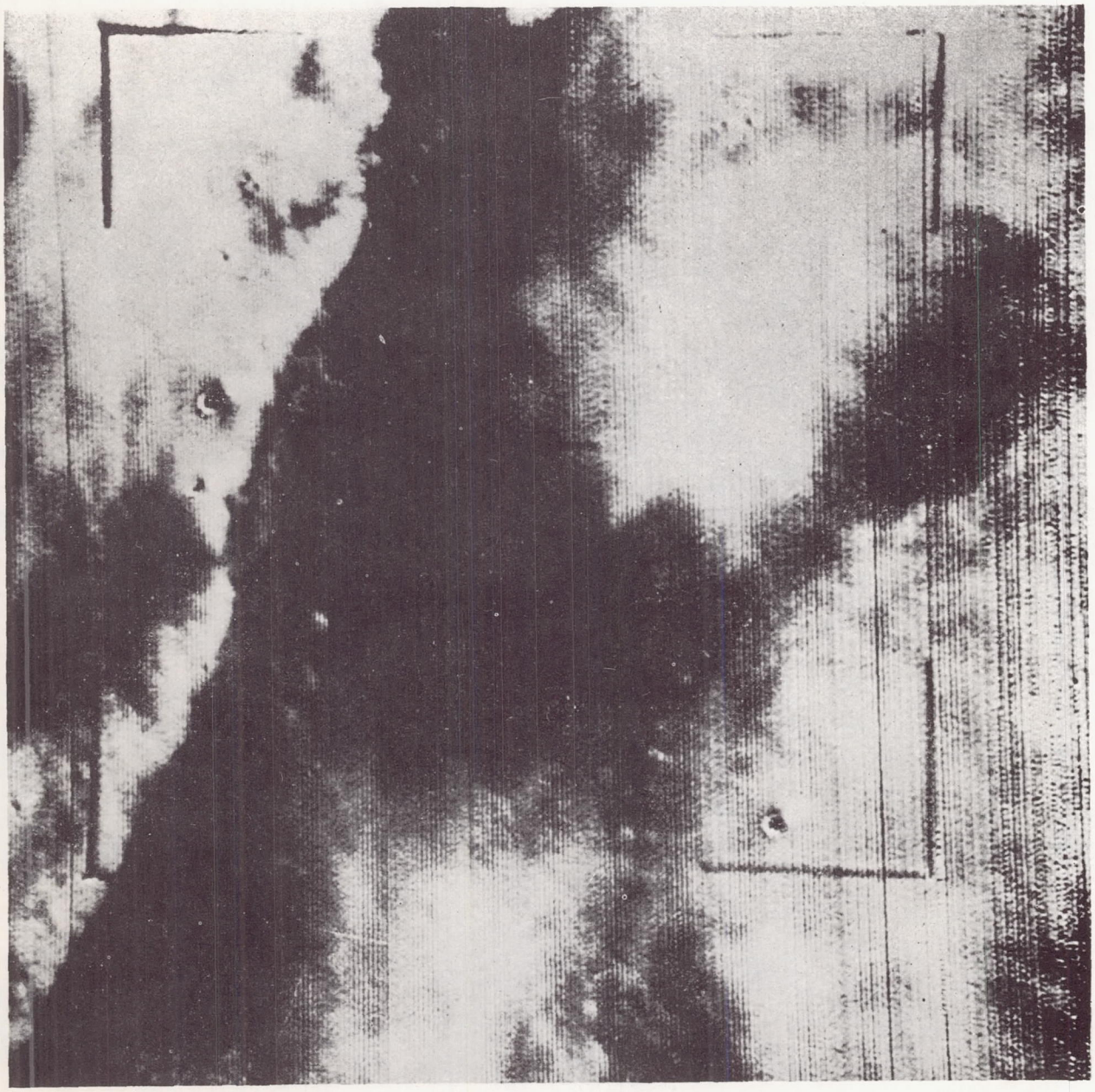

FIGURE 5.—Narrow-angle photograph showing details of cloudiness along a portion of line DD as indicated by the nearly square area outlined in figure 3. Picture was taken 30 sec. after the wide-angle photo in figure 3. (See legend to figure 4 regarding defects in narrow-angle camera.)

circulation existed over the eastern Pacific from the Gulf of Alaska southward toward about latitudes 30°–35°N. The major center of low pressure in this cyclonic complex had just moved northeastward to a position near 48°N., 140°W. in the previous 24 hours. The system with which we are concerned had its origin in the small perturbation located near 39°N., 155°W. In typical fashion this center and the cold front extending to its west were moving generally southeastward along the periphery of the main cyclone center. At 0000 GMT, April 4 (fig. 8b) a new center apparently started forming farther southward along the frontal trough at about 34°N., 150°W. By 1200 GMT, April 4 (fig. 8c) the system was organizing into a closed cyclonic circulation with pressures increasing to the north. Also, a weaker pressure minimum was located to the east along the main polar front near 33°N., 139°W. By 0000 GMT, April 5 (fig. 8d), one hour after the pictures in figures 1–5 were taken, an extensive cyclonic circulation had become established owing to both the deepening of the new cyclone center and the increases in pressures to the north of the

FIGURE 6.—Photograph of cloudiness west and southwest of cut-off cyclone in eastern Pacific on day following views in figures 1–5, showing broad, cyclonically curved band west of clear area closer to storm center. Picture was taken at about 2159 GMT, April 5, 1960 when TIROS I was located above point 6 in figure 8f.

Low. Note that the NAWAC frontal analysis on this map had been simplified in that the secondary cold front was dropped and therefore a front no longer extended into the storm center. Twelve hours later at 1200 GMT, April 5 (fig. 8e) the cyclone reached its lowest central pressure (about 999 mb.) and had about the strongest isobaric gradients and hence probably the strongest surface wind field (as viewed on 6-hourly charts). By 0000 GMT, April 6 (2 hours after the pictures shown in figs. 6 and 7 were taken) the storm had begun to fill and surface winds were weakening considerably (fig. 8f). Thus the two sets of TIROS pictures show portions of the storm about 12 hours prior to and about 12 hours after its most intense stage.

The history of the storm at upper levels is not especially notable except that a closed upper center was analyzed at 700 and 500 mb. as the center deepened. However, the paucity of radiosonde observations in the region left the precise intensity of the upper center somewhat in doubt.

FIGURE 7.—Photograph of cloudiness around center and southeast through southwest of cut-off cyclone in eastern Pacific on day following views in figures 1–5, showing pronounced spiral bands near center and several zones of cumuliform cloudiness well to the south of the center. Picture was taken at about 2200 GMT, April 5, 1960, one and a half minutes after figure 6, when TIROS I was located above point 7 in figure 8f.

4. RELATION OF THE CLOUD PICTURES TO CONVENTIONAL METEOROLOGICAL INFORMATION

Although the TIROS pictures can be compared visually with the standard synoptic weather data and charts once the satellite's location and general orientation are known, it is not until complete latitude-longitude grids are superimposed on the pictures that detailed and moderately accurate comparisons are feasible. Such gridding has been achieved for the pictures in this case by methods described in [8].

The pictures taken at about 2250 GMT, April 4, which have already been presented in figures 1–3, are shown in figures 9–11 with a 2° latitude-longitude grid, surface isobars and fronts from the NAWAC analysis, abbreviated surface synoptic reports, and pilot reports of clouds, all superimposed. The pictures are shown again in figures 12–14 with superimposed grid, 700-mb. contours, radiosonde reports, pilot reports of winds in the mid-troposphere, and vertical motion at 600 mb. as computed by the Joint Numerical Weather Prediction (JNWP) Unit.

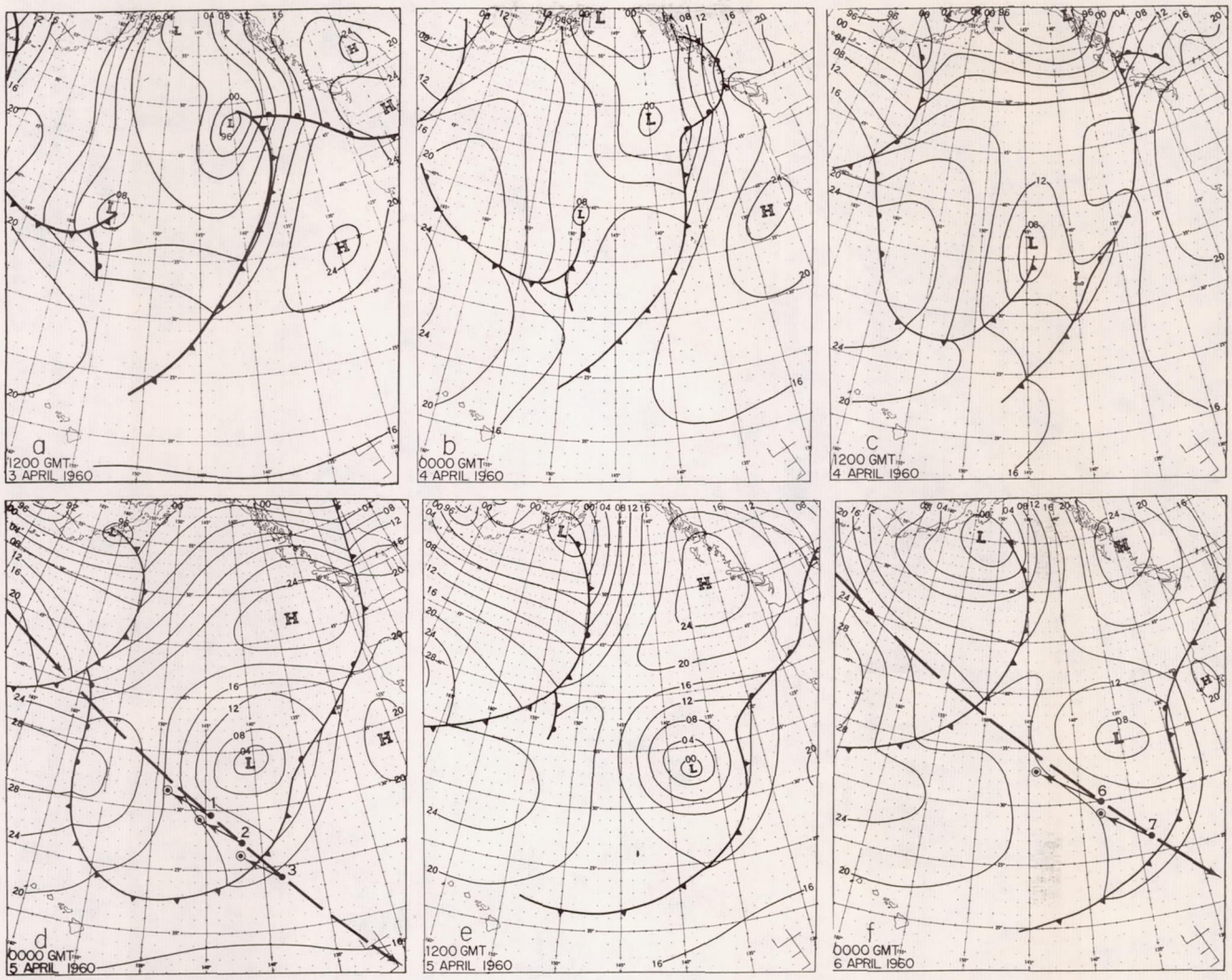

FIGURE 8.—Sequence of NAWAC sea level analyses at 12-hour intervals showing the evolution of cut-off cyclone in eastern Pacific. Paths of TIROS I on two days when pictures were taken of this area are shown in d and f. For wide-angle pictures discussed in this report, sub-satellite points are indicated by dots, principal points of pictures by circled dots, and horizontal orientation of camera by arrows in d and f. Numbers identify locations for pictures shown in figures 1–3, 6, 7.

All data except the pilot reports are for 0000 GMT, April 5.

The most striking feature of figures 9–14 is that most of the major bands are nearly perpendicular to the surface isobars and 700-mb. contours. Only line DD, which is related to the main cold front, and the northeastern end of line BB are closely parallel to the mid-tropospheric flow. It is well known however that there are frequently convergence lines in the westerly and northwesterly flow of cold air to the rear of well-defined cyclones. Such lines appeared frequently in the detailed analyses by members of the Bergen school (*cf.* [9]), some of them actually identified as "bent-back" occlusions or secondary cold fronts. In recent years, particularly on maps of a hemispheric scale, there has been more of a tendency to exclude these more minor systems from the analyses.

In the case under discussion here it appears that lines AA and BB are very likely convergence lines of this type. Close investigation of the position of line BB as compared with the secondary cold front analyzed on preceding NAWAC sea level charts (fig. 8) indicates rather strongly that line BB is indeed associated with this very same surface front. Its rather close fit with previous 6-hourly positions of the front as carried on the NAWAC analyses is illustrated in figure 15. In addition it is interesting that the surface analysis made by the Weather Bureau Forecast Center at San Francisco (not shown), which was consulted after the initial preparation of figure 15, retained the second front and its position coincides closely with that shown for line BB in figure 15.

Inspection of the superimposed 600-mb. vertical motion

569382—60——2

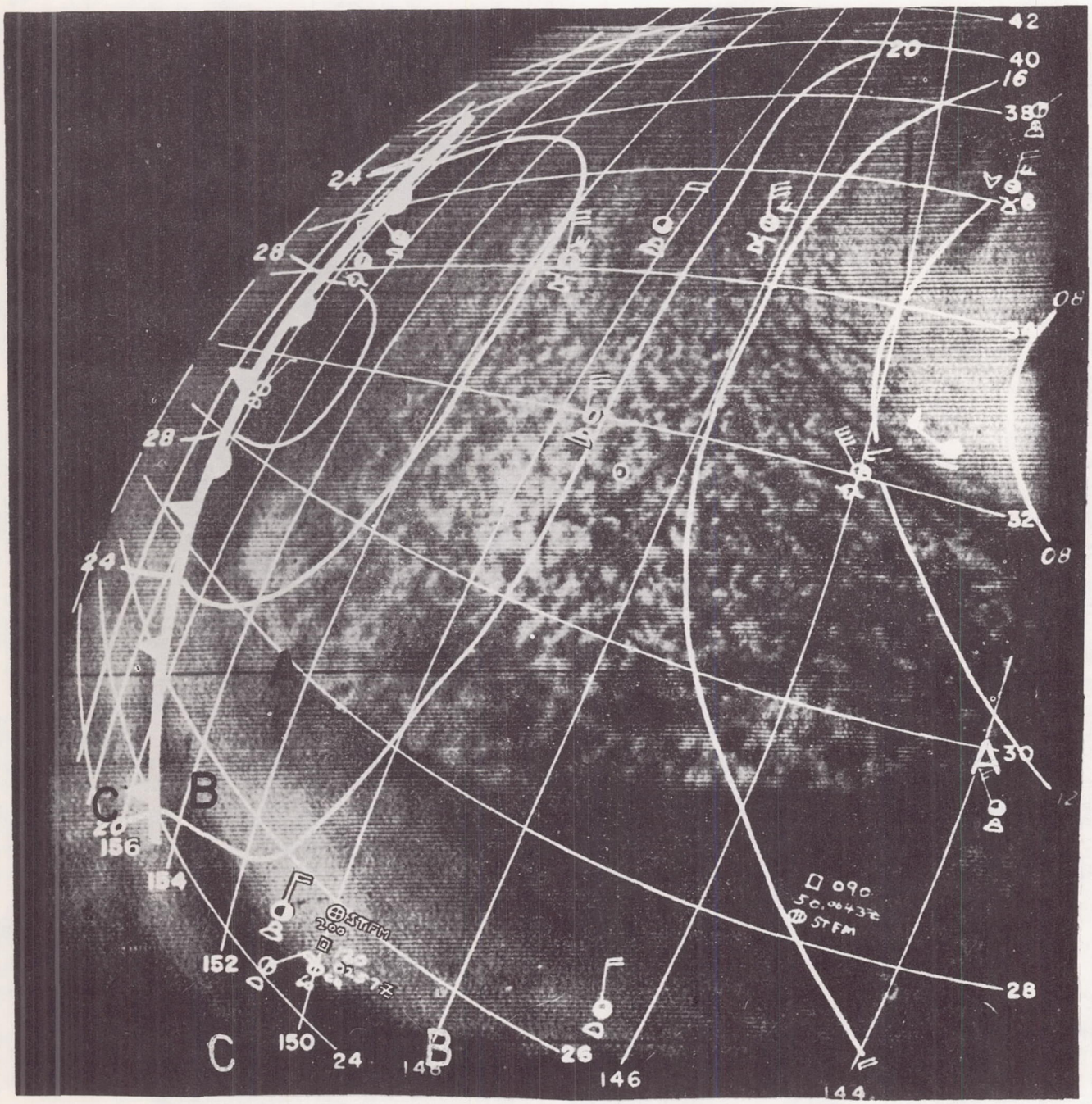

FIGURE 9.—Same picture as in figure 1 with superimposed 2° latitude-longitude grid; principal point of picture (circled dot); sea level fronts and isobars at 4-mb. intervals; abbreviated surface reports showing sky cover, cloud types, present weather, and winds; and pilot reports (squares), for times indicated, of types, amounts, and heights (in hundreds of ft.) of bases and/or tops of clouds. Time of superimposed data, except pilot reports, is 0000 GMT, April 5, 1960.

field, which consists of initial vertical velocities computed from a two-level baroclinic model by the JNWP Unit, shows a pattern of large-scale vertical motion which has been found to be typical of trough systems as exemplified by the 700-mb. contours in figures 12–14 (i.e., downward motion to the rear of the trough and upward motion ahead of the trough). It is notable that the area to the rear of line DD (fig. 14), which appears to be a zone of cloudiness extending upward into the middle and upper troposphere, is associated with the main polar front (fig. 11) where slight upward motion was calculated. However, the southwest-northeast orientation of this cloud band, with mostly clear

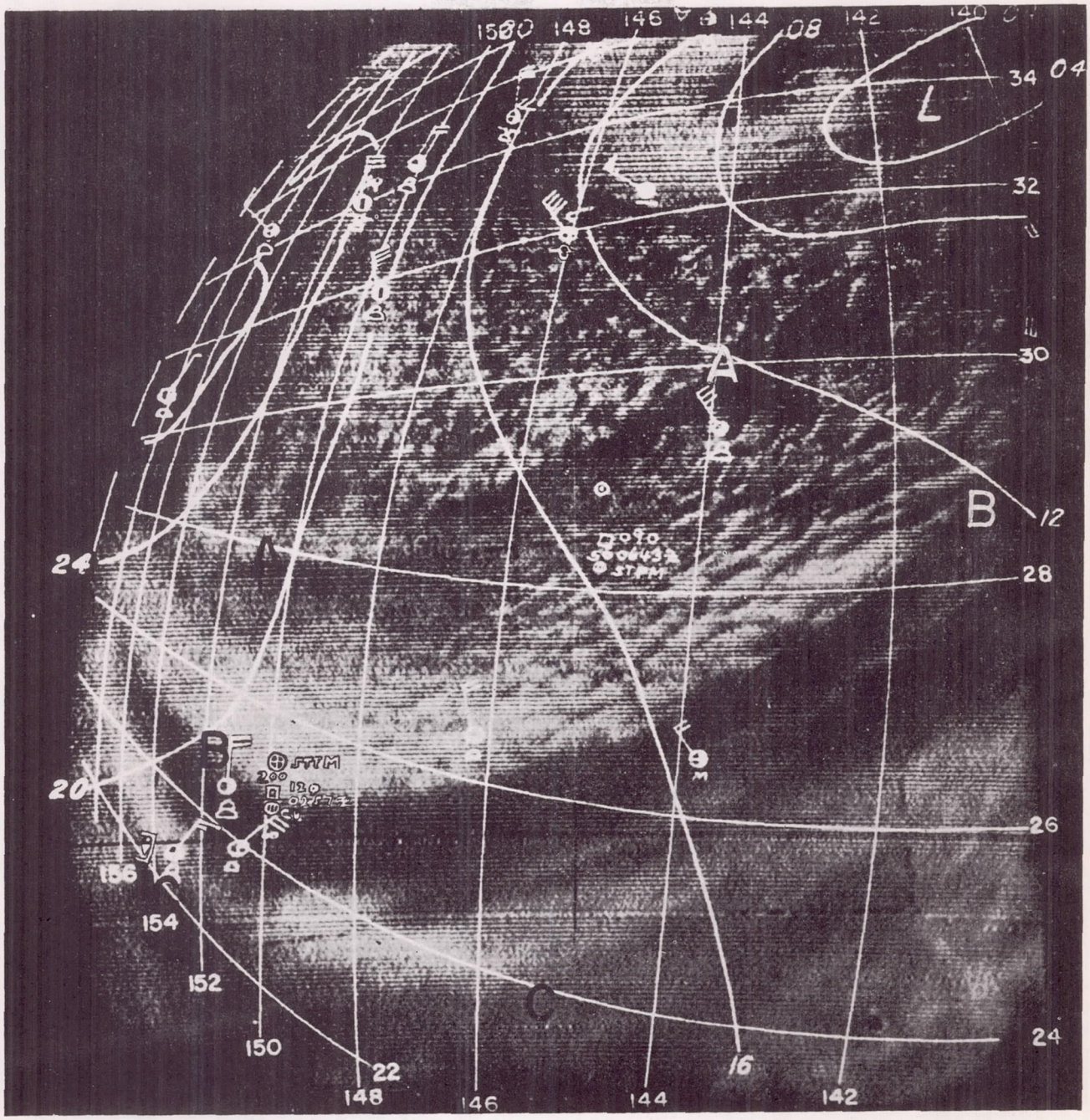

FIGURE 10.—Same picture as in figure 2 with superimposed grid and other items as in figure 9.

skies to the east of DD, suggests that the axis of maximum upward motion might be elongated southwestward to coincide more closely with this band.

Most of the remaining areas of the pictures, including lines AA, BB, CC, and the cloud areas behind them, are located where downward motion was computed. At first glance it seems surprising that such pronounced zones of cloudiness as those occurring along and to the rear of lines AA and BB should be found where the large-scale vertical motion was downward. However, this may indeed be physically correct since most evidence points to the fact that the cloudiness in these areas was of the cumuliform type which was very likely confined to approximately the lower 5000 ft. Certainly most of the clouds reported by ships in these areas were cumulus congestus and stratocumulus. A pilot report at 29.5° N., 145° W., about 8

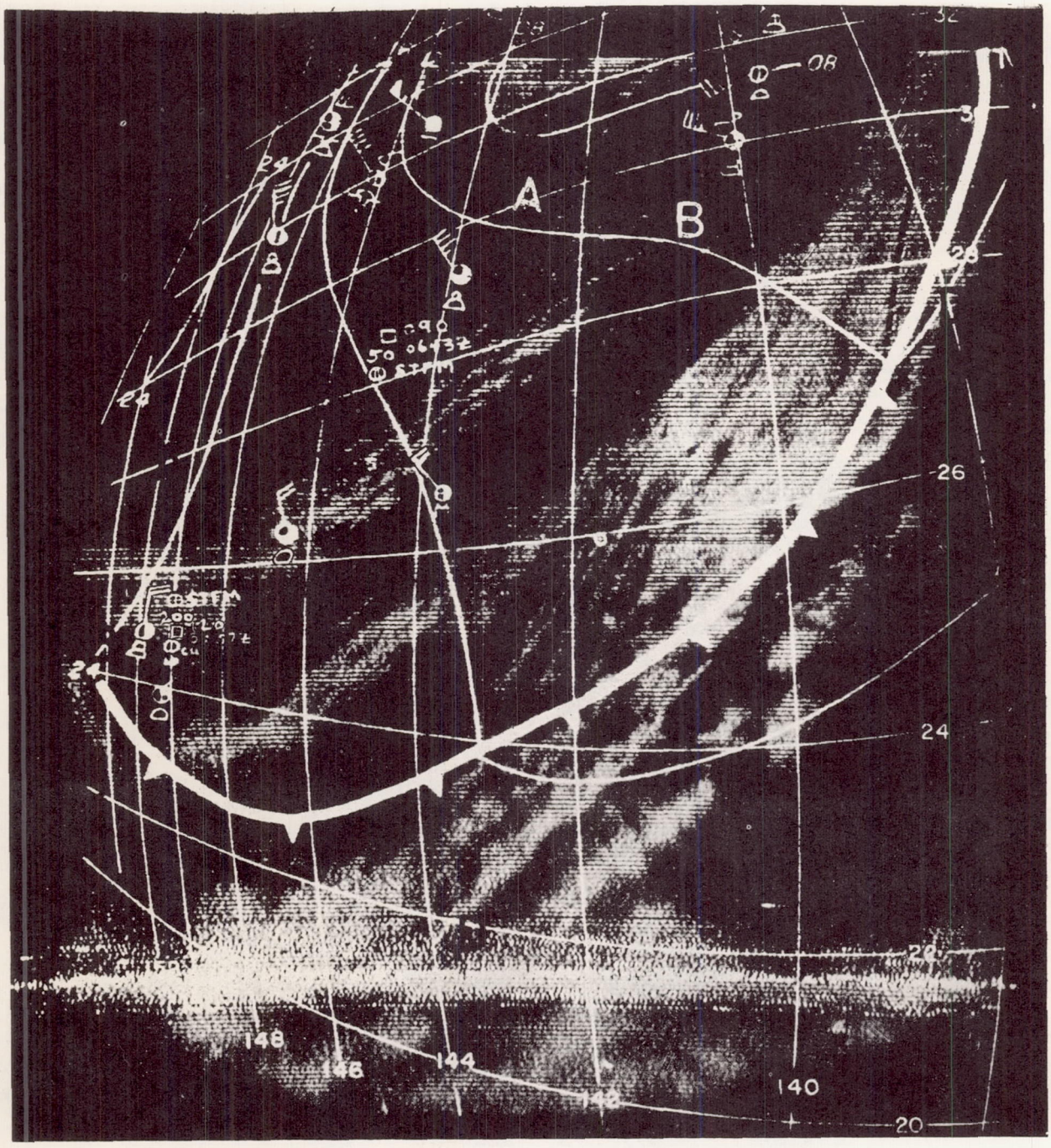

FIGURE 11.—Same picture as in figure 3 with superimposed grid and other items as in figure 9.

hours after the pictures were taken, indicated broken stratiform (presumably stratocumulus) clouds with tops at 5000 ft. The soundings at 35° N., 150° W. (fig. 16), which was well back in the cellular cloudiness to the rear of line AA, and the sounding at 30° N., 140° W. (fig. 17), which was practically on line BB, both reveal a moist, unstable layer of air from the surface to about 850 mb., with a layer of stable, dry air extending from above the pronounced inversion upward to near 600 mb. These soundings certainly suggest that cloudiness in their vicinities would have been confined to the instability type in the layer below the inversion. If convergence was indeed associated with lines AA and BB, it must therefore have been horizontal convergence and upward motion confined to this lower layer.

In portions of these areas, however, there is some evi-

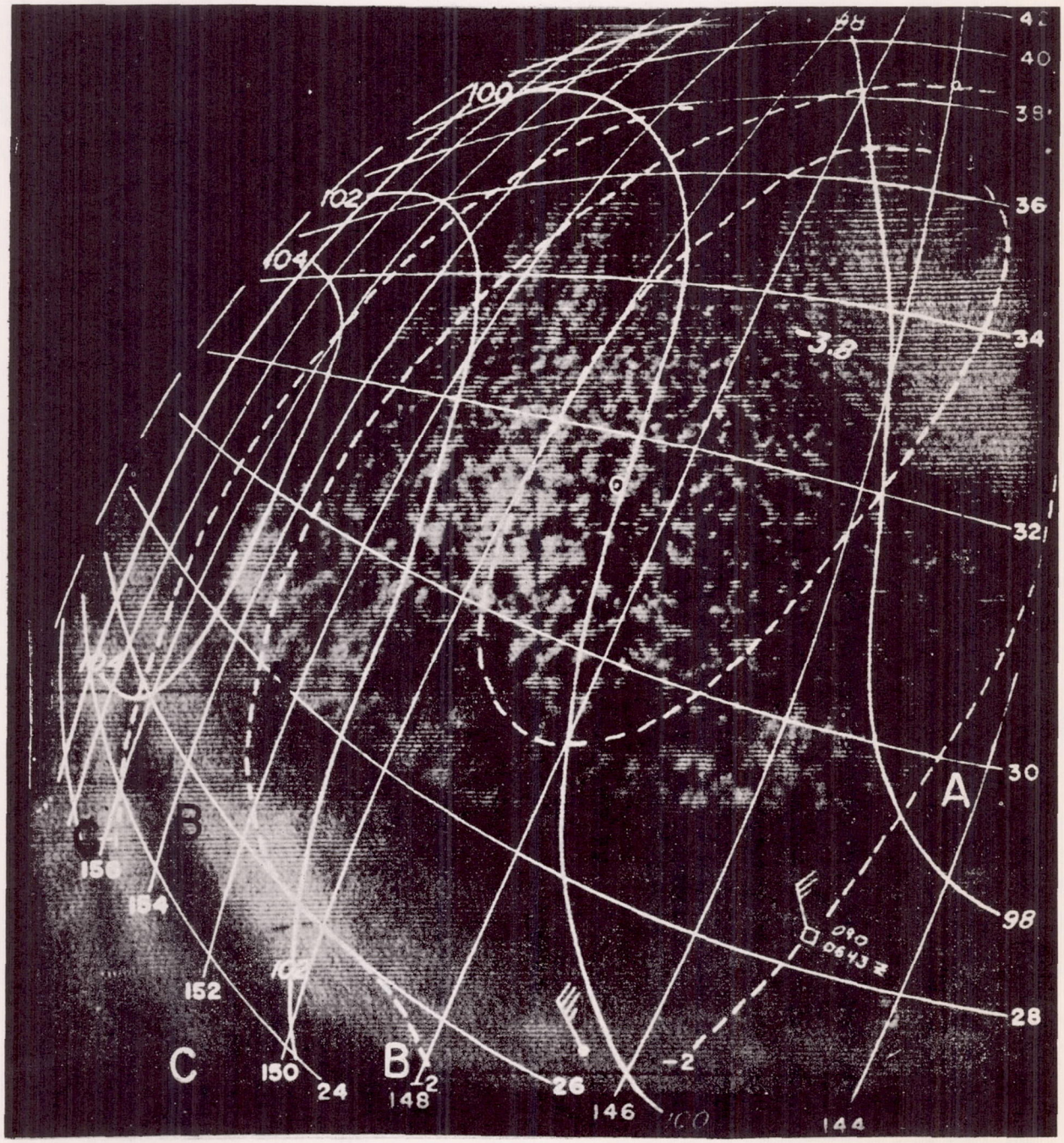

FIGURE 12.—Same picture as in figure 1 with superimposed 2° latitude-longitude grid; principal point of picture (circled dot); 700-mb. contours at 200-ft. intervals; 700-mb. winds; winds between 8000 and 12,000 ft. from aircraft measurements; and 600-mb. vertical motion in cm. sec.$^{-1}$ as computed routinely by the JNWP Unit. Time of superimposed data, except pilot reports, is 0000 GMT, April 5. 1960.

dence of middle cloudiness. Note the ship report of altostratus near 35° N., 148° W. which is just near the western edge of a solid-looking (apparently stratiform) cloud shield (fig. 9). Also the pilot report at 25° N., 150° W., approximately 4 hours after the picture was taken, shows an overcast of a stratiform type (presumably altostratus or cirrostratus) at an estimated base of 20,000 ft. (fig. 9). This report is also in a region where the cloudiness has a stratiform appearance. As the complete pilot report suggests, this upper cloud deck at this point overlay the lower, more extensive cumuliform cloudiness characteristic of the area behind line BB. The presence of middle cloudiness in

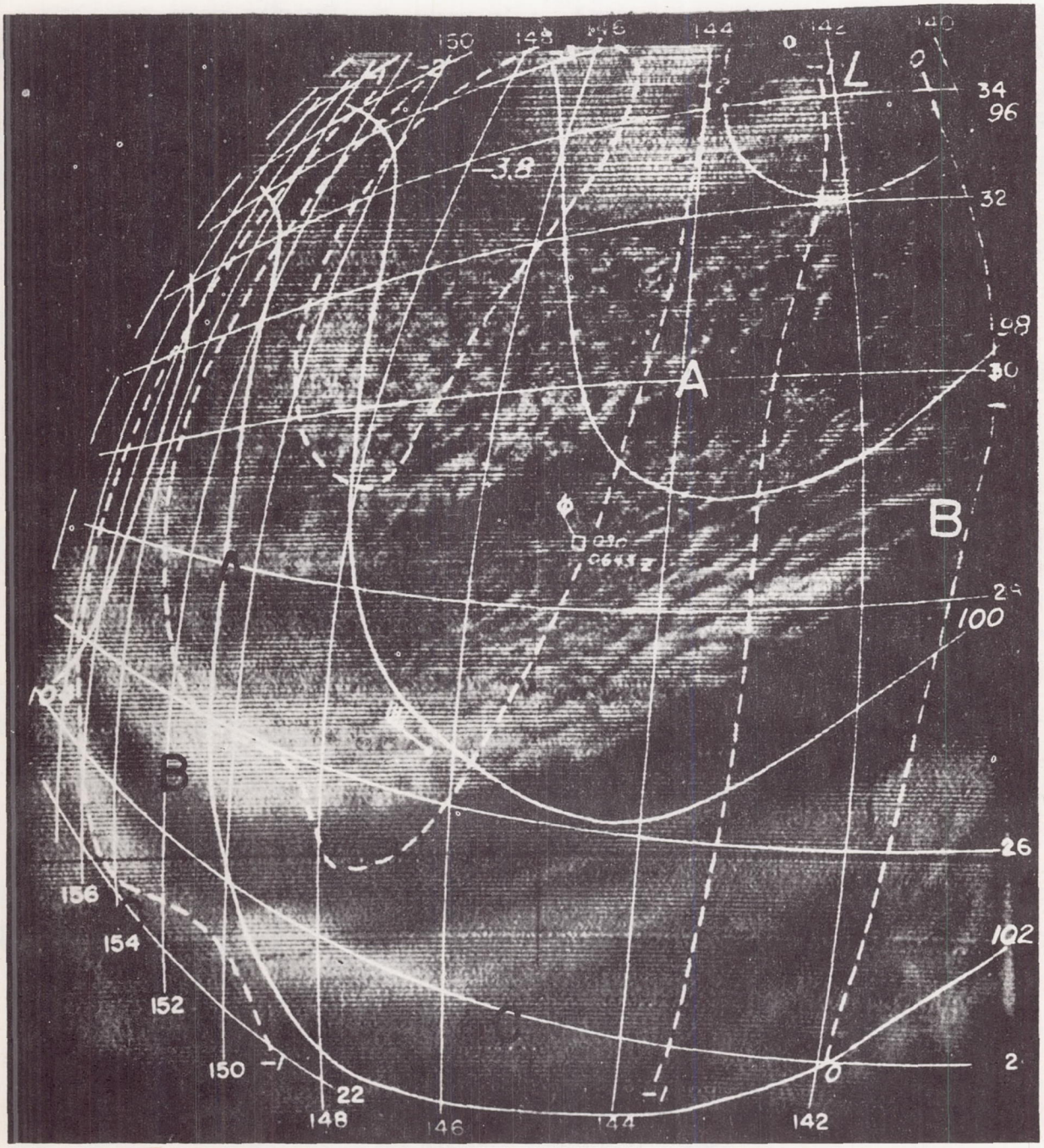

FIGURE 13.—Same picture as in figure 2 with superimposed grid and other items as in figure 12.

these areas suggests the likelihood of some large-scale upward motion in mid-troposphere.

Cridded pictures taken near 2200 GMT, April 5 (previously illustrated in figs. 6 and 7), are shown in figures 18–21 with superimposed NAWAC surface and 700-mb. analyses, abbreviated synoptic surface reports, and 600-mb. vertical motion, all of which are for 0000 GMT, April 6. It is notable that the broad banded cloud structure to the west of the cyclone (fig. 18) is closely oriented in the direction of the surface isobars. The ship reports show stratocumulus, cumulus congestus, and low clouds of bad weather in the area under this broad, bright band; there are also a few reports of an altostratus-altocumulus layer above the lower clouds. In view of the presence of middle cloudiness in this band, it is somewhat surprising that the 700-mb. contours are so different in orientation from the

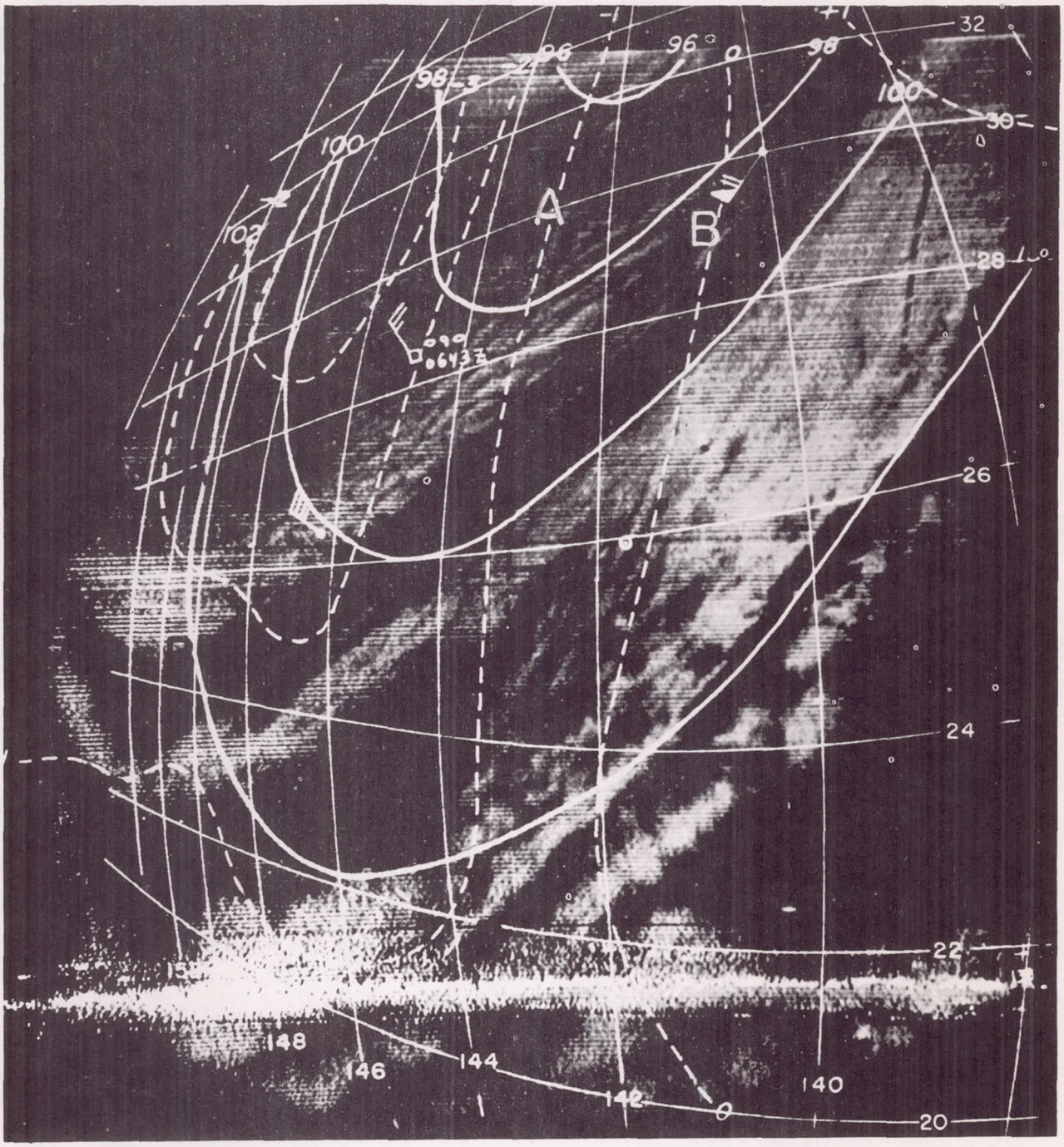

FIGURE 14.—Same picture as in figure 3 with superimposed grid and other items as in figure 12.

sea level isobars and the cloud band (e.g., the band and the contours are nearly perpendicular to each other near 34° N., 142° W. in fig. 20). The question thus arises as to whether the anticyclonic curvature in the 700-mb. contours is consistent with the pronounced cyclonic curvature of the sea level isobars. Twelve hours earlier the two analyses showed a close correspondence in flow patterns at the two levels (both strongly cyclonic) Although some height rises undoubtedly occurred in this 12-hour period, it does appear that this 700-mb. analysis eliminated the cyclonic curvature in the region of this cloud band too rapidly. It is likely that the 700-mb. contours actually did have an orientation more nearly parallel to the cloud band and to the surface isobars. In

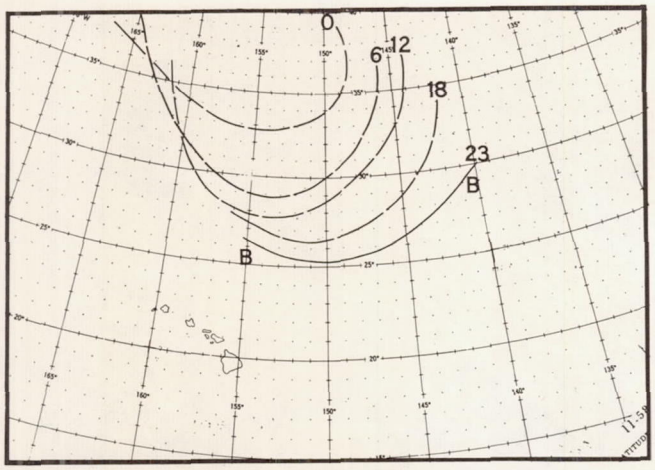

FIGURE 15.—Continuity of secondary cold front on April 4, 1960. Labeled positions for 0000, 0600, 1200, and 1800 GMT are from NAWAC sea level analyses. The position of line BB at 2300 GMT was derived from the gridded photograph in figure 10.

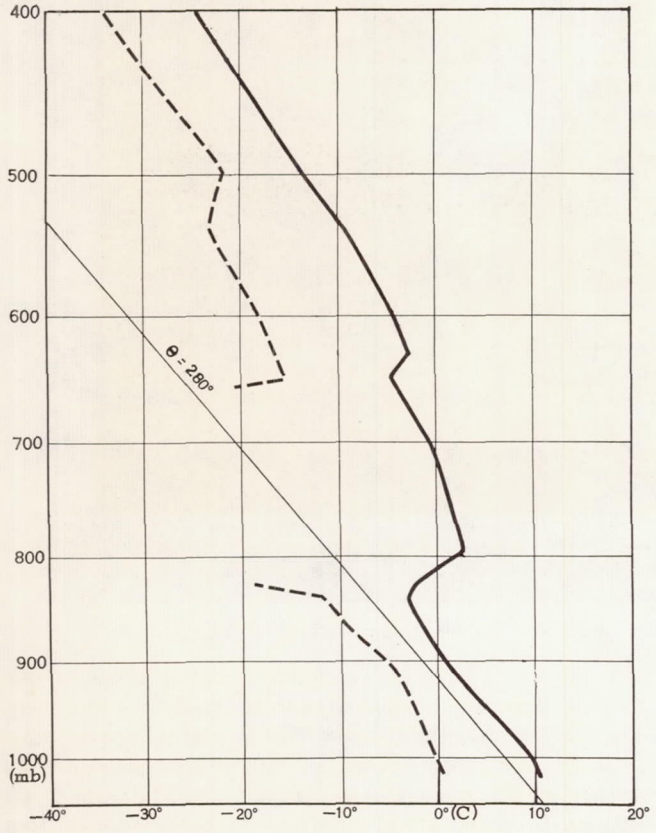

FIGURE 16.—Sounding at ship NHXN (34.9° N., 150.4° W.), 0000 GMT, April 5, 1960. Solid line shows temperature distribution; dashed line, dew point distribution.

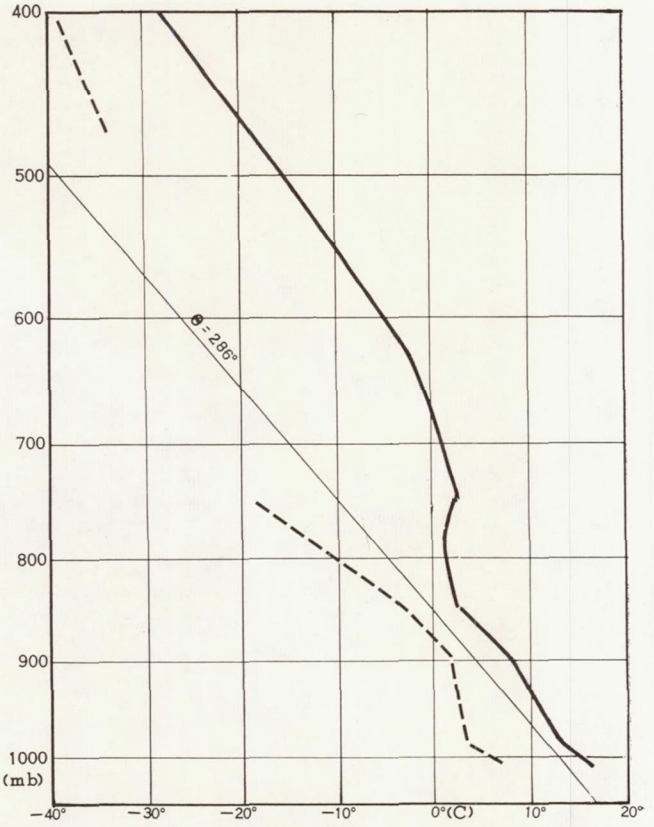

FIGURE 17.—Sounding at ship 4YN (30.0° N., 140.0° W.), 0000 GMT, April 5, 1960. Solid line shows temperature distribution: dashed line, dew point distribution.

fact it can be demonstrated readily that the contours can be reanalyzed in this fashion without violating any data.

The bands spiraling into the center of the storm as shown in figure 19 appear to line up with the surface flow north and just east of the center of the Low, although there is some uncertainty of this in view of the center's location toward the edge of the picture, where the accuracy of locating picture elements diminishes. The bands to the south of the cyclone center form a moderate angle of about 30°–45° with the surface isobars near 30° N., 134° W. and this increases to about 90° farther southwestward near 28° N., 138° W. It is probable that the forward edge of the spiral band which emanates from the center and runs approximately through 36° N., 134° W., southeastward to 32° N., 131° W., and thence southwestward through 28° N., 134° W. is the remnant of line BB in the pictures for the previous day (e.g., see fig. 10). This is supported by some rough trajectory calculations, based on the previous day's position of line BB, which show that this continuity from 24 hours earlier is within reason. The primary cold front appears to be mainly off the edge of the picture, but the cloud band near the northeastern and southeastern edges of the picture is very likely part of this frontal system and the suggestion is

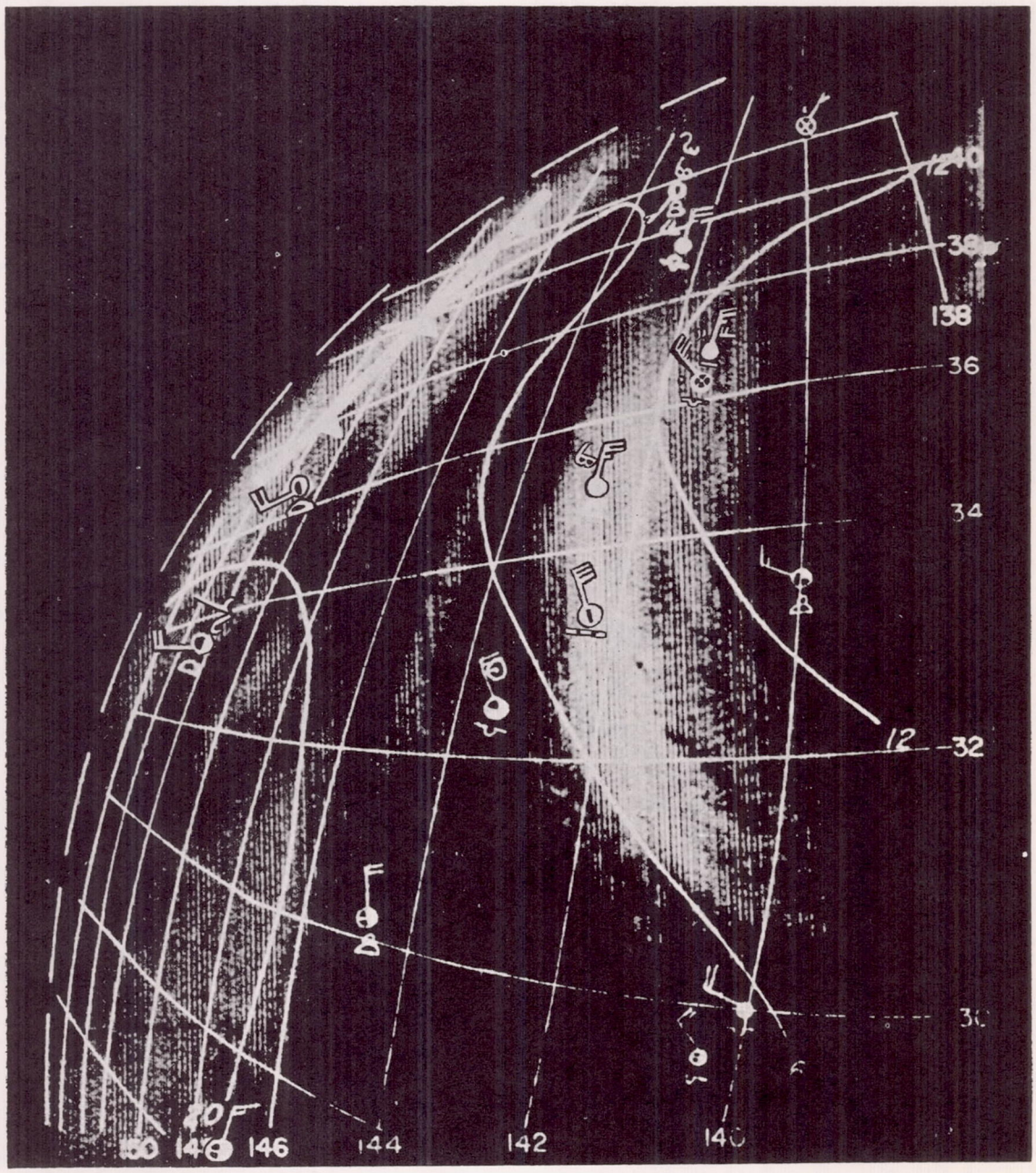

FIGURE 18.—Same picture as in figure 6 with superimposed grid and other items (except pilot reports) as in figure 9, except that time of superimposed data is 0000 GMT, April 6, 1960.

that the cloudiness and perhaps the front itself have spiraled into the region just north of the surface low center.

The vertical motion fields shown in figures 20 and 21 again fit in with the general broad-scale distribution expected around the mid-tropospheric trough associated with the cyclone. However, the solid-looking spiral bands and alternating clear areas near the cyclone center suggest that there may have been a similar spiraling of the vertical motion pattern in both the lower and middle troposphere. The JNWP vertical motion field is perforce constrained to a simpler pattern because of the general smoothing applied in the numerical calculations and because of the paucity of upper-air observations over this ocean area. It would be interesting to learn whether knowledge of such a spiral arrangement of vertical motion could sub-

569382—60——3

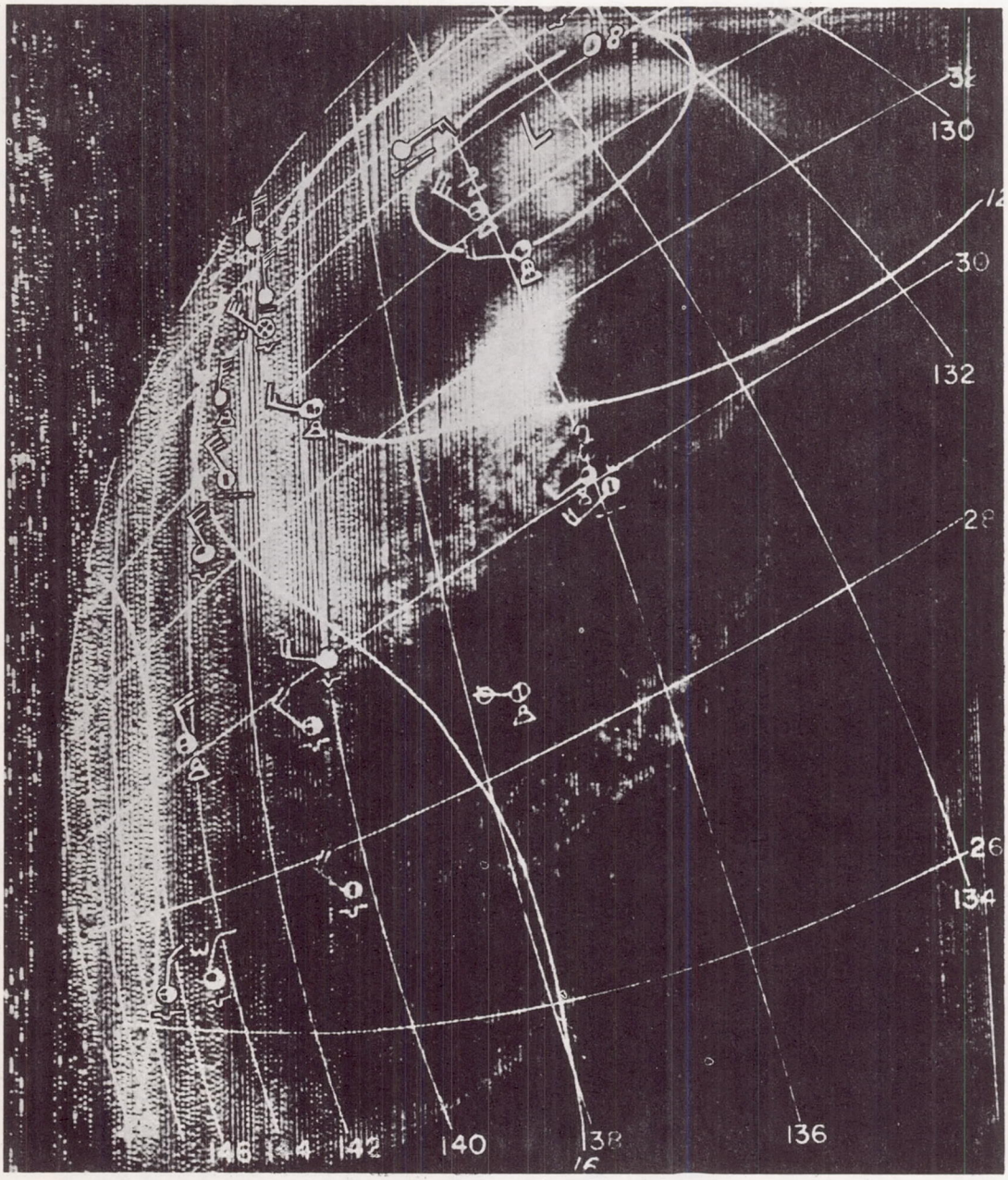

FIGURE 19.—Same picture as in figure 7 with superimposed grid and other items (except pilot reports) as in figure 9, except that time of superimposed data is 0000 GMT, April 6, 1960.

stantially improve predictions of the further evolution of the cyclone.

5 SUMMARY

The TIROS cloud pictures portray the details of the cloud structure around portions of this cut-off cyclone in the eastern Pacific in strikingly clear fashion. It has been shown that some of the major cloud bands in the southwestern portion of this cyclone were nearly perpendicular to the wind direction at both the surface and aloft. Also one of the most pronounced of these bands was identified as a secondary cold front along which the cyclonic development took place. The cloud patterns viewed by TIROS suggest possible modifications in the patterns of computed large-scale vertical motion in the middle troposphere. Regular views of entire storm areas, even at intervals of a day, would enhance our understanding of the life cycle and structure of systems such as the cut-off cyclone studied in this report.

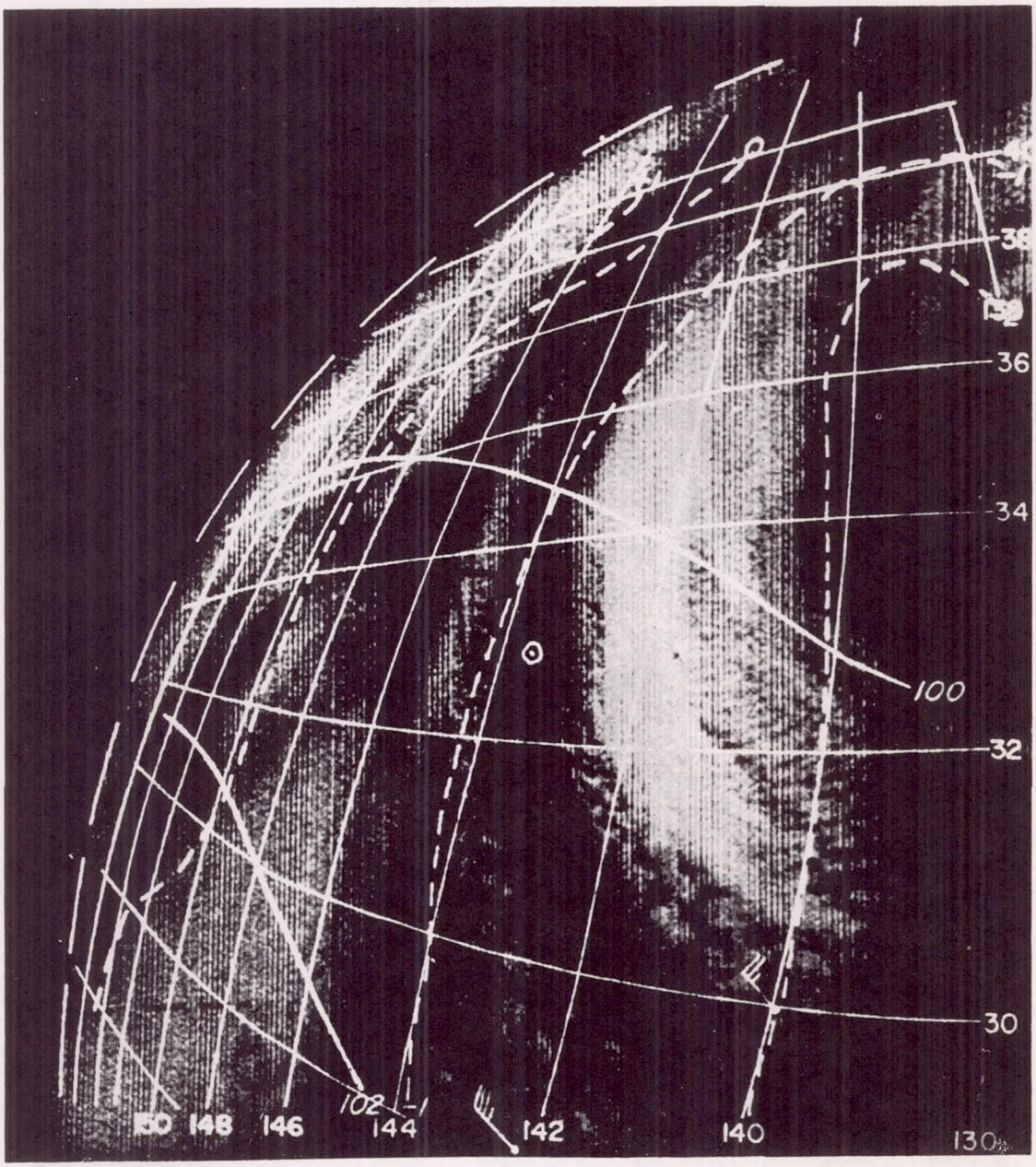

FIGURE 20.—Same picture as in figure 6 with superimposed grid and other items as in figure 12, except that time of superimposed data is 0000 GMT, April 6, 1960.

ACKNOWLEDGMENTS

The assistance of Louis Rubin in preparing the pictures with superimposed grids, isopleths, and plotted observations and of George E. Martin in fitting latitude-longitude grids to the pictures is sincerely appreciated.

REFERENCES

1. W. G. Stroud, "Initial Results of the TIROS I Meteorological Satellite," *Journal of Geophysical Research*, vol. 65, No. 5, May 1960, pp. 1643–1644.
2. S. Fritz and H. Wexler, "Cloud Pictures from Satellite TIROS I," *Monthly Weather Review*, vol. 88, No. 3, March 1960, pp. 79–87.
3. H. Wexler and S. Fritz, "TIROS Reveals Cloud Formation," *Science*, vol. 131, No. 3415, June 10, 1960, pp. 1708–1710.
4. A. F. Krueger and S. Fritz, "A Cellular Cloud Pattern Revealed by TIROS I," Section 8 of "Some Meteorological Results from TIROS I," Staff, Meteorological Satellite Laboratory, U.S. Weather Bureau, in a National Aeronautics and Space Administration Report on TIROS I (in press).
5. D. Fultz, "A Survey of Certain Thermally and Mechanically Driven Systems of Meteorological Interest," pp. 27–63 in *Fluid Models in Geophysics: Proceedings of the First Sym-*

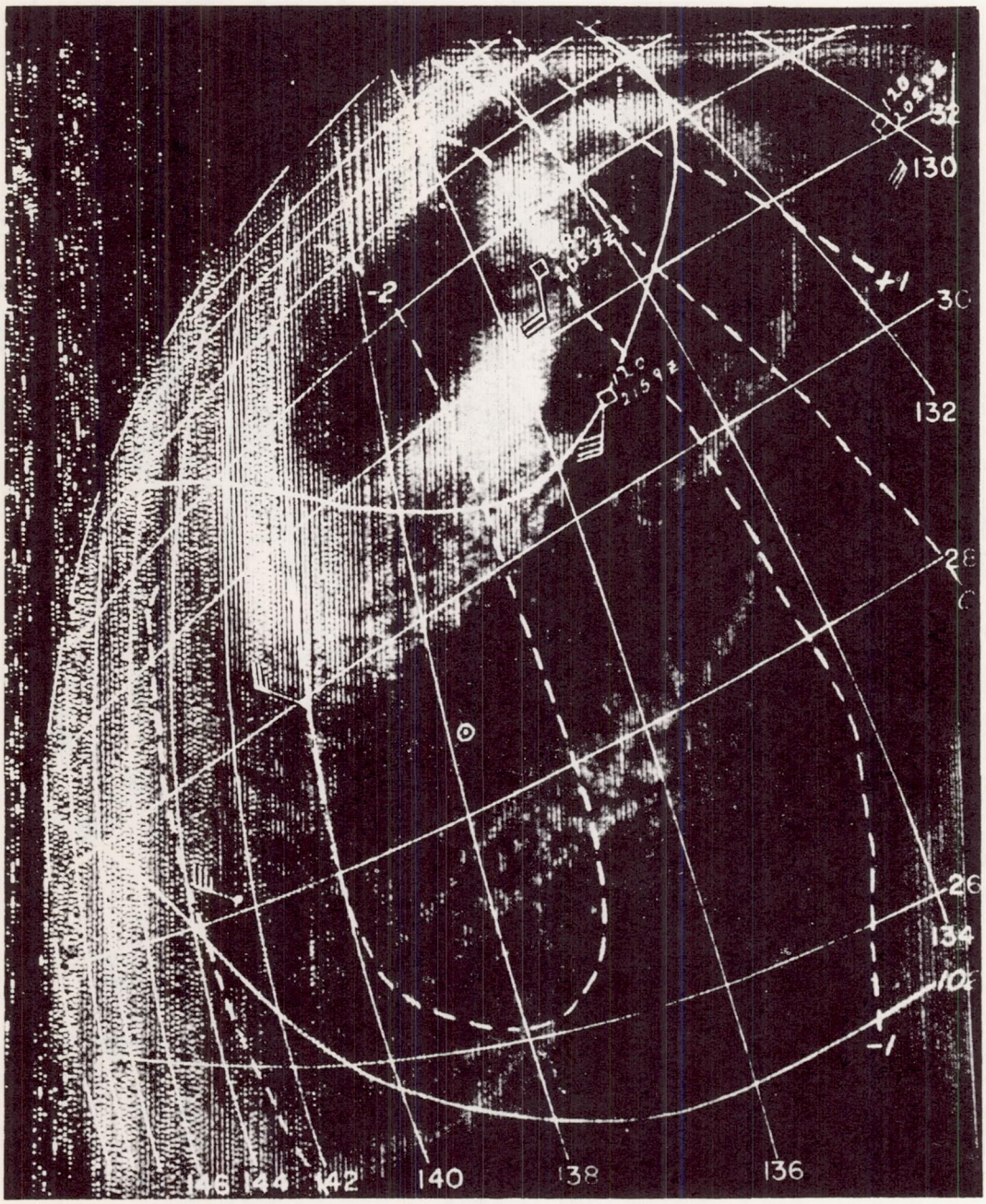

FIGURE 21.—Same picture as in figure 7 with superimposed grid and other items as in figure 12 except that time of superimposed data is 0000 GMT, April 6, 1960.

posium on the Use of Models in Geophysical Fluid Dynamics, Johns Hopkins University, Sept. 1–4, 1953, U.S. Office of Naval Research, Washington, D.C. 1956.

6. Y. Nakagawa and P. Frenzen, "A Theoretical and Experimental Study of Cellular Convection in Rotating Fluids," *Tellus*, vol. 7, No. 1, Feb. 1955, pp. 1–21.
7. H. Wexler, "Structure of Hurricanes as Determined by Radar," *Annals of the New York Academy of Sciences*, vol. 48, Art. 8, Sept. 15, 1947, pp. 821–845.
8. R. C. Doolittle, L. Miller, and I. Ruff, "Geographic Location of Cloud Features," Appendix 1 of "Some Meteorological Results from TIROS I," Staff, Meteorological Satellite Laboratory, U.S. Weather Bureau, in a National Aeronautics and Space Administration Report on TIROS I (in press).
9. C. L. Godske, T. Bergeron, J. Bjerknes, and R. C. Bundgaard, *Dynamic Meteorology and Weather Forecasting*, American Meteorological Society, Boston, 1957, 800 pp. (see Chapter 17, pp. 620–722).